High-spin through bond and space

Document status and date:
Published: 01/01/2001

Document Version:
Publisher's PDF, also known as Version of Record (includes final page, issue and volume numbers)

Please check the document version of this publication:

• A submitted manuscript is the version of the article upon submission and before peer-review. There can be important differences between the submitted version and the official published version of record. People interested in the research are advised to contact the author for the final version of the publication, or visit the DOI to the publisher's website.
• The final author version and the galley proof are versions of the publication after peer review.
• The final published version features the final layout of the paper including the volume, issue and page numbers.
Link to publication

High-spin through Bond and Space

Martin Struijk

High-spin through Bond and Space

PROEFSCHRIFT

ter verkrijging van de graad van doctor aan de Technische Universiteit Eindhoven, op gezag van de Rector Magnificus, prof.dr. M. Rem, voor een commissie aangewezen door het College voor Promoties in het openbaar te verdedigen op woensdag 21 maart 2001 om 16.00 uur

door

Martinus Pieter Struijk

geboren te Doesburg

Dit proefschrift is goedgekeurd door de promotoren:

prof.dr.ir. R. A. J. Janssen
en
prof.dr. E. W. Meijer

Table of Contents

4

Cation radicals of aniline oligomers with *meta* linkages   67

5

Towards ordering high-spin molecules:

Aniline oligomers with mesogenic groups   95

6

Oligo(verdazyl radicals) with mesogenic groups 117

7

Investigations on intramolecular spin coupling of cation radicals

through σ-bonds 137

List of abbreviations

ACN	acetonitrile
anal. calcd.	analytically calculated
ATR	attenuated total reflectance
BINAP	2,2'-bis(diphenylphosphino)-1,1'-binaphthyl
BPPFA	1-[1',2-bis(diphenylphosphino)ferrocenyl]ethyl-N,N-dimethylamine
C.T.	charge transfer
C.V.	cyclic voltammetry
dba	dibenzylideneacetone
DCM	dichloromethane
DMF	N,N-dimethylformamide
DMSO	dimethyl sulfoxide
DPPF	1,1'-bis(diphenylphosphino)ferrocene
ESR	electron spin resonance
Fc/Fc$^+$	ferrocene/ferrocenium
FCU	ferromagnetic coupling unit
FT	Fourier transform
hfac	hexafluoroacetylacetonate
HFIPA	hexafluoroisopropanol
HOMO	highest occupied molecular orbital
HPLC	high performance liquid chromatography
IR	infrared
LED	light emitting diode
LUMO	lowest unoccupied molecular orbital
MO	molecular orbital
mnt	maleonitrile
MSH	o-mesitylenesulfonylhydroxylamine
NBMO	non-bonding molecular orbitals
NBS	N-bromosuccinimide
NMR	nuclear magnetic resonance
PIFA	[bis(trifluoroacetoxy)iodo]benzene
PPFA	1-[2-(diphenylphosphino)ferrocenyl]ethyl-N,N-dimethylamine
PPF-OMe	1-[2-(diphenylphosphino)-ferrocenyl]ethyl methyl ether
PrCN	butyronitrile
SCE	saturated calomel electrode
SEC	size exclusion chromatography

spiro-TAD	2,2',7,7'-tetrakis-(*N*,*N*-diphenylamino)-9,9'-spirofluorene
spiro-MeOTAD	2,2',7,7'-tetrakis-(*N*,*N*-di-4-methoxyphenylamino)-9,9'-spirofluorene
SOMO	singly occupied molecular orbital
T_c	Curie temperature
TBAHF	tetrabutylammonium hexafluorophosphate
TCNE	tetracyanoethylene
TDAE	tetrakis(dimethylamino)-ethylene
TEMPO	2,2,6,6-tetramethyl-1-piperidinyloxy
TFA	trifluoroacetic acid
THF	tetrahydrofuran
$THI^{+\bullet}ClO_4^-$	thianthrenium perchlorate
TMS	trimethylsilane
TPD	*N*,*N*'-bis(3-methylphenyl)-*N*,*N*'-diphenylbenzidine
zfs	zero-field splitting

1

Organic ferromagnets

Abstract: *The design of molecular ferromagnetic materials and high-spin molecules requires knowledge of intra- and intermolecular spin-spin interactions. This chapter gives a short introduction and a discussion of important design parameters and concepts. A brief overview of recent literature in the area of organic ferromagnets is presented.*

1.1 Introduction

Tuneable molecular magnets remain a challenge for physical organic chemistry[1]. Magnetism results from the cooperative behavior of a large number of electron spins. Conventional magnets, like ferromagnetic iron, consist of magnetic domains containing a large number of unpaired electrons with strong interactions, resulting in an alignment of the electron spins in one direction.

Nature has a strong preference for pairing electron spins in an anti-parallel fashion. Therefore, most organic materials are diamagnetic (Figure 1.1, **A**) in which all electron spins are paired anti-parallel and their magnetic moments cancel. Due to the reactive nature of unpaired electrons only a limited number of organic materials consists of stable organic radicals. If interactions between the molecules are absent or weak a random orientation of the electron spins occurs, resulting in a paramagnetic material (**B**) with an overall cancellation of the electron magnetic moments in absence of an external magnetic field.
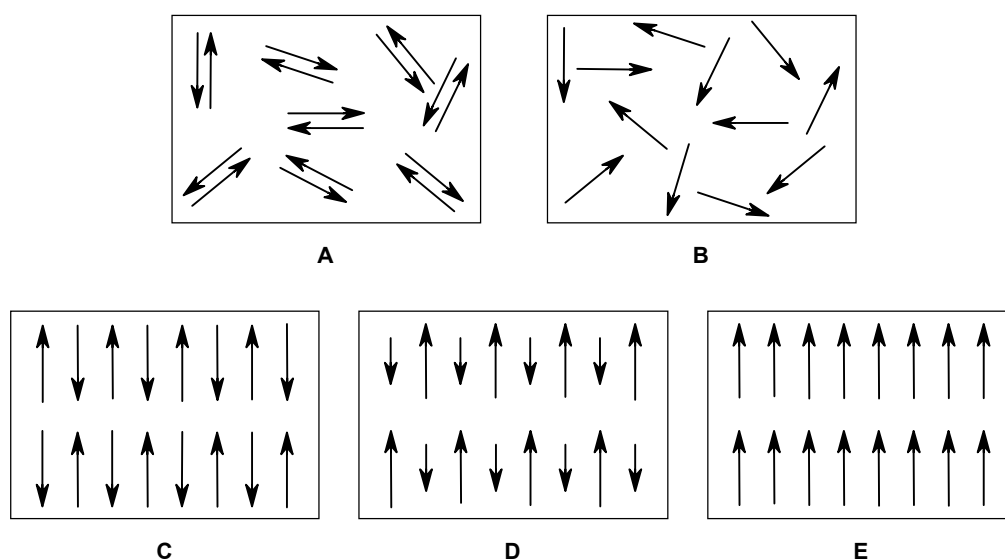
Figure 1.1. *Materials with different types of electron spin orientations; diamagnetic (A), paramagnetic (B), antiferromagnetic (C), ferrimagnetic (D), ferromagnetic (E).*

If non-negligible interaction between the unpaired electrons is present, a three dimensional ordering of the electron spins occurs below a critical temperature, T_c. The ordering can take several different forms. In an antiferromagnetic ordering (**C**) all spins align in an anti-parallel fashion so that the net magnetic moment is zero. In a ferrimagnetic material (**D**) an antiferromagnetic interaction between spins of different strength occurs, however, they do no cancel completely. Ferromagnetism (**E**) is a state in which all spins are aligned in one direction. The critical temperature, T_c, below which a

material becomes ferromagnetic is called the Curie temperature. At this temperature the interaction energy between the spins becomes larger than the thermal energy of the spins and a ordering of unpaired electron spins takes place. Since the interaction energies in most organic compounds are rather small, low T_c values are commonly observed.

The field of molecular magnets and organic ferromagnets can be subdivided into different types of materials depending on the nature of the spin carrier; organometallic complexes in which paramagnetic metals are bridged by organic ligands, organometallic complexes that are a combination of organic radicals with paramagnetic metals, and organic materials solely consisting of organic radicals.

A successful approach towards tunable materials with ferromagnetic properties was inspired by one of the first known inorganic complexes with magnetic properties; Prussian blue ($Fe_4[Fe(CN)_6]_3.15H_2O$)[2-4]. Prussian blue is a mixed valence compound in which iron is present in two different oxidation states, diamagnetic Fe^{2+} and paramagnetic Fe^{3+}. Verdaguer et al.[5] demonstrated that replacement of iron by a combination of other transition metals, such as vanadium and chromium, results in an organometallic complex ($V[Cr(CN)_6]$) which exhibits magnetic properties at room temperature ($T_c = 315$ K).

1   **2**   **3**

Figure 1.2. *Ferromagnetic complexes containing stable organic radicals.*

Organometallic magnetic compounds can also be constructed by mixing donor and acceptor molecules, which, after intermolecular electron transfer, are radicals and contain unpaired electrons. Miller et al.[6] showed that mixing a ferrocene donor with tetracyanoethylene (TCNE) as acceptor results in a sandwich structure **1** with a T_c of 4.8 K. Further experiments where TCNE was mixed with $V(C_6H_6)_2$ did not lead to a similar sandwich complex but resulted in the discovery of a room temperature magnetic material ($V(TCNE)_x.(CH_2Cl_2)_y$, $T_c \approx 400$ K)[7].

Combining stable organic radicals with paramagnetic transition metals has also proven to be a successful route towards molecular magnets. A prerequisite is the presence of coordination sites in the organic radical. Nitronyl nitroxide radicals are often used, because they combine chemical stability under ambient conditions with chelating sites and can be modified synthetically. By systematic preparation of numerous nitronyl nitroxide complexes with transition metals, Gatteschi et al.[8-10] succeeded in the preparation of Mn^{2+} complex **2** (R = methyl, ethyl, *i*-propyl), which shows ferromagnetic properties (T_c < 8 K). Kahn et al.[11] started off with preparing transition metals complexes with organic ligands. However, a switch towards the use of organic monoradicals with transition metals[12] proved to be more successful, improving the Curie temperature of these type of complexes to 22.5 K with **3**.
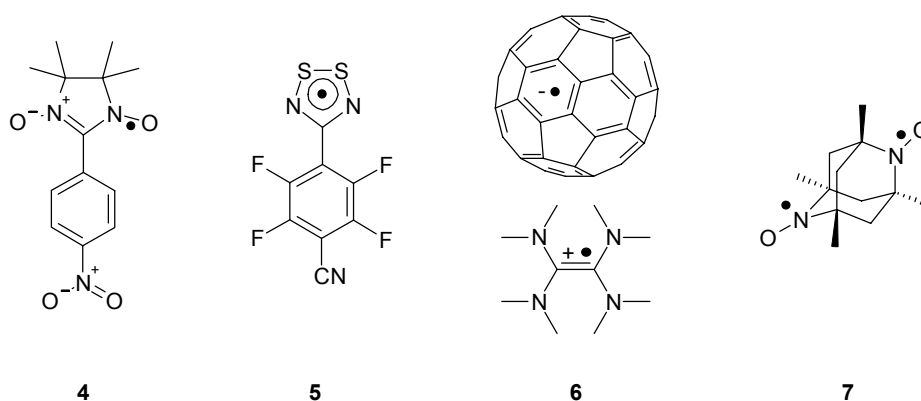
Figure 1.3. *Purely organic ferromagnetic materials.*

The development of purely organic ferromagnets started with the discovery that *p*-nitrophenyl-nitronyl-nitroxide (**4**) exhibits a ferromagnetic coupling between the radicals in the crystalline phase[13,14]. Soon, Kinoshita and co-workers found that this compound even exhibits bulk ferromagnetic properties below 0.7 K (T_c) for the β and γ crystalline phases[15-17]. These findings led to a systematic investigation of a large variety of stable organic monoradical derivatives and their crystalline phases[18]. Most of these monoradicals exhibit very low Curie temperatures, typically below 4 K, because the interactions between the molecules are very weak. A positive exception is the dithiadiazolyl radical **5** of Banister et al.[19,20] This type of radicals normally dimerises in a diamagnetic fashion, but careful substitution and preparation led to a crystalline β-phase with ferromagnetic properties below 36 K.

During their research on the *n*-doping of fullerenes, Wudl et al.[21] discovered that the donor-acceptor complex of C_{60} with tetrakis(dimethyamino)-ethylene (TDAE) (**6**) shows ferromagnetic properties below 16 K. This triggered the preparation of similar

complexes containing fullerene derivatives with different donors[22]. The origin of the ferromagnetic interactions in these complexes remained unclear until recently[23].

Another interesting type of organic ferromagnet is *N,N'*-dioxy-1,3,5,7-tetramethyl-2,6-diazaadamantane **7** of Chiarelli et al.[24,25] (T_c = 1.5 K). This molecule contains two radicals, which couple in a parallel fashion resulting in a high-spin molecule. Not only the intramolecular coupling is ferromagnetic, but at its transition temperature also the intermolecular coupling becomes ferromagnetic, yielding a pure organic ferromagnet.

The design of organic ferromagnetic materials requires stable unpaired electrons and strong ferromagnetic interactions. This requires control over both the spin coupling in the molecule (intramolecular) and the spin coupling between the molecules (intermolecular). Both subjects will be discussed separately with examples in the following paragraphs

1.2 Intramolecular spin alignment

Non-Kekulé molecules are part of the class of alternant hydrocarbons. In non-Kekulé molecules not all π-electrons can be rearranged to form π-bonds and as a consequence two or more unpaired electrons will be present, resulting in an open-shell configuration. In contrast, in Kekulé molecules all π-electrons form π-bonds resulting in a closed-shell configuration. In a high-spin molecule, the unpaired electrons have a parallel spin alignment caused by intramolecular ferromagnetic spin coupling. The nature of these spin-spin interactions can be predicted using several models. Two of these models will be discussed briefly.

In a polyradical, the unpaired electrons are located in separate almost degenerate singly occupied non-bonding molecular orbitals (NBMO's). The different radicals interact via an exchange coupling (J), which according to the Heitler-London model[26], can be subdivided in an antiferromagnetic contribution (kinetic exchange βS, negative) and a ferromagnetic contribution (coloumb exchange K, positive). In order the accomplish a ferromagnetic interaction, the antiferromagnetic term should be very small or zero. This is achieved when the NBMO's have zero overlap integral ($S = 0$, orthogonal). For a ferromagnetic coupling or high-spin state, the exchange integral (K) must be unequal to zero. This can be achieved if the unpaired electrons are localized in the same region of space and close enough to interact with each other. The preference for parallel spin alignment is expressed in Hund's rule and results from the fact that coulombic repulsions between electrons are diminished substantially if they have parallel spins. The Heitler-London model suggests that to achieve strong ferromagnetic

coupling between two electrons, the associated molecular orbitals should occupy the same region of space, yet have a quantum chemical overlap integral of zero.

8

S = 0

9

S = 1
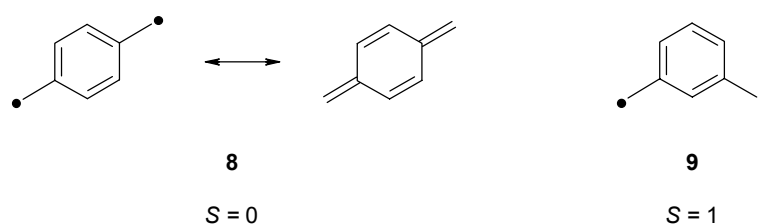
Figure 1.4. *Isomers of benzoquinodimethane*

There are two simple methods to predict the multiplicity of the ground state of non-Kekulé molecules. These methods will be illustrated using the classical example of isomeric *meta-* and *para*-benzoquinodimethane. The model developed by Longuet-Higgins[27] predicts that an alternant hydrocarbon contains $x = (N-2T)$ NBMO's in which N is the number of carbon atoms and T is the maximum number of double bonds. The *para*-isomer can be drawn with a maximum number of four double bonds (Figure 1.4) and as a consequence there are zero NBMO's (8-2*4 = 0). The *meta*-isomer can only be drawn with three double bonds, so there are two NBMO's in the molecule, each occupied with one unpaired electron. Application of Hund's rule (parallel spins) results in a triplet spin state ($S = x/2 = 1$).

8

S = 0

9

S = 1
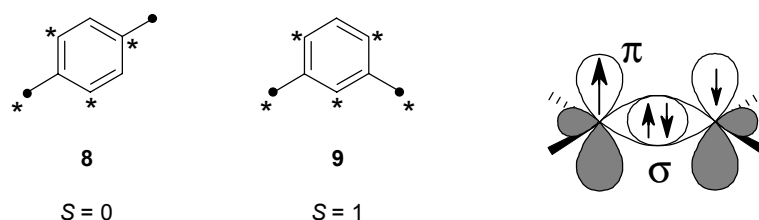
Figure 1.5. *Spin polarization in benzoquinodimethanes (left) according to Hund's rule (right).*

In the second model, developed by Ovchinnikov[28], the carbon atoms of an alternant hydrocarbon are starred (n*) and unstarred (n) in alternating fashion so that every starred atom has only unstarred atoms as nearest neighbors. If n* > n, the spin state S is given by: $S = (n$*$-n)/2$. Application to the isomeric benzoquinodimethane molecules (Figure 1.5), results in $S = (4-4)/2 = 0$ or singlet state for the *para*-isomer and $S = (5-3)/2 = 1$ or triplet state for the *meta*-isomer. The theoretical basis of this method relies on a full MO calculation including configuration interaction, of the sign and magnitude of the spin densities at the carbon atoms. The result of such calculations shows that the starred atoms have a large positive spin density and the unstarred atoms have a small negative spin density. This is called the spin polarization mechanism, where large

positive spin densities induce small negative spin densities on the neighboring atoms. Spin polarization can be rationalized by inspection of a molecular bond between to atoms of a conjugated molecule (Figure 1.5). Because of a more favorable exchange, the electrons in the π-orbital and σ-orbital on one atom will have similar spin orientations. Since the σ-orbital also contains an electron of the neighboring atom it must have an anti-parallel alignment (Pauli's principle) resulting in a π-electron with opposite spin at the other atom.

There are two important shortcomings in these two methods. Although the sign of the exchange coupling is correctly predicted in many cases, the magnitude of the exchange coupling is not taken into account. In case of a very weak interaction, nearly degenerate low–spin and high-spin states might result. Other molecular structural details determine now which one is the lowest in energy. This important shortcoming has been addressed by Borden and Davidson[29], introducing the concepts of joint, disjoint, and non-disjoint NBMO's. However, it is not necessary to understand these concepts in relation to this thesis and therefore they will not be explained in detail. Another shortcoming is that the spin state of polyradicals containing heterocycles, which actively participate in the exchange pathway, is not always predicted correctly.

1.3 High-spin molecules

1.3.1 Design concepts

Since the mechanisms of intramolecular spin alignment are rather well understood, high-spin molecules can rationally be designed and synthesized. A number of concepts exist for designing high-spin molecules[30]. A precise control over substitution pattern and quantitative generation of unpaired electrons are common denominators in these concepts. The simplest concept is the regular alternation of spin carrying units and ferromagnetic coupling units (FCU's) along a single chain (Figure 1.6, **A**). It allows for simple construction methodologies and strong intramolecular spin coupling since the radicals are close together. A drawback of this concept is the need for quantitative generation of the spins on the chain. If there is one radical missing or spin defect along the chain, this generally results in an antiferromagnetic coupling between the two segments and a canceling of the magnetic moments.
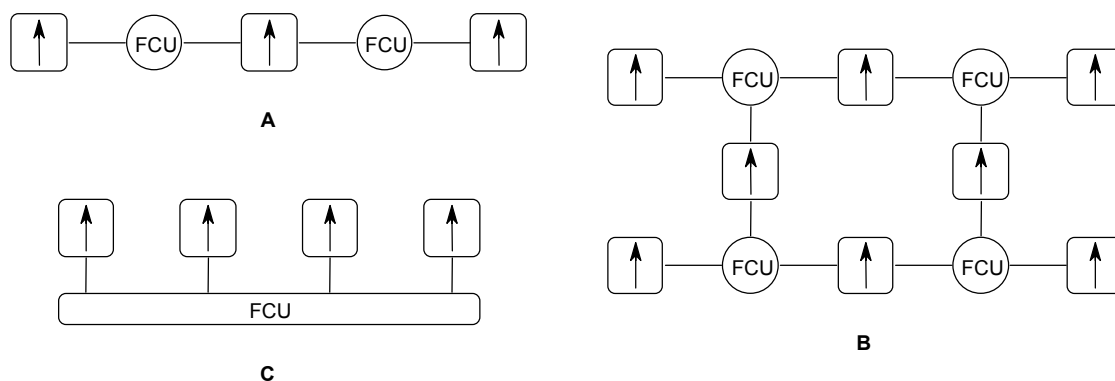
Figure 1.6. *Design concepts for high-spin molecules.* **A:** *Linear alternating chain;* **B:** *Double cable;* **C:** *FCU backbone with pendant radicals.*

The construction of a double cable in which several exchange pathways between the two parallel chains are present is a way to overcome the problem of spin defects (**B**). Here, a spin defect along one of the chains does not interrupt the ferromagnetic coupling in the whole molecule and a high-spin molecule will result. A different approach to overcome the disastrous effects of spin defects in linear chains is the concept of pendant radicals positioned along a π-conjugated backbone (**C**). Because the intramolecular exchange pathway is secured along the backbone, a spin defect does not necessarily reverse the spin coupling in the molecule. However, distances between the radicals are generally longer, resulting in weaker interactions. This concept is often used for the design of high-spin polymers, to overcome problems associated with the non-quantitative generation of radicals.
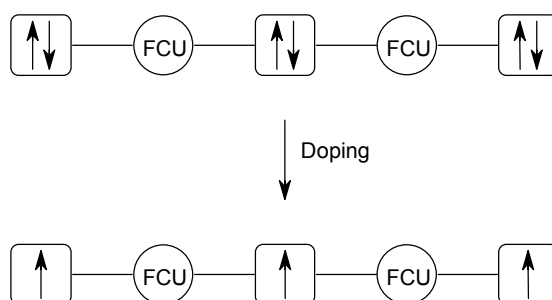
Figure 1.7. *Polaronic organic ferromagnet.*

The stability of ionic radicals combined with the precise control over their spin state by doping, led Fukotome et al.[31] to propose the concept of the polaronic organic ferromagnet (Figure 1.7). In this case the spin carrier units are made from a dopable segment.

The type of radical is an important choice in designing high-spin molecules. Important aspects are the stability of the radical at ambient temperature, the precise control over the spin state, possibilities for synthetic modification, and the strength of exchange couplings between the radicals. Since every radical has its pro's and con's, a large variety of high-spin molecules has been designed, synthesized, and characterized. There exists a number of excellent reviews and collections of papers that describe the literature in this field[32-38]. The following subparagraphs contain a selection of high-spin molecules reported, with an emphasis on the last five years, subdivided by the type of radical that has been used.

1.3.2 Carbenes

The first high-spin quintet ($S = 2$) dicarbene **10** was simultaneously reported by Itoh[39] and Wasserman et al.[40] This type of radicals is photochemically generated at cryogenic temperatures. In this process one of the diazo precursors is cleaved by a photon of light after which a chain reaction in the molecule results in a quantitative formation of the corresponding carbene radicals. This very efficient generation of multiple radicals resulted in the preparation of high-spin molecules with an increasing number of carbene units by Iwamura and co workers, of which nonacarbene **11** is the largest reported[41,42]. Over the years, they evolved from linear molecules via star-shaped compounds to highly branched structures. In these latter molecules intramolecular reaction of the reactive carbene units tended to give lower spin states than expected[43,44]. This limiting factor stimulated the group of Tomioka[45,46] to search for more stable carbene radicals. The first of which was a polybrominated carbene radical that was used to construct high-spin molecule **12**. The latest improvement in this area is carbene radical **13**, which is stable at room temperature for minutes[47]. Here, the carbene center is protected by sterical congestion and the electronically stabilizing influence of the bromo and trifluoromethyl groups. Replacement of all the bromo groups by the better stabilizing trifluoromethyl groups was not possible for synthetic reasons.

10

11

12

13
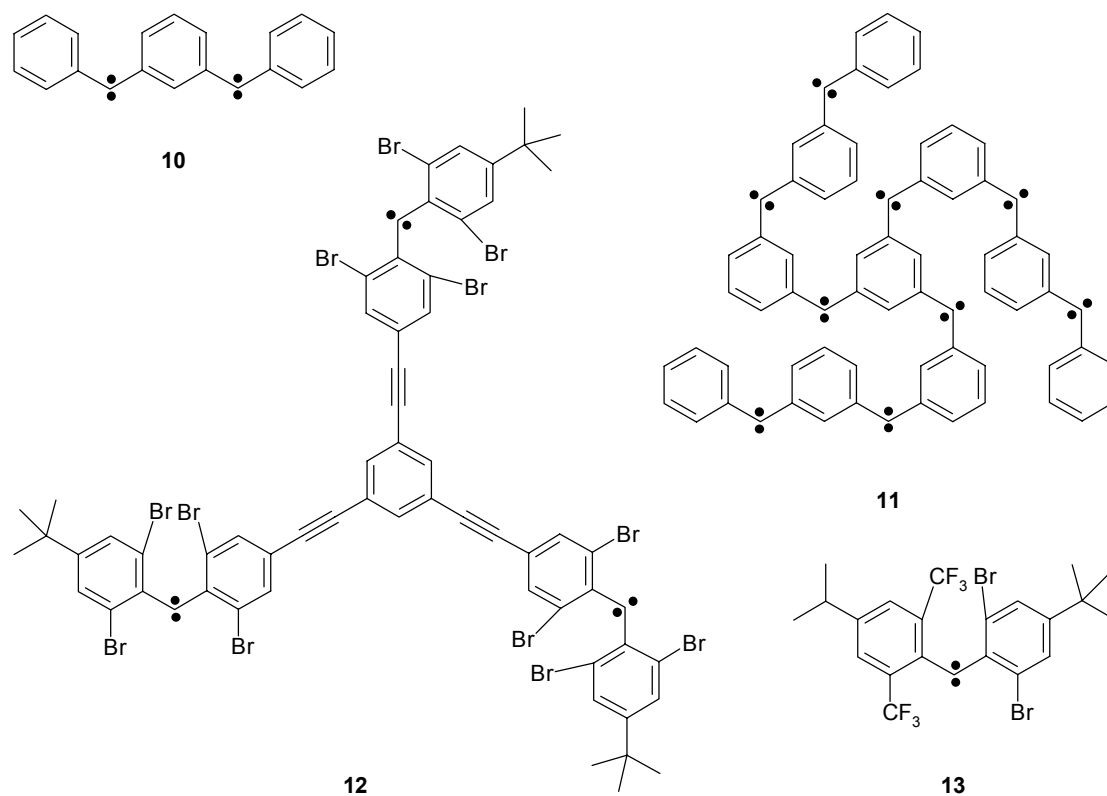
Figure 1.8. *High-spin molecules based on carbene radicals.*

1.3.3 Triarylmethyl radicals

The classical examples in this category are Schlenk's diradical[48] (**14**) and Leo's triradical[49] (**15**). Both the groups of Rajca and Veciana have effectively used this type of radical to construct high-spin molecules with higher spin states.

14

15

16

R =
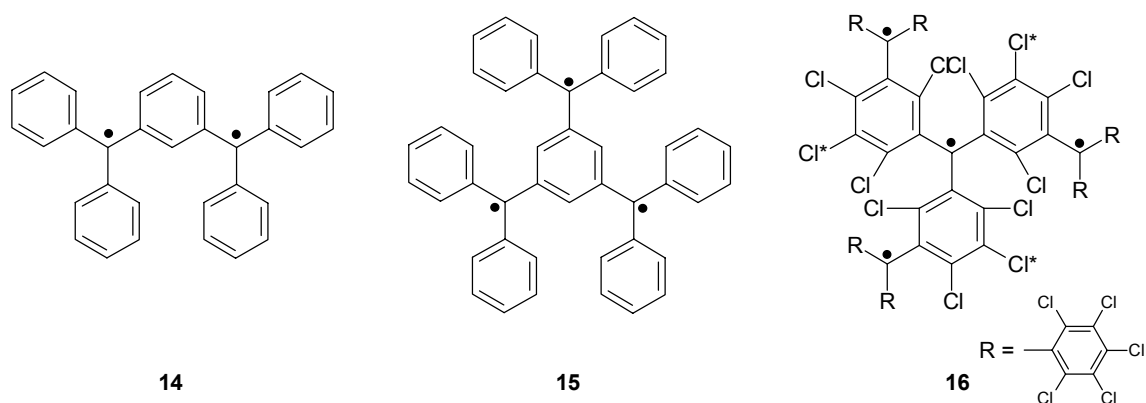
Figure 1.9. *High-spin molecules based on triarylmethyl radicals*

Although less reactive than carbenes, triarylmethyl type radicals have a limited stability and must be kept at low temperature. Ballester[50] solved this problem by using perchlorinated phenyl rings creating a radical with a very high temperature stability. The group of Veciana[51] used these radicals for the construction high-spin molecules (**16**). Although different synthetic routes were tried, steric congestion limits the extension of these high-spin molecules to higher homologues[52].

A large variety of dendritic oligo(triarylmethyl) radicals has been synthesized by the group of Rajca. Using calix(4)renes, the double cable concept proved to be effective in creating high-spin molecules with large spin states which do not suffer from one or more defects[53]. The latest example is **17**, which is currently the world record for oligomeric high-spin molecules with a $S = 10$ spin state (20 radicals !)[54]. Since theoretically a $S = 12$ state is expected, the chance to find a radical at any triarylmethyl center was calculated to be 98 % according to a magnetization study. These polyradicals are created from the corresponding methoxy-derivative precursor by treatment with Na/K alloy and subsequent oxidation of the generated polyanion with iodine.
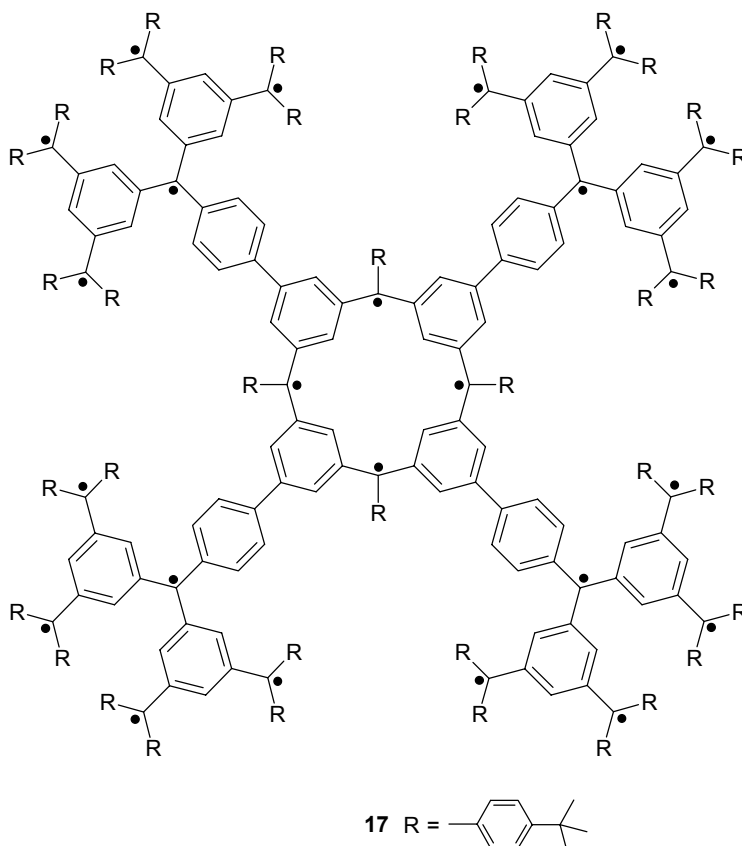
Figure 1.10. *Calix(4)rene with branched substituents of Rajca et al.*

1.3.4 Nitroxide radicals

Nitroxide radicals are frequently used for all kind of purposes because of their stability and synthetic accessibility. These radicals have been used in various different strategies towards organic ferromagnets over the past decades. A number of high-spin molecules containing nitroxide radicals have been constructed[55,56]. Weak intramolecular ferromagnetic couplings are generally observed due to the more localized nature of nitroxide radicals, sometimes even resulting in low spin states[57,58].

The latest developments in high-spin molecules made from nitroxide radicals concern the combination of different radicals in one molecule, so called heterospin molecules. Iwamura et al.[59] prepared molecules in which imino nitroxide and/or nitronyl nitroxide radicals are connected via a diphenyl nitroxide radical (**18**). All three molecules show quartet ground states with an antiferromagnetic intermolecular coupling within the single crystals. The imino nitroxide radicals (**18b,c**) do not have a resonance contribution to the exchange interactions between the radicals in the molecule and as a result have a weaker intramolecular ferromagnetic coupling.

18a R1 = R2 = O
  b R1 = O, R2 = -
  c R1 = R2 = -

19a 2,7
  b 2,8
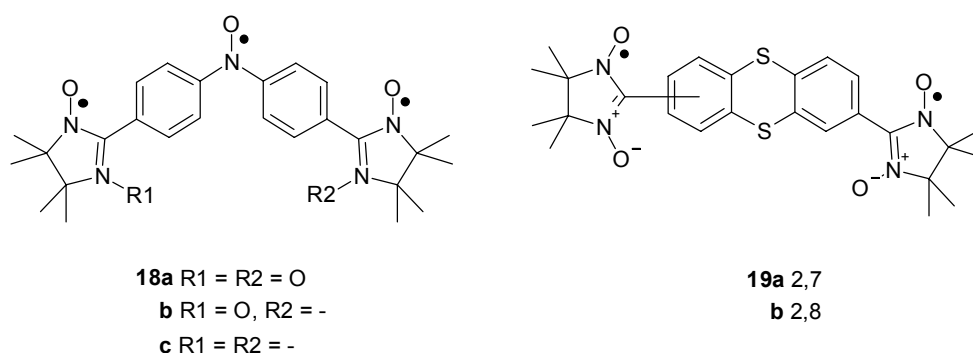
Figure 1.11. *Nitroxide radicals with high-spin properties.*

A different and interesting strategy has been described by Sugawara et al.[60] in which two nitronyl nitroxides are coupled to a thianthrene molecule acting as ferromagnetic coupler (**19**). Since thianthrene is known to produce stable cation radicals when oxidized, this molecule is an example of an electronically controllable spin system. The spin states of the neutral forms can be predicted with the spin polarization mechanism assuming that the lone pair on sulfur acts as a carbon-carbon double bond. In accordance, molecules **19a** and **19b** have a weak ferro- and antiferromagnetic intramolecular coupling, respectively. Surprisingly both the 2,7- and 2,8-isomer possess a quartet ground state in the singly oxidized triradical state. Apparently the spin alignment mechanisms in neutral and oxidized molecules are different, and the latter

has been rationalized in terms of a space-sharing of the three singly occupied molecular orbitals.

1.3.5 Ion radicals

The concept of the polaronic organic ferromagnet has proven to be a valuable model to design and construct high-spin molecules over the past decade. Triaryl aminium radicals are very popular because of their stability and delocalization of the spin density into the aryl groups, giving rise to strong intramolecular ferromagnetic interactions. Therefore, this paragraph will be focused on high-spin molecules containing aniline units. Both Wienk et al.[61-63] (**20**, **21a+b**) and Blackstock et al.[64] (**21b+c**) reported oligoanilines with an alternating *meta-para* topology, exhibiting a high-spin ground state and stability at ambient temperatures of the corresponding cation radicals.

20 n = 1, 2
R = H, Phenyl

21a R = H, R' = H
b R = Phenyl, R' = H
c R = Anisyl, R' = MeO
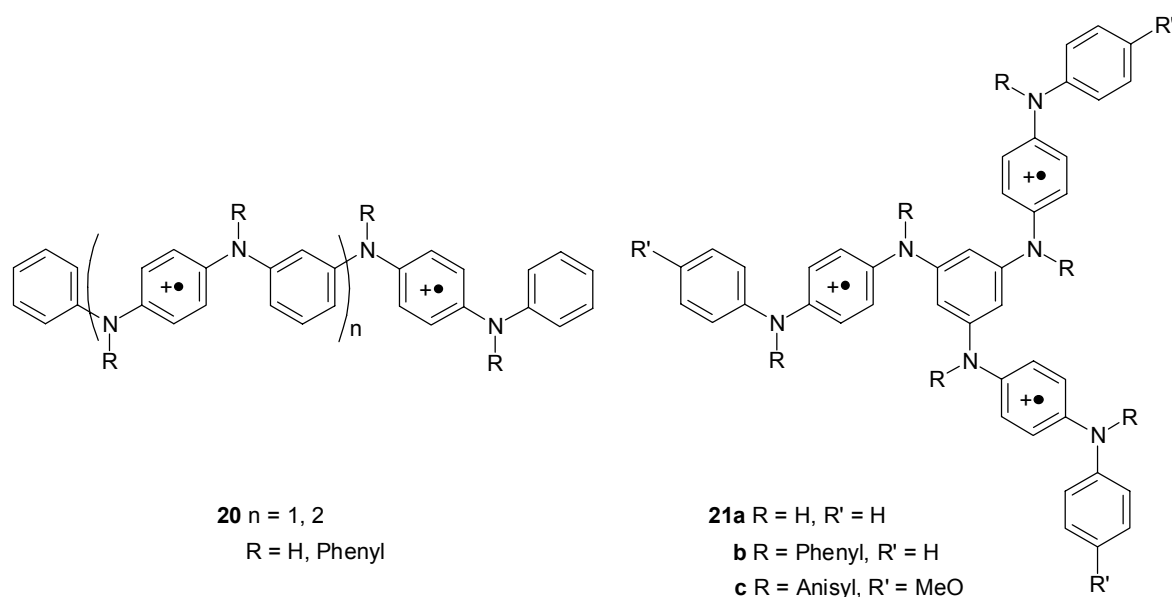
Figure 1.12. *High-spin m-p-oligoanilines.*

Nishide et al.[65] prepared a triplet high-spin molecule with two diphenylamine moieties connected to a π-conjugated stilbene backbone (**22**). This molecule has been studied as model compound for the high-spin polymer with pendant ionic radicals (**30**). Van Meurs et al.[66] used a similar strategy for the construction of head-to-tail coupled oligo(1,4-phenylenevinylene)s (**23**) and oligo(1,4-phenyleneethynylene)s with pendant 1,4-benzenediamine motifs. The corresponding di(cation radicals) exhibited a triplet ground state and stability at ambient temperatures.

22 R = OMe, *t*-Butyl   **23** n = 0, 1
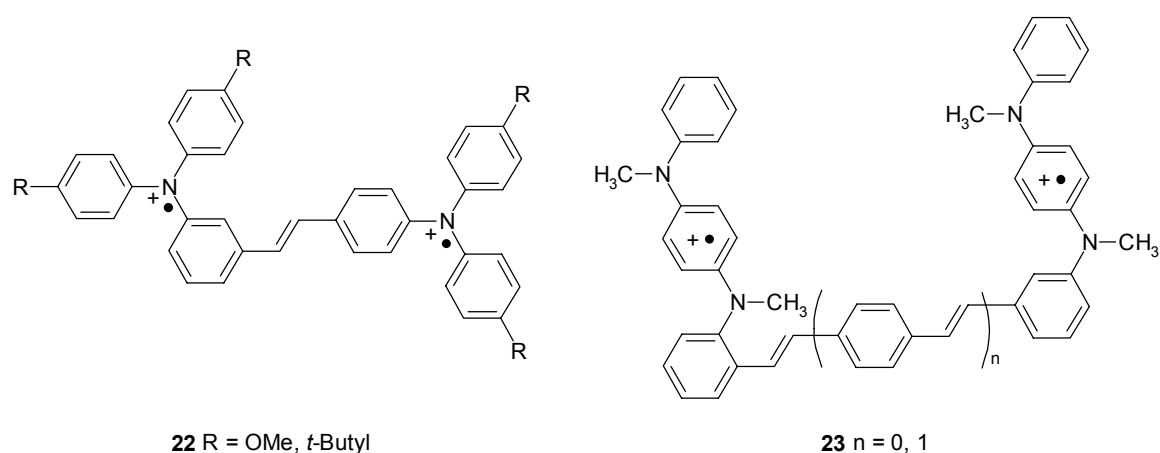
Figure 1.13. *Triplet state arylamine cation radicals*

Naphthalene is known to act as a ferromagnetic coupling unit if substituted at the appropriate positions[67]. Blackstock and Selby constructed two 2,7-bis(amino)naphthalenes (**24**) which possess a triplet state after oxidation to the corresponding di(cation radical). Surprisingly the methoxy substituted substrate (**24b**) showed solution stable behavior in contrast to their 1,3-benzene substituted derivative reported previously[68].

24a R = N—(⟨⟩—OMe)₂
  b R = OMe   **25**   **26** R = R' = *p*-Me, *m*-OMe, *p*-OMe, CO₂*t*-Bu
                                          R = CO₂*t*-Bu, R' = *p*-OMe
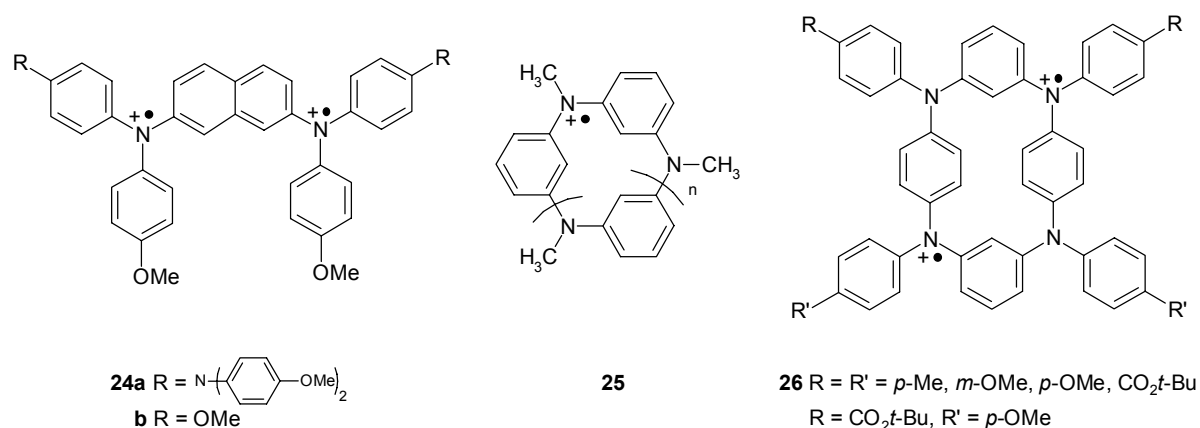
Figure 1.14. *Naphtalene and azacyclophanes as design element in high-spin molecules.*

Both Hartwig et al.[69] and Tanaka et al.[70] have prepared azacyclophanes as model compounds for the construction of high-spin molecules with multiple intramolecular exchange pathways. The *N*-methyl-azametacyclophanes (**25**, n=1-6) of Tanaka showed irreversible oxidation behavior due to the localized nature of the cation radicals. In contrast, the tetraazacyclophanes (**26**) of Hartwig and co-workers showed reversible oxidation behavior and triplet states according to ESR spectroscopy.

1.4 High-spin polymers

True high-spin polyradicals are the ultimate goal in the preparation of high-spin organic molecules. The polydisperse nature of polymers tends to frustrate the total control over the spin state and intelligent designs and/or doping procedures are necessary. Up to now the polyradicals reported are generally possessing lower spin states as compared to monodisperse high-spin oligomers, as a consequence of problems associated with the quantitative generation of radicals in a polymer. The pendant radical approach as mentioned in paragraph 1.3.1 is a promising strategy to overcome the problem of spin defects[71,72]. The field of π-conjugated polymers is a valuable source of π-conjugated backbones for pendant high-spin polymers. As a consequence a wide variety of regioregular substituted poly(phenylenevinylene) and poly(phenyleneethynylene) polyradicals have been synthesized and characterized. In these polyradicals, nitroxide, galvinoxyl, and phenoxyl radicals are most often used.
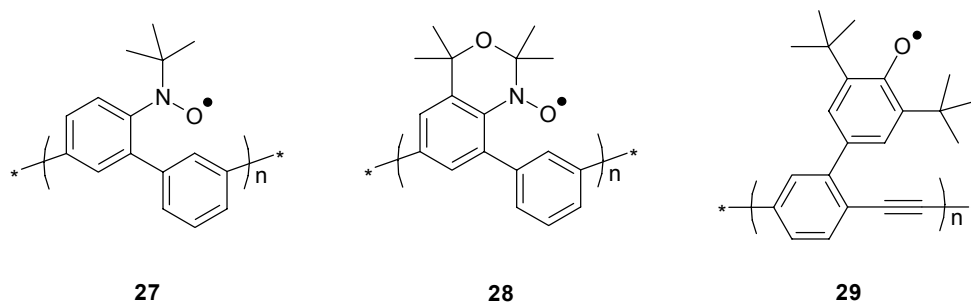
Figure 1.15. *Pendant high-spin polymers based on neutral radicals*

Miura et al.[73,74] have prepared two pendant poly(nitroxide radical)s with a poly(1,3-phenylene) backbone. Although polyradical **27** (n = 18) was stable and 80 % of the spins were generated, a low spin state was observed attributed to twisting of the nitroxide moieties and subsequent antiferromagnetic intramolecular coupling. To prevent the twisting of the nitroxide radical, polyradical **28** with cyclic nitroxides was prepared and an intramolecular ferromagnetic interaction was observed, but the multiplicity of the ground state was not reported.

The group of Nishide has been strongly involved in the preparation of pendant high-spin radicals. Phenoxy radicals were used in combination with a poly(1,4-phenyleneethynylene) backbone[75], **29**. However, only 60 % of the total number of possible radicals was generated. The extension from a linear backbone to a hyper-branched or star-shaped backbone made from phenylenevinylene units proved to be more successful in generating higher spin states[76]. Here magnetization studies revealed an average of 7 ferromagnetically coupled spins. As a logical follow-up of aminium

biradical **22**, an analogous poly(1,2-phenylenevinylene) (**30**, n=12) was prepared and oxidized to the poly(cation radical)[77]. On average a quintet state was established for **30**.

The most successful approach to obtain very high-spin polymers has been reported by Rajca et al.[78] Using the 'double cable' strategy (Figure 1.6, **B**), a polycalix[4]arene precursor was synthesized and after subsequent reduction and oxidation, the polyether precursor was transformed into the poly(triarylmethyl radical) **31**. For a polymer with an $M_n > 10^5$ Da, a $S_n > 40$ spin state was found at 1.8 K.

30

31 R =
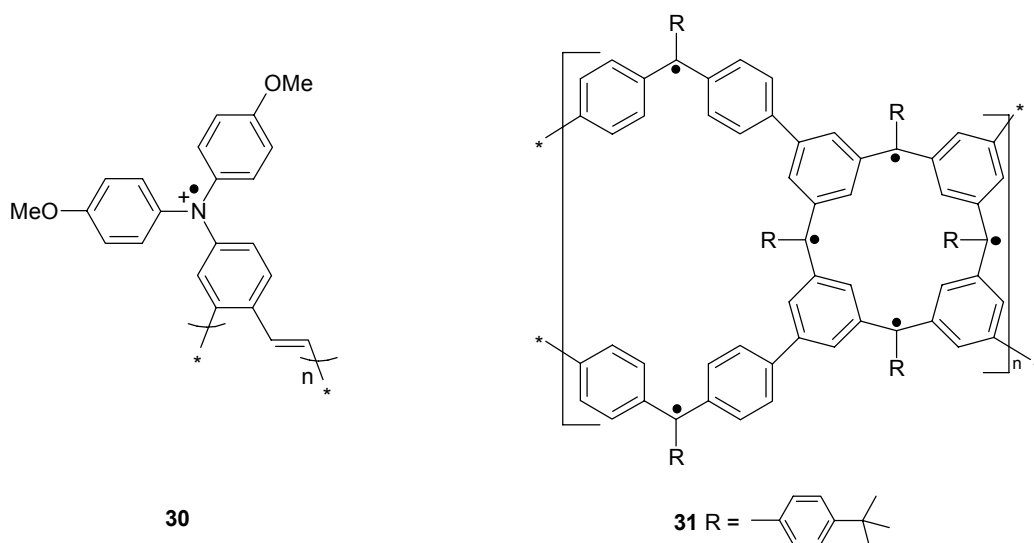
Figure 1.16. *High-spin polymer with pendant ionic radicals by Nishide et al. (left) and the high-spin polymer with the highest number of spins (S > 40) reported by Rajca et al. (right).*

1.5 Intermolecular spin alignment

Intermolecular spin coupling between the individual magnetic molecules is crucial for the development of future organic ferromagnetic materials. A number of models has been put forward to predict intermolecular spin-spin interactions. Basically, these models are a modification of the spin polarization mechanism used to describe intramolecular spin coupling. McConnell proposed a description for through-space interactions of unpaired electrons (McConnell Model I)[79]. The most important outcome of this model is that ferromagnetic interactions will occur between atoms carrying opposite spin density. Ab initio MO calculations for the stacking of two benzyl radicals in different orientations confirm this prediction[80](Figure 1.17). Here only the *ortho* and *para* orientations result in an intermolecular ferromagnetic coupling. A further extension of these calculations to other types of radicals suggests that exchange interactions can be strengthened if the spin polarization in the molecule is enhanced by

introducing more radicals in one molecule[81]. In other words, high-spin molecules may have stronger exchange interactions. Therefore Yamaguchi et al.[82] proposed the design and preparation of disk type liquid crystalline high-spin molecules, which might result in an one-dimensional high-spin stack.

geminal : S = 0   ortho : S = 1   meta : S = 0   para : S = 1
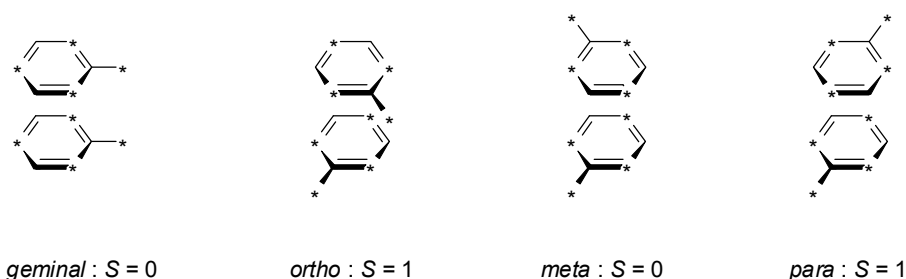
Figure 1.17. *Stacking of benzyl radicals with different orientations. Starred atoms have positive spin densities.*

The second model by McConnell[83] (McConnell model II) predicts that in charge transfer complexes consisting of alternating donor and acceptor molecules, a ferromagnetic alignment of the unpaired electrons can occur if either the neutral acceptor or donor molecule has a triplet ground state. Later on Kollmar and Kahn[84,85] suggested, in a more detailed theoretical study on the McConnell model II, that this model is too simple and cannot account for the ferromagnetic behavior found for the ferromagnetic decamethylferrocenium tetracyanoethenide CT-complex by Miller et al.[86]. Therefore, application of McConnell model II seems to be difficult. Nevertheless, several different modifications to this model have been proposed and investigated experimentally[87,88].

An interesting modification of McConnell model I by Buchachenko[89] suggests the co-crystallisation of monoradicals with bi- or triradicals in a regular alternating fashion. If the intermolecular spin coupling is anti-ferromagnetic between the monoradical and the oligoradical, it results in opposite spin orientations. All the monoradicals would have an opposite spin compared to the spin of the oligoradicals, yielding an organic ferrimagnet.

A promising strategy to achieve intermolecular spin coupling is the use of non-covalent bonds as effective exchange path ways, like e.g. dipole-dipole interactions, metal ion complexation, or hydrogen bonds. In the first purely organic molecular magnet dipole-dipole interactions between nitrophenyl nitronyl nitroxides are responsible for the intermolecular ferromagnetic interaction observed in single crystals. It is also possible to use metals as a ferromagnetic coupler between organic free radicals. Paramagnetic metal ions can make a positive contribution to the total spin state.

Hydrogen bonding between monoradicals in single crystals[90,91] has also a large potential to become a useful ferromagnetic coupler in high-spin molecules[92].

1.6 Organic/inorganic hybrids

The area of organic radical transition metal complexes has gained a considerable interest since the discovery of molecular magnets based on this principle[10]. Here, attention will be focused on metal-ligand complexes with more than one unpaired electron in the organic ligand. Nitronyl nitroxide biradicals are versatile radicals to construct metal/ligand complexes due to their ligating sites[93,94]. A large number of these nitroxide radicals have been synthesized, bearing additional groups for hydrogen bonding, charge transfer, or metal complexing purposes[95]. Especially pyridine derivatives have been very popular for the construction of metal-organic complexes. In a metal complex of a pyridine biradical species there are in principle three exchange interactions; one intramolecular interaction and two radical/metal interactions which can be opposite in sign.
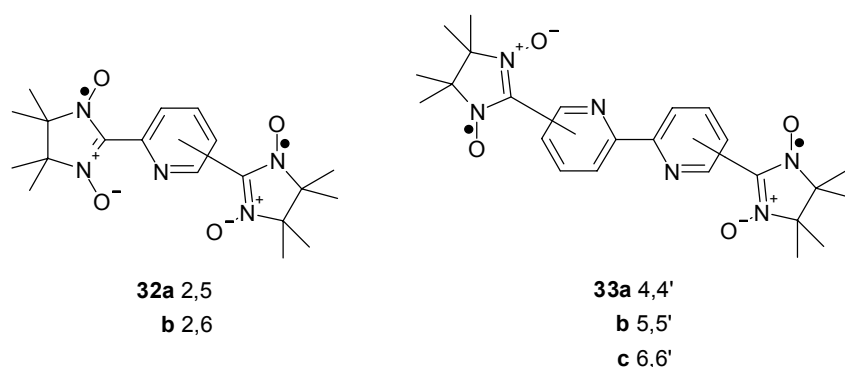
Figure 1.18. *Bis(nitronyl nitroxide) radicals connected by pyridine derivatives.*

Ziessel and co-workers have prepared a number of bis(nitronyl nitroxide) radicals containing chelating pyridine groups over the past six years[96-99]. In these type of compounds only the bis-substituted pyridines showed a through-bond intramolecular exchange interaction. As expected the 2,5-pyridine (**32a**) and the 2,6-pyridine (**32b**) showed an anti-ferromagnetic and a ferromagnetic coupling, respectively. The other molecules with pyridine derivatives had no through-bond interactions but an antiferromagnetic through-space interaction. Complexation of paramagnetic Ni(II), Cu(II), Co(II), or Mn(II) to the 6,6'-bis(nitronyl nitroxide)-2,2'-bipyridine **33c** revealed that only the Ni(II) perchlorate monohydrate cis-complex had a ferromagnetic

interactions through the metal for both radicals as well as a weak intermolecular ferromagnetic interaction.
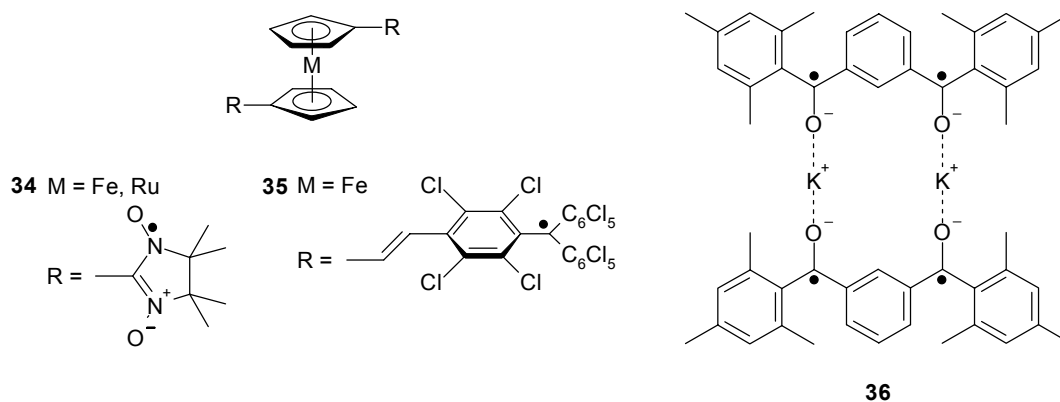
Figure 1.19. *Metal radical complexes of Veciana et al.(left) and Baumgarten et al.(right).*

Metallocenes have been investigated by Veciana et al.[100,101] as possible candidates for ferromagnetic coupling unit, using two different types radicals. Metallocenes can also act as a redox controlled spin coupler. In the case of the nitronyl nitroxide radicals (**34**) an antiferromagnetic through-space coupling dominated, which took place via a hydrogen bond between the two radicals. To overcome this problem, ferrocene molecule **35** substituted with two polychlorinated triarylmethyl radicals was prepared. ESR spectroscopy of the unoxidized biradical revealed a triplet state as well as a transition at half-field confirming the high-spin nature of this species.

An early example of organic radical/metal high-spin complexes was established by Hirota and Weismann[102-104]. A high-spin complex was reported consisting of two ketyl radical anions ferromagnetically bridged by two alkali metal ions. This observation inspired Baumgarten et al.[105] to construct a high-spin molecule, in which two bis(ketyl radical anion)s are bridged by lithium or potassium ions (**36**). In both cases a quintet state ($S = 2$) was observed when a bimolecular complex was formed by reduction to the tetraanion. Linear extension to a tetraketone was not successful, because spin pairing prevented the formation of higher spin states in one molecule.

37   **38**
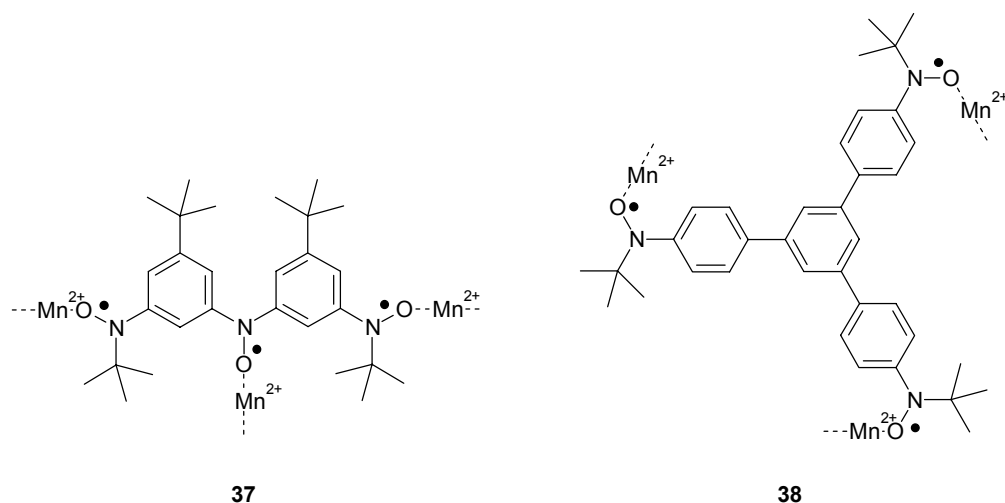
Figure 1.20. *Manganese tri(nitroxide) radical complexes of Iwamura et al.*

The group of Iwamura has reported some beautiful examples of organic high-spin molecules bridged by paramagnetic metal ions. The most successful example is complex **37** with a T_c of 46 K[106], which is the highest Curie temperature ever reported for a transition metal/organic radical complex. This was a logical step forward from complex **38**, which showed a T_c of 3.4 K[107]. The weak intramolecular ferromagnetic coupling in **38** was thought to be responsible for the weak intermolecular ferromagnetic coupling. Apparently, a high-spin molecule with strong intramolecular interactions, like **37**, exhibits stronger intermolecular ferromagnetic interactions.

39a M = Cu^{2+}
   b M = Mn^{2+}

40
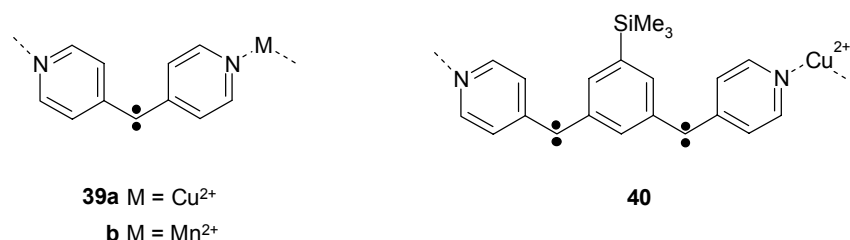
Figure 1.21. *One-dimensional oligo(carbene-metal) complexes.*

Other interesting examples by Iwamura and co-workers are the oligo{carbene radical-M(II)} complexes (Figure 1.21), which form one-dimensional ferromagnetic chains depending on the type of transition metal. Here the spin carriers are not used for metal chelating as in the previous examples. The 1:1 complexation of a diazodi(4-pyridyl)methane with Cu^{2+}(hexafluoroacetylacetonato = hfac)$_2$ (**39a**) or Mn^{2+}(hfac)$_2$ (**39b**) and subsequent photolysis of the diazo-moieties to the carbene biradical, resulted in a ferromagnetic and ferrimagnetic chain, respectively[108,109]. This methodology has been extended to a 1,3-benzene carrying two diazo(4-pyridyl)methane moieties, which after

irradiation of 1:1 complex **40** was converted to a one-dimensional ferromagnetic chain with antiferromagnetic interchain interactions[110].

1.7 H-bonds as exchange pathways

Hydrogen bonds represent non-covalent interactions which can serve as a ferromagnetic exchange pathway, since they are highly directional and relatively strong. No high-spin molecules have been reported up to now which have this type of non-covalent bond. However, the field of molecular magnets has some history in the use of hydrogen bonds for ferromagnetic interactions. A systematic survey of nitronyl nitroxide radicals bearing phenolic groups has been performed by Veciana et al.[90,111-114] Bulk ferromagnetism has been found for nitronyl nitroxide radical **41a**. Simultaneously Sugawara et al.[115,116] also found for 2,5-dihydroxybenzene nitronyl nitroxide **42a** bulk ferromagnetic properties below 0.5 K. Statistical analysis of a large number of nitronyl nitroxide monoradicals by Veciana et al.[117,118] revealed that there is no explicit relation between structure (crystal engineering) and magnetic properties.

41 n=1 **a** *ortho*
    b *meta*
    c *para*

42 n=2 **a** *ortho, meta*
    b *meta, meta*
    c *meta, para*

43a R = O
   b R = -
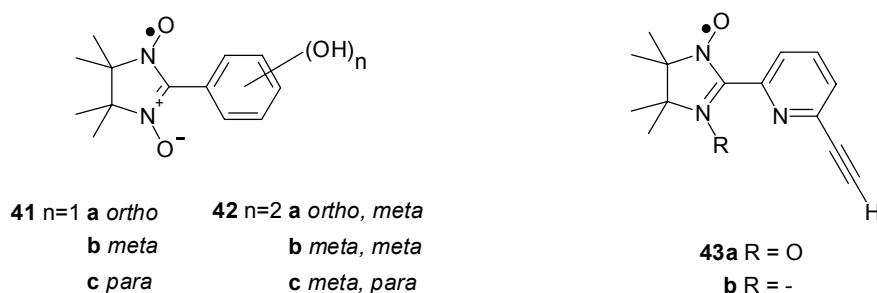
Figure 1.22. *Hydrogen bonding molecular magnets.*

The group of Ziessel prepared a number of nitroxide radicals with hydrogen bonding capabilities. Here acetylene substituted pyridine radicals were studied[119,120]. Imino nitroxide radical **43b** displays ferromagnetic properties in contrast to the nitronyl nitroxide **43a**. The crystal packing shows ferromagnetic chains in which the molecules are hydrogen bonded via the oxygen of the nitroxide and the acetylene-hydrogen. An interesting strategy for the preparation of layered magnetic materials has been designed and prepared by Papoutsakis et al.[121] The combination of ammidinium benzoate salt bridges and nitronyl nitroxides (**44**) gives rise to layered structures. Spin propagation via a spin polarization mechanism was observed for the secondary hydrogen bonds in the layer.
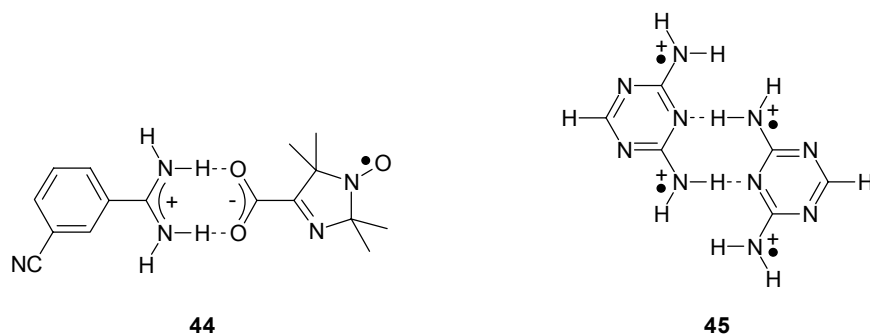
Figure 1.23. *Salt bridge with secondary hydrogen bonds by Papoutsakis et al. (left). Diaminotriazine di(cation radical) dimer of Zhang and Baumgarten (right).*

Zhang and Baumgarten [122,123] have studied the possibilities for spin propagation for hydrogen bonded dimers of high-spin molecules theoretically. Accordingly triplet diaminotriazine di(cation radical) **45** was predicted to exhibit an intermolecular ferromagnetic coupling through the H-bonds in the plane. However, through-space interactions of stacked hydrogen-bonded dimers are at least as strong as the interactions via the H-bonds in the plane and have a considerable contribution to the total high-spin ground state of the system.

1.8 Aim and scope of this thesis

Purely organic ferromagnets exhibiting magnetic properties at ambient temperatures do not exist yet. Several strategies exist to engage in this challenge, each with its own advantages and disadvantages. The advantage of using high-spin molecules to achieve this goal, is the prospect that if intermolecular interactions can be realized, higher Curie temperatures can be expected as compared to monoradicals. The examples in this introduction show that realization of non-covalent bonds between and ordering of high-spin molecules is still at an early stage. Especially, liquid crystalline high-spin molecules have not been reported and may form a new field in the area organic ferromagnetism. The aim of this thesis is twofold. First, owing to the recent progress in C-N bond formation synthetic methodologies, it is of interest to improve and extend the synthesis of high-spin molecules based on 1,4-benzenediamine moieties. These molecules have a fair chemical stability under ambient conditions and may be used for the construction of higher assemblies. The second goal is the realization of ordered high-spin molecules via liquid crystalline behavior.

In chapter 2 a short introduction into ESR-spectroscopy of high-spin molecules is given. This chapter has the purpose to provide insight into the ESR spectra and their interpretation as presented in the adjoining chapters. Topics that are dealt with are

some of the basic principles of ESR spectroscopy as well as solution spectra and frozen solution spectra of high-spin molecules and their temperature dependence.

In chapter 3 contemporary palladium/phosphine ligand catalyzed arylamine synthesis is used to synthesize a number of aniline oligomers with different topologies. These oligomers have been constructed from 1,4-benzenediamine moieties coupled to 1,3-benzene or 1,3,5-benzene ferromagnetic coupling units. The largest molecules prepared consist of eight aniline units with either methyl or phenyl substituents in alternating *meta-para* fashion. These oligomers have been characterized by means of cyclic voltammetry in chapter 4. Chemical oxidation of the oligomers to the corresponding oligo(cation radicals) has been monitored by UV/visible/nearIR spectroscopy and ESR spectroscopy. The observed properties are consistent with low energy high-spin states and show that the concept of a polaronic ferromagnet is viable for extension to longer systems. However, for the longest systems ESR spectroscopy is unable to unambiguously identify the multiplicity of the oligo(cation radicals).

In chapter 5 a first attempt towards discotic liquid crystalline high-spin molecules is described. Carbazoles allow facile substitution at the 3- and 6-position with e.g. mesogenic groups. Therefore, mixed carbazole aniline oligomers were prepared and characterized. The introduction of the carbazole, however, caused a decreased stability of the oligo(cation radicals) at ambient temperatures. Next, a star-shaped aniline oligomer with mesogenic groups at the periphery was synthesized and oxidized to the tri(cation radical). Although a low lying high-spin state could be confirmed, lyotropic or thermotropic liquid crystalline properties were not observed. In chapter 6 stable neutral verdazyl radicals are investigated instead of nitrogen-centered cation radicals. Here oxo-verdazyl radicals with dodecyl groups are used to construct a discotic liquid crystalline high-spin molecule. In addition to a 1,3,5-substituted benzene also a 2,6,10-substitued triphenylene core has been used to increase the rigidity of the core. Although, both triradicals exhibited a transition at half field with ESR-spectroscopy characteristic of ferromagnetic coupling of unpaired electrons, no unambiguous evidence could be found for a high-spin state or for liquid crystalline behavior.

In the last chapter two types of molecules are presented in which a ferromagnetic intramolecular coupling might occur via σ-bonds. Stable oxidation to the corresponding oligo(cation radical) could be accomplished electrochemically and chemically both for hexahydrotriazine as well as spiro molecules. However, these molecules showed no evidence for a ferromagnetic intramolecular interaction via σ-bonds and only low-spin states were observed with ESR-spectroscopy.

1.9 References

1.   Iwamura, H., *J. Phys. Org. Chem.* **1998**, *11*, 299.

2.   Holden, A. N.; Matthias, B. T.; Anderson, P. W.; Lewis, H. W., *Phys. Rev.* **1956**, *102*, 1463.

3.   Bozorth, R. M.; Williams, H. J.; Walsh, D. E., *Phys. Rev.* **1956**, *103*, 572.

4.   Kahn, O., *Nature* **1995**, *378*, 667.

5.   Ferlay, S.; Mallah, T.; Ouahes, R.; Veillet, P.; Verdaguer, M., *Nature* **1995**, *378*, 701.

6.   Miller, J. S.; Calabrese, J. C.; Epstein, A. J.; Bigelow, R. W.; Zhang, J. H.; Reiff, W. M., *J. Chem. Soc., Chem. Commun.* **1986**, 1026.

7.   Manriquez, J. M.; Yee, G. T.; McLean, R. S.; Epstein, A. J.; Miller, J. S., *Science* **1991**, *252*, 1415.

8.   Caneschi, A.; Gatteschi, D.; Laugier, J.; Rey, P., *J. Am. Chem. Soc.* **1987**, *109*, 2191.

9.   Caneschi, A.; Gatteschi, D.; Laugier, J.; Rey, P.; Sessoli, R.; Zanchini, C., *J. Am. Chem. Soc.* **1988**, *110*, 2795.

10.   Caneschi, A.; Gatteschi, D.; Sessoli, R., *Acc. Chem. Res.* **1989**, *22*, 392.

11.   Pei, Y.; Verdaguer, M.; Kahn, O., *J. Am. Chem. Soc.* **1986**, *108*, 7428.

12.   Stumpf, H. O.; Ouahab, L.; Pei, Y.; Grandjean, D.; Kahn, O., *Science* **1993**, *261*, 447.

13.   Awaga, K.; Inabe, T.; Nagashima, U.; Maruyama, Y., *J. Chem. Soc., Chem. Commun.* **1989**, 1617.

14.   Awaga, K.; Maruyama, *Chem. Phys. Lett.* **1989**, *158*, 556.

15.   Tamura, M.; Nakazawa, Y.; Shiomi, D.; Nozawa, K.; Hosokoshi, Y.; Ishikawa, M.; Takahashi, M.; Kinoshita, M., *Chem. Phys. Lett.* **1991**, *186*, 401.

16.   Takahashi, M.; Turek, P.; Nakazawa, Y.; Tamura, M.; Nozawa, K.; Shiomi, D.; Ishikawa, M.; Kinoshita, M., *Phys. Rev. Lett.* **1991**, *67*, 746.

17.   Kinoshita, M.; Turek, P.; Tamura, M.; Nozawa, K.; Shiomi, D.; Nakazawa, Y.; Ishikawa, M.; Takahashi, M.; Awaga, K.; Inabe, T.; Maruyama, Y., *Chem. Lett.* **1991**, 1225.

18.   Togashi, K.; Imachi, R.; Tomioka, K.; Tsuboi, H.; Ishida, T.; Nogami, T.; Takeda, N.; Ishikawa, M., *Bull. Chem. Soc. Jpn.* **1996**, *69*, 2821.

19.   Banister, A. J.; Bricklebank, N.; Clegg, W.; Elsegood, M. R. J.; Gregory, C. I.; Lavender, I.; Rawson, J. M.; Tanner, B. K., *J. Chem. Soc., Chem. Commun.* **1995**, *680*, 679.

20.   Banister, A. J.; Bricklebank, N.; Lavender, I.; Rawson, J. M.; Gregory, C. I.; Tanner, B. K.; Clegg, W.; Elsegood, M. R. J.; Palacio, F., *Angew. Chem., Int. Ed. Engl.* **1996**, *35*, 2533.

21.   Allemand, P. M.; Khemani, K. C.; Koch, A.; Wudl, F.; Holczer, K.; Donovan, S.; Gruner, G.; Thompson, J. D., *Science* **1991**, *253*, 301.

22.   Mrzel, A.; Omerzu, A.; Umek, P.; Mihailovic, D.; Jaglicic, Z.; Trontelj, Z., *Chem. Phys. Lett.* **1998**, *298*, 329.

23.   Narymbetov, B.; Omerzu, A.; Kabanov, V. V.; Tokumoto, M.; Kobayashi, H.; Mihailovic, D., *Nature* **2000**, *407*, 883.

24.   Chiarelli, R.; Rassat, A.; Rey, P., *J. Chem. Soc., Chem. Commun.* **1992**, 1081.

25.   Chiarelli, R.; Novak, M. A.; Rassat, A.; Tholence, J. L., *Nature* **1993**, *363*, 147.

26.   Kollmar, C.; Kahn, O., *Acc. Chem. Res.* **1993**, *26*, 259.

27.   Longuet-Higgins, H. C., *J. Chem. Phys.* **1950**, *18*, 265.

28.   Ovchinnikov, A. A., *Theoretica Chimica Acta* **1978**, *47*, 297.

29.   Borden, W. T.; Davidson, E. R., *J. Am. Chem. Soc.* **1977**, *99*, 4587.

30.   Iwamura, H., *Pure App. Chem.* **1993**, *65*, 57.

31.   Fukutome, H.; Takahashi, I.; Ozaki, M., *Chem. Phys. Lett.* **1987**, *133*, 34.

32.   Gatteschi, D.; Kahn, O.; Miller, J. S.; Palacio, F. (Eds.), *Magnetic Molecular Materials,* Kluwer Academic Publishers, Dordrecht **1991**.

33.   Kahn, O. (Ed.), *Magnetism: A Supramolecular Function,* Kluwer Academic Publishers, Dordrecht **1996**.

34.   K. Itoh, J. S. Miller ,T. Takui (Eds.), *Proc. Conf. on Molecule Based Magnets, Mol. Cryst. Liq. Cryst.* **1997**, *306.*

35.   Lahti, P. M. (Ed.), *Magnetic Properties of Organic Materials,* Marcel Dekker, Inc., New York **1999**.

36.   O. Kahn (Ed.), *Proc. Conf. on Molecule Based Magnets, Mol. Cryst. Liq. Cryst.* **1999**, *334.*

37.   Miller, J. S.; Epstein, A. J., *Angew. Chem., Int. Ed. Engl.* **1994**, *33*, 385.

38.   Rajca, A., *Chem. Rev.* **1994**, *94*, 871.

39.   Itoh, K., *Chem. Phys. Lett.* **1967**, *1*, 235.

40.   Wasserman, E.; Murray, R. W.; Yager, W. A.; Trozzolo, A. M.; Smolinsky, G. J., *J. Am. Chem. Soc.* **1967**, *89*, 5076.

41.   Nakamura, N.; Inoue, K.; Iwamura, H.; Fujioka, T.; Sawaki, Y., *J. Am. Chem. Soc.* **1992**, *114*, 1484.

42.   Nakamura, N.; Inoue, K.; Iwamura, H., *Angew. Chem., Int. Ed. Engl.* **1993**, *32*, 872.

43.   Matsuda, K.; Nakamura, N.; Inoue, K.; Koga, N.; Iwamura, H., *Bull. Chem. Soc. Jpn.* **1996**, *69*, 1483.

44.   Matsuda, K.; Nakamura, N.; Inoue, K.; Koga, N.; Iwamura, H., *Chem. Eur. J.* **1996**, *2*, 259.

45.   Tomioka, H.; Watanabe, T.; Hirai, K.; Furukawa, K.; Takui, T.; Itoh, K., *J. Am. Chem. Soc.* **1995**, *117*, 6376.

46.   Tomioka, H.; Hattori, M.; Hirai, K.; Sato, K.; Shiomi, D.; Takui, T.; Itoh, K., *J. Am. Chem. Soc.* **1998**, *120*, 1106.

47.   Tomioka, H.; Hattori, M.; Hirai, K.; Murata, S., *J. Am. Chem. Soc.* **1996**, *118*, 8723.

48.   Schlenk, W.; Brauns, M., *Ber. Dtsch. Chem. Ges.* **1915**, *48*, 661.

49.   Leo, M., *Ber. Dtsch. Chem. Ges.* **1937**, *70*, 1691.

50.   Ballester, M., *Acc. Chem. Res.* **1985**, *18*, 380.

51.   Veciana, J.; Rovira, C.; Ventosa, N.; Crespo, M. I.; Palacio, F., *J. Am. Chem. Soc.* **1993**, *115*, 57.

52.   Ruizmolina, D.; Veciana, J.; Palacio, F.; Rovira, C., *J. Org. Chem.* **1997**, *62*, 9009.

53.   Rajca, A.; Lu, K.; Rajca, S., *J. Am. Chem. Soc.* **1997**, *119*, 10335.

54.   Rajca, A.; Wongsriratanakul, J.; Rajca, S.; Cerny, R., *Angew. Chem., Int. Ed.* **1998**, *37*, 1229.

55.   Ishida, T.; Iwamura, H., *J. Am. Chem. Soc.* **1991**, *113*, 4238.

56.   Kanno, F.; Inoue, K.; Koga, N.; Iwamura, H., *J. Phys. Chem.* **1993**, *97*, 13267.

57. Kanno, F.; Inoue, K.; Koga, N.; Iwamura, H., *J. Am. Chem. Soc.* **1993**, *115*, 847.

58. Fujita, J.; Tanaka, M.; Suemune, H.; Koga, N.; Matsuda, K.; Iwamura, H., *J. Am. Chem. Soc.* **1996**, *118*, 9347.

59. Tanaka, M.; Matsuda, K.; Itoh, T.; Iwamura, H., *J. Am. Chem. Soc.* **1998**, *120*, 7168.

60. Izuoka, A.; Hiraishi, M.; Abe, T.; Sugawara, T.; Sato, K.; Takui, T., *J. Am. Chem. Soc.* **2000**, *122*, 3234.

61. Wienk, M. M.; Janssen, R. A. J., *J. Am. Chem. Soc.* **1997**, *119*, 4492.

62. Wienk, M. M.; Janssen, R. A. J., *Chem. Commun.* **1996**, 267.

63. Wienk, M. M.; Janssen, R. A. J., *J. Am. Chem. Soc.* **1996**, *118*, 10626.

64. Stickley, K. R.; Selby, T. D.; Blackstock, S. C., *J. Org. Chem.* **1997**, *62*, 448.

65. Michinobu, T.; Takahashi, M.; Tsuchida, E.; Nishide, H., *Chem. Mater.* **1999**, *11*, .

66. Vanmeurs, P. J.; Janssen, R. A. J., *J. Org. Chem.* **2000**, *65*, 5712.

67. Biewer, M. C.; Biehn, C. R.; Platz, M. S.; Despres, A.; Migirdicyan, E., *J. Am. Chem. Soc.* **1991**, *113*, 616.

68. Stickley, K. R.; Blackstock, S. C., *J. Am. Chem. Soc.* **1994**, *116*, 11575.

69. Hauck, S. I.; Lakshmi, K. V.; Hartwig, J. F., *Org. Lett.* **1999**, *1*, 2057.

70. Ito, A.; Ono, Y.; Tanaka, K., *J. Org. Chem.* **1999**, *64*, 8236.

71. Abdelkader, M.; Drenth, W.; Meijer, E. W., *Chem. Mater.* **1991**, *3*, 598.

72. Vlietstra, E. J.; Nolte, R. J. M.; Zwikker, J. W.; Drenth, W.; Meijer, E. W., *Macromolecules* **1990**, *23*, 946.

73. Oka, H.; Tamura, T.; Miura, Y.; Teki, Y., *J. Mater. Chem.* **1999**, *9*, 1227.

74. Oka, H.; Tamura, T.; Miura, Y.; Teki, Y., *Polym. J.* **1999**, *31*, 979.

75. Nishide, H.; Maeda, T.; Oyaizu, K.; Tsuchida, E., *J. Org. Chem.* **1999**, *64*, 7129.

76. Nishide, H.; Miyasaka, M.; Tsuchida, E., *Angew. Chem., Int. Ed.* **1998**, *37*, 2400.

77. Takahashi, M.; Nakazawa, T.; Tsuchida, E.; Nishide, H., *Macromolecules* **1999**, *32*, 6383.

78. Rajca, A.; Rajca, S.; Wongsriratanakul, J., *J. Am. Chem. Soc.* **1999**, *121*, 6308.

79. McConnell, H. M., *J. Chem. Phys.* **1963**, *39*, 1910.

80. Yamaguchi, K.; Fueno, T.; Nakasuji, K.; Murata, I., *Chem. Lett.* **1986**, 629.

81. Yamaguchi, K.; Fukui, H.; Fueno, T., *Chem. Lett.* **1986**, 625.

82. Yamaguchi, K.; Toyoda, Y.; Nakano, M.; Fueno, T., *Synth. Met.* **1987**, *19*, 87.

83. McConnell, H. M., *Proc. R.A. Welch Found. Chem. Res.* **1967**, *11*, 144.

84. Kollmar, C.; Kahn, O., *J. Am. Chem. Soc.* **1991**, *113*, 7987.

85. Kollmar, C.; Couty, M.; Kahn, O., *J. Am. Chem. Soc.* **1991**, *113*, 7994.

86. Miller, J. S.; Calabrese, J. C.; Epstein, A. J.; Bigelow, R. W.; Zhang, J. H.; Reiff, W. M., *J. Chem. Soc., Chem. Commun.* **1986**, 1026.

87. Breslow, R., *Pure App. Chem.* **1982**, *54*, 927.

88. Lepage, T. J.; Breslow, R., *J. Am. Chem. Soc.* **1987**, *109*, 6412.

89. Buchachenko, A. L., *Proc. Acad. Sci. USSR* **1979**, 107.

90. Hernandez, E.; Mas, M.; Molins, E.; Rovira, C.; Veciana, J., *Angew. Chem., Int. Ed. Engl.* **1993**, *32*, 882.

91. Okuno, T.; Otsuka, T.; Awaga, K., *J. Chem. Soc., Chem. Commun.* **1995**, *828*, 827.

92. Zhang, J. P.; Baumgarten, M., *Chem. Phys.* **1997**, *222*, 1.

93. Caneschi, A.; Dei, A.; Gatteschi, D., *J. Chem. Soc., Chem. Commun.* **1992**, *631*, 630.

94. Caneschi, A.; Chiesi, P.; David, L.; Ferraro, F.; Gatteschi, D.; Sessoli, R., *Inorg. Chem.* **1993**, *32*, 1445.

95. Nakatsuji, S.; Anzai, H., *J. Mater. Chem.* **1997**, *7*, 2161.

96. Luneau, D.; Romero, F. M.; Ziessel, R., *Inorg. Chem.* **1998**, *37*, 5078.

97. Romero, F. M.; Luneau, D.; Ziessel, R., *Chem. Commun.* **1998**, *552*, 551.

98. Luneau, D.; Laugier, J.; Rey, P.; Ulrich, G.; Ziessel, R.; Legoll, P.; Drillon, M., *J. Chem. Soc., Chem. Commun.* **1994**, *742*, 741.

99. Ziessel, R.; Ulrich, G.; Lawson, R. C.; Echegoyen, L., *J. Mater. Chem.* **1999**, *9*, 1435.

100. Elsner, O.; Ruizmolina, D.; Vidalgancedo, J.; Rovira, C.; Veciana, J., *Chem. Commun.* **1999**, *580*, 579.

101. Jurgens, O.; Vidalgancedo, J.; Rovira, C.; Wurst, K.; Sporer, C.; Bildstein, B.; Schottenberger, H.; Jaitner, P.; Veciana, J., *Inorg. Chem.* **1998**, *37*, 4547.

102. Hirota, N.; Weissman, S. I., *J. Am. Chem. Soc.* **1964**, *86*, 2538.

103. Brown, I. M.; Weissman, S. I.; Snyder, L. C., *J. Chem. Phys.* **1965**, *42*, 1105.

104. Hirota, N., *J. Am. Chem. Soc.* **1967**, *89*, 32.

105. Baumgarten, M.; Gherghel, L.; Wehrmeister, T., *Chem. Phys. Lett.* **1997**, *267*, 175.

106. Inoue, K.; Hayamizu, T.; Iwamura, H.; Hashizume, D.; Ohashi, Y., *J. Am. Chem. Soc.* **1996**, *118*, 1803.

107. Inoue, K.; Iwamura, H., *J. Am. Chem. Soc.* **1994**, *116*, 3173.

108. Sano, Y.; Tanaka, M.; Koga, N.; Matsuda, K.; Iwamura, H.; Rabu, P.; Drillon, M., *J. Am. Chem. Soc.* **1997**, *119*, 8246.

109. Karasawa, S.; Sano, Y.; Akita, T.; Koga, N.; Itoh, T.; Iwamura, H.; Rabu, P.; Drillon, M., *J. Am. Chem. Soc.* **1998**, *120*, 10080.

110. Karasawa, S.; Tanaka, M.; Koga, N.; Iwamura, H., *Chem. Commun.* **1997**, 1359.

111. Cirujeda, J.; Ochando, L. E.; Amigo, J. M.; Rovira, C.; Rius, J.; Veciana, J., *Angew. Chem., Int. Ed. Engl.* **1995**, *34*, 55.

112. Cirujeda, J.; Hernandezgasio, E.; Rovira, C.; Stanger, J. L.; Turek, P.; Veciana, J., *J. Mater. Chem.* **1995**, *5*, 243.

113. Cirujeda, J.; Mas, M.; Molins, E.; Depanthou, F. L.; Laugier, J.; Park, J. G.; Paulsen, C.; Rey, P.; Rovira, C.; Veciana, J., *J. Chem. Soc., Chem. Commun.* **1995**, *710*, 709.

114. Veciana, J.; Cirujeda, J.; Rovira, C.; Vidalgancedo, J., *Adv. Mater.* **1995**, *7*, 221.

115. Sugawara, T.; Matsushita, M. M.; Izuoka, A.; Wada, N.; Takeda, N.; Ishikawa, M., *J. Chem. Soc., Chem. Commun.* **1994**, 1723.

116. Matsushita, M. M.; Izuoka, A.; Sugawara, T.; Kobayashi, T.; Wada, N.; Takeda, N.; Ishikawa, M., *J. Am. Chem. Soc.* **1997**, *119*, 4369.

117. Deumal, M.; Cirujeda, J.; Veciana, J.; Novoa, J. J., *Adv. Mater.* **1998**, *10*, 1461.

118. Deumal, M.; Cirujeda, J.; Veciana, J.; Novoa, J. J., *Chem. Eur. J.* **1999**, *5*, 1631.

119. Romero, F. M.; Ziessel, R.; Bonnet, M.; Pontillon, Y.; Ressouche, E.; Schweizer, J.; Delley, B.; Grand, A.; Paulsen, C., *J. Am. Chem. Soc.* **2000**, *122*, 1298.

120. Romero, F. M.; Ziessel, R.; Drillon, M.; Tholence, J. L.; Paulsen, C.; Kyritsakas, N.; Fisher, J., *Adv. Mater.* **1996**, *8*, .

121.   Papoutsakis, D.; Kirby, J. P.; Jackson, J. E.; Nocera, D. G., *Chem. Eur. J.* **1999**, *5*, 1474.

122.   Zhang, J. P.; Wang, R. S.; Baumgarten, M., *Mol. Cryst. Liq. Cryst. Sci. Technol., Sect. A* **1997**, *306*, 119.

123.   Zhang, J. P.; Baumgarten, M., *Chem. Phys.* **1997**, *214*, 291.

2

ESR of high-spin molecules

Abstract: *An introductory overview of the theory of electron spin resonance spectroscopy on high-spin organic molecules is presented.*

2.1 Introduction to ESR spectroscopy

This chapter provides a short introduction to electron spin resonance (ESR) spectroscopy with an emphasis on the subjects required to interpret and analyze the ESR spectra of organic radicals and high-spin molecules. A more extensive and complete introduction into ESR spectroscopy can be found in several excellent textbooks [1-4].

2.1.1 The free electron

The free electron possesses spin angular momentum **S**. For an electron $S = ½$. The eigenvalues for the projection of the spin angular momentum on to some specified direction are labeled with M_S, running in integral steps from $+S$ to $-S$. Hence, for the electron the values of M_S are $+½$ and $-½$. These spin states are commonly referred to as α and β, or parallel and antiparallel, respectively. The physical manifestation of electron spin is that the electron has a magnetic moment $\mathbf{\mu}_e$. The magnetic moment is proportional to the angular momentum:

$$\mathbf{\mu}_e = -g_e \mu_B \mathbf{S} \tag{1}$$

In (1) μ_B is the Bohr magneton defined as $\mu_B = eh/4\pi m_e$, where e and m_e are the electron charge and mass, respectively and h is Planck's constant. The factor g_e is called the free-electron g-factor and its value is 2.00232.

The classical energy of a magnetic moment $\mathbf{\mu}$ in a field $\mathbf{B}$ is given by the scalar product:

$$E = -\mathbf{\mu} \cdot \mathbf{B} \tag{2}$$

The Hamiltonian for a free electron in a magnetic field (Zeeman term) is obtained by combining (2) with the operator defined in (1):

$$H = H_{Ze} = g_e \mu_B \mathbf{S} \cdot \mathbf{B} \tag{3}$$

When the field is chosen along the z-direction ($\mathbf{B} = (0, 0, B_0)$), the scalar product simplifies to:

$$H = g_e \mu_B B_0 S_z \tag{4}$$

The spin states $\left| S, M_S \right\rangle$ of the free electron are eigenfunctions of the S_z-operator, with eigenvalues M_S. As a result, the eigenfunctions of Hamiltonian (4) correspond to the two spin states of the electron with energies:

$$E = \left\langle S, M_S \left| H \right| S, M_S \right\rangle = g_e \mu_B B_0 M_S \tag{5}$$

This is illustrated in Figure 2.1. In the absence of a magnetic field the spin states are degenerate. Application of a magnetic field B_0 removes this degeneracy. The antiparallel spin state ($M_S = -\frac{1}{2}$) has a lower energy than the parallel ($M_S = \frac{1}{2}$) spin state. The energy difference is proportional to the strength of the magnetic field. The ESR experiment involves transitions between the spin states in a magnetic field by applying radiation with a frequency ν that satisfies the resonance condition for a free electron:

$$\Delta E = h\nu = g_e \mu_B B_0 \tag{6}$$

Continuous wave ESR spectrometers generally work at constant frequency and variable magnetic field. One of the commonly used frequency ranges for ESR spectrometers is the X-band (9-10 GHz). By substituting the physical constants in (6) and taking the frequency $\nu = 9.5$ GHz the resulting magnetic field at resonance is 3390 Gauss (0.3390 T). The detection of the ESR signal involves a small modulation of the applied magnetic field at a frequency of 100 kHz combined with lock-in amplification. As a consequence, ESR spectra are obtained as the first derivative of an absorption signal with respect to the magnetic field.
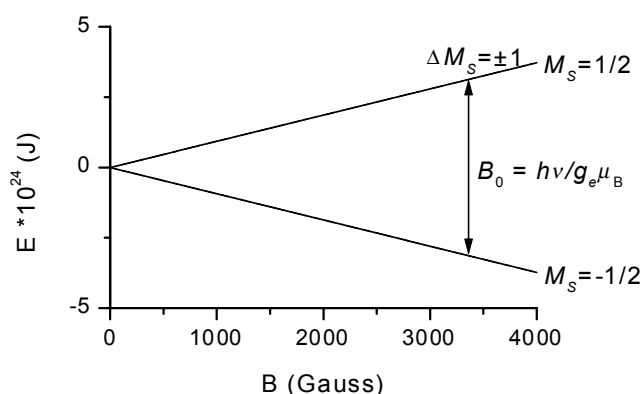

Figure 2.1. *State energies and $\Delta M_S = \pm 1$ transition for a doublet system ($S = \frac{1}{2}$) according to (6), $B_0 = 3390$ G, $\nu = 9.5$ GHz, $g_e = 2.00232$.*

2.1.2 Nuclear hyperfine interactions

Nuclei with an odd number of protons and nuclei with an odd number of neutrons possess the property of nuclear spin angular momentum I. Examples are hydrogen ¹H with $I = \frac{1}{2}$ and nitrogen ¹⁴N with $I = 1$. The interaction of an unpaired electron with magnetic nuclei gives rise to nuclear hyperfine interactions. These hyperfine interactions originate from two processes, the isotropic or Fermi contact interaction and anisotropic or dipolar interaction. The latter corresponds to the classical dipole-dipole interaction between the magnetic dipoles of the electron and the nucleus. The anisotropic coupling vanishes to zero in motionally averaged systems (solutions) and can only be determined for radicals in a rigid matrix (crystals, powders, frozen solutions). The Fermi contact interaction results from the unpaired electron density at the nucleus. Because only s-orbitals have a non-zero value at the nucleus, unpaired electrons in p-, d- and f-orbitals do not contribute directly to the isotropic hyperfine coupling. The Fermi contact interaction is isotropic and is readily observed in solution ESR. The spin Hamiltonian which only considers the spin-dependent contributions and the complete electronic terms, for the unpaired electron of an organic radical in a magnetic field experiencing isotropic hyperfine interaction is given by: [5]

$$H = H_{Ze} + H_{hf} = g_e \mu_B B_0 S_z + \sum_n A_n \mathbf{S} \cdot \mathbf{I}_n \tag{7}$$

The sum runs over all magnetic nuclei n present in the radical and A_n is the hyperfine coupling constant for nucleus n. When the coupling constants are small relative to the microwave frequency this relation can be simplified to:

$$H = g_e \mu_B B_0 S_z + \sum_n A_n S_z I_{z,n} \tag{8}$$

The energies of the various spin states are then given by:

$$E\left(M_S, \{M_{i,n}\}\right) = g_e \mu_B B_0 M_S + \sum_n A_n M_S M_{i,n} \tag{9}$$

The allowed transitions must meet the ESR selection rules $\Delta M_S = \pm 1$ and $\Delta M_{i,n} = 0$. If n equivalent nuclei are present in a system, the maximum number of transitions becomes $((2nI+1)*(2S+1))/2$, e.g. two ¹⁴N nuclei with one unpaired electron results in 5 lines. The intensities of the transitions in ESR depend on the degeneracy of the energy levels, for nuclei with $I = \frac{1}{2}$ the binomial triangle of Pascal can be used.

2.1.3 Molecules with S > ½

When two electrons occupy different molecular orbitals, it is possible to construct four electronic configurations, which can be divided into a singlet state ($S = 0$, $M_S = 0$, $2S + 1 = 1$) and a triplet state ($S = 1$, $M_S = \pm 1$ or $M_S = 0$, $2S + 1 = 3$). At zero magnetic field, the degeneracy of the three triplet spin sublevels is generally lifted. This is called zero-field splitting and originates from the classical magnetic dipole-dipole interaction of the magnetic moments associated with the two electrons. The dipole-dipole interaction for the coupling of two unpaired electrons can be described with a spin Hamiltonian:

$$H = H_d = \mathbf{S} \cdot \mathbf{D} \cdot \mathbf{S} \tag{10}$$

The spin-spin coupling tensor $\mathbf{D}$ is traceless and symmetric. In the principal axis system of $\mathbf{D}$ the Hamiltonian becomes:

$$H = -XS_x^2 - YS_y^2 - ZS_z^2 \tag{11}$$

In this equation the X, Y and Z values are the eigenvalues of $\mathbf{D}$ in the directions x, y, and z, respectively. Because $\mathbf{D}$ is a traceless tensor ($X + Y + Z = 0$), only two independent parameters exist, commonly known as the zero-field splitting parameters D and E. Introduction of $D = -(3/2)Z$ and $E = -(1/2)(X - Y)$ and adding the term for the interaction of the electron spin with the magnetic field leads to expression of the spin Hamiltonian of a molecule with $S > ½$:

$$H = H_{Ze} + H_d = g_e \mu_B \mathbf{S} \cdot \mathbf{B} + D\left(S_z^2 - \frac{1}{3}S^2\right) + E(S_x^2 - S_y^2) \tag{12}$$

In (12) the hyperfine term H_{hf} is neglected because it is usually less then H_d (H_{Ze} $\gg H_d > H_{hf}$). For axially symmetric molecules X and Y are the same and hence $E = 0$. Using (12) it is possible to calculate the energies of the triplet spin sublevels $M_S = \pm 1$ and $M_S = 0$ as a function of the orientation and strength of the magnetic field. If $\mathbf{B}$ is chosen parallel to the z-axis ($\mathbf{B} = B_z$):

$$E_{\pm 1} = \frac{1}{3}D \pm g_e \mu_B B_z \qquad \text{and} \qquad E_0 = -\frac{2}{3}D \tag{13}$$

While for $\mathbf{B}$ parallel to the x-axis ($\mathbf{B} = B_x$):

$$E_{\pm 1} = -\frac{1}{6}D \pm \frac{1}{2}\sqrt{D^2 + 4g_e^2 \mu_B^2 B_x^2} \quad \text{and} \qquad E_0 = \frac{1}{3}D \tag{14}$$

The energies of the triplet sublevels are plotted as a function of the magnetic field B in Figure 2.2. In this plot the values for the different variables (D, g_e) were taken from the experimental results reported in Chapter 4, zero-field splitting constants are given in frequency units (MHz)[6]. Two $\Delta M_S = \pm 1$ transitions are possible for each direction of the magnetic field and two consequently two ESR lines are expected for a triplet state molecule in a magnetic field. The splitting between the two ESR transitions depends on D and on the orientation of the molecule with respect to the magnetic field. The splitting will be large ($2D$) when B is parallel to z and small (D) when B is parallel to x. For a randomly oriented ensemble of molecules the ESR spectrum will represent a sum spectrum over all possible orientations of the molecules with respect to the magnetic field. Because the ESR spectrum is usually recorded as the first derivative of the absorption, the ESR spectrum of a triplet state ($S = 1$) molecule in a frozen solution exhibits four transitions (Figure 2.3).

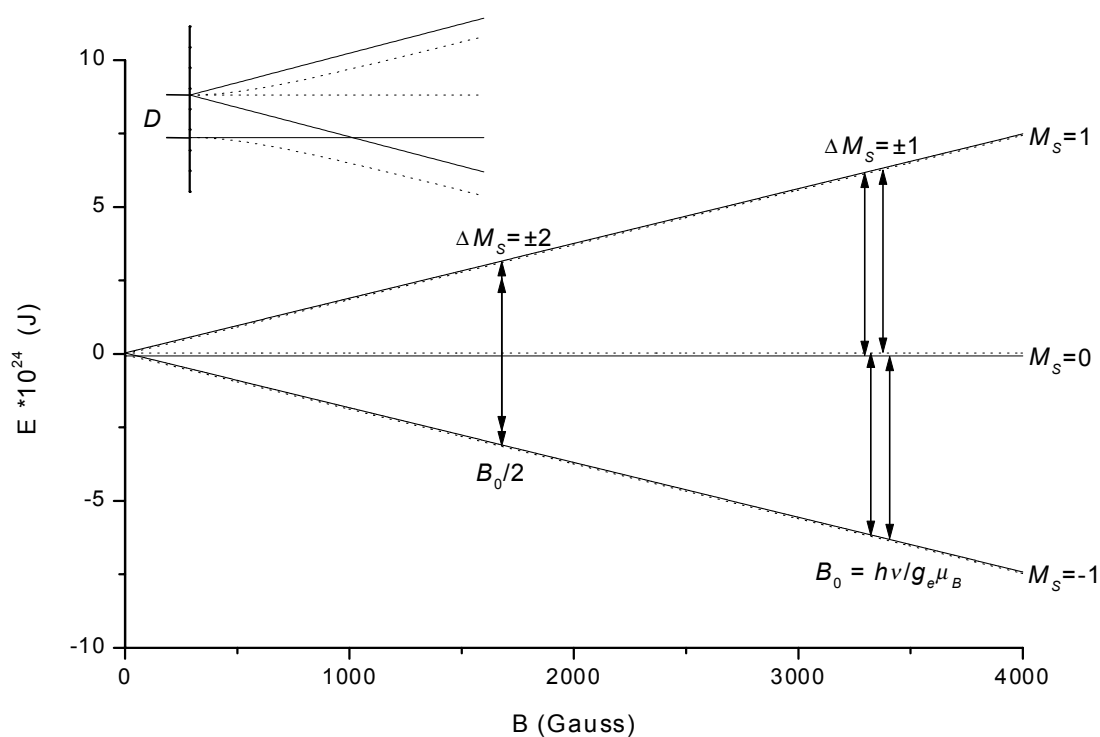**Figure 2.2.** *State energies and transitions for a randomly oriented triplet molecule (S = 1) with axial symmetry. Solid lines are B∥axis z, dotted lines are B∥axis x. Inset shows magnified low field area. D = 155 MHz, E = 0 MHz, B_0 = 3355 G, v = 9.435 GHz, g_e = 2.009273.*
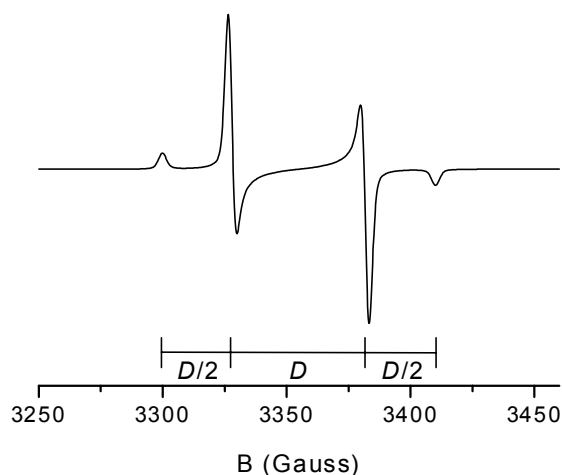
Figure 2.3. *Simulated ΔM$_S$ = ±1 ESR spectrum for a randomly oriented triplet system (S = 1) with axial symmetry. D = 155 MHz, B$_0$ = 3355 G, ν = 9.435 GHz, g$_e$ = 2.009273.*

In addition to the two allowed $\Delta M_S = \pm 1$ transitions, the ESR spectrum of a triplet state molecule often exhibits a 'forbidden' $\Delta M_S = \pm 2$ transition which occurs at approximately half of the normal magnetic field. For a triplet state molecule with axial symmetry $\Delta M_S = \pm 2$ transitions are expected at $B_z = h\nu/(2g_e\mu_B)$ and $B_x = [(h\nu)^2 - D^2]^{\frac{1}{2}}/(2g_e\mu_B)$.

A similar approach can be used to describe the ESR spectrum of a quartet system ($S = 3/2$). Equation (12) for $S = 3/2$ results in a 4×4 determinant from which four eigenvalues are obtained corresponding with the energies of the four spin sublevels. For an axially symmetric quartet state molecule ($E = 0$), the limiting situations in which B is parallel to the z-axis or parallel to the x-axis can be solved, leading to two sets of four energy levels given by (15) and (16) and plotted in Figure 2.4.

$$E_{\frac{1}{2},-\frac{1}{2}} = \pm \frac{1}{2} g_e \mu_B B_z - D$$

$$E_{\frac{3}{2},-\frac{3}{2}} = \pm \frac{3}{2} g_e \mu_B B_z + D \tag{15}$$

$$E_{\frac{3}{2}} = \frac{1}{2} g_e \mu_B B_x + \left[\left(g_e \mu_B B_x \right)^2 + D^2 - g_e \mu_B B_x D \right]^{\frac{1}{2}}$$

$$E_{\frac{1}{2}} = -\frac{1}{2} g_e \mu_B B_x + \left[\left(g_e \mu_B B_x \right)^2 + D^2 + g_e \mu_B B_x D \right]^{\frac{1}{2}}$$

$$E_{-\frac{1}{2}} = \frac{1}{2} g_e \mu_B B_x - \left[\left(g_e \mu_B B_x \right)^2 + D^2 - g_e \mu_B B_x D \right]^{\frac{1}{2}} \tag{16}$$

$$E_{-\frac{3}{2}} = -\frac{1}{2} g_e \mu_B B_x - \left[\left(g_e \mu_B B_x \right)^2 + D^2 + g_e \mu_B B_x D \right]^{\frac{1}{2}}$$
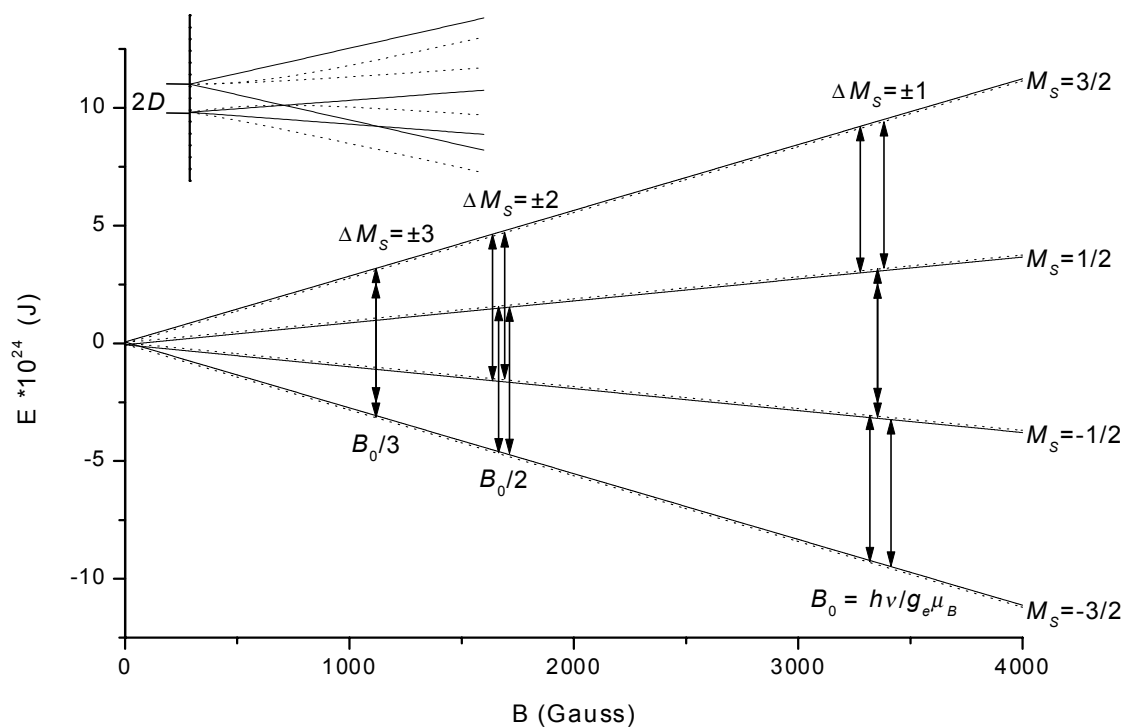
Figure 2.4. *State energies and transitions for randomly oriented quartet molecule (S = 3/2) with axial symmetry. Solid lines are B∥axis z, dotted lines are B∥axis x. Inset shows magnified low field area. D = 90 MHz, B_0 = 3355 G, v = 9.435 GHz, g_e = 2.009273*

For a quartet state molecule three $\Delta M_S = \pm 1$ transitions are possible for each direction of the magnetic field (Figure 2.4) and hence three ESR lines are expected for a $S = 3/2$ molecule in a magnetic field. Similar to the ESR spectrum of the triplet state, the splitting between the lines depends on the orientation of the magnetic field and attains a maximum value of $2D$ when B is parallel to z and a minimum value of D when B is parallel to x. For randomly oriented quartet state molecules again all possible orientations in between these limiting situations have to be considered. Simulation of an axially symmetric quartet system results in an ESR spectrum with five lines (Figure 2.5). While the $\Delta M_S = \pm 2$ ESR spectrum of an axially symmetric triplet state molecule only consists of a single line, two $\Delta M_S = \pm 2$ transitions occur at half field for a quartet state for each orientation of the magnetic field. As a result of the averaging over all orientations, the $\Delta M_S = \pm 2$ ESR spectrum of a quartet state has a similar pattern to the $\Delta M_S = \pm 1$ spectrum of a triplet state molecule where the transitions parallel to x are D apart and the transitions parallel to z are $2D$ apart.

In principle also a single $\Delta M_S = \pm 3$ transition at one-third field is present for a quartet state molecule. The observation of such a $\Delta M_S = \pm 3$ signal, however, is often

hampered by the low intensity of this forbidden transition. In general the ESR signals of the $\Delta M_S = \pm 1$, $\Delta M_S = \pm 2$, and $\Delta M_S = \pm 3$ transitions have relative intensities of $1 : (D/B_0)^2 : (D/B_0)^4$, respectively[7,8]. As a consequence, the ESR signal intensity decreases dramatically upon going from normal via half to one third field resulting in an extremely low signal for the $\Delta M_S = \pm 3$ transition.
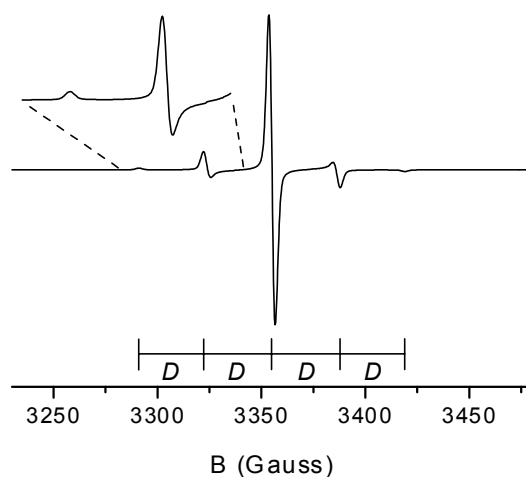
Figure 2.5. *Simulated $\Delta M_S = \pm 1$ ESR spectrum for a randomly oriented quartet system ($S = 3/2$) with axial symmetry. $D = 90$ MHz, $B_0 = 3355$ G, $v = 9.435$ GHz, $g = 2.009273$.*

2.1.4 The dipole-dipole interaction

There are two different interactions that contribute to the spin-spin Hamiltonian defined in equation (10). These are spin-spin and spin-orbit coupling. Because the spin-orbit coupling is negligible for light nuclei, spin-spin coupling is the most important contribution to **D** in organic high-spin molecules. The elements D_{ij} of the spin-spin coupling tensor **D** follow from the classical dipole-dipole interaction Hamiltonian and can be written as:

$$D_{ij} = -\frac{1}{2}\left(\frac{\mu_0}{4\pi h}\right)g_e^{\,2}\mu_B^2\left\langle\frac{r^2\delta_{ij}-3ij}{r^5}\right\rangle \tag{17}$$

where $i, j = $ x, y, z; μ_0 is magnetic permeability in vacuum and the bracket notation indicates that the integration is performed over the entire many-electron wavefunction. For an axially symmetric system ($E = 0$), D_{zz} (or $-Z$, the diagonal term of **D**) provides an estimate to the average distance (d) between the unpaired electrons in the molecule. By substituting $r = i = j = d$ and taking $D = -3/2{*}Z$, (17) can be transformed into:[3]

$$D = -\left(\frac{3\mu_0}{8\pi h}\right)g_e{}^2\mu_B^2\left\langle d^{-3}\right\rangle \qquad (18)$$

For practical purposes this equation is written as $D = 7.8 \times 10^4\ d^{-3}$, with D in MHz and d in Å.

2.1.5 Curie law

The transition energies involved in ESR spectroscopy are small ($\Delta E = g_e\mu_B B_0 = 6.252\ 10^{-24}$ J at X-band) in relation to the thermal energy kT. All spin sublevels are therefore populated at temperatures above 0 K resulting in a Boltzmann distribution of spins between the upper and lower spin sublevels. Since the ESR spectrometer probes the (small) differences between the populations in the upper and lower spin sublevels, the intensity of the ESR signal is temperature dependent. The Boltzmann distribution $\exp(-\Delta E/kT)$ describes the population ratio of two spin sublevels separated by $\Delta M_S = \pm 1$. Because $g_e\mu_B B_0$ is small compared to kT at ordinary temperatures it follows that $\exp(-\Delta E/kT) \approx 1 - \Delta E/kT$. Hence, the populations of the two spin levels (separated by $\Delta M_S = \pm 1$) are almost equal and a simple calculation shows that $\frac{1}{2}N(1 + \Delta E/2kT)$ are in the low spin state and $\frac{1}{2}N(1 - \Delta E/2kT)$ are in the high spin state. The signal intensity I of a $\Delta M_S = \pm 1$ ESR transition at thermal equilibrium is proportional to the difference in population, $Ng_e\mu_B B_0/2kT$, and therefore linear with the reciprocal temperature. This is equivalent to the Curie law for magnetization:

$$I = \frac{C}{T} \qquad (19)$$

In principle, the ground state of a high-spin molecule can be determined using variable temperature ESR measurements. A linear increase of the intensity of the ESR signal with the inverse temperature according to Curie's law reveals that there is no thermal population or depopulation of the spin state of the molecule in that temperature range. Unfortunately, the interpretation of Curie-law behavior for the ESR signal intensity may be twofold. Either the high-spin state is the lowest energy state separated by a substantial difference compared to the thermal energy kT from the low-spin state, or the energy difference with the lower spin state is extremely small. In the latter case the low-spin and high-spin states are degenerate and a change in temperature does not shift the thermal equilibrium between these states.

2.2 Concluding remarks

This short introduction to electron spin resonance (ESR) spectroscopy shows that the interpretation and analysis of ESR spectra of high-spin molecules can provide valuable information on the delocalization of the unpaired electrons via hyperfine interactions en zero-field splittings. The multiplicity of the ground state and the relative ordering of the different spin states can be assessed from the temperature dependence of the ESR signal intensity.

2.3 References

1.   Wertz, J. E.; Bolton, J. R., *Electron Spin Resonance, Elemental Theory and Practical Applications*, McGraw-Hill, New York **1972**.

2.   Carrington, A.; McLachlan, A. D., *Introduction to Magnetic Resonance*, Chapman and Hall, London **1979**.

3.   Weil, J. A.; Bolton, J. R.; Wertz, J. E., *Electron Paramagnetic Resonance, Elemental Theory and Practical Applications*, John Wiley & Sons, New York **1993**.

4.   Atherton, N. M., *Principles of Electron Spin Resonance*, Ellis Horwood Limited, London **1993**.

5.   It is common to use upper case A's for coupling constants in MHz and lower case a's for coupling constants in Gauss.

6.   In this thesis the commonly known convention is used that all parameters in a spin hamiltonian are assumed to be in energy units. Division by h is required to convert to frequency units.

7.   Brickmann, J.; Kothe, G., *J. Chem. Phys.* **1973**, *59*, 2807.

8.   Weissman, S. I.; Kothe, G., *J. Am. Chem. Soc.* **1975**, *97*, 2537.

3

Synthesis of aniline oligomers with *meta* linkages

Abstract: A series of aniline oligomers is synthesized using a palladium/phosphine ligand catalyst system. These oligomers consist of para-substituted benzenediamine motifs connected by meta-substituted benzene rings in several different topologies, ranging from linear to branched molecules. The two largest molecules reported here consist of eight aniline units with different substituents connected in a linear alternating meta-para fashion.

3.1 Introduction

Already for more then a century polyanilines attracts the attention of researchers active in science and technology. Their chemical and physical nature are such that optical, magnetic and electronic properties are tunable by synthesis or physical manipulation. The 'synthetic metal' behavior of polyaniline, having a high electric conductivity when doped, is one of these important properties. Like most modern polymers, polyaniline can be processed easily, giving it an important place in today's research programs on plastic electronics.

Parallel to the research of polyanilines, synthesis routes for oligoanilines were developed allowing for better control over purity and length, and enabling detailed studies. A commonly encountered phenomenon is the deprotonation of the nitrogen bound hydrogens upon oxidation, which led to the development of oligoanilines with other groups on that position e.g. methyl or phenyl[1,2]. Some of the *N*-methyl-oligoanilines reported[3] showed the tendency to dimerise when doped to the cation radical state, the *N*-phenyl-oligoanilines however exhibited increased solubility in absence of dimerisation.

R = H, Phenyl
n = 1,2

R = H,   R' = H
R = Phenyl, R' = H
R = Anisyl, R' = MeO
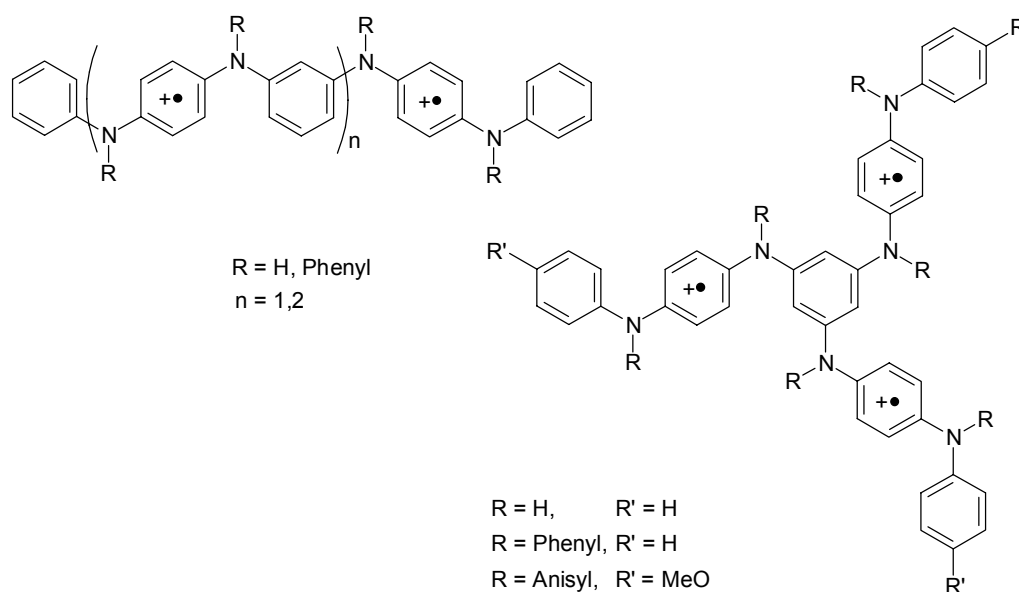
Figure 3.1. *High-spin m-p-Oligoanilines reported in literature. Linear oligomers and star-shaped oligomers with R=H or Phenyl and R'=H by Wienk et al.[4-6] Star-shaped oligomers with R=Phenyl, R'=H and R=Anisyl, R'=MeO by Blackstock et al.[7]*

The unusual stability of unpaired electrons in oxidatively doped oligo- and polyanilines attracted the attention of researchers in the field of organic ferromagnetism[4-18]. Oligoanilines with alternating *meta-para* topology were synthesized

and characterized both by Wienk et al.[4-6] and Blackstock et al.[7] having a ground state high-spin state and stability at ambient temperatures of the corresponding cation radicals (Figure 3.1). This combination of a high-spin ground state with stability at ambient temperatures make it worthwhile to investigate the *m-p*-oligoaniline polyradicals further. Wienk synthesized the aniline oligomers by using Ullmann reactions, in which an arylamine is coupled to an aryl halide in a copper catalyzed reaction. The preparation of longer and more complex aniline oligomers is severely limited using this type of coupling reaction. Therefore, the objective of this chapter is the preparation of longer and branched *m-p*-aniline oligomers using improved synthetic methodology. The redox, optical, and high-spin properties of the aniline oligomers will be presented in chapter 4.

3.2 Introduction into arylamine synthesis

The construction of carbon-nitrogen bonds in aryl amines has proved to be difficult over the last century. Existing synthetic methodologies used high temperatures and rather drastic reaction conditions. A widely used reaction is the Ullmann-Goldberg reaction[19,20] using copper and/or copper iodide as a catalyst (Scheme 3.1, top), in which an amine is coupled to an aryliodide. This reaction type has evolved over the years using for example phase-transfer catalysis[21], but reactive iodobenzenes remain necessary, and products are often difficult to isolate and suffer from colored impurities.

An alternative route to anilines is condensation of hydroxybenzenes with aryl amines using iodine as a catalyst under removal of water[22] (Scheme 3.1, middle). Especially with 1,3,5-trihydroxybenzene (phloroglucinol) this reaction gives good yields. This coupling is limited to the synthesis of secondary anilines. The use of condensing agents, preventing the back reaction, improves the reaction so that milder conditions can be applied. A series of oligomers has been synthesized by Tanaka et al. [23] using a titanium alkoxide aryloxide as a condensing agent.

Ortho- or *para*-fluoro-nitrobenzenes can also be applied in a nucleophilic aromatic substitution reaction (Scheme 3.1, bottom) for the synthesis of aromatic amines[24]. This strategy was used and improved for the synthesis of a series of branched oligoanilines using DMSO as solvent and the more reactive 2,4-dinitrofluorobenzene as building block[25].
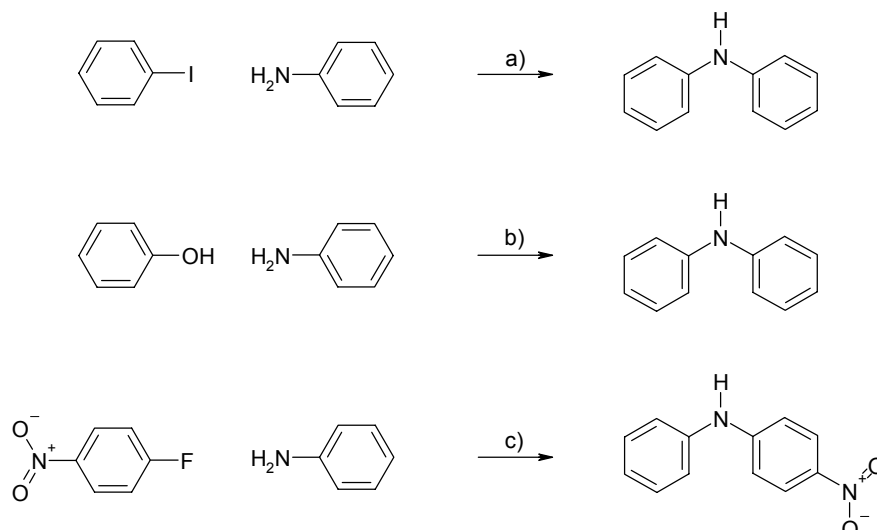
Scheme 3.1. *General reaction types for the preparation of anilines. Reactions and conditions: a) Cu and/or CuI, strong base, high boiling solvent, reflux, b) I_2 or condensing agent e.g. Ti(n-BuO)₃(OC₆H₄OMe), reflux, c) base, H_2O, ±200 °C.*

The classic example of the synthesis of linear oligoanilines is the work of Honzl and co-workers[26]. The oligomers were obtained using a double condensation reaction of a *p*-benzenediamine with diethyl succinylosuccinate (or succinylosuccinic acid diethyl ester) (Scheme 3.2). This was followed by oxidation, ester hydrolysis and decarboxylation by vacuum sublimation. Using this strategy Honzl was able to obtain a *p*-aniline hexamer. Later on Wudl et al.[27] used a modified Honzl synthesis for the preparation of *p*-octaaniline using the diacid instead of the diethyl ester.
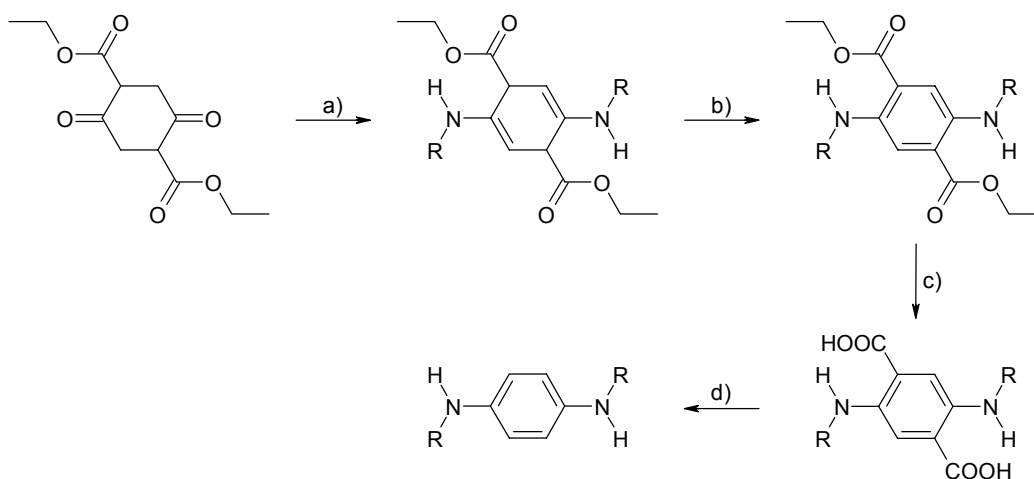
Scheme 3.2. *Synthesis route of Honzl and co-workers for the preparation of oligo-anilines. Reactions: a) condensation with primary aromatic amine, b) oxidation with 2,3,5,6-tetrachloro-[1,4]benzoquinone, c) hydrolysis with NaOH/ethanol, d) decarboxylation by sublimation.*

The synthesis route to linear *m-p*-oligoanilines of Wienk et al.[4,5] uses the Ullmann methodology to prepare hydrogen and phenyl substituted oligomers (Scheme 3.3). For the hydrogen substituted oligomers it is necessary to use protecting acetyl-groups during the synthesis, similar to the work of Ito et al. on *m*-oligoanilines[28]. This protecting group however has a dramatic influence on the solubility of the oligomer precursors, making it difficult to prepare longer oligomers. The phenyl-substituted tetraamine is made by coupling 4-iodo-*N,N*-diphenylaniline twice to *N,N'*-diphenyl-1,3-benzenediamine, which was prepared in a three-step synthesis, starting from 1,3-benzenediamine using Ullmann methodology.
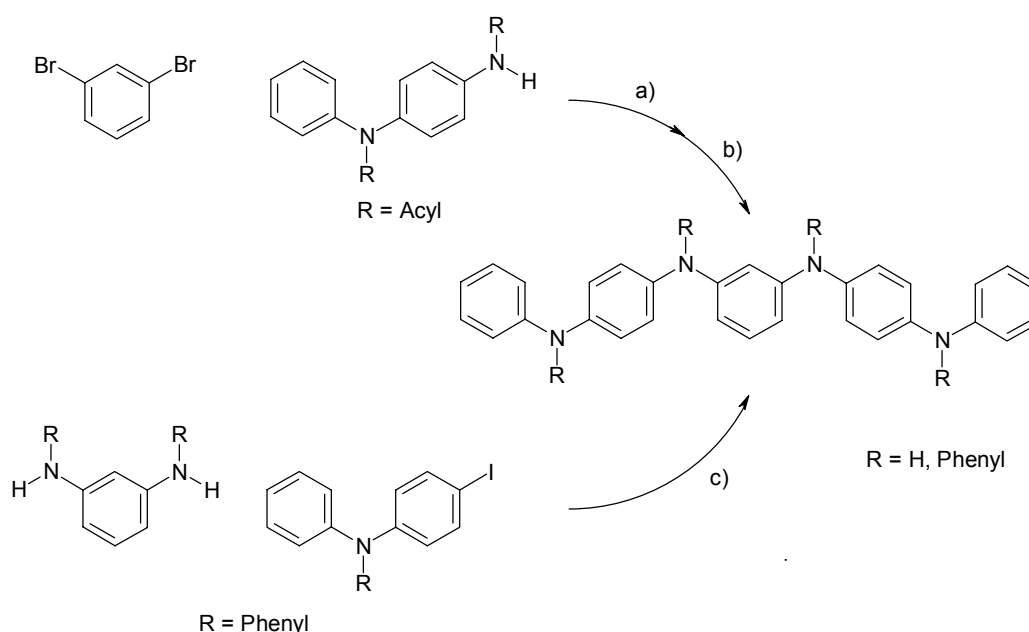
Scheme 3.3. *Synthesis route of Wienk et al.[4,6] for the tetraamine oligomers. Reactions and conditions: a) CuI, K₂CO₃, ethoxyethyl ether, reflux, 24 h, b) NaOH, water/ethanol, reflux, 24 h, c) n-BuLi, CuI, Ph₂O, 200 °C, 48 h.*

A Knoevenagel reaction of phloroglucinol with a primary aromatic amine has been used by both Blackstock et al.[7] and Wienk et al.[5] to synthesize star-shaped oligoanilines. Where the former uses *N*-phenyl-*p*-benzenediamine and a sixfold Ullmann coupling with iodobenzene, the later starts with aniline followed by a threefold Ullmann coupling with 4-iodo-*N,N*-diphenylaniline (Scheme 3.4).
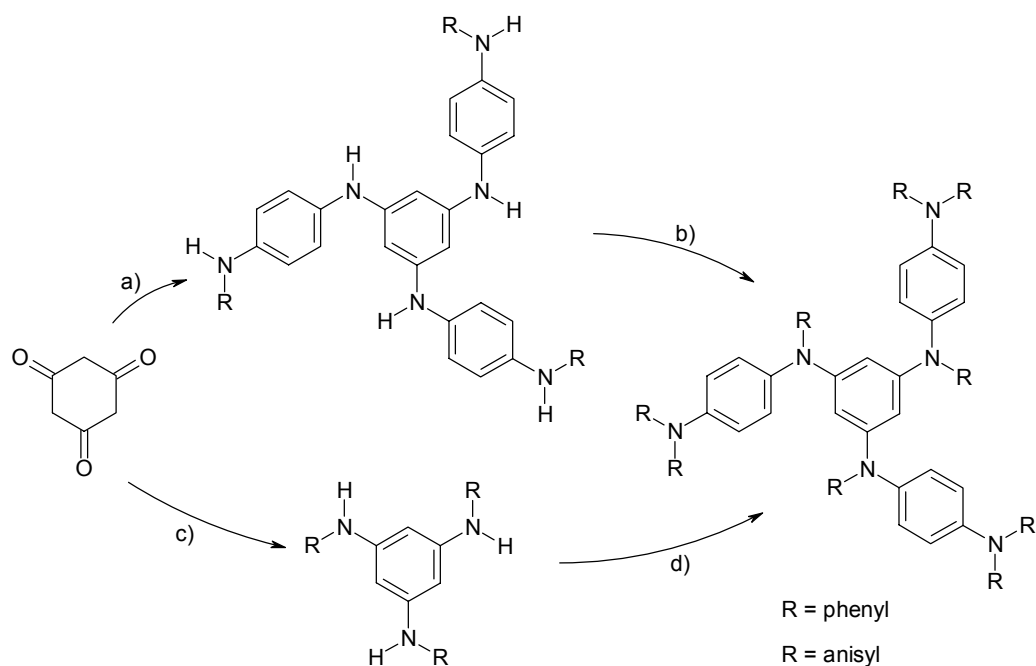
Scheme 3.4. *Synthesis routes of Blackstock et al.[7] (top) and Wienk et al.[5] (bottom) for the star-shaped oligomers. Reactions and conditions: a) N-phenyl-1,4-benzenediamine or N-anisyl-1,4-benzenediamine, I₂, 160 °C, 1h, b) iodobenzene or iodoanisole, KOH, Cu, Ph₂O, 180 °C, 44 h, c) aniline, I₂, 190 °C, 6h, d) 4-iodo-N,N-diphenylaniline, NaH, CuI, Ph₂O, 200 °C, 48 h.*

The synthesis of aromatic amines has made a giant leap forward over the past five years. The introduction of palladium catalysis for carbon-nitrogen bond formation in aniline synthesis can be attributed to Migita and co-workers[29] (Scheme 3.5, top). They found that *N,N*-diethyl-amino-tributyltin could be coupled to various bromobenzenes using a palladium(II) phosphine-ligand complex. Chloro- or iodobenzenes, however, proved to be much less reactive in this route.
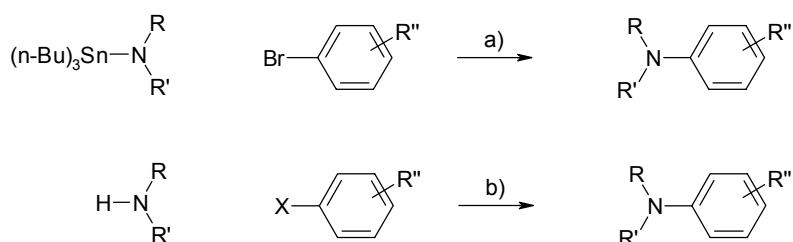
Scheme 3.5. *Palladium-catalyzed reactions of aryl halides with allylic or aromatic amines. Reactions and conditions: a) PdCl₂((o-tolyl)₃P)₂, toluene, 100 °C, b) NatBuO, Pd(II)(ligand)Cl₂ or Pd(0)(ligand), THF or toluene , 80-100 °C,*

It took almost a decade before palladium-catalyzed C-N coupling reactions received renewed attention. Originally following the strategy of Migita[29], Hartwig and Buchwald

independently coupled different aminostannanes[30] or in-situ generated aminostannanes[31] to aryl bromides. It was found that the organotin compounds could be replaced by unsubstituted amines when sodium *t*-butoxide was used as base[32,33] (Scheme 3.5, bottom). This important simplification allowed for a reaction between a primary or secondary amine and a bromo- or iodobenzene. This methodology has shown to be very successful during the last years for the preparation of various amines.

Reductive Elimination of Arylamine
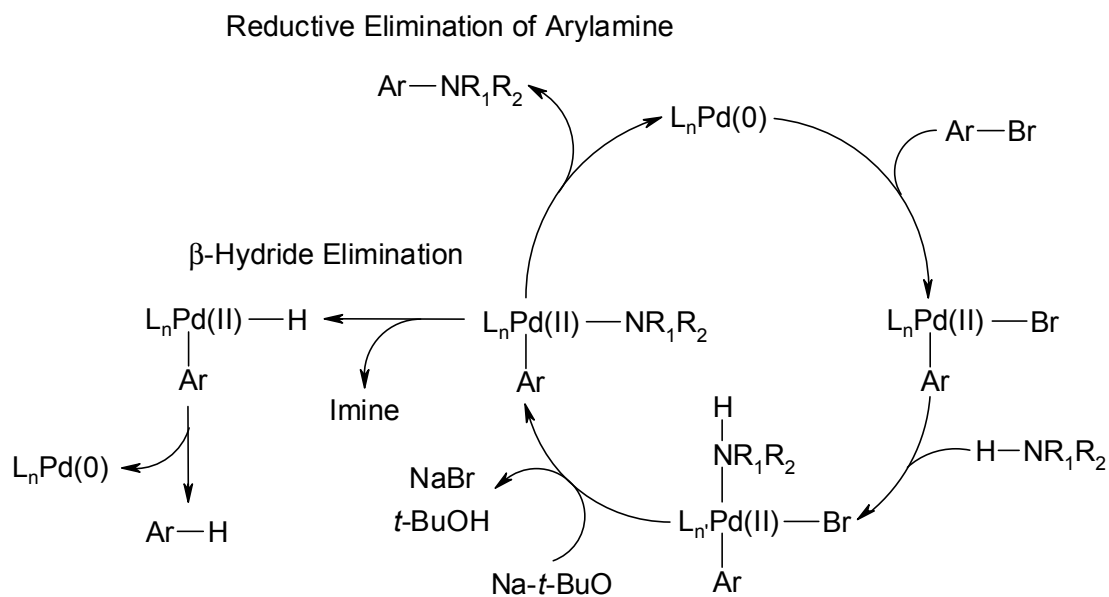
Scheme 3.6. *A simplified catalytic cycle of palladium mediated C-N bond formation by reductive elimination of arylamine.*

Both Hartwig[34] and Buchwald[35] explain in approximately the same way the mechanism of the palladium catalysis (Scheme 3.6). The catalytic cycle of the palladium-catalyzed arylamine synthesis starts with a Pd(0)/Ligand complex, in situ formed from mixing tris(dibenzylideneacetone)dipalladium(0) (Pd$_2$(dba)$_3$) with an appropriate phosphine ligand. Oxidative addition of the aryl bromide results in a Pd(II) complex that coordinates the amine enhancing the acidity of the N-H. Reaction of this complex with a base yields the important aryl amido intermediate, which affords the desired arylamine and the starting Pd(0) complex via reductive elimination. An important side reaction is the β-hydride elimination resulting in an imine and a dehalogenated arene. Increasing the nucleophilicity of the amine or increasing the electrophilicity of the aryl bromide reaction favors the reductive elimination reaction. So alkylamines react faster than diarylamines as do aryl bromides with electron-withdrawing substituents compared to electronically neutral aryl bromides. Other factors that influence the ratio between β-hydride elimination and reductive elimination are the number of coordinating phosphines in the aryl amido intermediate. For monodentate phosphines, like the

sterically hindered tri-*o*-tolylphosphine, the complex that undergoes elimination is a three-coordinate aryl amido complex having only one phosphine ligand. This complex has high reaction rates for both reductive and β-hydride eliminations. The formation of bis-amine complexes, when using primary amines, is another side reaction that occurs during these palladium catalyzed reactions. There are also other side reactions occurring for which the mechanism is still unclear and are worth investigating, e.g. the dehalogenation reaction that takes place during the preparation of triarylamines, despite the absence of β-hydrogens in the reactants. The catalyst system was improved using chelating ligands, e.g. 1,1'-bis(diphenylphosphino)ferrocene (DPPF)[36], 2,2'-bis(diphenylphosphino)-1,1'-binaphthyl (BINAP)[37,38] or 1-[2-(diphenylphosphino)-ferrocenyl]ethyl methyl ether (PPF-OMe)[39]. For chelating ligands with two coordinating phosphine groups, like BINAP, the aryl amido intermediate is a four-coordinate complex which has a much slower rate of β-hydride elimination compared to the reductive elimination. Variation of the base, e.g. cesium carbonate[40] made it possible to accommodate various functional groups in both the aryl halogen and aryl amine.

Recently catalyst systems have been developed which even allow for reactions to be performed at room temperature[41,42] and/or use of aryl chlorides. The use of tri-*tert*-butylphosphine as a sterically hindered monodentate ligand[43] made it possible to do a broad range of coupling reactions that previously needed a variety of different ligands. Despite this tremendous progress, reaction conditions still need to be fine tuned for the optimal palladium/ligand amount and ratio as well as for the base, reaction time, and temperature.

Parallel to these improvements, the attention has been focused on the synthesis of well-defined oligoanilines[44,45] and several poly(*N*-aryl aniline)s[46,47]. Surprisingly, these recent publications show that the synthesis of *N*-aryl-anilines works best with monodentate phosphine ligands like tri-*o*-tolylphosphine or tri-*tert*-butylphosphine.

3.3 Synthesis of linear *N*-methyl substituted aniline oligomers

At the start of our investigations on the synthesis of linear m-p-aniline oligomers, the development of a palladium-catalyzed arylamine coupling was at an early stage and a limited number of couplings were known. E.g., the synthesis of triarylamines by this promising method was not yet developed, but couplings involving *N*-methylaniline had been demonstrated. This was one of the reasons for choosing a methyl group as substituent on the *m*-*p*-oligoaniline framework instead of the phenyl substituted oligomers prepared by Wienk [5]. Another reason for using a methyl group instead of a

phenyl group lies in the fact that it is expected not to participate in the delocalisation of the unpaired electron in the oxidized 1,4-benzenediamine unit, the resulting increased spin density at the nitrogen atoms could enhance the ferromagnetic coupling between two cation radicals in the same molecule. For increased solubility, it would be even more preferable to have a longer alkyl-group so that the solubility of the products is enhanced. Exploratory experiments with a hexyl group instead of a methyl group revealed that coupling a *N*-hexylaniline with an aryl bromide using the palladium catalyst system available at that time, resulted in longer reaction times with only trace amounts of the desired product being formed. It is also very likely that the product would be a viscous oil and so much more prone to oxidation by air. This in contrast to a methyl group which generally affords crystalline products with better air-stability.

The availability of starting materials always plays a major role in the development of a synthetic route. In the use of palladium catalysis for the coupling of aryl halides with aryl amines a choice must be made between coupling 1,3-benzenediamine with 1,4-dibromobenzene or coupling 1,4-benzenediamine with 1,3-dibromobenzene. The donating effect of an amine group is larger on the para-position than on the meta position. Hence, after dibromobenzene has reacted once with an aryl amine the remaining bromide is less deactivated when it is on meta position than when it is on the para position. An additional advantage of using 1,3-dibromobenzene is the fact that it is a liquid and can be used as solvent as well as reactant when only a single coupling to a secondary amine is preferred.
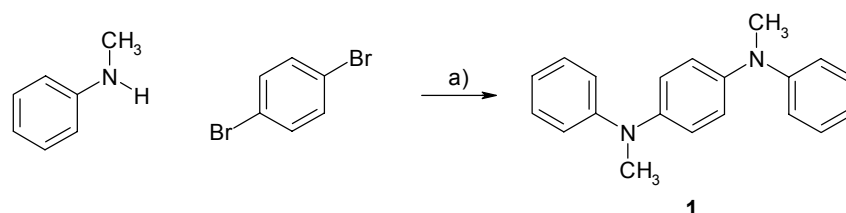
Scheme 3.7. *Synthesis of dimer **1**. Reaction conditions: a) NatBuO, Pd₂(dba)₃, S-BINAP, toluene, 90 °C, 18 h, 75 %.*

Dimer **1** was synthesized from *N*-methylaniline and 1,4-dibromobenzene using the palladium(0)/BINAP catalyst system developed by Buchwald[37] (Scheme 3.7). Column chromatography was used to purify **1** from the side products, *N*-methyl-*N*-phenyl-4-bromobenzeneamine in which only one bromine was substituted and *N*-methyl-*N*-phenylbenzeneamine caused by β-hydride elimination. Compound **1** will serve as reference compound in the series of linear oligomers.
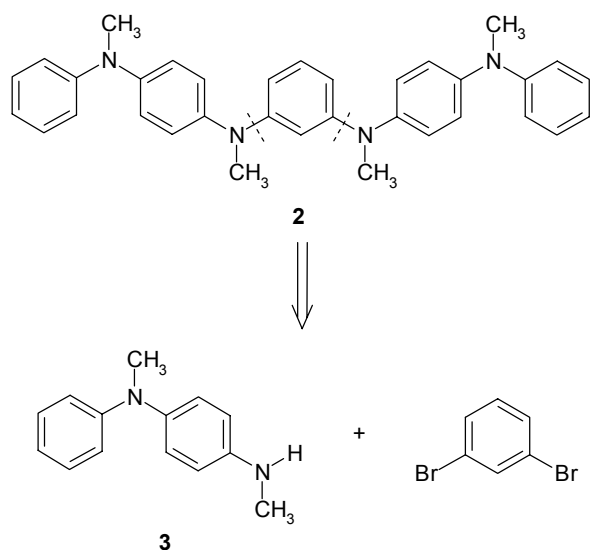
Scheme 3.8. *Retrosynthesis of tetramer 2.*

From a retrosynthetic point of view the following two building blocks should be available for the synthesis tetraamine **2**; *N,N'*-dimethyl-*N*-phenyl-1,4-benzenediamine **3** and 1,3-dibromobenzene (Scheme 3.8). For the synthesis of **3** there are in principle several options, since *N*-phenyl-1,4-benzenediamine is commercially available it is a convenient precursor for the synthesis of **3**. One of its advantages is the fact that it contains the arylamine framework and only methylation of the amine groups has to be accomplished in a controlled way in order to get to **3**.
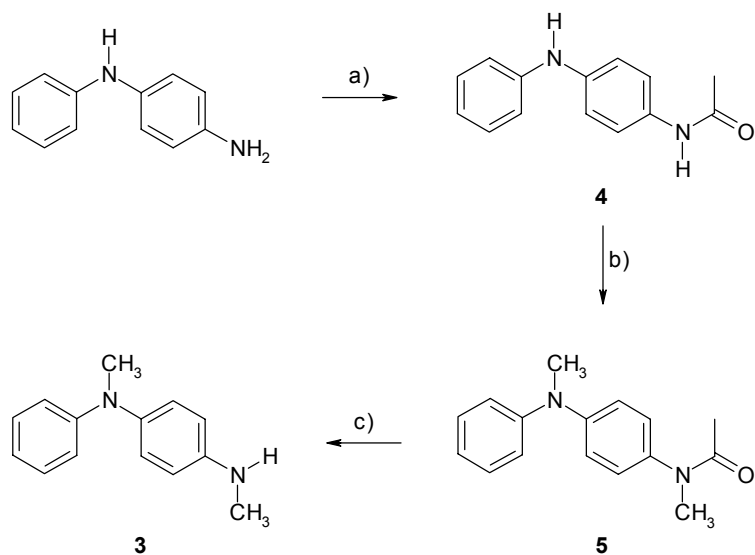
Scheme 3.9. *Synthesis of 3. Reactions and conditions: a) acetic anhydride, acetic acid, reflux, 3 h, 95 %, b) iodomethane, NaOH, K₂CO₃, (n-Bu)₄NHSO₄, toluene, reflux, 18 h, 70 %, c) NaOH, ethanol/water 2/1 (v/v), reflux, 48 h, 90 %.*

Protection of the primary amine was achieved by a classic acylation reaction. This protecting group is stable under the reaction conditions used for the methylation of the amines in which tetrabutylammonium hydrogensulfate is used as a phase transfer catalyst[48]. The methylation reaction was performed at reflux temperature, enhancing the solubility of compound **4**, resulting in methylation of the diphenylamine group as well as the acetamide group. For deprotection of intermediate **5** sodium hydroxide in a water/ethanol mixture was used.
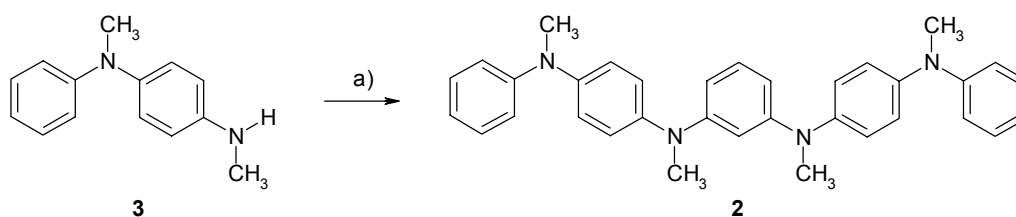
Scheme 3.10. *Synthesis of tetramer **2**. Reactions and conditions: a) 1,3-dibromobenzene, NatBuO, Pd₂(dba)₃, S-BINAP, toluene, 90 °C, 48 h, 30 %.*

The tetramer **2** was made by reacting 1,3-dibromobenzene twice with **3** using slightly more than two equivalents (Scheme 3.10). After cooling the reaction mixture, the product crystallized together with NaBr formed during the reaction. Adding diethyl ether, however, dissolved the tetramer by which the salts could be filtered and **2** could be purified by crystallization from toluene.

Scheme 3.11. *Two possible synthesis routes for building block **6**. Reactions and conditions: a) acetic anhydride, acetic acid, reflux, b) iodomethane, NaOH, K₂CO₃, (n-Bu)₄NHSO₄, toluene, reflux, c) NaOH, ethanol/water 2/1 (v/v), reflux, d) LiAlH₄, 1,4-dioxane, 40 °C, 6 h, 50 %.*
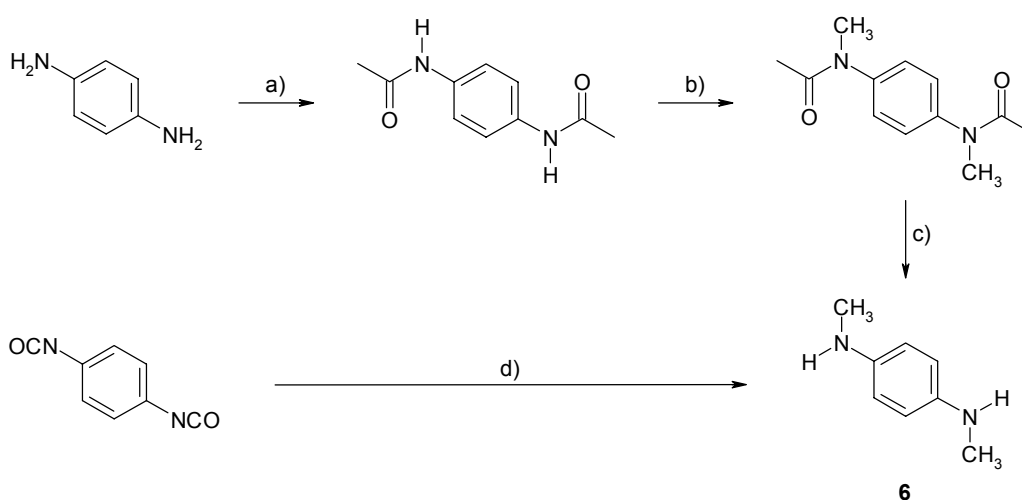
In principle, building block **6**, needed for the synthesis of the longer oligomers, can be made by the same synthetic sequence of acylation, methylation, and deacylation (Scheme 3.11, top route) as used for the synthesis of **3**.
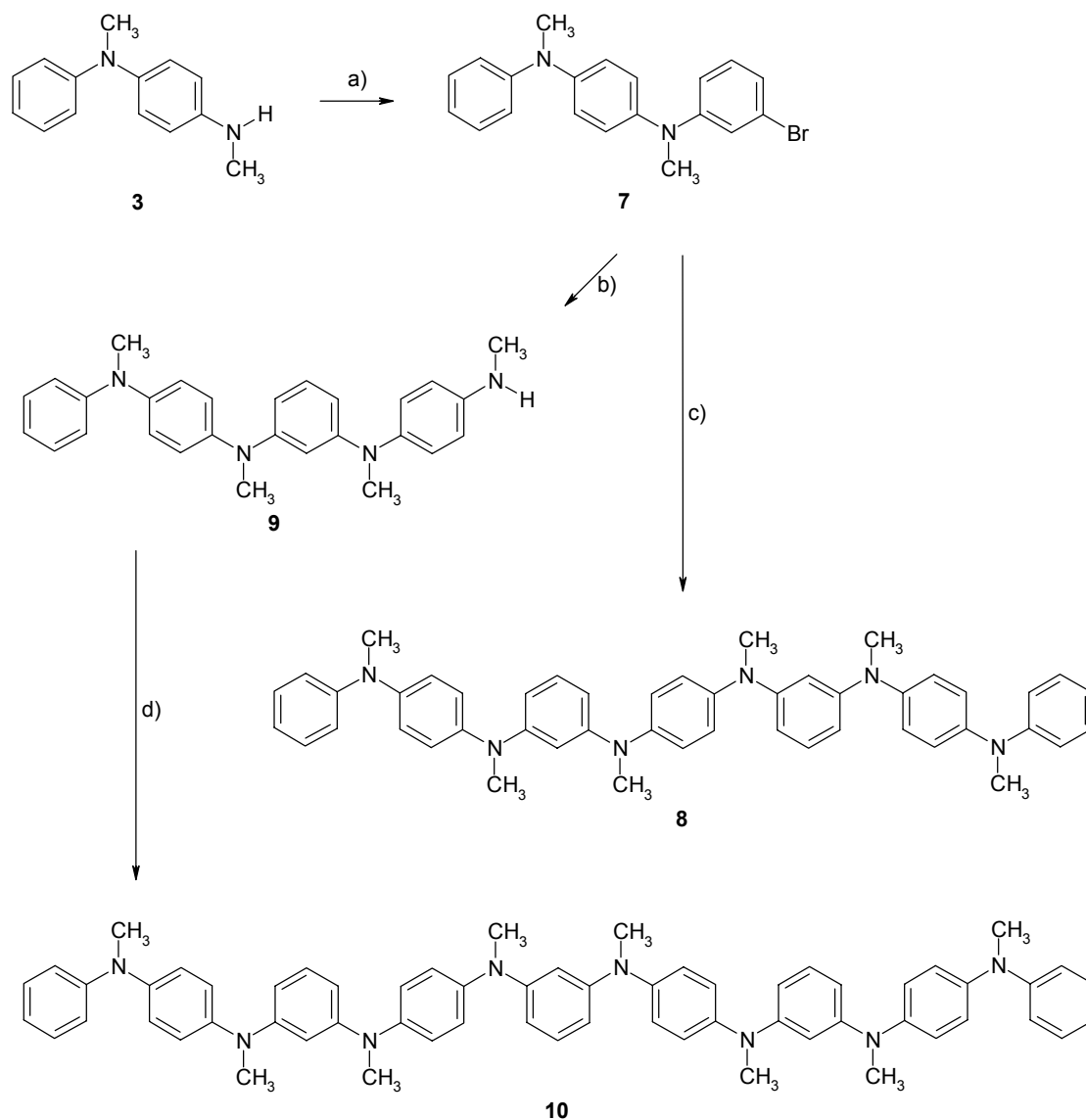
Scheme 3.12. *Synthesis of hexamer **8** and octamer **10**. Reactions and conditions: a) 1,3-dibromobenzene, NatBuO, Pd₂(dba)₃, S-BINAP, 90 °C, 4 h, 85 %, b) **6**, NatBuO, Pd₂(dba)₃, PPFA, toluene, 90 °C, 60 h, 50 %, c) **6**, NatBuO, Pd₂(dba)₃, PPFA, toluene, 90 °C, 52 h, 51 %, d) 1,3-dibromobenzene, NatBuO, Pd₂(dba)₃, PPFA, toluene, 90 °C, 72 h, 35 %.*

This route is, however, hampered by the insoluble nature of intermediate product *N,N'*-diacetyl-1,4-benzenediamine which gives rise to low yields in the subsequent methylation reaction. An alternative route towards **6** is the reduction of 1,4-benzenediisocyanate with lithium aluminum hydride in an exothermic reaction (Scheme

3.11, bottom route). Although the original procedure[49] only describes the reduction of monoisocyanates, it could successfully be applied for the reduction of a diisocyanate, provided the reaction mixture was stirred vigorously to prevent gelation. This convenient one-step procedure for synthesizing **6** resulted in a modest yield, on the same order of magnitude as the overall yield of the tedious and elaborate acylation, methylation and deacylation sequence. The fact that product **6** has a melting point close to room temperature makes it prone to oxidation by air.

The second key-intermediate for the synthesis of longer oligomers is arylbromide **7** (Scheme 3.12). Pure 1,3-dibromobenzene is an advantageous reagent for the preparation of aryl bromide **7**. Due to its dual role as solvent and as reactant the formation of tetramer **2** could be fully suppressed, leaving debromination, resulting in dimer **1**, as the major side-reaction.

Having synthon **7** available, reaction with diamine **6** was now possible. Depending on the stoichiometry used, this reaction yields either the hexamer **8**, or **9** as a precursor to the octamer (Scheme 3.12). During the course of this investigation, a new palladium/ligand catalyst system[39] became available, which surpresses the β-hydride elimination side-reaction. This 1-[2-(diphenylphosphino)ferrocenyl]ethyl-*N*,*N*-dimethylamine (PPFA) ligand gave also cleaner reaction mixtures and was used in subsequent reactions. Due to the limited solubility of octamer **10** and the inorganic salts in toluene/diethyl ether, they are filtered off during work-up. Aqueous treatment of the residue and crystallization from toluene yielded the octamer **10**. It should be noted that all secondary amines during this synthesis route are very susceptible towards oxidation by air resulting in a yellow/brown color within hours.

3.4 Synthesis of branched *N*-methyl substituted aniline oligomers

A frequently used ferromagnetic coupling unit in organic high-spin molecules, together with *meta*-benzene, is the 1,3,5-benzenetriyl unit. Incorporation of this unit in high-spin molecules provides the opportunity to extend intramolecular ferromagnetism from one dimension to two dimensions. An extensive variety of polyradicals containing the 1,3,5-benzenetriyl unit have been reported[50-57]. In the area of aniline research, this unit has been used in networks or dendritic structures containing aminium cation radicals[14,58] or high-spin 1,3,5-triaminobenzenes[11,59]. As mentioned in paragraph 3.1, high-spin oligo *m-p*-anilines with this structural element have been synthesized and characterized by Blackstock[7] and Wienk[5] (Figure 3.1). Since alkyl substituted star-

shaped oligoanilines have not been reported, the synthesis and high-spin characteristics of substitution pattern for *N*-methyl oligoanilines is of interest.

For this reason star-shaped oligoaniline **11** has been synthesized from 1,3,5-tribromobenzene and **3** (Scheme 3.13). After the usual workup the resulting white solid was not pure and contaminated with an unidentified side product bearing a great resemblance with product **11**. The difference in polarity was so small that several attempts to purify **11** from this side product using silica gel thin layer chromatography failed. It was then decided to only purify a small amount (100 mg) by means of preparative HPLC, which was enough to perform all measurements for the full characterization of compound **11**. This elaborate purification of **11** shows that a Knoevenagel reaction as described in paragraph 3.2 is probably more convenient for the preparation of star-shaped oligoanilines
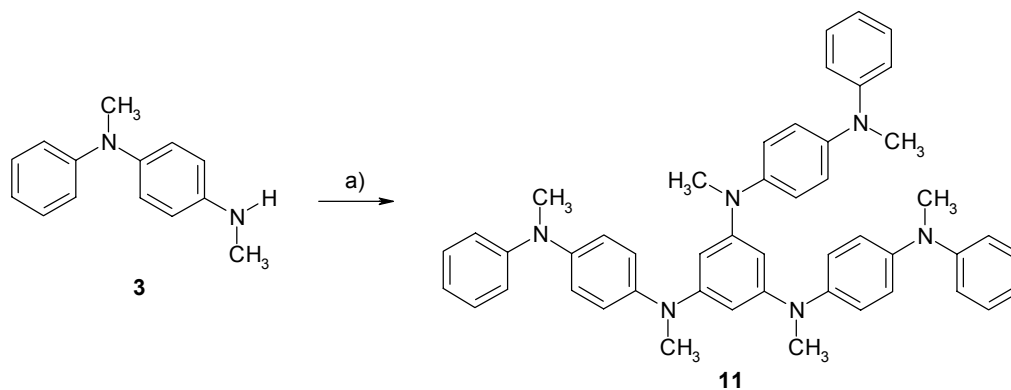
Scheme 3.13. *Synthesis of star-shaped hexamer **11**. Reactions and conditions: a) 1,3,5-tribromobenzene, NatBuO, Pd₂(dba)₃, PPFA, toluene, 90 °C, 72 h.*

In addition to create high-spin oligoanilines with alternating *meta-para* topology, it is also possible to make high-spin molecules from oligoanilines with a *meta*-topology only. In contrast to the *m-p*-oligoanilines, every amine in these *m*-oligoanilines must be oxidized to the cation radical state. This increased charge density results often in a limited stability in the oxidized state[9,13,28,59], unless the *ortho-* and/or *para*-positions [11,15] of the phenyl groups connected to the amine are blocked with alkyl or alkoxy groups.

It is also possible to circumvent these problems by connecting a stabilizing substituent, such as an electron releasing *para*-aminophenyl, to the amine. The *para*-aminophenyl makes it possible to delocalise the unpaired electron and charge in the side group. The simplest oligomer in this series is compound **14** (Scheme 3.14). In order to synthesize this oligomer, primary amine **13** had to be prepared. Coincidentally it was found during the synthesis of **3**, that the protected primary amine **12** can be synthesized when the methylation step is carried out at ambient temperature instead of reflux. After

hydrolysis of the acetyl group compound **13** was isolated. Reacting **13** with aryl bromide **7** in a 2:1 ratio, yielded the desired oligomer **14**.
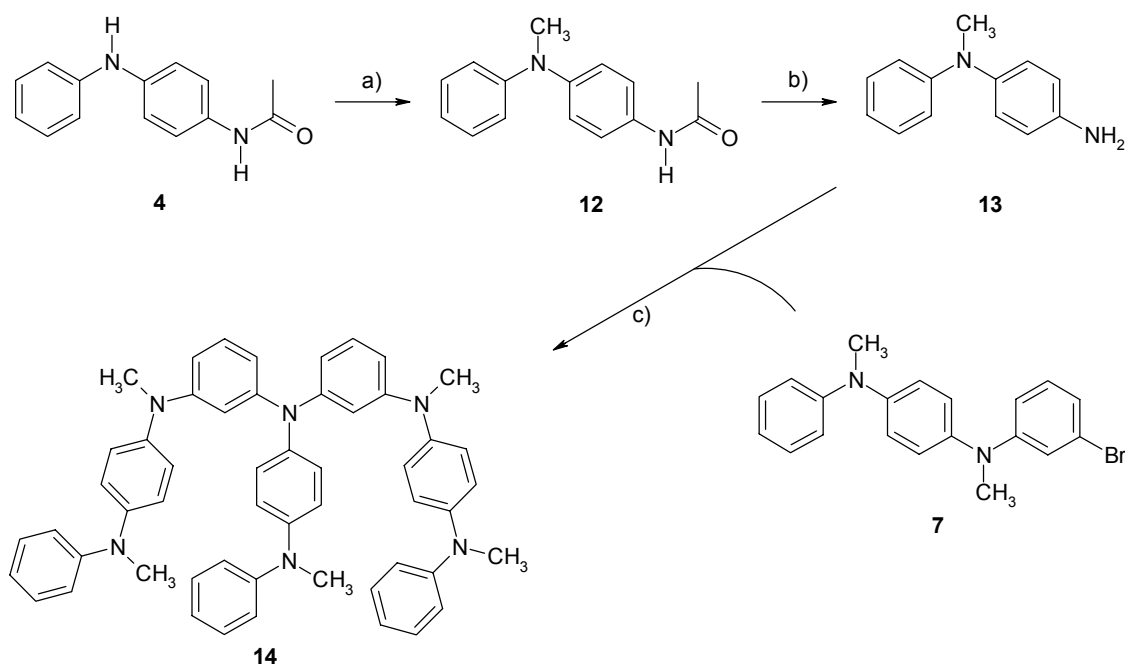
Scheme 3.14. *Synthesis of branched hexamer **14**. Reactions and conditions: a) iodomethane, NaOH, K₂CO₃, (n-Bu)₄NHSO₄, toluene, 295K, 18 h, 51 %, b) NaOH, ethanol/water 2/1 (v/v), reflux, 48 h, 88 %, c) NatBuO, Pd₂(dba)₃, PPFA, toluene, 90 °C, 20 h, 30 %.*

3.5 Synthesis of a linear *N*-phenyl substituted aniline octamer

The synthesis of a *N*-phenyl-*m-p*-aniline octamer is of interest because this would allow for comparison of two differently substituted octa-amines with each other; one with methyl groups and one with phenyl groups. With the development of the PPFA ligand catalyst system, palladium catalyzed C-N couplings could also be used in triarylamine synthesis, although later on it appeared that triarylamines could also be synthesized using the first generation catalyst with the tri-*o*-tolylphosphine ligand. Therefore, the synthetic strategy involved is the same as for the *N*-methyl series and consists of using 1,4-benzenediamine derivatives for coupling with 1,3-dibromobenzene. This is different from the strategy used by Wienk et al.[5,6] in the preparation of *N*-phenyl substituted *m-p*-oligoanilines up to the hexamer using Ullmann couplings.

The synthesis of *N,N,N'*-triphenyl-1,4-benzenediamine **15** has been reported in literature[2] using Ullmann chemistry, resulting in a poor yield. The dilemma faced in making this compound, is the use of just one reaction and tedious purification of the

product or using multiple reaction steps, e.g. protecting group chemistry to ensure that only the desired products are formed. The use of an acetyl group on the primary amine has been attempted in combination with palladium/tri-*o*-tolylphosphine catalyst system, but under these reaction conditions the acetyl group was partly cleaved. Also a strategy which involves creating the benzenediamine framework by coupling e.g. diphenylamine with 4-bromo-1-nitrobenzene, followed by reduction of the nitro group and reaction of the primary amine with bromobenzene would still involve at least three reaction steps.
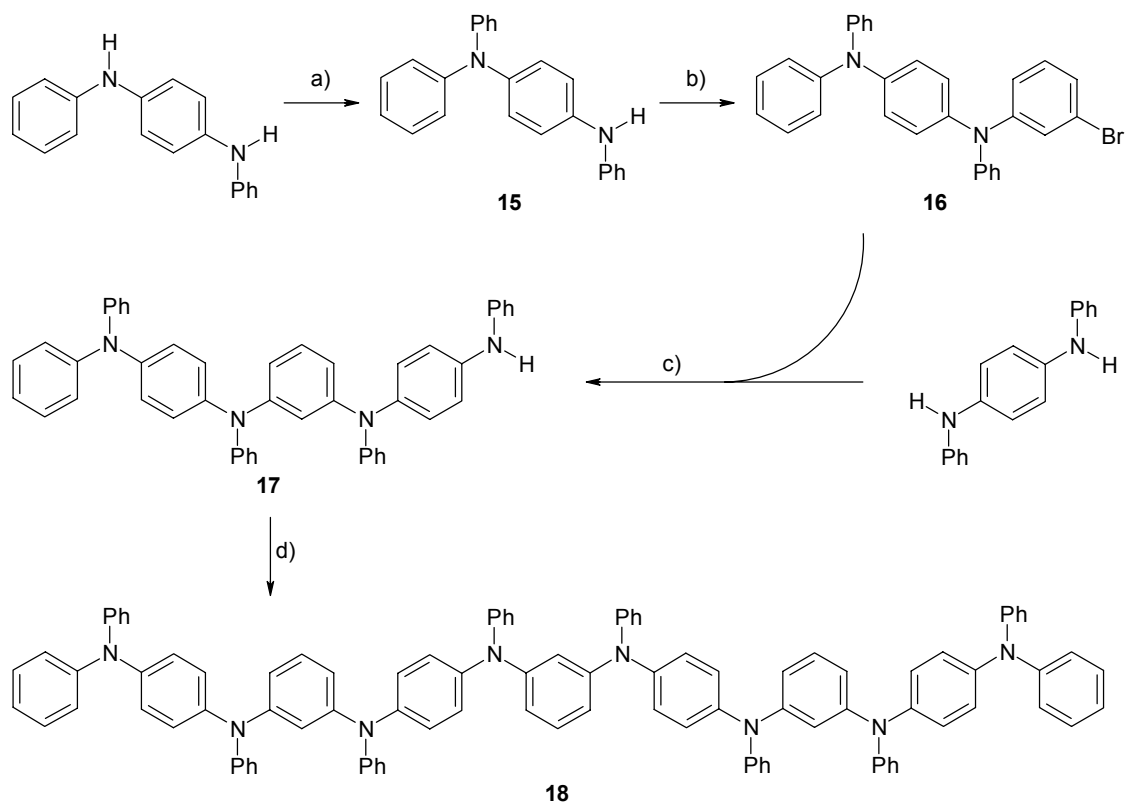
Scheme 3.15. *Synthesis of octamer 18. Reactions and conditions: a) bromobenzene, NatBuO, Pd₂(dba)₃, S-BINAP, toluene, 90 °C, 22 h, 51 %, b) 1,3-dibromobenzene, NatBuO, Pd₂(dba)₃, PPFA, toluene, 90 °C, 45 h, 64 %, c) NatBuO, Pd₂(dba)₃, PPFA, toluene, 90 °C, 90 h, 76 %, d) 1,3-dibromobenzene, NatBuO, Pd₂(dba)₃, PPFA, toluene, 90 °C, 96 h, 29 %.*

It was found that reacting *N*-phenyl-1,4-benzenediamine with bromobenzene using palladium/tri-*o*-tolylphosphine as a catalyst, produced the desired secondary amine in 50 % isolated yield (Scheme 3.15), a twofold increase compared to the Ullmann chemistry[2]. In addition, the resulting compound was white instead of orange/yellow as has been repeatly found using the Ullmann chemistry. The remainder of the synthetic sequence is similar as used previously for the preparation of **10**. By using 1,3-dibromobenzene as solvent and reactant for the next reaction aryl bromide **16** was primarily formed, but due to a longer reaction time more side reactions occurred. Commercially available *N,N'-*

diphenyl-1,4-benzenediamine was reacted with **16**, yielding not only primary amine **17**, but also the *N*-phenyl substituted hexamer in substantial amounts. Finally the octamer **18** was obtained by reacting two equivalents of **17** with 1,3-dibrombenzene. The isolation of octamer **18** was accomplished in a similar fashion as for octamer **10**.

3.6 Conclusion

The synthesis of oligoanilines has improved tremendously in the last five years in terms of purity, yields and ease of synthesis. This made it possible using a palladium/ligand catalyst system to design and synthesize oligomers in a controlled way having different topologies. The synthesis of two octa-aniline oligomers **10** and **18** clearly shows that the limiting factor changed from synthesis to solubility. In this respect the star-shaped and branched oligomers are promising candidates in the pursue of larger molecules. They combine solubility with a good stability towards oxidation by air. In principle the only limit to the size of these anilines are time and imagination as shown by Hartwig et al[47]. Although it must be mentioned that every individual coupling reaction using reactants different than described in literature needs to be fine-tuned in terms of ligands and/or reaction conditions.

3.7 Experimental section

General techniques. All reagents and solvents were used as received. Toluene was distilled from sodium prior to use in reactions. For column chromatography Merck silica gel 60 was used. Melting points are uncorrected and determined using a Buchi melting point apparatus. NMR spectra were recorded on a Bruker AM-400 spectrometer at frequencies of 400.1 and 100.6 MHz for ^{1}H and ^{13}C nuclei. Tetramethylsilane (TMS) was used as an internal standard for ^{1}H NMR and $CDCl_3$ or acetone-d6 for ^{13}C NMR. Fourier-transform infrared (FT-IR) spectra were recorded on a Perkin-Elmer 1605 FT-IR spectrophotometer or on a Perkin-Elmer Spectrum One UATR FT-IR spectrophotometer. Elemental analyses were performed on a Perkin-Elmer 2400 Series II CHN Analyzer. Kugelrohr was performed on a Buchi GKR-51 Apparatus.

***N,N′*-Dimethyl-*N,N′*-diphenyl-1,4-benzenediamine (dimer) (1).** An oven-dried Schlenk flask was charged with *N*-methylaniline (0.13 g, 1.2 mmol), 1,4-dibromobenzene (0.13 g, 0.55 mmol), sodium *tert*-butoxide (0.18 g, 1.9 mmol), Pd$_2$(dba)$_3$ (2.6 mg, 2.8 μmol), and *S*-BINAP (5.1 mg, 8.2 μmol). After purging with argon, toluene (5 ml) was added. The reaction mixture was heated for 18 h at 90 °C and cooled to room temperature. The mixture was taken up in diethyl ether, filtered over Celite 545 and concentrated in vacuo. The residue was crystallized twice from methanol, resulting in white needle crystals (0.12 g, 75%). mp 151-152 °C; ^{1}H NMR (CDCl$_3$): δ 7.25 (m, 4H), 7.02 (s, 4H), 6.95 (d, *J* = 7.9 Hz, 4H), 6.88 (t, *J* = 7.3 Hz, 2H), 3.30 (s, 6H); ^{13}C NMR (CDCl$_3$): δ 149.30, 143.81, 129.06, 123.33, 119.82, 118.19, 40.26; IR (KBr, cm^{-1}) 3053, 2872, 2806, 1594, 1493, 1336, 1250, 1181, 1126, 1083, 1024, 987, 864, 859, 839, 747, 691, 592, 512. Anal Calcd for C$_{20}$H$_{20}$N$_2$: C, 83.29; H, 6.94; N, 9.71. Found: C, 83.05; H, 6.93; N, 9.48.

N′-Acetyl-N-phenyl-1,4-benzenediamine (4). *N*-phenyl-1,4-benzenediamine (7.40 g, 40.1 mmol) and acetic anhydride (4.51 g, 44.1 mmol) were dissolved in acetic acid (100 ml). The reaction mixture was refluxed for 3 h and cooled to room temperature. The mixture was concentrated and crystallized from toluene to give **4**(8.6 g, 95%). mp 158 °C; ^{1}H NMR (CDCl$_3$): δ 7.39 (d, *J* = 8.79 Hz, 2H), 7.26 (m, 2H), 7.16 (s, 1H), 7.03 (m, 4H), 6.89 (t, *J* = 7.36 Hz, 1H), 5.18 (s, 1H) 2.15 (s, 3H); ^{13}C NMR (CDCl$_3$): δ 168.30, 143.46, 139.61, 131.49, 129.32, 121.71, 120.64, 118.86, 117.13, 24.34. Anal Calcd for C$_{14}$H$_{14}$N$_2$O: C, 74.32; H, 6.23; N, 12.38. Found: C, 74.08; H, 6.14; N, 12.53.

N′-Acetyl-N,N′-dimethyl-N-phenyl-1,4-benzenediamine (5). Diamine **4** (5.97 g, 26.4 mmol), powdered sodium hydroxide (18.0 g, 0.45 mol), powdered potassium carbonate (23.5 g, 0.17 mol), tetrabutylammonium hydrogen sulfate (1.5 g, 4.4 mmol), and iodomethane (20 ml, 0.32 mol) were added to toluene (30 ml). The reaction mixture was refluxed for 18 h and cooled to room temperature. Ethyl acetate was added and the salts were removed by filtration. The residue was concentrated and crystallized from petroleum ether (60-80) resulting in pale yellow crystals (4.7 g, 70%). mp 112-114 °C; ^{1}H NMR (CDCl$_3$): δ 7.33 (m, 2H), 7.12 (d, *J* 7.75 Hz, 2H), 7.07 (t, *J* = 7.33 Hz, 1H), 7.01 (d, *J*= 11.72 Hz, 2H), 6.92 (d, *J*= 11.70 Hz, 2H), 3.31 (s, 3H), 3.23 (s, 3H), 1.87 (s, 3H); ^{13}C NMR (CDCl$_3$): δ 170.95, 148.28, 136.33, 129.45, 127.54, 123.21, 122.97, 118.27, 40.26, 31.18, 22.33. Anal Calcd for C$_{16}$H$_{18}$N$_2$O: C, 75.56; H, 7.13; N, 11.01. Found: C, 75.41; H, 7.19; N, 11.12.

N,N′-Dimethyl-N-phenyl-1,4-benzenediamine (3). Diamine **5** (4.5 g, 17.7 mmol) and sodium hydroxide (5.4 g, 0.14 mol) were dissolved in ethanol/water (125 ml, 2:1 *(v/v))*. The reaction mixture was refluxed for 48 h and cooled to room temperature. The mixture was extracted with ethyl acetate, the combined organic layers were dried over MgSO$_4$, and the solvent was evaporated. Column chromatography (SiO$_2$, hexane/CH$_2$Cl$_2$ 2:1) resulted in a colorless viscous liquid (3.4 g, 90%). ^{1}H NMR (CDCl$_3$): δ 7.16 (m, 2H), 7.01 (d, *J* = 8.76 Hz, 2H), 6.71 (m, 3H), 6.59 (d, *J* = 8.73 Hz, 2H), 3.6 (s, 1H), 3.21 (s, 3H), 2.81 (s, 3H); ^{13}C NMR (CDCl$_3$): δ 150.06, 146.64, 139.08, 128.75, 127.29, 117.17, 114.31, 113.22, 40.39, 30.96.

N,N′-Bis[4-(methylphenylamino)phenyl]-N,N′-dimethyl-1,3-benzenediamine (tetramer) (2). An oven-dried Schlenk flask was charged with **3** (0.26 g, 1.2 mmol), 1,3-dibromobenzene (0.13 g, 0.55 mmol), sodium *tert*-butoxide (0.16 g, 1.7 mmol), Pd$_2$(dba)$_3$ (5.2 mg, 5.7 μmol), and S-BINAP (10.9 mg, 17.5 μmol). After purging with argon, dry toluene (4 ml) was added. The reaction mixture was heated for 48 h at 90 °C and cooled to room temperature. The mixture was taken up in diethyl ether, filtered over Celite 545 and concentrated in vacuo. Column chromatography (SiO$_2$, heptane/CH$_2$Cl$_2$ 2:1) and crystallization from toluene resulted in a white powder (82 mg, 30%). mp 175-176 °C; ^{1}H NMR (CDCl$_3$): δ 7.25-7.20 (m, 4H), 7.12 (t, *J* = 8.1 Hz, 1H), 7.01 (s, 8H), 6.91 (d, *J* = 7.7 Hz, 4H), 6.85 (t, *J* = 7.3 Hz, 2H), 6.58 (t, *J* = 2.2 Hz, 1H), 6.51 (dd, *J* = 8.1, 2.2 Hz, 2H), 3.28 (s, 6H), 3.27 (s, 6H); ^{13}C NMR (CDCl$_3$): δ 150.13, 149.35, 143.99, 143.35, 129.52, 129.01, 123.50, 122.72, 119.59, 117.87, 111.04, 109.37, 40.35; IR (KBr, cm^{-1}): 3055, 2952, 2869, 2806, 1594, 1497, 1325, 1253, 1184, 1130, 1088, 1026, 990, 952, 870, 839, 751, 695, 580, 510. Anal Calcd for C$_{34}$H$_{34}$N$_4$: C, 81.88; H, 6.87; N, 11.23. Found: C, 81.75; H, 6.93; N, 10.75.

N,N′-Dimethyl-1,4-benzenediamine (6). Lithium aluminum hydride (1.80 g, 47.4 mmol) was suspended in dry dioxane (40 ml) and a suspension of 1,4-benzenediisocyanate (3.2 g, 20 mmol) in dry dioxane (25 ml) was added in 1 h. The temperature was carefully monitored and was not allowed to rise above 40 °C (exothermic reaction !!). After 6 h at 40 °C, water (5 ml), 12 N NaOH (50 ml) were carefully added. The reaction mixture was filtered and concentrated in vacuo. After Kugelrohr distillation at 110 °C, a wet colorless solid was obtained (1.38 g, 50 %), which was used without additional purification. ^{1}H NMR (CDCl$_3$): δ 6.58 (s, 4H), 3.25 (s, 2H), 2.79 (s, 6H); ^{13}C NMR (CDCl$_3$): δ 141.84, 114.23, 31.89.

***N*-(3-Bromophenyl)-*N,N'*-dimethyl-*N'*-phenyl-1,4-benzenediamine (7).** An oven-dried Schlenk flask was charged with **3** (2.89 g, 13.6 mmol), sodium *tert*-butoxide (1.82 g, 18.9 mmol), Pd$_2$(dba)$_3$ (35.4 mg, 38.7 μmol), and S-BINAP (65.3 mg, 0.104 μmol). After purging with argon, 1,3-dibromobenzene (30 ml) was added. The reaction mixture was heated for 4 h at 90 °C and cooled to room temperature. The mixture was taken up in diethyl ether, filtered over Celite 545 and concentrated in vacuo. The excess 1,3-dibromobenzene was removed by distillation. Kugelrohr distillation at 200 °C resulted in a pale yellow oil (4.25 g, 85%) which became a solid in time. mp 100 °C; ^{1}H NMR (CDCl$_3$): δ 7.31-7.26 (m, 2H), 7.06-6.94 (m, 9H), 6.89 (d, *J* = 8.65 Hz, 1H), 6.72 (dd, *J* = 8.33, 2.24 Hz, 1H), 3.32 (s, 3H), 3.26 (s, 3H); ^{13}C NMR (CDCl$_3$): δ 150.73, 148.95, 145.64, 141.7, 130.08. Anal Calcd for C$_{20}$H$_{19}$BrN$_2$: C, 65.32; H, 5.21; N, 7.63. Found: C, 65.72; H, 5.29; N, 7.74.

***N,N'*-Bis[*N*-(*N*-methyl-*N*-phenyl-4-aminophenyl)-*N*-methyl-3-aminophenyl]-*N,N'*-dimethyl-1,4-benzenediamine (hexamer) (8).** An oven-dried Schlenk flask was charged with **7** (0.57 g, 1.6 mmol), **6** (0.09 g, 0.07 mmol), sodium *tert*-butoxide (0.23 g, 2.4 mmol), Pd$_2$(dba)$_3$ (4.0 mg, 4.3 μmol), and PPFA (5.7 mg, 13.0 μmol). After purging with argon, toluene (8 ml) was added. The reaction mixture was heated for 52 hours at 90 °C and cooled to room temperature. The mixture was taken up in chloroform, filtered over Celite 545 and concentrated in vacuo. The residue was twice crystallized from toluene, resulting in a white powder (0.24 g, 51 %). mp 210-212 °C; ^{1}H NMR (CDCl$_3$): δ 7.25-7.20 (m, 4H), 7.10 (t, *J* = 8.1 Hz, 2H), 7.00 (s, 12H), 6.91 (d, *J* = 7.7 Hz, 4H), 6.85 (t, *J* = 7.3 Hz, 2H), 6.56 (t, *J* = 2.2 Hz, 2H), 6.56 (dt, *J* = 8.1, 2.6 Hz, 4H), 3.27 (s, 6H), 3.26 (s, 6H), 3.25 (s, 6H); ^{13}C NMR (CDCl$_3$): δ 150.18, 150.10, 149.49, 144.03, 143.55, 143.29, 129.50, 129.02, 123.53, 122.97, 122.64, 119.57, 117.84, 110.94, 110.81, 109.06, 40.37; IR (KBr, cm^{-1}): 3027, 2902, 2816, 1592, 1495, 1326, 1260, 1178, 1134, 960, 853, 815, 763, 692, 593, 508. Anal Calcd for C$_{48}$H$_{43}$N$_6$: C, 81.32; H, 6.82; N, 11.85. Found: C, 81.55; H, 6.89; N, 11.53.

***N*-[*N*-(*N*-methyl-*N*-phenyl-4-aminophenyl)-*N*-methyl-3-aminophenyl]-*N,N'*-dimethyl-1,4-benzenediamine (9).** An oven-dried Schlenk flask was charged with **7** (1.94 g, 5.3 mmol), **6** (1.44 g, 10.6 mmol), sodium *tert*-butoxide (0.71 g, 7.4 mmol), Pd$_2$(dba)$_3$ (14.1 mg, 15.3 μmol), and PPFA (20 mg, 46 μmol). After purging with argon, toluene (25 ml) was added. The reaction mixture was heated for 60 h at 90 °C and cooled to room temperature. The mixture was taken up in dichloromethane, filtered over Celite 545 and concentrated in vacuo. Column chromatography (SiO$_2$, heptane/CH$_2$Cl$_2$ (1:3) and crystallization from heptane/toluene (9:1 *(v/v)*), resulted in a white powder (1.1 g, 50 %). ^{1}H NMR (acetone-d$_6$): δ 7.21-7.17 (m, 2H), 7.05-6.95 (m, 7H), 6.85 (d, *J* = 7.7 Hz, 2H), 6.78 (t, *J* = 7.3 Hz, 1H), 6.61 (d, *J* = 8.6 Hz, 2H), 6.38 (t, *J* = 2.2 Hz, 1H), 6.34 (dd, *J* = 7.8, 2.2 Hz, 1H), 6.31 (dd, *J* = 8.1, 2.2 Hz, 1H), 4.92 (s, 1H), 3.25 (s, 3H), 3.22 (s, 3H), 3.16 (s, 3H), 2.77 (s, 3H); ^{13}C NMR (acetone-d$_6$): δ 152.61, 151.15, 151.02, 148.84, 146.31, 143.78, 130.44, 130.33, 130.09, 128.34, 125.43, 122.49, 120.13, 118.17, 113.90, 110.59, 108.88, 107.77, 41.12, 40.99, 40.92, 31.07.

***N,N'*-Bis{*N*-[*N*-(*N*-methyl-*N*-phenyl-4-aminophenyl)-*N*-methyl-3-aminophenyl]-*N*-methyl-4-aminophenyl}-*N,N'*-dimethyl-1,3-benzenediamine (octamer) (10).** An oven-dried Schlenk flask was charged with **9** (0.9 g, 2.1 mmol), 1,3-dibromobenzene (0.24 g, 1 mmol), sodium *tert*-butoxide (0.29 g, 3.0 mmol), Pd$_2$(dba)$_3$ (5.3 mg, 5.8 μmol), and PPFA (7.7 mg, 17.4 μmol). After purging with argon, toluene (10 ml) was added. The reaction mixture was heated for 72 hours at 90 °C and cooled to room temperature. The mixture was taken up in dichloromethane, filtered and the remaining white solid was washed with water and crystallized twice from toluene, resulting in a white powder (30 mg, 35 %). mp 208-209 °C; ^{1}H NMR (CDCl$_3$, 323 K): δ 7.25-7.20 (m, 4H), 7.10 (t, *J* = 8.1 Hz, 2H), 7.00 (s, 12H), 6.91 (d, *J* = 7.7 Hz, 4H), 6.85 (t, *J* = 7.3 Hz, 2H), 6.56 (t, *J* = 2.2 Hz, 2H), 6.56 (dt, *J* = 8.1, 2.6 Hz, 4H), 3.26 (s, 6H), 3.24 (s, 6H), 3.23 (s, 6H), 3.22 (s, 6H); ^{13}C NMR (CDCl$_3$, 323K); δ 150.46, 150.43, 150.36, 149.62, 144.30, 143.91, 143.77, 143.58, 129.53, 129.06, 123.55, 123.11, 122.97, 122.74, 119.74, 118.12, 111.14, 111.00, 110.94, 104.40, 109.17, 40.35; IR (KBr, cm^{-1}):

3025, 2900, 2815, 1594, 1497, 1326, 1261, 1175, 1132, 1113, 1065, 959, 851, 814, 762, 691, 593, 506. Anal Calcd for $C_{62}H_{62}N_3$: C, 81.00; H, 6.80; N, 12.18. Found: C, 80.54; H, 6.87; N, 11.98.

***N,N',N''*-Tris(*N*-methyl-*N*-phenyl-4-aminophenyl)-*N,N',N''*-trimethyl-1,3,5-benzenetriamine (11).** An oven-dried Schlenk flask was charged with **3** (1.80 g, 8.48 mmol), 1,3,5-tribromobenzene (0.88 g, 2.8 mmol), sodium *tert*-butoxide (0.90 g, 9.4 mmol), Pd$_2$(dba)$_3$ (22.1 mg, 24.2 µmol), and PPFA (28.1 mg, 63.7 µmol). After purging with argon, dry toluene (10 ml) was added. The reaction mixture was heated for 72 h at 90 °C and cooled to room temperature. The mixture was taken up in diethyl ether and filtered over Celite 545 and concentrated in vacuo. Column chromatography (SiO$_2$, hexane/CH$_2$Cl$_2$ 3:1) resulted in a impure white powder. 100 mg of this powder was purified by means of preparative HPLC (reversed phase, THF/water 65:35) resulting in 90 mg pure white powder. mp 134-136 °C; ^{1}H NMR (CDCl$_3$): δ 7.23-7.19 (m, 6H), 7.02-6.99 (m, 12H), 6.88 (d, J = 7.73 Hz, 6H), 6.83 (t, J = 7.3 Hz, 3H), 6.20 (s, 3H), 3.26 (s, 9H), 3.24 (s, 9H); ^{13}C NMR (CDCl$_3$): δ 150.57, 149.39, 144.13, 142.93, 128.99, 123.67, 122.15, 119.37, 117.57, 103.47, 40.39, 40.34; IR (ATR, cm^{-1}): 3032, 2876, 2812, 1594, 1575, 1493, 1453, 1321, 1258, 1238, 1187, 1177, 1132, 1112, 1091, 1029, 990, 972, 870, 839, 823, 755, 748, 736, 717, 694, 651, 595, 576. Anal Calcd for $C_{48}H_{48}N_6$: C, 81.3; H, 6.8; N, 11.9. Found: C, 80.71; H, 6.78; N, 11.59.

***N'*-Acetyl-*N*-methyl-*N*-phenyl-1,4-benzenediamine (12).** Diamine **2** (4.5 g, 20 mmol), powdered sodium hydroxide (6.6 g, 0.17 mol), powdered potassium carbonate (16 g, 0.12 mol), tetrabutylammonium hydrogen sulfate (1.2 g, 3.5 mmol), and iodomethane (15 ml, 0.24 mol) were added to toluene (15 ml). The reaction mixture was stirred for 18 h at room temperature. Ethyl acetate was added and the salts were removed by filtration. Evaporation of the solvent, column chromatography (SiO$_2$, heptane/ethyl acetate.1:4) and crystallization from petroleum ether (60-80) resulting resulted in pale yellow crystals (2.46 g, 51%). mp 108 °C; ^{1}H NMR (CDCl$_3$): δ 7.32-7.26 (m, 2H), 7.12-6.97 (m, 7H), 5.94 (s, 1H), 3.24 (s, 3H), 1.89 (s, 3H); ^{13}C NMR (CDCl$_3$): δ 170.97, 142.97, 142.20, 136.85, 129.34, 127.84, 121.70, 118.58, 117.43, 37.18, 22.30. Anal Calcd for $C_{15}H_{15}N_2O$: C, 75.29; H, 6.32; N, 11.71. Found: C, 75.18; H, 6.74; N, 11.85.

***N*-Methyl-*N*-phenyl-1,4-benzenediamine (13).** Diamine **12** (0.36 g, 1.5 mmol) and sodium hydroxide (0.40 g, 10 mmol) were dissolved in ethanol/water (15 ml, 2:1 *(v/v))*. The reaction mixture was refluxed for 48 h and cooled to room temperature. The mixture was extracted with ethyl acetate, the combined organic layers were dried over MgSO$_4$, and the solvent was evaporated. Column chromatography (SiO$_2$, heptane/CH$_2$Cl$_2$ 2:1) resulted in a pale yellow viscous liquid (0.18 g, 88%). ^{1}H NMR (CDCl$_3$): δ 7.19-7.14 (m, 2H), 6.98 (d, J = 8.6 Hz, 2H), 6.76-6.71 (m, 3H), 6.68 (d, J = 8.6 Hz, 2H), 3.60 (s, 2H), 3.22 (s, 3H); ^{13}C NMR (CDCl$_3$): δ 149.96, 143.35, 140.40, 128.81, 127.03, 117.55, 116.13, 114.77, 40.41.

***N,N*-Bis[*N*-(*N*-methyl-*N*-phenyl-4-aminophenyl)-*N*-methyl-3-aminophenyl]-*N'*-methyl-*N'*-phenyl-1,4-benzenediamine (14).** An oven-dried Schlenk flask was charged with **7** (0.74 g, 2.0 mmol), **13** (0.18 g, 0.91 mmol), sodium *tert*-butoxide (0.24 g, 2.5 mmol), Pd$_2$(dba)$_3$ (5.4 mg, 5.9 µmol), and PPFA (6.7 mg, 15.2 µmol). After purging with argon, toluene (10 ml) was added. The reaction mixture was heated for 20 hours at 90 °C and cooled to room temperature. The mixture was taken up in diethyl ether, filtered over Celite 545 and concentrated in vacuo. Column chromatography (SiO$_2$, heptane/CH$_2$Cl$_2$ 2:1) and crystallization from ethanol resulted in a white powder (0.20 g, 30%). mp 64 °C; ^{1}H NMR (CDCl$_3$): δ 7.24-7.17 (m, 6H), 7.13 –6.83 (m, 29H), 6.70 (t, J = 2.0 Hz, 1H), 6.59 (t, J = 2.0 Hz, 1H), 6.55 (d, J = 7.49 Hz, 2H), 6.51 (dt, J = 8.1, 2.5 Hz, 2H), 3.25 (s, 12H), 3.20 (s, 3H); ^{13}C NMR (CDCl$_3$): δ 150.13, 149.95, 149.28, 148.68, 147.89, 144.43, 143.84, 143.75, 143.53, 143.49, 141.55, 129.51, 129.01, 128.95, 125.92, 123.48, 123.33, 123.25, 123.01, 122.93, 122.02, 121.87, 119.68, 119.59, 118.01, 117.85, 115.28, 113.50, 112.42, 111.40, 111.13, 109.66, 40.29; IR (ATR, cm^{-1}): 3051, 2872, 2807, 1591, 1506, 1485, 1325, 1259, 1171, 1130, 1111, 1089, 1026, 991, 941, 863, 823, 748, 693, 601, 571. Anal Calcd for $C_{53}H_{50}N_6$: C, 82.6; H, 6.5; N, 10.9. Found: C, 81.76; H, 6.43; N, 10.57.

N,N',N'-Triphenyl-1,4-benzenediamine (15). An oven-dried Schlenk flask was charged with N,N'-diphenyl-1,4-benzenediamine (0.26 g, 1.0 mmol), sodium *tert*-butoxide (0.15 g, 1.6 mmol), Pd$_2$(dba)$_3$ (9 mg, 9.8 µmol), and P(*o*-tolyl)$_3$ (12 mg, 39 µmol). After purging with argon, bromobenzene (145 µl, 1.4 mmol) and toluene (4 ml) were added. The reaction mixture was heated for 22 h at 90 °C and cooled to room temperature. The mixture was taken up in diethyl ether, filtered over Celite 545 and concentrated in vacuo. Column chromatography (SiO$_2$, heptane/CH$_2$Cl$_2$ 2:1) afforded white crystals (0.17 g, 51%). mp 125-127 °C; ^{1}H NMR (CDCl$_3$): δ 7.28-7.17 (m, 6H), 7.15-6.82 (m, 13H), 5.6 (bs, 1H); ^{13}C NMR (CDCl$_3$): δ 148.02, 141.41, 129.33, 129.08, 126.65, 123.15, 121.98, 120.56, 119.40, 117.12; IR (ATR, cm^{-1}): 3385, 3037, 1598, 1585, 1507, 1485, 1400, 1310, 1275, 1175, 1157, 1104, 1076, 1027, 1011, 994, 894, 875, 850, 830, 746, 691, 650, 634, 619, 609, 584. Anal Calcd for C$_{24}$H$_{20}$N$_2$: C, 85.68; H, 5.99; N, 8.33. Found: C, 83.54; H, 5.88; N, 8.08.

N-(3-Bromophenyl)-N,N',N'-triphenyl-1,4-benzenediamine (16). An oven-dried Schlenk flask was charged with **15** (3.41 g, 10.1 mmol), sodium *tert*-butoxide (1.52 g, 15.8 mmol), Pd$_2$(dba)$_3$ (25.2 mg, 27.5 µmol), and PPFA (31.0 mg, 70.2 µmol). After purging with argon, 1,3-dibromobenzene (40 ml) was added. The reaction mixture was heated for 45 h at 90 °C and cooled to room temperature. The mixture was taken up in diethyl ether, filtered over Celite 545 and concentrated in vacuo. The excess 1,3-dibromobenzene was removed by vacuum distillation. Column chromatography (SiO$_2$, heptane/CH$_2$Cl$_2$ 5:1) and crystallization from hexane resulted in white crystals (3.19 g, 64%). mp 128 °C; ^{1}H NMR (CDCl$_3$): δ 7.29-7.23 (m, 6H), 7.20-7.19 (m, 1H), 7.12-7.09 (m, 6H), 7.06-6.95 (m, 10H), 6.20-6.19 (m, 1H); ^{13}C NMR (CDCl$_3$): δ 149.37, 147.69, 147.14, 143.70, 141.74, 130.30, 129.39, 129.23, 126.02, 125.10, 125.03, 124.56, 124.39, 124.01, 123.29, 122.76, 122.65, 121.01; IR (ATR, cm^{-1}): 3036, 1585, 1505, 1484, 1331, 1308, 1266, 1178, 1153, 1118, 1105, 1072, 1027, 1005, 956, 918, 895, 831, 816, 761, 746, 711, 699, 689. Anal Calcd for C$_{30}$H$_{23}$BrN$_2$: C, 73.32; H, 4.71; N, 5.70. Found: C, 73.19; H, 4.71; N, 5.70.

N-[N-(N,N-Diphenyl-4-aminophenyl)-N-phenyl-3-aminophenyl]-N,N'-diphenyl-1,4-benzenediamine (17). An oven-dried Schlenk flask was charged with **16** (2.36 g, 4.8 mmol), N,N'-diphenyl-1,4-benzenediamine (1.94 g, 7.5 mmol), sodium *tert*-butoxide (1.14 g, 11.9 mmol), Pd$_2$(dba)$_3$ (13.0 mg, 14.2 µmol), and PPFA (16.1 mg, 36.5 µmol). After purging with argon, toluene (40 ml) was added. The reaction mixture was heated for 90 h at 90 °C and cooled to room temperature. The mixture was taken up in dichloromethane, filtered over Celite 545 and concentrated in vacuo. Column chromatography (SiO$_2$, heptane/CH$_2$Cl$_2$ (1:1) afforded a pale yellow powder (2.45 g, 76%). mp 88-90 °C; ^{1}H NMR (CDCl$_3$): δ 7.25-7.15 (m, 12H), 7.10-6.88 (m, 22H), 6.85 (t, *J*=2.0 Hz, 1H), 6.63 (t, *J*=6.7 Hz, 2H), 5.57 (bs, 1H);^{13}C NMR (CDCl$_3$): δ 148.44, 147.81, 147.46, 142.73, 142.68, 141.20b, 129.56b, 129.29b, 129.12b, 129.03b, 126.62, 125.55, 125.43, 123.62, 123.56, 123.11, 122.27, 121.97, 120.45b, 119.39b, 118.01b, 117.04b; IR (ATR, cm^{-1}): 3032, 1584, 1504, 1482, 1266, 1171, 1110, 1075, 1028, 875, 828, 749, 695, 628. Anal Calcd for C$_{48}$H$_{38}$N$_4$: C, 85.94; H, 5.71; N, 8.35. Found: C, 85.78; H, 5.58; N, 8.30.

N,N'-Bis{N-[N-(N,N-diphenyl-4-aminophenyl)-N-phenyl-3-aminophenyl]-N-phenyl-4-aminophenyl}-N,N'-diphenyl-1,3-benzenediamine (18). An oven-dried Schlenk flask was charged with **17** (0.93 g, 1.4 mmol), 1,3-dibromobenzene (0.17 g, 0.72 mmol), sodium *tert*-butoxide (0.29 g, 3.0 mmol), Pd$_2$(dba)$_3$ (4.0 mg, 4.4 µmol), and PPFA (4.5 mg, 10 µmol). After purging with argon, dry toluene (5 ml) was added. The reaction mixture was heated for 96 h at 90 °C and cooled to room temperature. The mixture was taken up in diethyl ether and filtered. The residue was washed with water and taken up in chloroform dried over MgSO$_4$, filtered and concentrated in vacuo. The resulting solid was dissolved in DMF and precipitated in methanol resulting in a white powder (0.30 g, 29%). mp 255-258 °C; ^{1}H NMR (CDCl$_3$): δ 7.24-7.16 (m, 20H), 7.08-7.05 (m, 23H), 6.99-6.92 (m, 26H), 6.85-6.83 (m, 3H), 6.66-6.60 (m, 6H); ^{13}C NMR (CDCl$_3$): δ 148.48, 147.80, 147.48, 142.85, 142.59, 142.54, 129.65, 129.15, 129.05, 125.48, 125.30, 123.71, 123.59, 122.36, 122.33, 118.49, 117.39; IR (ATR, cm^{-1}): 3036, 1585, 1505, 1485, 1312, 1266, 1170, 1148, 1115, 1076, 1028, 859, 830,

774, 754, 733, 707, 693, 677, 649, 643, 629.Anal Calcd for $C_{102}H_{78}N_8$: C, 86.53; H, 5.55; N, 7.91. Found: C, 86.88; H, 5.60; N, 8.14.

3.8 References

1. Moll, T.; Heinze, J., *Synth. Met.* **1993**, *55*, 1521.
2. Strohriegl, P.; Jesberger, G.; Heinze, J.; Moll, T., *Makromol. Chem.* **1992**, *193*, 909.
3. Cauquis, G.; Serve, D., *Anal. Chem.* **1972**, *44*, 2222.
4. Wienk, M. M.; Janssen, R. A. J., *J. Am. Chem. Soc.* **1996**, *118*, 10626.
5. Wienk, M. M.; Janssen, R. A. J., *J. Am. Chem. Soc.* **1997**, *119*, 4492.
6. Wienk, M. M.; Janssen, R. A. J., *Chem. Commun.* **1996**, 267.
7. Stickley, K. R.; Selby, T. D.; Blackstock, S. C., *J. Org. Chem.* **1997**, *62*, 448.
8. Yoshizawa, K.; Tanaka, K.; Yamabe, T.; Yamauchi, J., *J. Chem. Phys.* **1992**, *96*, 5516.
9. Yoshizawa, K.; Chano, A.; Ito, A.; Tanaka, K.; Yamabe, T.; Fujita, H.; Yamauchi, J.; Shiro, M., *J. Am. Chem. Soc.* **1992**, *114*, 5994.
10. Nakamura, Y.; Iwamura, H., *Bull. Chem. Soc. Jpn.* **1993**, *66*, 3724.
11. Stickley, K. R.; Blackstock, S. C., *J. Am. Chem. Soc.* **1994**, *116*, 11575.
12. Ito, A.; Ota, K.; Tanaka, K.; Yamabe, T.; Yoshizawa, K., *Macromolecules* **1995**, *28*, 5618.
13. Yano, M.; Sato, K.; Shiomi, D.; Ichimura, A.; Abe, K.; Takui, T.; Itoh, K., *Tetrahedron Lett.* **1996**, *37*, 9207.
14. Bushby, R. J.; Ng, K. M., *Chem. Commun.* **1996**, 659.
15. Sato, K.; Yano, M.; Furuichi, M.; Shiomi, D.; Takui, T.; Abe, K.; Itoh, K.; Higuchi, A.; Katsuma, K.; Shirota, Y., *J. Am. Chem. Soc.* **1997**, *119*, 6607.
16. Selby, T. D.; Blackstock, S. C., *J. Am. Chem. Soc.* **1999**, *121*, 7152.
17. Selby, T. D.; Blackstock, S. C., *Org. Lett.* **1999**, *1*, 2053.
18. Hauck, S. I.; Lakshmi, K. V.; Hartwig, J. F., *Org. Lett.* **1999**, *1*, 2057.
19. Ullmann, F., *Ber. Dtsch. Chem. Ges.* **1903**, *36*, 2382.
20. Goldberg, I.; Nimerovsky, M., *Ber. Dtsch. Chem. Ges.* **1907**, *40*, 2451.
21. Gauthier, S.; Fréchet, J. M. J., *Synthesis* **1987**, 383.
22. Buu-Hoï, N. P., *J. Chem. Soc.* **1952**, 4346.
23. Ochi, M.; Furusho, H.; Tanaka, J., *Bull. Chem. Soc. Jpn.* **1994**, *67*, 1749.
24. Lantz, R. L.; Obellianne, P., *Bul. Soc. Chim. Belg.* **1956**, 311.
25. Hall Jr, H. K.; Polis, D. W., *Polym. Bull.* **1987**, *17*, 409.
26. Honzl, J.; Tlustakova, M., *J. Polym. Sci. C* **1968**, 451.
27. Lu, F.-L.; Wudl, F.; Nowak, M.; Heeger, A. J., *J. Am. Chem. Soc.* **1986**, *108*, 8311.
28. Ito, A.; Saito, T.; Tanaka, K.; Yamabe, T., *Tetrahedron Lett.* **1995**, *36*, 8809.
29. Kosugi, M.; Kameyama, M.; Migita, T., *Chem. Lett.* **1983**, 927.
30. Paul, F.; Patt, J.; Hartwig, J. F., *J. Am. Chem. Soc.* **1994**, *116*, 5969.
31. Guram, A. S.; Buchwald, S. L., *J. Am. Chem. Soc.* **1994**, *116*, 7901.
32. Louie, J.; Hartwig, J. F., *Tetrahedron Lett.* **1995**, *36*, 3609.
33. Guram, A. S.; Rennels, R. A.; Buchwald, S. L., *Angew. Chem., Int. Ed. Engl.* **1995**, *34*, 1348.

34.   Hartwig, J. F., *Angew. Chem., Int. Ed.* **1998**, *37*, 2047.

35.   Wolfe, J. P.; Wagaw, S.; Marcoux, J. F.; Buchwald, S. L., *Acc. Chem. Res.* **1998**, *31*, 805.

36.   Driver, M. S.; Hartwig, J. F., *J. Am. Chem. Soc.* **1996**, *118*, 7217.

37.   Wolfe, J. P.; Wagaw, S.; Buchwald, S. L., *J. Am. Chem. Soc.* **1996**, *118*, 7215.

38.   Wolfe, J. P.; Buchwald, S. L., *J. Org. Chem.* **2000**, *65*, 1144.

39.   Marcoux, J. F.; Wagaw, S.; Buchwald, S. L., *J. Org. Chem.* **1997**, *62*, 1568.

40.   Wolfe, J. P.; Buchwald, S. L., *Tetrahedron Lett.* **1997**, *38*, 6359.

41.   Old, D. W.; Wolfe, J. P.; Buchwald, S. L., *J. Am. Chem. Soc.* **1998**, *120*, 9722.

42.   Wolfe, J. P.; Buchwald, S. L., *Angew. Chem., Int. Ed.* **1999**, *38*, 2413.

43.   Hartwig, J. F.; Kawatsura, M.; Hauck, S. I.; Shaughnessy, K. H.; Alcazarroman, L. M., *J. Org. Chem.* **1999**, *64*, 5575.

44.   Singer, R. A.; Sadighi, J. P.; Buchwald, S. L., *J. Am. Chem. Soc.* **1998**, *120*, 213.

45.   Sadighi, J. P.; Singer, R. A.; Buchwald, S. L., *J. Am. Chem. Soc.* **1998**, *120*, 4960.

46.   Goodson, F. E.; Hartwig, J. F., *Macromolecules* **1998**, *31*, 1700.

47.   Goodson, F. E.; Hauck, S. I.; Hartwig, J. F., *J. Am. Chem. Soc.* **1999**, *121*, 7527.

48.   Koziara, A.; Zawadzki, S.; Zwierak, A., *Synthesis* **1979**, 527.

49.   Finholt, A. E.; Anderson, C. D.; Agre, C. L., *J. Org. Chem.* **1953**, *18*, 1338.

50.   Cordes, A. W.; Haddon, R. C.; Hicks, R. G.; Oakley, R. T.; Palstra, T. T. M.; Schneemeyer, L. F.; Waszczak, J. V., *J. Am. Chem. Soc.* **1992**, *114*, 5000.

51.   Kothe, G.; Nowak, C.; Denkel, K.-H.; Ohmes, E.; Zimmermann, H., *Angew. Chem.* **1970**, *82*, 521.

52.   Dulog, L.; Kim, J. S., *Angew. Chem., Int. Ed. Engl.* **1990**, *29*, 415.

53.   Okada, K.; Imakura, T.; Oda, M.; Kajiwara, A.; Kamachi, M.; Sato, K.; Shiomi, D.; Takui, T.; Itoh, K.; Gherghel, L.; Baumgarten, M., *J. Chem. Soc., Perkin Trans. 2* **1997**, 1059.

54.   Matsuda, K.; Nakamura, N.; Inoue, K.; Koga, N.; Iwamura, H., *Bull. Chem. Soc. Jpn.* **1996**, *69*, 1483.

55.   Veciana, J.; Rovira, C.; Ventosa, N.; Crespo, M. I.; Palacio, F., *J. Am. Chem. Soc.* **1993**, *115*, 57.

56.   Kanno, F.; Inoue, K.; Koga, N.; Iwamura, H., *J. Phys. Chem.* **1993**, *97*, 13267.

57.   Rajca, A.; Rajca, S.; Wongsriratanakul, J., *J. Am. Chem. Soc.* **1999**, *121*, 6308.

58.   Torrance, J. B.; Oostra, S.; Nazzal, A., *Synth. Met.* **1987**, *19*, 709.

59.   Sasaki, S.; Iyoda, M., *Chem. Lett.* **1995**, 1011.

4

Cation radicals of aniline oligomers with *meta* linkages

Abstract: *Oligo(cation radicals) obtained from linear and branched m-p-aniline oligomers are characterized by means of cyclic voltammetry, UV/visible/nearIR spectroscopy, and ESR spectroscopy. The observed properties are consistent with low-energy high-spin states. The largest oligomers, being octaanilines with either N-methyl or N-phenyl groups, show the limited capability of ESR spectroscopy to unambiguously identify the quintet (S = 2) states for nitrogen-centered oligo(cation radicals).*

4.1 Introduction

The high electric conductivity of polyaniline originates from the π-conjugation along the backbone combined with a low ionization potential, making it possible to create stable charges by doping with an oxidizing agent. In general doping of π-conjugated organic polymers creates highly energetic charged radicals that rearrange to a less energetic quinoidal form. Polyaniline based materials are an exception to this general principle, here the radicals are better stabilized making this the lower energetic state (Scheme 4.1). Polyaniline can be regarded as consisting of a chain of *p*-benzenediamine units with electron-rich properties able to bear a stable cation radical when oxidized. The diarylamine bearing the cation radical is stabilized by the donating effect of the aniline-unit at the *para*-position. Both functional groups are chemically indistinguishable, allowing for delocalisation of the charge over the 1,4-benzenediamine unit by π-conjugation, adding to the stability of the system. Manipulation of the substituents allows for tuning of the redox properties of the material.
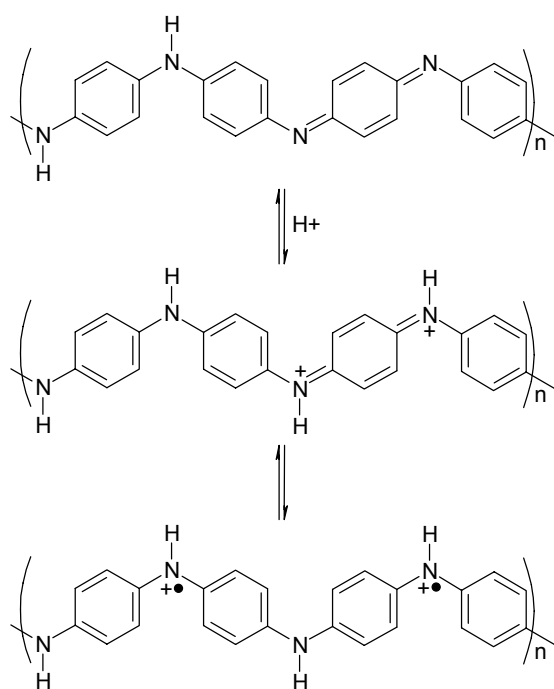
Scheme 4.1. *Doping of poly-p-aniline resulting in conducting polyaniline with an average of one cation radical per two aniline units. Step 1: protonation of the imines, step 2: redox reaction between protonated imines and amines.*

Many different concepts and strategies towards organic ferromagnets have been developed during the second half of the previous century, leading to the discovery of organic materials with magnetic properties[1-5]. The fact that very few organic

polyradicals reported show stability at ambient temperatures, stimulated Fukutome[6] to put forward the concept of the polaronic organic ferromagnet, proposing a polymer where π-conjugated segments are alternated with ferromagnetic coupling units (FCU) (Figure 4.1). The π-conjugated segments are then reductively or oxidatively doped, generating stable unpaired electrons or spins on every unit which may result in a high-spin polyradical. The unusual stability of the cation radicals in doped polyaniline attracted the attention of researchers in the field of organic ferromagnets. This led to the development of various materials containing aniline derivatives as spin carriers in organic ferromagnets[7-21].
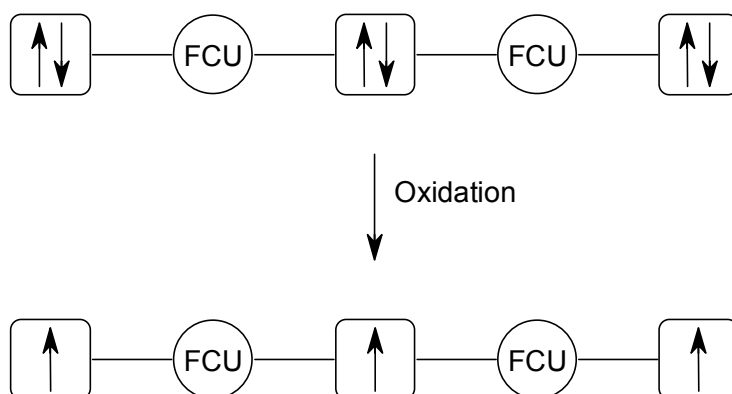

Figure 4.1. *Schematic representation of the polaronic organic ferromagnet. Doping, in this case oxidation, creates unpaired electrons aligned via a ferromagnetic coupling unit(FCU).*

Combination of the concept of the polaronic organic ferromagnet with polyaniline implies the introduction of *meta*-benzene as FCU in the polyaniline chain. As a result two basic structures are possible candidates for high-spin polyradicals; poly-*m-p*-aniline and poly-*m*-aniline (Figure 4.2).

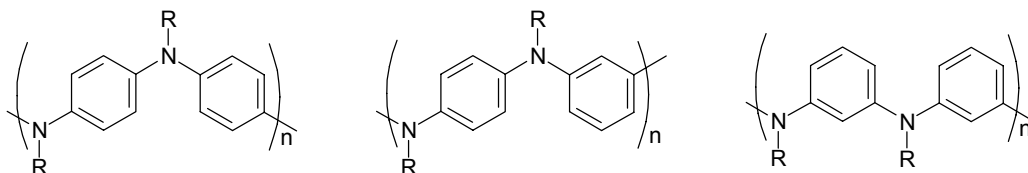**Figure 4.2.** *Three topologically different polyanilines; left: poly-p-polyaniline, middle: poly-m-p-aniline, right: poly-m-aniline.*

Oligomers with alternating *meta-para* topology were synthesized and characterized both by Wienk et al.[16-18] and Blackstock et al.[14]. The corresponding oligo(cation radicals) exhibit a ground state high-spin state and are stable at ambient temperatures (Figure 3.1).
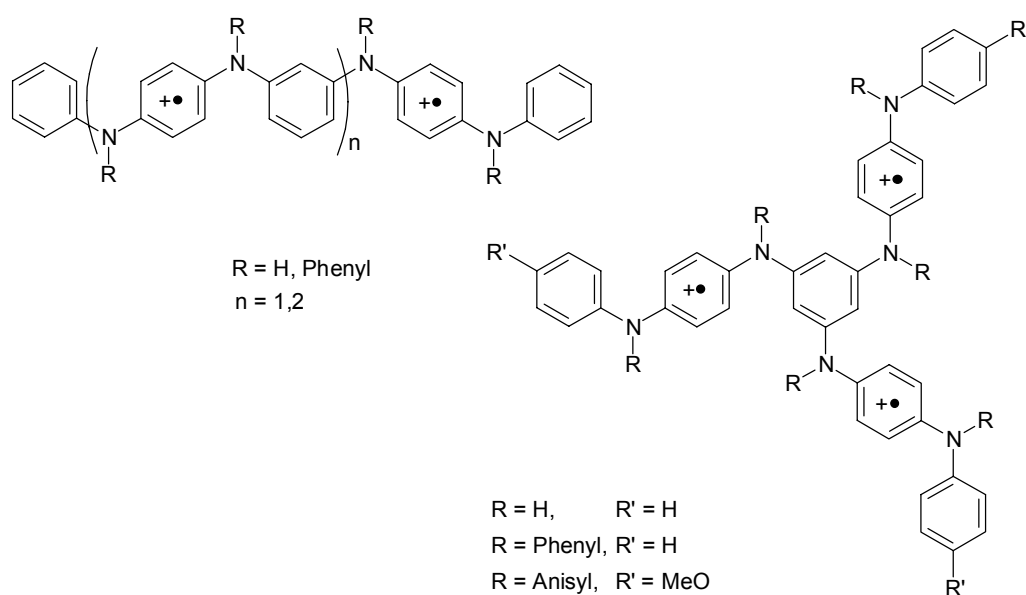
Figure 4.3. *High-spin m-p-oligoanilines reported in literature. Linear oligomers and star-shaped oligomers with R=H or Phenyl and R'=H by Wienk et al.[16-18] Star-shaped oligomers with R=Phenyl, R'=H and R=Anisyl, R'=MeO by Blackstock et al.[14]*

Oligomers of poly-*m*-aniline with R=H reported in literature showed unstable behavior of the cation radicals when oxidized[22,23]. Later on this problem has been overcome by substituting the nitrogens with phenyl-groups that are blocked at the *para*-positions with electron donating groups[10,12,15,24](Figure 4.4). Still low temperatures are necessary to keep the oxidized compounds stable.

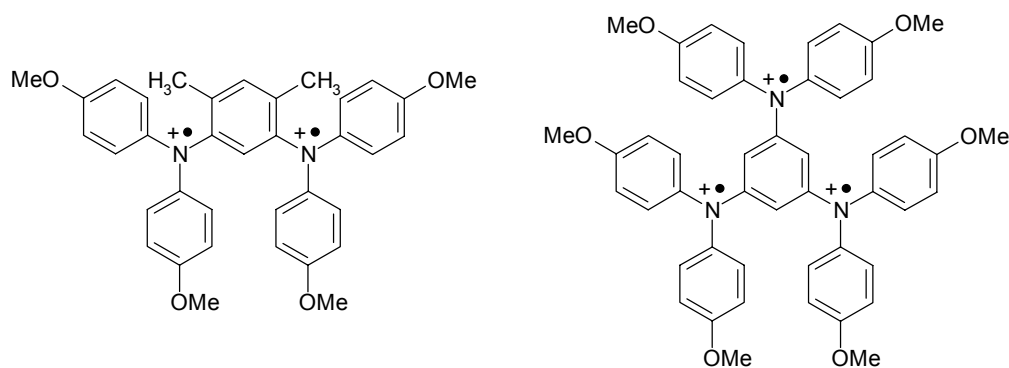**Figure 4.4.** *Substituted oligo-m-anilines with stable high-spin states of the corresponding cation radicals at low temperatures. Left: 1,3-Bis(diarylamino)benzene of Itoh et al.[12], right: hexaanisyl-1,3,5-triaminobenzene of Blackstock et al.[10]*

In chapter 3 the synthesis of several *N*-methyl oligoanilines and a *N*-phenyl-*m*-*p*-octaaniline was reported (Figure 4.5). These oligomers were synthesized for the purpose

of studying their magnetic properties. Therefore, in this chapter they are characterized using cyclic voltammetry (C.V.), UV/visible/nearIR spectroscopy, and electron spin resonance spectroscopy (ESR spectroscopy) in order to determine the redox, optical and high-spin properties of these oligoanilines.
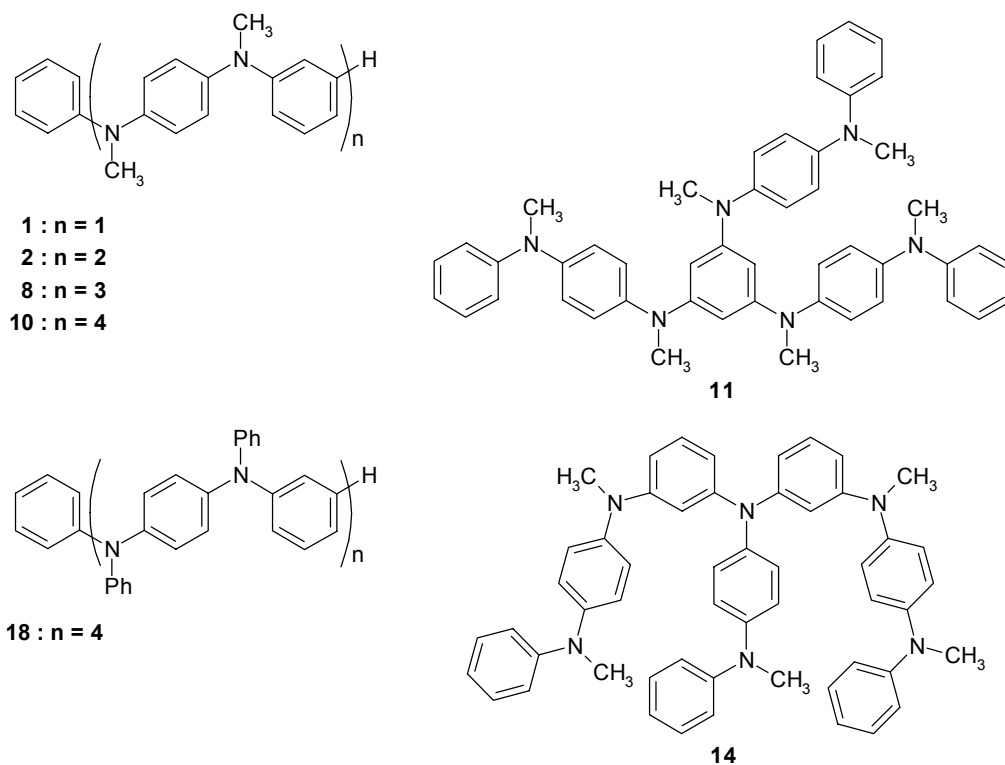

1 : n = 1
2 : n = 2
8 : n = 3
10 : n = 4

18 : n = 4

11

14

Figure 4.5. *Oligoanilines characterized in this chapter.*

Electrochemistry by means of cyclic voltammetry provides information on the redox behavior and the chemical stability of the different redox states. The availability of a series of linear oligomers opens the opportunity to study the influence of oligomer length on the oxidation potential. The oxidation of oligoanilines can also be accomplished with oxidizing agents and can be monitored with UV/visible/nearIR spectroscopy. The optical properties of the oligoanilines change when they are oxidized, exhibiting characteristic absorption bands for each oxidation state. These specific absorption bands allow to monitor the tuning of the oligoaniline to the desired oligo(cation radical) oxidation state. ESR spectroscopy can be used to study the spin state of the oligo(cation radicals). ESR spectra reveal information on the interactions between the unpaired electrons and on the interaction of the unpaired electron(s) with the magnetic nuclei. In a dilute frozen solution there are no intermolecular interactions between the spins of the different molecules. From the ESR-spectrum information on distance and (anti-)ferromagnetic spin alignment between the unpaired electrons can be obtained.

4.2 Cation radicals of linear *N*-methyl substituted aniline oligomers

4.2.1 Cation radicals by cyclic voltammetry

The redox behavior of the *N*-methyl substituted oligomers (**1**, **2**, **8**, **10**) is depicted in Figure 1.8 and the oxidation potentials are summarized in Table 4.1. The cyclic voltammogram of dimer **1** shows two one-electron oxidations and their corresponding reduction waves. The first oxidation occurs at 0.41 V resulting in the cation radical of **1**; increasing the voltage leads to the dication at 1.01 V. The anodic and cathodic waves are separated by 110 mV, which is almost double the theoretically expected value of 59 mV for a one-electron process. Measuring at different scan rates, typically 50, 100, and 200 mV/s shows that a decrease of the scan rate results in a decrease of this gap. Since both oxidation processes are chemically reversible it can be concluded that this *para*-benzenediamine unit provides stable cation radicals and dications in solution at ambient temperature upon one- and two-electron oxidation, respectively.
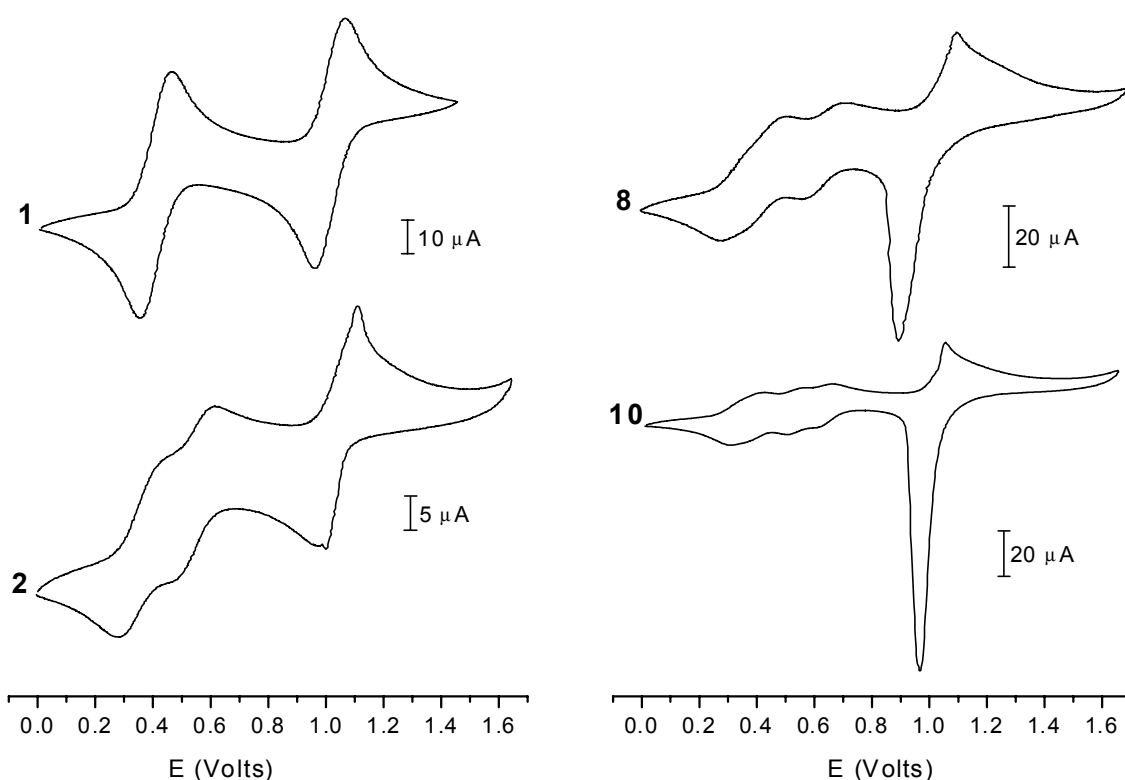

Figure 4.6. *Cyclic voltammograms of linear N-methylaniline oligomers; top, left: dimer **1**; bottom, left: tetramer **2**; top, right: hexamer **8**; bottom, right: octamer **10**. Conditions: 0.1 M TBAHF in CH$_2$Cl$_2$ at 295 K, scan rate 100 mV/s. Potential vs. SCE reference and calibrated against Fc/Fc$^+$ couple at 0.46 V.*

The oxidation potentials of **1** have been reported previously for three different media, dichloromethane[25], chloroform[26] and acetonitrile[27], against Ag/Ag$^+$, but only the first two publications report a value vs. Fc/Fc$^+$, which allows for comparison. Using the reported Fc/Fc$^+$ value, E_1^0 and E_2^0 values can be recalculated to the internal standard Fc/Fc$^+$ = 0.46V used here. Cauquis and Serve[26] (Fc/Fc$^+$ = –0.35 V) found 0.38 and 0.88 V whereas Moll and Heinze[25] (Fc/Fc$^+$ = 0.35 V) found 0.51 and 1.01 V for the E_1^0 and E_2^0 respectively. These values are in the same range as the values found here, 0.41 and 1.01 V. A striking difference, however, is the 0.5 V difference between E_1^0 and E_2^0 compared to 0.6 V reported here.

The redox characteristics of tetramer **2** show a similar behavior. The cation radical is formed at 0.36 V, which is 50 mV lower in comparison with the dimer. Apparently the extra *para*-benzenediamine unit, although not conjugated due to the 1,3-benzene linkage, exerts an electron releasing influence and lowers the first oxidation potential. The presence of a cation radical in the tetramer makes it more difficult, due to electrostatic repulsion, to oxidize the molecule to the di(cation radical), resulting in a higher value of the second oxidation potential; 0.53 V. The splitting between the two pairs of anodic and cathodic waves are 160 mV for the first as well as the second oxidation wave and show a similar scan rate dependence as found for **1**. The third wave is an unresolved two-electron oxidation and corresponds to the formation of the tri- and tetracation at 1.04 V with a peak-to-peak separation of 130 mV. The abnormal shape of this redox wave is likely to result from the limited solubility of the highly charged state.

Table 4.1. *Electrochemical data of the linear N-methylaniline oligomers* [a]

	E_1^0(V)	E_2^0(V)	E_3^0(V)	E_4^0(V)	E_5^0(V)
Dimer **1**	0.41	1.01			
Tetramer **2**	0.36	0.53	1.04[b]		
Hexamer **8**	0.33	0.44	0.64	1.00[b]	
Octamer **10**	0.38[b]	0.38[b]	0.55	0.64	1.02[b]

[a] *Conditions: 0.1 M TBAHF in CH$_2$Cl$_2$, 295 K. Potential vs. SCE reference and calibrated against Fc/Fc$^+$ couple at 0.46 V.* [b] *Peaks are unresolved.*

The first redox wave in the cyclic voltammogram of hexamer **8** can be regarded as a two-electron oxidation positioned at 0.39 V. A careful look however, reveals a small shoulder from which an approximation for two one-electron oxidation potentials can be made with a peak-peak separation of 110 mV. E_1^0 decreases from 0.41 V to 0.33 V going from the dimer **1** to the hexamer **8**. This can be explained if we consider that the cation radical is localized at the central unit which carries two electron donating units on both sites stabilizing the charge. When hexamer **8** is oxidized to the di(cation radical) state,

the two positive charges will repel each other and likely be localized at the terminal *para*-benzenediamine units. This, in turn, increases the oxidation potential for the third wave, which is positioned at the significantly higher potential of 0.64 V.

The octamer **10** possesses one additional unit but the effect on the oxidation potential is small. When the cation radical is formed it will probably be located on one of the two central units, which are chemically identical. In terms of stabilization of the charge they behave similar with respect to the central unit of the hexamer as described above, and E_1^0 will not be expected to be much different. Oxidation to the di(cation radical) creates an extra charge which can be localized at the two ends of the molecule without much repulsion from the central cation radical and therefore E_2^0 will be lower then the E_2^0 of the hexamer. This results in the observed two-electron redox wave at 0.38 V, which cannot be resolved. The second redox wave at 0.55 V leads to the formation of the tri(cation radical). This third oxidation step bears much resemblance with the second oxidation step of the tetramer **2** that has a value of 0.53 V and $E_4^0 = 0.64$ V is approximately at the same value as E_3^0 of the hexamer, because in both cases a charge has to be created in between two units that are already oxidized. From these considerations it can be expected that the oxidation potentials for the formation of multiple cation radicals on even longer oligomers will be in the range of 0.33 to 0.64 V.

The redox waves of hexamer **8** to the hexacation and of octamer **10** to the octacation are unresolved and exhibit a very large reduction peak. This cathodic wave is more pronounced for the longer oligomers. The same observation was made by Moll and Heinze[25] for the *N*-methyl-*p*-hexamer, they explain that this phenomenon is caused by the insoluble nature of these highly charged states, causing precipitation on the working electrode. Reconsidering the cyclic voltammogram of tetramer **2**, there is already a small indication of the same behavior because the anodic and cathodic waves have not the same intensity. All oligomers show a substantial potential gap between the oxidation towards the multiple cation radical state and the fully oxidized state. This gap makes is possible to tune the oxidation state of the molecule in their highest oligo(cation radical) state.

4.2.2 Optical properties of the cation radicals

The electronic absorption spectrum of neutral dimer **1** in dichloromethane shows two bands at 4.05 and 4.94 eV (Figure 4.7), similar to the values found by Weller and Grellmann[28] of 5.0 eV (248 nm) and 4.08 eV (304 nm), obtained in methylcyclohexane.
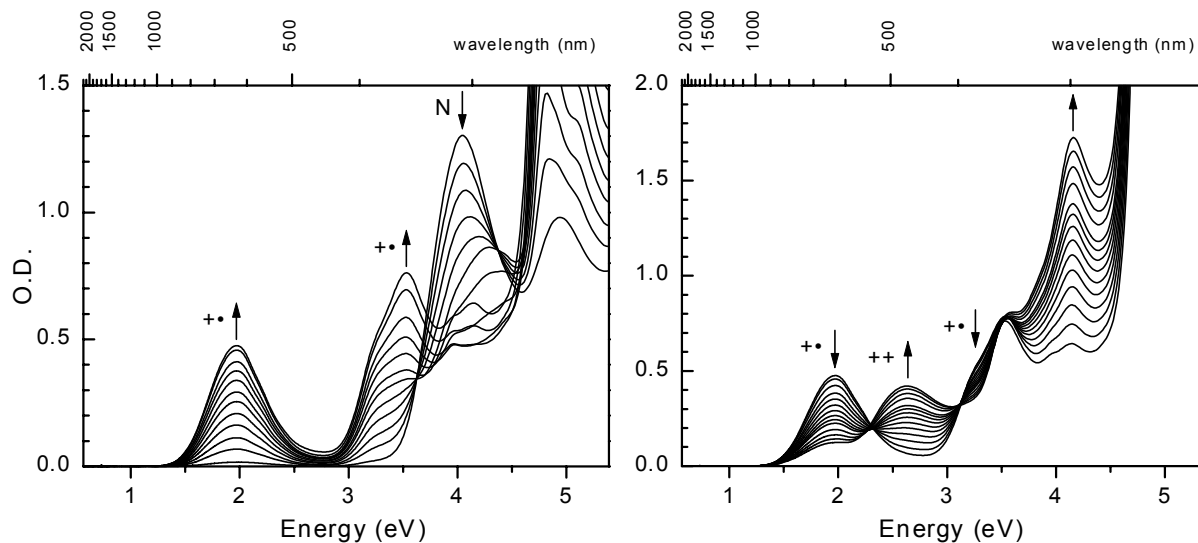
Figure 4.7. *UV/visible/nearIR spectra recorded during the conversion of **1** by stepwise oxidation with THI$^{+\bullet}$ClO$_4^-$ in CH$_2$Cl$_2$ at 295 K; left: from the neutral state to the cation radical; right: from the cation radical to the dication.*

The band at 4.05 eV decreases upon stepwise addition of small quantities of THI$^{+\bullet}$ClO$_4^-$. Although the accompanying band at 4.94 eV increases upon addition of oxidant, this increase is actually due to the formation of neutral thianthrene (4.82 eV), which results from the reduction of thianthrenium. Two new absorption bands appear, which are attributed to the formation of cation radicals, one at 1.98 eV and one as a shoulder of the neutral band at 3.25-3.50 eV. They reach their maximum intensity at 1.97 and 3.53 eV, after addition of one equivalent of THI$^{+\bullet}$ClO$_4^-$. Cauquis and Serve[26] observed three absorption bands at 1.99 (623 nm), 3.48 (356 nm) and 3.91 eV (317 nm) respectively for electrochemically generated **1**$^{+\bullet}$ in chloroform. A careful look at the absorption spectrum of **1**$^{+\bullet}$ in Figure 4.7 shows also a small third absorption at 4.13 eV, which might be shifted to higher energy due to the presence of the large thianthrene absorption. Further oxidation leads to a decrease of the cation radical bands and new absorption bands are observed at 2.63 and 4.16 eV. They are indicative for removal of a second electron from the *para*-benzenediamine and the formation of a dication of **1** (**1**$^{2+}$). The reversibility of the whole oxidation process was checked by reduction of the solution with an excess of hydrazine monohydrate, resulting in a recovery of the spectrum of neutral **1**.

From the spectral information a molecular orbital diagram can be constructed for the different oxidation states (Figure 4.8). The removal of one electron from the HOMO of **1** results in two absorptions typical for a cation radical, one at low energy for the HOMO-SOMO transition and one at high energy for the SOMO-LUMO transition. Further oxidation leads to an absorption band corresponding to the new HOMO-LUMO

transition, which for π-conjugated systems is often positioned in between the two cation radical absorptions.
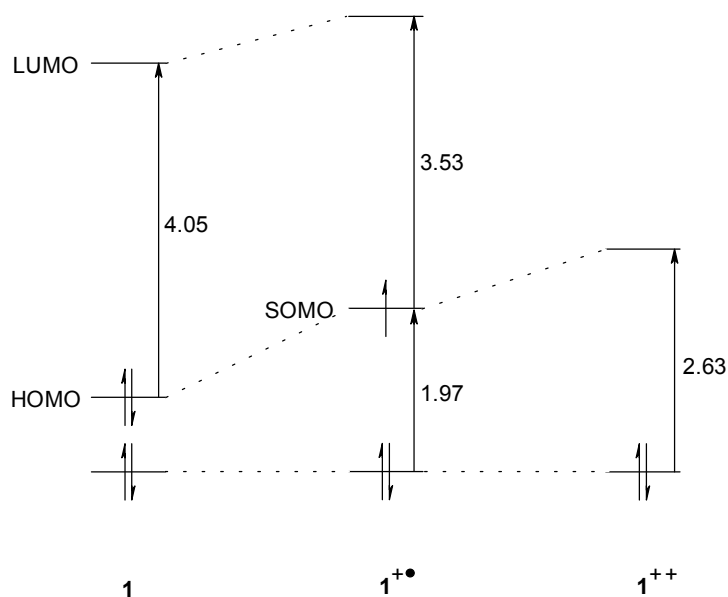
Figure 4.8. *Molecular orbital diagram of **1** as function of the oxidation state based on information derived from the electronic absorption spectra. Transitions are depicted with vertical arrows, numbers are in eV. The position of the penultimate highest occupied molecular orbital is assumed to be constant.*
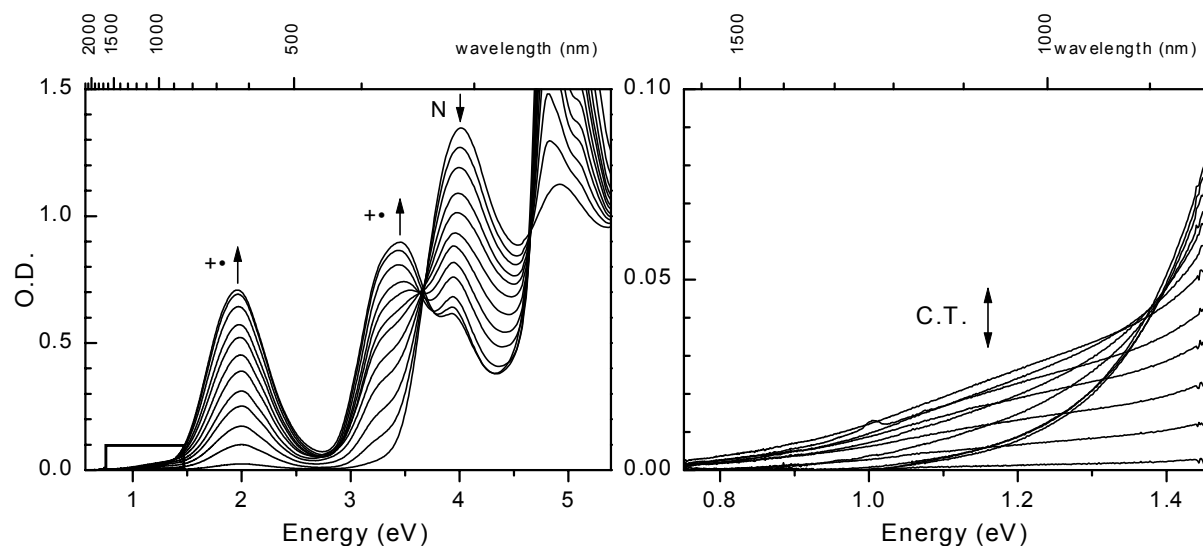
Figure 4.9. *UV/visible/nearIR spectra recorded during the conversion of **2** by stepwise oxidation with THI*$^{+\bullet}$*ClO₄*$^{-}$ *in CH₂Cl₂ at 295 K; left: from neutral state to the di(cation radical), a black rectangular area is drawn around the position of charge transfer band; right: Magnified nearIR area from figure shown on the left.*

In dichloromethane the spectrum of neutral **2** shows bands at 4.01 eV and 4.91 eV, which decrease on addition of THI$^{+\bullet}$ClO$_4^-$ (Figure 4.9), to give the cation radical absorption bands at 1.96, 3.45, and 3.93 eV. This oxidation process shows a similar behavior as for dimer **1**, indicating that the conjugation length of the molecule has not increased. This is due to the *meta*-benzene linkage in the molecule, which results in localization of each cation radical to one *para*-benzenediamine unit. When the low energy area of the spectra recorded during oxidation is magnified, a charge transfer band (C.T. band) is observed. This band reaches a maximum when tetramer **2** is oxidized to the mono(cation radical) state. In this situation half of the molecule is oxidized and the other half is in the neutral state, a so-called mixed valence molecule. The C.T. band represents the intramolecular electron transfer from the reduced side to the oxidized side of the molecule. Further oxidation to the di(cation radical) state results in the gradual disappearance of this band, which is in full agreement with its assignment to a C.T. band of a mixed valence state.
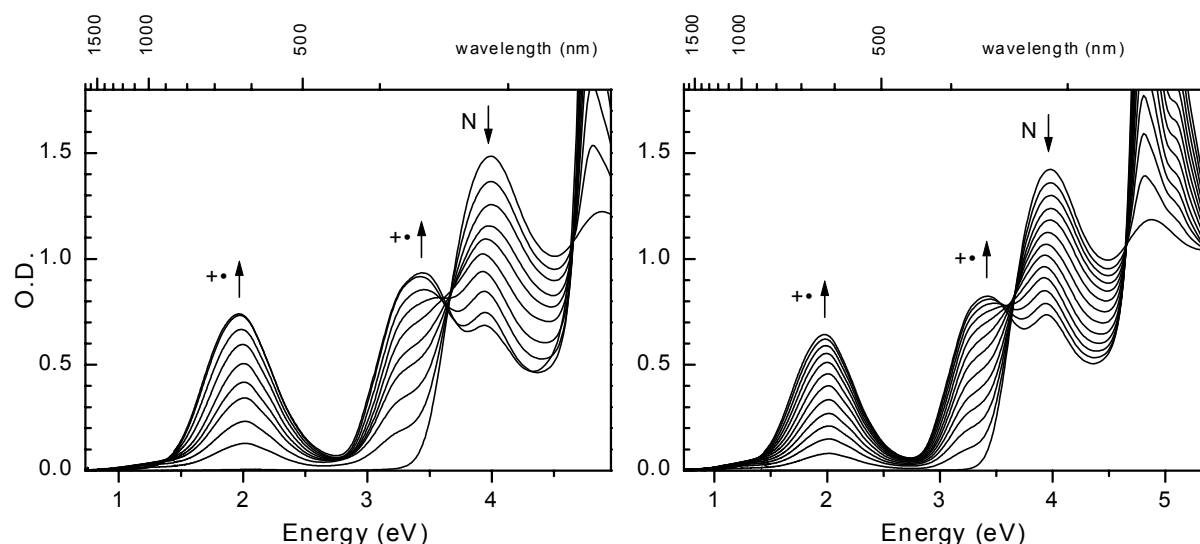
Figure 4.10. *UV/visible/nearIR spectra recorded during the conversion of hexamer **8** (left) and octamer **10** (right) by stepwise oxidation with THI$^{+\bullet}$ClO$_4^-$ in CH$_2$Cl$_2$ at 295 K from the neutral state to the tri(cation radical) and tetra(cation radical) respectively.*

The electronic absorption spectra recorded for the same stepwise oxidation experiment done with hexamer **8** and octamer **10** show a similar result (Figure 4.10). In these experiments the C.T. band is also present but less intense. The optical data of the linear *N*-methylaniline oligomers are summarized in table 4.2.

Table 4.2. *Optical data of the linear N-methylaniline oligomers* [a]

	Neutral, eV (nm)		Oligo(cation radical), eV (nm)		
Dimer **1**	4.05 (306)	4.94 (251)	1.97 (629)	3.53 (351)	3.91 (317)
Tetramer **2**	4.01 (309)	4.91 (253)	1.96 (633)	3.45 (359)	3.93 (316)
Hexamer **8**	3.99 (311)	4.88 (254)	1.97 (629)	3.44 (360)	3.94 (315)
Octamer **10**	3.98 (312)	4.88 (254)	1.98 (626)	3.43 (362)	3.94 (315)

[a] *Conditions: CH$_2$Cl$_2$, oxidation with THI$^{+\bullet}$ClO$_4^-$, 295 K.*

Cation radicals of π-conjugated organic materials tend to form spinless dimers and this processes may restrict the use of these materials for creating polaronic ferromagnets[29]. To check whether *N*-methylaniline oligomers are sensitive to this phenomenon, a variable temperature experiment was conducted with the di(cation radical) of tetramer **2** in dichloromethane (Figure 4.11). In the temperature range of 185 to 295 K, no absorption bands could be detected that can be attributed to the formation of dimers, which are usually apparent as shoulders approximately 0.3 eV to higher energy. The sole effect observed is a slight increase of the spectrum as a result of the temperature dependent volume and hence increasing concentration.
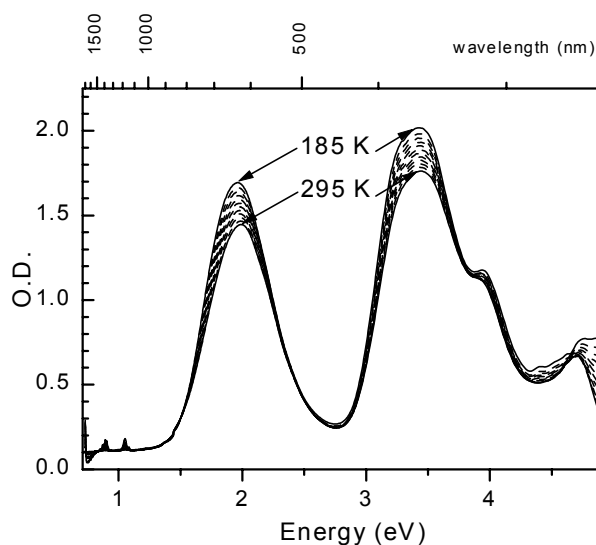

Figure 4.11. *Temperature dependent UV/visible/nearIR spectra of the di(cation radical) of tetramer **2** from T=295 K to T=185 K with steps of 10 K. Di(cation radical) of tetramer **2** was obtained by oxidation with [bis(trifluoracetoxy)iodo]benzene (PIFA) in CH$_2$Cl$_2$/TFA (95/5 (v/v)) at 295 K.*

4.2.3 Electron spin resonance spectroscopy

The previous paragraphs have shown that oligo-*N*-methyl anilines can be oxidized to the corresponding oligo(cation radicals).
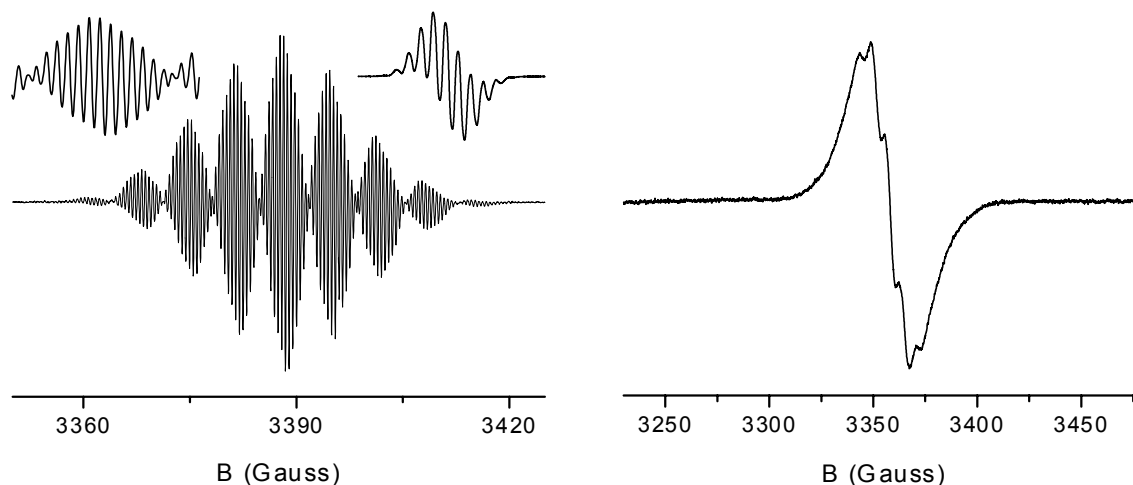

Figure 4.12. *ESR spectra of the cation radical of dimer **1** in CH₂Cl₂ obtained by oxidation with THI⁺•ClO₄⁻. Left: recorded at room temperature, inset left shows magnified central area, inset right shows 11-band spectrum recorded at higher modulation amplitude. Right: recorded at 120 K.*

The ESR spectrum of $\mathbf{1}^{+\bullet}$ dissolved in CH_2Cl_2 and recorded at T = 295 K (Figure 4.12, left spectrum) shows a highly resolved hyperfine coupling pattern at low modulation amplitude. Increasing the modulation amplitude reduces the resolution but clearly shows the outer wings of the spectrum (Figure 4.12, left spectrum, right inset). Combining both spectra results in the conclusion that the spectrum consists of 11 lines separated by a coupling of about 18.3 MHz and that each of these lines is split into 14 lines separated by ~1.4 MHz (Figure 4.12, left spectrum, left inset). The spectrum could be fully simulated with the following parameters: A_N = 18.3 MHz (2N); A_H = 18.3 MHz (6H); A_H = 5.9 MHz (4H); A_H = 2.8 MHz (6H); A_H = 1.4 MHz (4H). These hyperfine splittings are assigned to the coupling of the unpaired electron with the two nitrogen atoms, the six hydrogen nuclei of the methyl groups, the four hydrogen nuclei of the central 1,4-benzenediamine unit, the *ortho-* and *para*-hydrogen nuclei and the *meta*-hydrogen nuclei of the terminal phenyl rings, respectively. In frozen solution much of the hyperfine couplings are unresolved as a result of dipolar interactions and only the largest coupling can be observed (Figure 4.12, right spectrum).

The ESR spectrum of $\mathbf{2}^{+\bullet}$ in CH_2Cl_2 recorded at room temperature shows an 11-line pattern as observed for $\mathbf{1}^{+\bullet}$. Reducing the modulation amplitude reveals that each of these 11 lines is further splitted into about 12 lines similar to the results for $\mathbf{1}^{+\bullet}$.

Oxidation of **2** with two equivalents of PIFA in butyronitrile/TFA yields the di(cation radical) of **2** ($\mathbf{2^{2(+\bullet)}}$). At ambient temperature only a broad featureless ESR spectrum is obtained. The frozen solution ESR spectrum of $\mathbf{2^{2(+\bullet)}}$ at 120 K reveals an ESR spectrum characteristic of a triplet state ($S = 1$) with axial symmetry (Figure 4.13, left). The absence of a central line in the $\Delta M_S = \pm 1$ region indicates that almost no doublet impurity is present and the presence of a $\Delta M_S = \pm 2$ transition at half field gives direct spectral evidence of the triplet state of this di(cation radical) (Figure 4.13, left, inset). Zero-field splitting parameters, $D = 153$ MHz; $E \approx 0$ MHz, were obtained by simulation of the $\Delta M_S = \pm 1$ ESR spectrum. An average distance of $d = 7.97$ Å between the two unpaired electrons can be estimated[30] from the D parameter. Typically only a narrow unresolved spectrum was observed for samples of $\mathbf{2^{2(+\bullet)}}$ dissolved in butyronitrile or CH_2Cl_2 without the addition of TFA. This phenomenon has been noticed also in previous studies on high-spin oligoanilines[17,21], but so far no clear explanation exists about the origin of this effect. The addition of acid leads to a reversible protonation of the amines, which results in higher oxidation potentials for these class of compounds. Magnetic susceptibility measurements by Hartwig et al.[21] on tetraazacyclophanes are consistent with this observed behavior. Therefore, the position of triplet and singlet energy levels seem to change depending on the solvent[17]. Since TFA is commonly used in ESR samples to ensure cation radical stability and to quench trace nucleophiles in the solvent[14,19], this phenomenon might be more widespread then the number of reports would indicate.

Figure 4.13. *ESR spectra and temperature dependence of the ESR signal intensity of the di(cation radical) of tetramer **2** in butyronitrile/TFA (95/5 (v/v)) obtained by oxidation with PIFA. Left: recorded at 120 K, inset right shows half-field signal recorded at 4 K. Right: ΔM$_S$=±1 (●) signal and ΔM$_S$=±2 (○) signal as a function of the reciprocal temperature. Solid lines are linear fits to Curie's law.*

A variable temperature ESR experiment was performed for $2^{2(+\bullet)}$ in the range of 4 – 100 K to determine whether the triplet state corresponds to the ground state. The signal intensities of $2^{2(+\bullet)}$ for the $\Delta M_S = \pm 1$ and $\Delta M_S = \pm 2$ transitions follow a linear behavior with the reciprocal temperature, corresponding to Curie's law of $I = C/T$ (Figure 4.13, right). This experiment demonstrates that in the range of 4 – 100 K no thermal change of the population of the triplet state occurs. Hence, the triplet state is the ground state and separated from the excited low-spin (singlet) state by a substantial energy gap of a few hundreds calories per mole, or an extremely small energy gap is present resulting in a degeneracy of the singlet and triplet state. In either case the triplet state is a low-energy state.
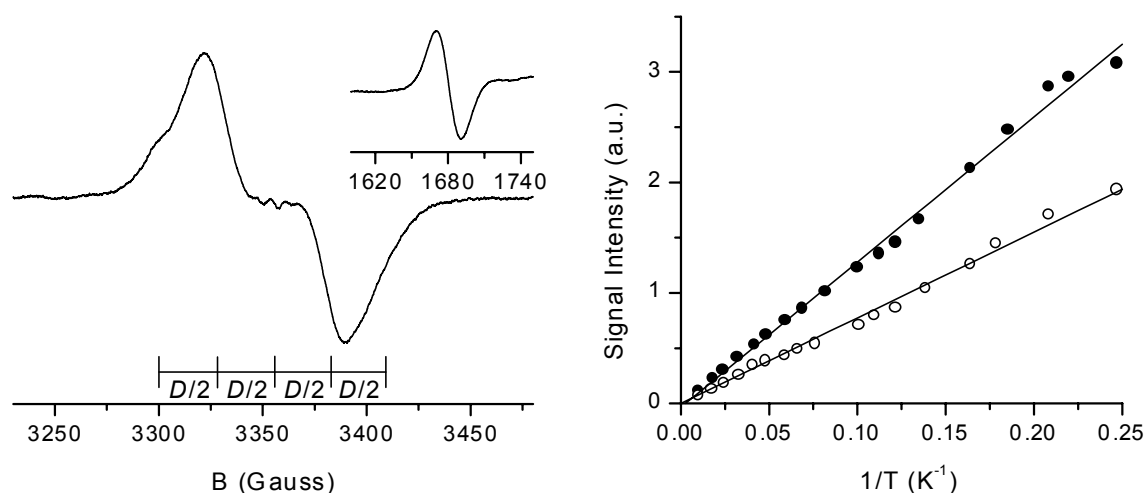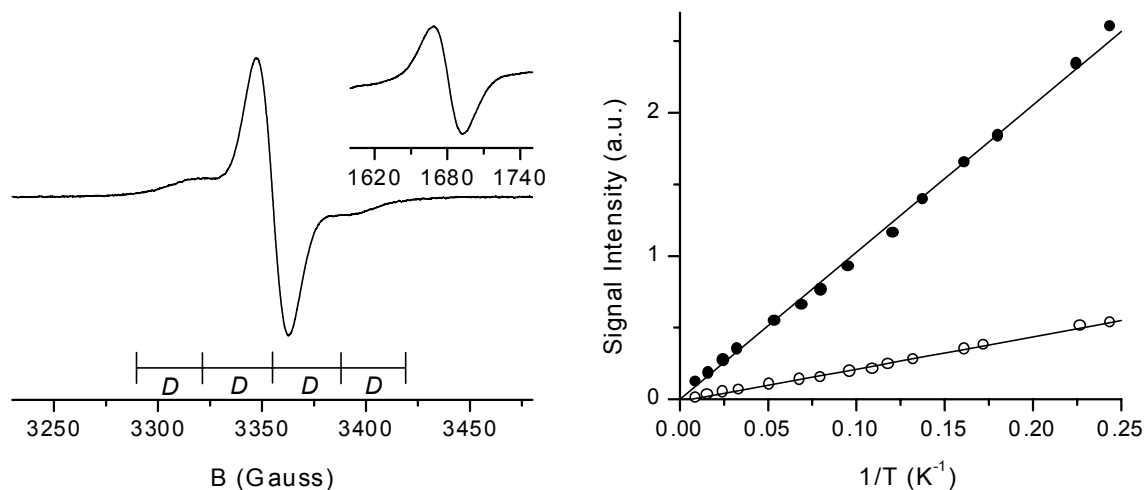

Figure 4.14. *ESR spectra and temperature dependence of the ESR signal intensity of the tri(cation radical) of hexamer 8 in butyronitrile/TFA (95/5 (v/v)) obtained by oxidation with THI$^{+\bullet}$ClO$_4^-$. Left: recorded at 120 K, inset right shows half-field signal recorded at 4 K. Right: $\Delta M_S = \pm 1$ (●) signal and $\Delta M_S = \pm 2$ (○) signal as a function of the reciprocal temperature, solid lines are linear fits to Curie's law.*

The ESR spectrum of the cation radical of **8** dissolved in CH_2Cl_2 at room temperature shows the characteristic 11-line hyperfine splitting attributed to the coupling of the unpaired electron with two ^{14}N nuclei and six ^1H nuclei of two methyl groups. Here no additional hyperfine couplings could be observed for the aromatic hydrogens. The tri(cation radical) of **8** ($8^{3(+\bullet)}$)was obtained by addition of three equivalents of THI$^{+\bullet}$ClO$_4^-$ to neutral **8** in butyronitrile/TFA. The frozen-solution ESR spectrum of $8^{3(+\bullet)}$ recorded at 120 K exhibits the characteristics of a quartet ($S = 3/2$) state (Figure 4.14, left): especially the broad shoulders next to the central line indicate the presence of quartet species. This spectrum can be simulated with $S = 3/2$ and zero-filed splitting parameters, $D = 91$ MHz and $E \approx 0$ MHz. The simulation reveals that the

intense central line can not completely be explained by the presence of a quartet state and that doublet impurities (S = ½) are likely to present in the sample. The broad $\Delta M_S = \pm 2$ transition at half field confirms the presence of the quartet state at normal field (Figure 4.14, left graph, right inset).

In theory also a $\Delta M_S = \pm 3$ transition at one third field might be observed, since tri(cation radical) has a quartet state. This would unambiguously identify $\mathbf{8}^{3(+\bullet)}$ as having a S = 3/2 spin state. Unfortunately, no indication for a $\Delta M_S = \pm 3$ transition could be found in the ESR spectra. The reason for this lack of observation lays in the fact that the ESR signal intensities at normal field, half field and one third field have the following ratio[31,32]; $1:(D/B_0)^2:(D/B_0)^4$, where B_0 is the magnetic field. In the present case $D/B_0 \approx 10^{-2}$, and hence the ESR signal intensity decreases dramatically upon going from normal via half to one third field resulting in an undetectable $\Delta M_S = \pm 3$ transition.
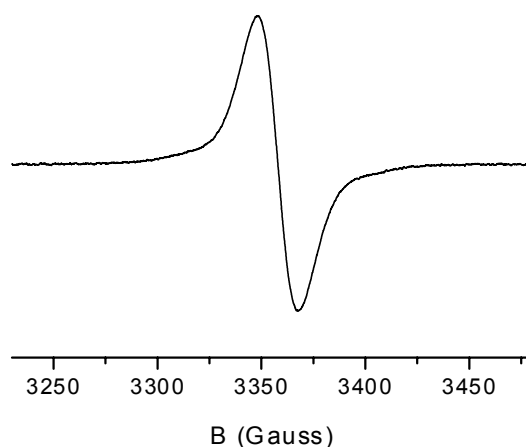
Figure 4.15. *ESR spectrum of the tetra(cation radical) of octamer **10** in butyronitrile/TFA (95/5 (v/v)) obtained by oxidation with THI$^{+\bullet}$ClO$_4^-$ recorded at 120 K.*

Variable temperature ESR spectroscopy was used to investigate the ground state spin multiplicity of $\mathbf{8}^{3(+\bullet)}$. For the $\Delta M_S = \pm 1$ transition the signal intensity of $\mathbf{8}^{3(+\bullet)}$ was deduced from the broad shoulders corresponding to the quartet state to avoid any possible interference with the doublet impurity. Both $\Delta M_S = \pm 1$ and $\Delta M_S = \pm 2$ transitions follow Curie's law (Figure 4.14, right), in the temperature range of 4 – 100 K. Similar to the previous conclusion for $\mathbf{2}^{2(+\bullet)}$, this result indicates that the quartet state of $\mathbf{8}^{3(+\bullet)}$ is a low-energy state. No conclusion, however, can be obtained for the quartet-doublet energy gap $\mathbf{8}^{3(+\bullet)}$, because the absence of population or depopulation of the quartet state as a function of the temperature is consistent with a gap that is either much smaller or much larger than the thermal energy (4 – 100 K: ΔE_{QD} < 8 cal/mol or ΔE_{QD} > 200 cal/mol)[33-35].

Octaaniline **10** was oxidized similarly to the previous oligoanilines using four equivalents of oxidizing agent in butyronitrile/TFA, yielding tetra(cation radical) **10** (**10**$^{4(+\bullet)}$). The ESR spectrum of **10**$^{4(+\bullet)}$ (Figure 4.15) reveals no features which can be contributed to a quintet ($S = 2$) state. Part of the explanation is that the observed D value decreases going via a di-, tri- to a tetraradical, resulting in a decrease of the spectral width. In addition, the outer-most features of the ESR spectrum are expected to decrease in intensity with increasing spin multiplicity. Due to the broad lines resulting from hyperfine couplings of the unpaired electrons with the ^{1}H and ^{14}N nuclei all dipolar couplings may be obscured. Although small changes in the spectrum can be observed when going stepwise through the different oxidation states and UV/visible/nearIR spectroscopy indicates that the correct fourfold oxidation state is reached (absence of neutral or dication absorptions), no conclusive evidence is found for a high-spin state.

4.3 Cation radicals of the branched *N*-methyl substituted aniline oligomers

The branched oligomers **11** and **14** described in chapter 3 (Figure 4.5) have been investigated for their redox behavior, optical properties and spin-spin interactions of the cation radicals.

4.3.1 Cation radicals by cyclic voltammetry

Electrochemistry was carried out in a 0.1 M tetrabutylammonium hexafluorophosphate (TBAHF) dichloromethane solution as described in paragraph 4.1. The cyclic voltammogram of star-shaped oligomer **11** (Figure 4.16) shows three consecutive one-electron oxidations at 0.33, 0.48 and 0.64 V all with a peak-peak separation of 75 mV. These oxidation potentials are comparable with the values of 0.33, 0.44 and 0.64 V, found for linear hexamer **8**, indicating that the stabilizing effect of two unoxidized *para*-benzenediamine units on the cation radical state is not influenced by the different topology of **11** compared to **8**. However the second oxidation potential corresponding to the formation of the di(cation radical), is slightly higher for **11**. This seems plausible, since the two charges are likely to be much closer together in **11**$^{2(+\bullet)}$ than in case of **8**$^{2(+\bullet)}$. The highest oxidation states suffer from the same solubility problems as encountered with the linear oligomers. The effect is even more pronounced compared to linear hexamer **8**. The cyclic voltammogram is chemically fully reversible up to 1.6 V vs. SCE.
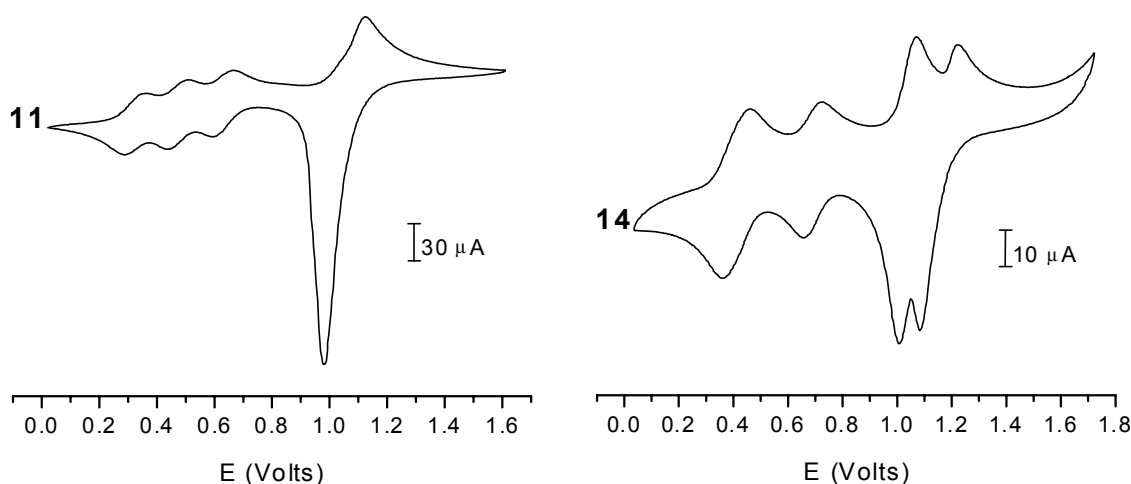
Figure 4.16. *Cyclic voltammograms of branched N-methylaniline oligomers; left: star shaped hexamer **11**; right: branched hexamer **14**. Conditions: 0.1 M TBAHF in CH₂Cl₂ at 295 K, scan rate 100 mV/s. Potential vs. SCE reference and calibrated against Fc/Fc⁺ couple at 0.46 V.*

The cyclic voltammogram of **14** reveals four chemically reversible redox waves (Figure 4.16.) A striking feature is the 2 : 1 intensity ratio of both first and second wave, and third and fourth wave. In the first, two-electron, oxidation at 0.41 V, the terminal 1,4-benzenediamine moieties of the molecule are oxidized. The central 1,4-benzenediamine moiety of the molecule is slightly different with respect to the substitution pattern. It consists both of a triphenylamine part and a *N*-methyl-diphenylamine part. The extra phenyl group has an electron withdrawing effect (compared to the methyl group), increasing E_3^0 to 0.69 V. The central triarylamine has probably a propeller shaped geometry which affects the conjugation and might explain why the first redox wave is unresolved, although the charges seem to be closer together in **14**$^{2(+\bullet)}$ compared with the linear hexamer **8**$^{2(+\bullet)}$, that has a resolved E_1^0 and E_2^0. The oxidation to the hexacation proceeds in two steps, first two-electrons are removed at 1.04 V then one electron is removed at 1.14 V. This splitting is attributed to the same chemical in equivalency of the 1,4-benzenediamine units as described above.

Table 4.3. *Electrochemical data of the branched N-methylaniline Oligomers[a]*

	E_1^0(V)	E_2^0(V)	E_3^0(V)	E_4^0(V)	E_5^0(V)
11	0.33	0.48	0.64	1.05[b]	
14	0.41[b]	0.41[b]	0.69	1.04[b]	1.14

[a] *Conditions: 0.1 M TBAHF in CH₂Cl₂, 295 K. Potential vs. SCE reference and calibrated against Fc/Fc⁺ couple at 0.46 V.* [b] *Peaks are unresolved.*

4.3.2 Optical properties of the cation radicals

The UV/visible/nearIR measurements were carried out as described in paragraph 4.1. The electronic absorption spectrum of neutral star-shaped hexamer **11** in dichloromethane shows bands at 4.01 and 4.90 eV (Figure 4.17) which decrease upon stepwise addition of small quantities of $THI^{+\bullet}ClO_4^-$. Two new absorption bands, attributed to the formation of cation radicals, appear initially at 2.04 eV and as a shoulder of the neutral absorption at ~ 3.5 eV. At approximately one third of the oxidation process, so in the mono(cation radical state), a shift of -0.1 eV of the low energy absorption band occurs. Apparently the spectrum changes when the di(cation radical) is generated. At present it is not known whether this shift reflects a conformational change or is a result of an electronic effect. Further oxidation leads to the tri(cation radical) state of **11**, which exhibits three absorption bands at 1.94, 3.48 and, 3.88 eV respectively.
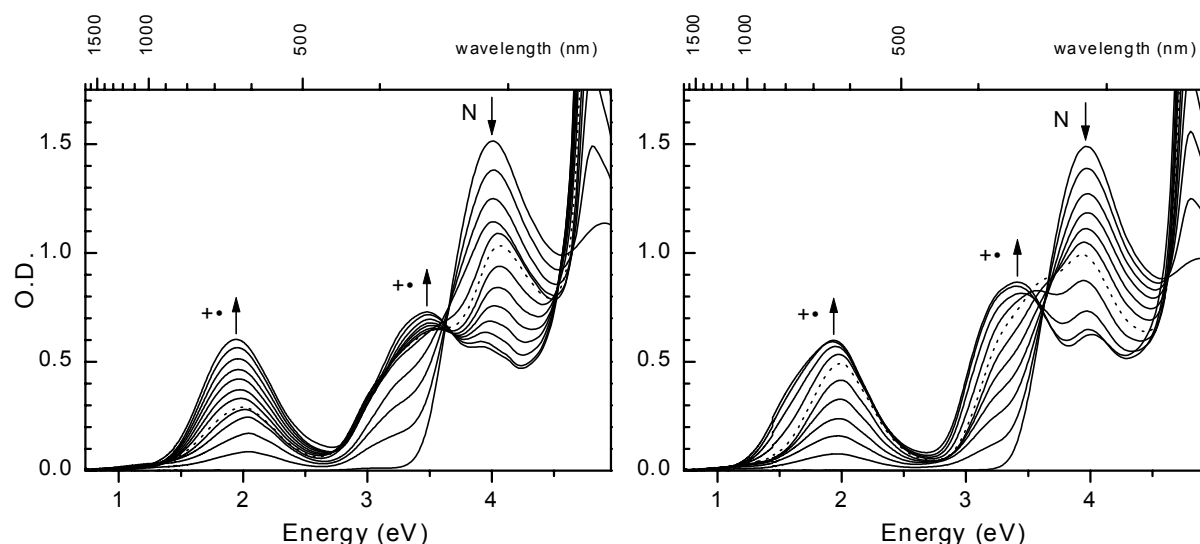
Figure 4.17. *UV/visible/nearIR spectra recorded during the conversion of hexamers **11** (left) and **14** (right) by stepwise oxidation with $THI^{+\bullet}ClO_4^-$ in CH_2Cl_2 at 295 K from the neutral state to the tri(cation radical).*

The optical spectra of branched hexamer **14**, with two neutral absorptions at 3.96 and 4.89 eV, reveal the same oxidation sequence as observed with cyclic voltammetry (Figure 4.17). First the two terminal 1,4-benzenediamine moieties of the molecule are oxidized, as inferred from the appearance of two cation radical absorption bands, one at 1.97 eV and one as a shoulder of the neutral band at ~ 3.25 eV. At two thirds of the oxidation process, the cation radical absorption bands exhibit a red shift reaching their maximum at 1.92, 3.41, and 4.01 eV, for the tri(cation radical) state of **14**. Clearly the absorption of the central 1,4-benzenediamine moiety of the molecule is different in the

cation radical state as compared to the outer parts. This is due to the fact that there is a triarylamine group present in the central 1,4-benzenediamine, which has different absorption compared to a *N*-methyldiarylamine group. The neutral absorption of both molecules **11** and **14** reappeared after addition of hydrazine hydrate demonstrating the reversibility of the oxidation process.

Table 4.4. *Optical data of the branched N-methylaniline oligomers* [a]

	Neutral, eV (nm)		Tri(cation radical), eV (nm)		
11	4.01 (309)	4.90 (253)	1.94 (639)	3.48 (356)	3.88 (320)
14	3.96 (313)	4.89 (254)	1.92 (646)	3.41 (364)	4.01 (309)

[a] *Conditions: CH$_2$Cl$_2$, oxidation with THI$^{+\bullet}$ClO$_4^-$, 295 K.*

4.3.3 Electron spin resonance spectroscopy

The oxidation of **11** by addition of three equivalents of THI$^{+\bullet}$ClO$_4^-$ yields **11**$^{3(+\bullet)}$, resulting in an anisotropic ESR spectrum with a 5-line well resolved zero-field splitting corresponding to a quartet ($S = 3/2$) state (Figure 4.18, left), especially the two lines next to the central line are an indication for the presence of quartet species. Simulation of this spectrum provides the zero-field parameters, $D = 89$ MHz and $E \approx 0$ MHz, similar to the values found for **8**$^{3(+\bullet)}$. The observation of a $\Delta M_S = \pm 2$ transition at half field confirms the presence of a high-spin state (Figure 4.18). Also in this case a $\Delta M_S = \pm 3$ transition at one third field could not be observed due to the reasons described in paragraph 4.2.3.

Figure 4.18. *ESR spectra and temperature dependence of the ESR signal intensity of the tri(cation radical) of star shaped hexamer **11** in butyronitrile/TFA (95/5 (v/v)) obtained by oxidation with THI$^{+\bullet}$ClO$_4^-$. Left: recorded at 120 K, inset right shows half-field signal recorded at 4 K. Right: $\Delta M_S = \pm 1$ (●) signal and $\Delta M_S = \pm 2$ (○) signal as a function of the reciprocal temperature, solid lines are linear fits to Curie's law.*

The oxidation of **14** with three equivalents of THI$^{+\bullet}$ClO$_4^-$ in butyronitrile/TFA yields **14**$^{3(+\bullet)}$ which after cooling down to 120 K results in an anisotropic ESR spectrum showing a characteristic 5-line splitting for a quartet ($S = 3/2$) state (Figure 4.19). The broad shoulders next to the central line and the $\Delta M_S = \pm 2$ transition at half field confirm the high-spin nature of this species. From simulation of the ESR spectrum, the zfs parameters, $D = 87$ MHz and $E \approx 0$ MHz are obtained. Also in this case the intense central line cannot completely be attributed to the presence of only quartet species, as found for **8**$^{3(+\bullet)}$, and hence an additional doublet impurity is present.

Variable temperature ESR spectroscopy was performed to investigate the ground state spin multiplicity of **11**$^{3(+\bullet)}$ and **14**$^{3(+\bullet)}$. For the $\Delta M_S = \pm 1$ transition the ESR signal intensities of **11**$^{3(+\bullet)}$ and **14**$^{3(+\bullet)}$ were taken from the broad shoulders corresponding to the $S = 3/2$ states. The $\Delta M_S = \pm 1$ and $\Delta M_S = \pm 2$ transitions of both molecules follow Curie's law ($I = C/T$) (Figure 4.18 and Figure 4.19, right graphs), and indicate that the quartet state is the ground state, although a possible degeneracy with the corresponding doublet state cannot be excluded for similar reasons as described for **8**$^{3(+\bullet)}$.
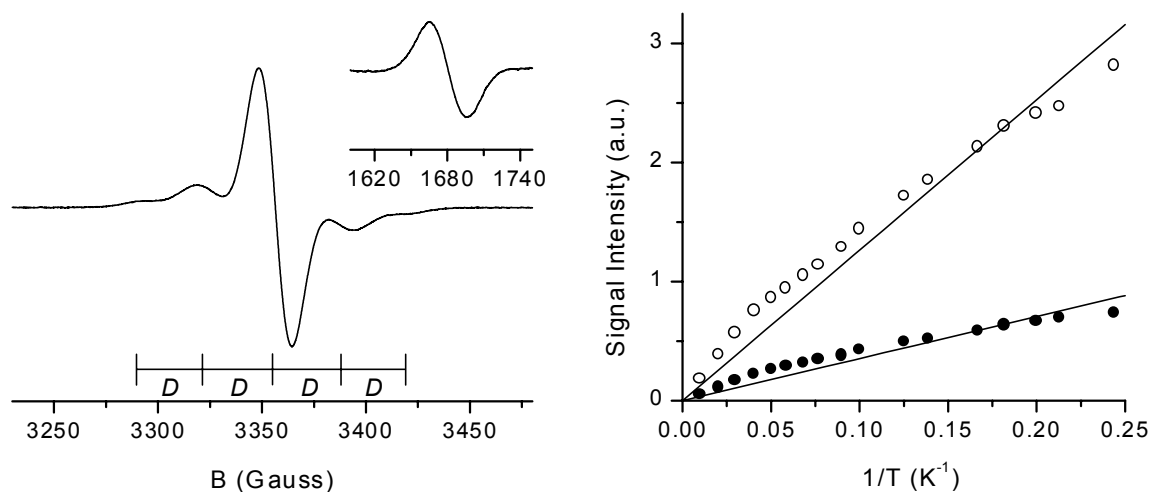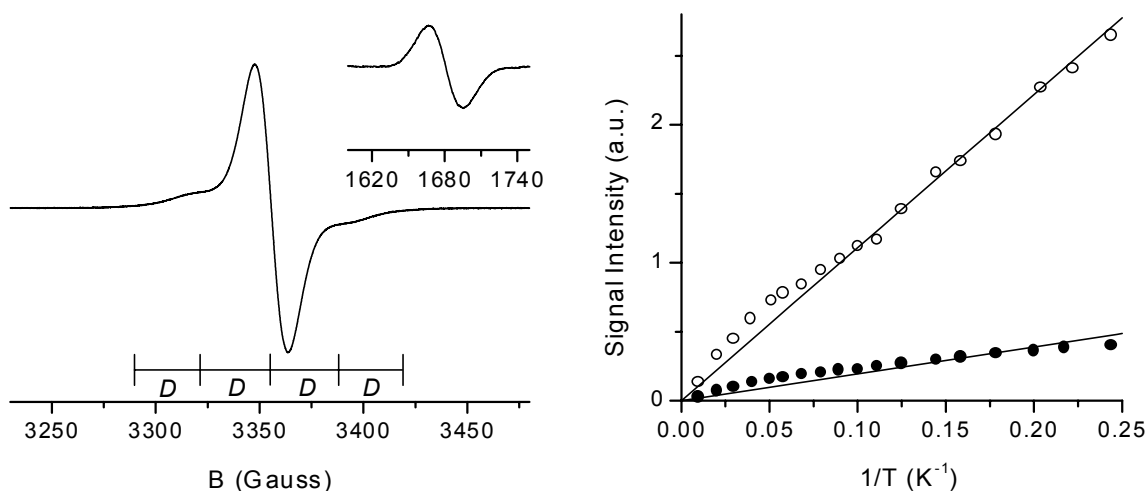

Figure 4.19. *ESR spectra and temperature dependence of the ESR signal intensity of the tri(cation radical) of branched hexamer **14** in butyronitrile/TFA (95/5 (v/v)) obtained by oxidation with THI$^{+\bullet}$ClO$_4^-$. Left: recorded at 120 K, inset right shows half-field signal recorded at 4 K. Right: $\Delta M_S = \pm 1$ (●) signal and $\Delta M_S = \pm 2$ (○) signal as a function of the reciprocal temperature, solid lines are linear fits to Curie's law.*

4.4 Cation radicals of the *N*-phenyl substituted aniline octamer

4.4.1 Cation radicals by cyclic voltammetry

An electrochemical investigation was conducted for *N*-phenyl-*m*-*p*-octaaniline **18** by means of cyclic voltammetry at scan rates of 25, 50, 100 and 200 mV/s. The cyclic

voltammogram of **18** reveals two sets of clustered oxidation waves at around 0.7 V, yielding the tetra(cation radical) and at around 1.2 V resulting in the octacation (Figure 4.20). The chemical reversibility of the process and thus the stability of the generated cation radicals was established by running multiple scan cycles which showed no variation in signal or intensity. The clustering of the oxidation waves makes it difficult to obtain precise peak to peak separations of the anodic and cathodic waves. However, a first estimate results in values between 70 to 90 mV with a small dependency on the scan rate of ±5 mV. The first oxidation wave that occurs at 0.56 V, is a two electron process whereas the two following waves are one-electron processes, clearly showing that electrostatic repulsion by ions already present in the molecule increases the oxidation potential of the 1,4-benzenediamine unit, to be oxidized next.
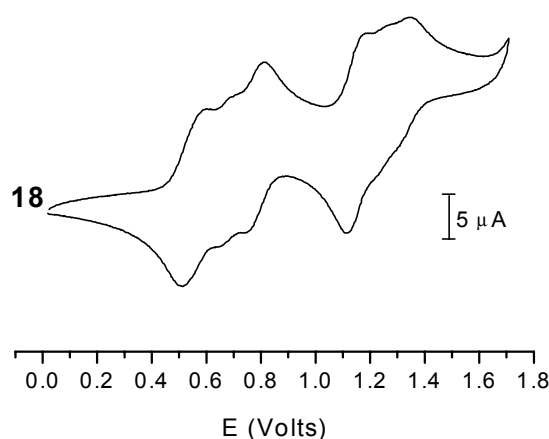
Figure 4.20. *Cyclic voltammogram of* **18***. Conditions: 0.1 M TBAHF in CH₂Cl₂ at 295 K, scan rate 100 mV/s. Potential vs. SCE reference and calibrated against Fc/Fc⁺ couple at 0.46 V.*

The oxidation potentials of **18** are listed in Table 4.5 and are consistent with the values found by Wienk[17] for the linear tetramer and hexamer. The first oxidation potential of these compounds can be found around 0.55 V whereas the last oxidation potential towards the poly(cation radical) state can be expected around 0.74 V similar to the values reported here.

Table 4.5. *Electrochemical data of octamer* **18** [a]

	E_1^0(V)	E_2^0(V)	E_3^0(V)	E_4^0(V)	E_5^0(V)	E_6^0(V)
18	0.56[b]	0.68	0.78	1.15[b]	1.24	1.33

[a] *Conditions: 0.1 M TBAHF in CH₂Cl₂, 295 K. Potential vs. SCE reference and calibrated against Fc/Fc⁺ couple at 0.46 V.* [b] *Peaks are unresolved.*

Comparing the electrochemical results obtained for the different substituted oligoanilines the following remark can be made. The values for the oxidation potentials of the *N*-methyl oligoanilines are on average 0.15 V lower compared to oxidation potentials of the *N*-phenyl oligoanilines. In contrast to what was found for the oligo(dication)s of the *N*-methyl-oligoanilines, the tetra(dication) of **18** is soluble in CH₂Cl₂ indicated by the normal cathodic wave resulting from the absence of precipitation on the working electrode.

4.4.2 Optical properties of the oligo(cation radical)

UV/visible/nearIR spectroscopy allows for monitoring the optical properties of **18** during a stepwise oxidation process (Figure 4.21). The spectrum of **18** shows a clear maximum at 3.93 eV although at higher energy a shoulder can be observed. Stepwise oxidation reveals two cation radical bands at 1.43 and 3.02 eV as well as a small shoulder at 3.44 eV, which becomes clearly visible after complete oxidation to the tetra(cation radical) state. The increasing absorption band at 4.81 eV is due to the presence of neutral thianthrene. Further oxidation would lead to the octacation of **18** yielding an absorption of which the beginning can just be observed at 2.11 eV in between the two cation radical absorptions in the last spectrum. After addition of hydrazine hydrate the spectrum of neutral **18** is recovered, consistent with the observed chemical reversibility from cyclic voltammetry.
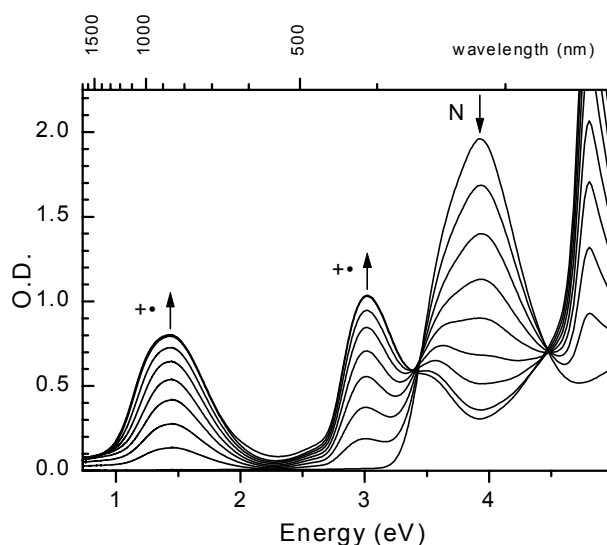

Figure 4.21. *UV/visible/nearIR spectra recorded during the conversion of **18** by stepwise oxidation with THI⁺•ClO₄⁻ in CH₂Cl₂ at 295 K from the neutral state to the tetra(cation radical).*

Comparison of the optical spectra of the poly(cation radical)s of the different oligomers shows that in contrast to the neutral absorptions, the cation radical absorptions of a *N*-methyl-oligoaniline are on average ±0.45 eV higher in energy than those of a *N*-phenyl-oligoaniline. Both types of anilines show a typical shoulder at the UV-side of the high energy cation radical band, which is not due to incomplete oxidation of the molecule but seems to be inherently connected to the cation radical state.

Table 4.6. *Optical data of the N-phenylaniline octamer* [a]

	Neutral, eV (nm)	Tetra(cation radical), eV (nm)		
18	3.93 (316)	1.43 (867)	3.02 (411)	3.44 (360)

[a] *Conditions: CH₂Cl₂, oxidation with THI⁺•ClO₄⁻, 295 K.*

4.4.3 Electron spin resonance spectroscopy

ESR experiment on a frozen solution of the tetra(cation radical) of **18** (**18**$^{4(+•)}$) reveal a broad almost featureless spectrum (Figure 4.22). Partial oxidation of the molecule, results in an intermediate triplet state. Further oxidation gives a narrow intense central line in the ΔM_S=±1 region, which widens going from **18**$^{3(+•)}$ to **18**$^{4(+•)}$ ending up with small shoulders next to the central line. This can be rationalized by the fact that a quartet state should give a 5-line spectrum with a central line whereas a quintet state should give 6 lines without a central line. So the transition from **18**$^{3(+•)}$ to **18**$^{4(+•)}$ results in an increase in the splitting of the central line but, as could be observed for the quartet molecules, lower spin states are very likely to be present.
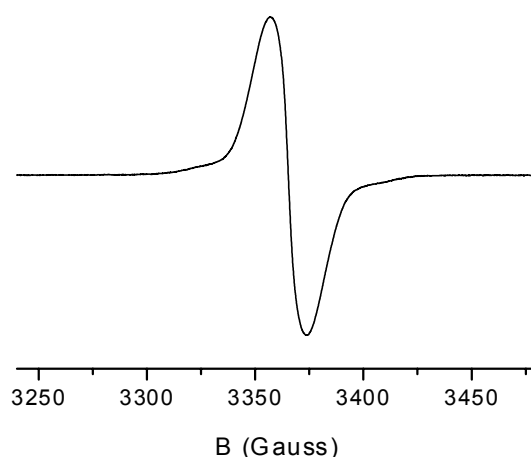

Figure 4.22. *ESR spectrum of the tetra(cation radical) of octamer **18** in butyronitrile/TFA (95/5 (v/v)) obtained by oxidation with THI⁺•ClO₄⁻ recorded at 120 K.*

The absence of a clear $\Delta M_S = \pm 2$ transition at half field at 120 K does not support the identification of a high-spin state either, although the additional zero-field coupling will likely broaden the $\Delta M_S = \pm 2$ signal of a quintet state. Since the ESR intensity is inversely related to the temperature according to Curie's law, a $\Delta M_S = \pm 2$ transition might be observed at 4 K. The same problems which arose for the ESR spectroscopic identification of the *N*-methyl-octaaniline $\mathbf{10}^{3(+\bullet)}$ quintet state hamper here the attempted observation of a quintet state.

4.5 Conclusion

All experimental results lead to the conclusion that stable oligo(cation radicals) can be obtained from *N*-methyl-oligoanilines. The di(cation radicals) and tri(cation radicals) were shown to have a low energy high-spin state. The presence of methyl groups results in larger zero-field *D* parameters compared to hydrogens or phenyl groups (Table 4.7), indicating a reduced average distance between the unpaired electrons in the oligo(cation radicals), possibly due to a lesser extent of delocalization.

Table 4.7. *Zero-field parameter D for the different substituted oligo-m-p-anilines*[17]

D	Methyl (MHz)	Phenyl (MHz)	Hydrogen (MHz)
$\mathbf{2}^{2(+\bullet)}$	153	110	118
$\mathbf{8}^{3(+\bullet)}$	91	77	73
$\mathbf{11}^{3(+\bullet)}$	89	68	
$\mathbf{14}^{3(+\bullet)}$	87		

The slightly reduced oxidation potential is advantageous for generating stable cation radicals but this positive effect is countered by the less soluble nature of the linear compounds. The branched topology of **14** is in this respect an interesting new compound combining solubility with easy oxidation and high-spin states. It offers the possibility to make an all *meta*-polyaniline that could combine helix twisting and lyotropic liquid crystalline behavior with high-spin states, if flexible alkyl chains are connected to the phenyl groups of the amine at the *para*-position. The inability to positively identify the quintet states for $\mathbf{10}^{4(+\bullet)}$ and $\mathbf{18}^{4(+\bullet)}$ clearly shows the limitations of ESR spectroscopy for the identification of higher spin states for nitrogen centered cation radicals with broad coupling patterns. Magnetization studies should therefore confirm the nature of the spin states in these octaanilines.

4.6 Experimental section

General techniques. Nitrosonium tetrafluoroborate (NOBF$_4$, Aldrich), trifluoroacetic acid (TFA, Acros), hydrazine hydrate (Acros), phosphorus pentoxide (P$_2$O$_5$, Acros), [Bis(trifluoroacetoxy)iodo]benzene (PIFA, Aldrich), and acetonitrile (ACN, Biosolve DNA-synthesis grade) were used as received. Potassium iodide (KI, Merck) was dried in a vacuum oven for 1 day at 100 °C. Purification of *n*-butyronitrile (PrCN, Acros 98%) was carried out according to the method of Van Duyne and Reilley[36] by heating it twice at 75 °C with stirring for several hours with a mixture of 7.5 g of Na$_2$CO$_3$ and 11.5 g of KMnO$_4$ and distillation afterwards. The last distillation was followed by drying the butyronitrile over an alumina column (ICN Alumina B super I). Dichloromethane (Acros c.p. stabilized with ethanol) was distilled from P$_2$O$_5$ [37]. Thianthrenium perchlorate (THI$^{+•}$ClO$_4^-$) was synthesized according to literature procedures[38]. Syringes used were SGE gas-tight syringes with removable needle and teflon tipped plungers.

General procedure for determination of the active THI$^{+•}$ClO$_4^-$ concentration in solution: A solution of 1.00 mM KI in ACN was slowly added with a syringe to 100 µl of a THI$^{+•}$ClO$_4^-$ solution. The intense purple solution changes to a faintly pink color upon addition of KI. The transition from faintly pink to slightly yellow can be observed with the naked eye and usually occurs by addition of one more drop of KI solution. This procedure was carried out in triplo for more accurate determination of the active content. By this way the right amount of oxidizing THI$^{+•}$ClO$_4^-$ could be added to a neutral compound with an accuracy of ±5 µl.

Cyclic Voltammetry: Cyclic voltammograms were obtained in dichloromethane with 0.1 M tetrabutylammonium hexafluorophosphate (TBAHF, Fluka electrochemical grade) as supporting electrolyte using a Potentioscan Wenking POS73 potentiostat. A platinum disk (diameter 5 mm) was used as working eletrode, the counter electrode was a platinum plate (5*5 mm^2) and a saturated calomel electrode (SCE) was used as reference electrode, internally calibrated vs. Fc/Fc$^+$ (0.46 V vs. SCE). Typical concentration of the substrates in C.V. experiments was 1 mg/ml. All experiments were conducted in a glovebox under nitrogen atmosphere.

UV/visible/nearIR spectroscopy: UV/visible/nearIR experiments (200 − 3300 nm) were recorded with a Perkin Elmer Lambda 900 spectrometer with a path length of 10 mm. Oxidation experiments were carried out by adding oxidant solution by a syringe through a teflon-lined septum sealing the cuvette, under magnetic stirring (Rank. Bros. Ltd. electronic stirrer model 200) of the substrate solution under inert conditions. Typical concentration of the oxidant was 0.7 10^{-3} M for THI$^{+•}$ClO$_4^-$ and 10^{-3} M for NOBF$_4$. The concentration of substrate solutions were 0.07 10^{-3} M according to the number of 1,4-benzenediamine units in the substrate. Variable temperature experiments down to 185 K were performed with an Oxford Optistat^{DN} cryostat connected to an Oxford ITC 601 temperature controller in 10 K steps under nitrogen atmosphere.

ESR spectroscopy: ESR spectra were recorded on a Bruker ESP300E spectrometer operating with an X-band microwave bridge ER042 MRH connected to standard or TMH cavity equipped with an ER4111 variable temperature unit. Variable temperature ESR experiments were obtained using an Oxford 3120 temperature controller connected to a continuous flow cryostat in the range of 4 − 100 K. Saturation of the ESR signal during these experiments was avoided by using microwave powers which were within a range where signal intensities are proportional to the square root of the microwave power at 4K. Typically 8 µW for the $\Delta M_S=\pm 1$ transition and 2 − 4 mW for the $\Delta M_S=\pm 2$ transition.
ESR samples were prepared in a glovebox by adding the appropriate amount of oxidant in butyronitrile (±1 mM) with a syringe to 100 µl of the oligoaniline in butyronitrile/TFA (95/5 (v/v)) under stirring or shaking. The concentration of 1,4-benzenediamine units was approximately 10^{-3} M for all oligoaniline solutions. The resulting solution was then transferred into an ESR quartz-tube. As a result of the inaccuracy of the determination of the

active THI$^{+\bullet}$ClO$_4^-$ amount in solution, the usual procedure was to prepare three samples with −5 µl, +0 µl, +5 µl as compared to amount of oxidator solution needed for the right oxidation state of the compound.

4.7 References

1.   Kahn, O. (Ed.), *Magnetism: A Supramolecular Function,* Kluwer Academic Publishers, Dordrecht **1996**.

2.   Gatteschi, D.; Kahn, O.; Miller, J. S.; Palacio, F. (Eds.), *Magnetic Molecular Materials,* Kluwer Academic Publishers, Dordrecht **1991**.

3.   Lahti, P. M. (Ed.), *Magnetic Properties of Organic Materials,* Marcel Dekker, Inc., New York **1999**.

4.   O. Kahn (Ed.), *Proc. Conf. on Molecule Based Magnets, Mol. Cryst. Liq. Cryst.* **1999**, *334.*

5.   K. Itoh, J. S. Miller ,T. Takui (Eds.), *Proc. Conf. on Molecule Based Magnets, Mol. Cryst. Liq. Cryst.* **1997**, *306.*

6.   Fukutome, H.; Takahashi, I.; Ozaki, M., *Chem. Phys. Lett.* **1987**, *133*, 34.

7.   Yoshizawa, K.; Tanaka, K.; Yamabe, T.; Yamauchi, J., *J. Chem. Phys.* **1992**, *96*, 5516.

8.   Yoshizawa, K.; Chano, A.; Ito, A.; Tanaka, K.; Yamabe, T.; Fujita, H.; Yamauchi, J.; Shiro, M., *J. Am. Chem. Soc.* **1992**, *114*, 5994.

9.   Nakamura, Y.; Iwamura, H., *Bull. Chem. Soc. Jpn.* **1993**, *66*, 3724.

10.   Stickley, K. R.; Blackstock, S. C., *J. Am. Chem. Soc.* **1994**, *116*, 11575.

11.   Ito, A.; Ota, K.; Tanaka, K.; Yamabe, T.; Yoshizawa, K., *Macromolecules* **1995**, *28*, 5618.

12.   Yano, M.; Sato, K.; Shiomi, D.; Ichimura, A.; Abe, K.; Takui, T.; Itoh, K., *Tetrahedron Lett.* **1996**, *37*, 9207.

13.   Bushby, R. J.; Ng, K. M., *Chem. Commun.* **1996**, 659.

14.   Stickley, K. R.; Selby, T. D.; Blackstock, S. C., *J. Org. Chem.* **1997**, *62*, 448.

15.   Sato, K.; Yano, M.; Furuichi, M.; Shiomi, D.; Takui, T.; Abe, K.; Itoh, K.; Higuchi, A.; Katsuma, K.; Shirota, Y., *J. Am. Chem. Soc.* **1997**, *119*, 6607.

16.   Wienk, M. M.; Janssen, R. A. J., *J. Am. Chem. Soc.* **1996**, *118*, 10626.

17.   Wienk, M. M.; Janssen, R. A. J., *J. Am. Chem. Soc.* **1997**, *119*, 4492.

18.   Wienk, M. M.; Janssen, R. A. J., *Chem. Commun.* **1996**, 267.

19.   Selby, T. D.; Blackstock, S. C., *J. Am. Chem. Soc.* **1999**, *121*, 7152.

20.   Selby, T. D.; Blackstock, S. C., *Org. Lett.* **1999**, *1*, 2053.

21.   Hauck, S. I.; Lakshmi, K. V.; Hartwig, J. F., *Org. Lett.* **1999**, *1*, 2057.

22.   Ito, A.; Saito, T.; Tanaka, K.; Yamabe, T., *Tetrahedron Lett.* **1995**, *36*, 8809.

23.   Sasaki, S.; Iyoda, M., *Chem. Lett.* **1995**, 1011.

24.   Yoshizawa, K.; Hatanaka, M.; Ago, H.; Tanaka, K.; Yamabe, T., *Bull. Chem. Soc. Jpn.* **1996**, *69*, 1417.

25.   Moll, T.; Heinze, J., *Synth. Met.* **1993**, *55*, 1521.

26.   Cauquis, G.; Serve, D., *Anal. Chem.* **1972**, *44*, 2222.

27.   Cauquis, G.; Delhomme, H.; Serve, D., *Tetrahedron Lett.* **1972**, *13*, 1965.

28.   Weller, H.; Grellmann, K.-H., *J. Am. Chem. Soc.* **1983**, *105*, 6268.

29.   Van Haare, J. A. E. H.; Van Boxtel, M.; Janssen, R. A. J., *Chem. Mater.* **1998**, *10*, 1166.

30. Weil, J. A.; Bolton, J. R.; Wertz, J. E., *Electron Paramagnetic Resonance, Elemental Theory and Practical Applications*, John Wiley & Sons, New York **1993**.

31. Brickmann, J.; Kothe, G., *J. Chem. Phys.* **1973**, *59*, 2807.

32. Weissman, S. I.; Kothe, G., *J. Am. Chem. Soc.* **1975**, *97*, 2537.

33. Iwamura, H.; Koga, N., *Acc. Chem. Res.* **1993**, *26*, 346.

34. Kanno, F.; Inoue, K.; Koga, N.; Iwamura, H., *J. Phys. Chem.* **1993**, *97*, 13267.

35. Ling, C.; Lahti, P. M., *J. Am. Chem. Soc.* **1994**, *116*, 8784.

36. Van Duyne, R. P.; Reilley, C. N., *J. Am. Chem. Soc.* **1986**, *44*, 142.

37. Armarego, W. L. F.; Perrin, D. D., *Purification of Laboratory Chemicals*, Butterworth-Heinemann, Oxford **1997**.

38. Murata, Y.; Shine, H. J., *J. Org. Chem.* **1969**, *34*, 3368.

5

Towards ordering high-spin molecules:
Aniline oligomers with mesogenic groups

Abstract: *A first attempt to create liquid crystalline discotic stacks as an intermediate step towards intermolecular ferromagnetic coupling between high-spin molecules is reported. Oligo(cation radicals) made from mixed carbazole aniline oligomers and branched m-p-aniline oligomers with mesogenic groups were synthesized and characterized by means of cyclic voltammetry, UV/visible/nearIR spectroscopy and ESR spectroscopy.*

5.1 Introduction

One of the major challenges in the area of organic high-spin molecules is to realize intermolecular ferromagnetic coupling through space. A mechanism that predicts the (anti-) ferromagnetic behavior of spin-spin interactions between organic radicals was put forward by McConnell[1] in 1963. The McConnell model I describes a stack of radicals, in which atoms with positive spins densities have an interactions with atoms of neighboring radicals with small negative spin densities. This antiparallel spin coupling could give a ferromagnetic spin alignment of the unpaired electrons of the different radicals, creating a stack with an overall magnetic moment. A prerequisite of such an organic ferromagnetic material based on high-spin molecules would be that it incorporates a high degree of order and/or symmetry.
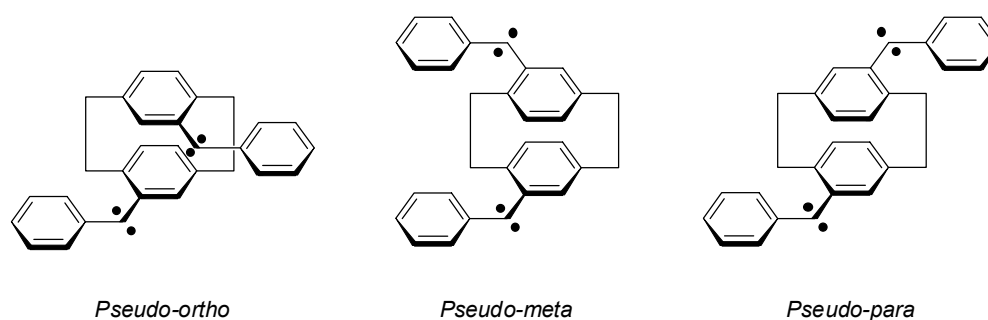

Pseudo-ortho   Pseudo-meta   Pseudo-para

Figure 5.1. *[2.2]paracyclophanes of Iwamura et al.[2,3] with intramolecular spin-spin coupling. Left: pseudo-ortho; middle: pseudo-meta; right: pseudo-para.*

The McConnell model I was originally intended to describe intermolecular interactions. It took more than 20 years before the model was verified experimentally by Iwamura[2,3]. Iwamura used ingeniously designed [2.2]paracyclophanes substituted with two diphenylcarbenes (Figure 5.1) to demonstrate that intramolecular spin coupling occurs through space via the two benzene rings stacked on top of each other. If the two biradical carbene moieties are positioned in either a *pseudo-ortho* or *pseudo-para* configuration, it results in a ferromagnetic spin coupling because atoms with opposite spin density interact, yielding quintet ($S = 2$) molecules. On the other hand, positioning of the biradicals in a pseudo-meta configuration, results in a low-spin $S = 0$ molecule due to an anti-ferromagnetic spin coupling. In this latter case, atoms with similar spin density signs are stacked on top of each other, resulting in an anti-ferromagnetic coupling.

The possibility to stack high-spin molecules with a triazine coupling unit has been theoretically investigated by Zhang and Baumgarten[4]. The calculations show, in agreement with the McConnell model I, that the stability of the high-spin ground state

versus low-spin can be traced back to the number of atoms with reversed signs of π-spin density in neighboring molecules coupled to each other. One experimental example of intermolecular interactions similar to the McConnell model resulting in ferromagnetic interactions in a molecular material has been reported for the charge transfer salt $NH_4Ni(mnt)_2.H_2O$ (mnt = maleonitrile)[5].
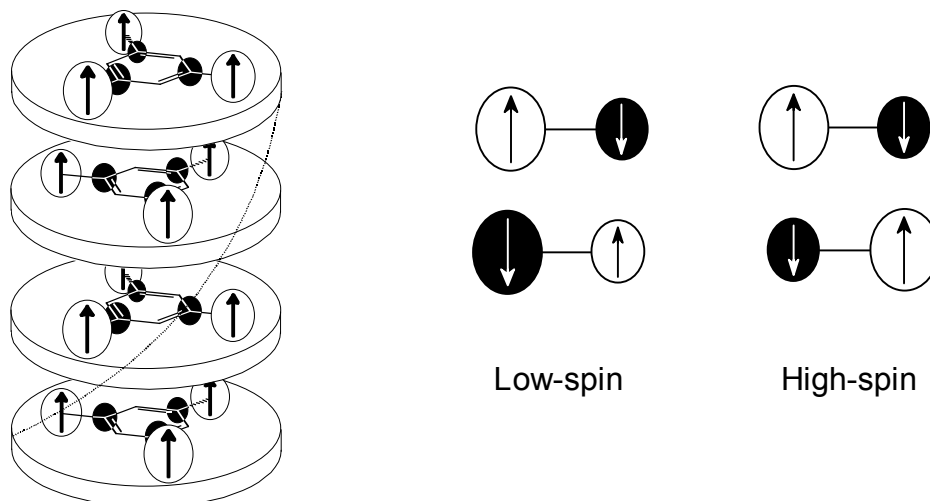

Figure 5.2. *The McConnell Model I envisioned on a stack of discotic quartet molecules (S = 3/2) with a (helical) twist of 60° (left). Alternation of positive (white) and negative (black) spin densities resulting in a high-spin (right) or low-spin (middle) stack, with or without twist respectively.*

An intriguing question, concerning the stacking of high-spin molecules, is the possibility that by using an extended rigidified aromatic core with C_3 symmetry and flexible solubilizing substituents R of suitable dimension, the molecule exhibits discotic liquid crystalline behavior. Discotic liquid crystals often exhibit some kind of helicity, especially when the R group is chiral[6-9]. A 60° twisted geometry of the disks provides the required orientation for the McConnell mechanism to become operative. By the rotation, regions of positive and negative spin density in adjacent molecules in the stack overlap vertically in space and might result in a high-spin complex. This helical twisting behavior would favor the alternation of large positive and small negative spin densities in the columnar stack of high-spin molecules (Figure 5.2). In other words if there would be no helical twist, the radicals in the column would be stacked on top of each other, and one would end up in low-spin situation, whereas the opposite could be true if there is a twist. Clearly such a three-dimensional organization must result from a fine balance of many different interactions. Therefore, ferromagnetic coupling via liquid crystalline cooperative behavior is an extremely challenging goal, which has not been pursued until now.
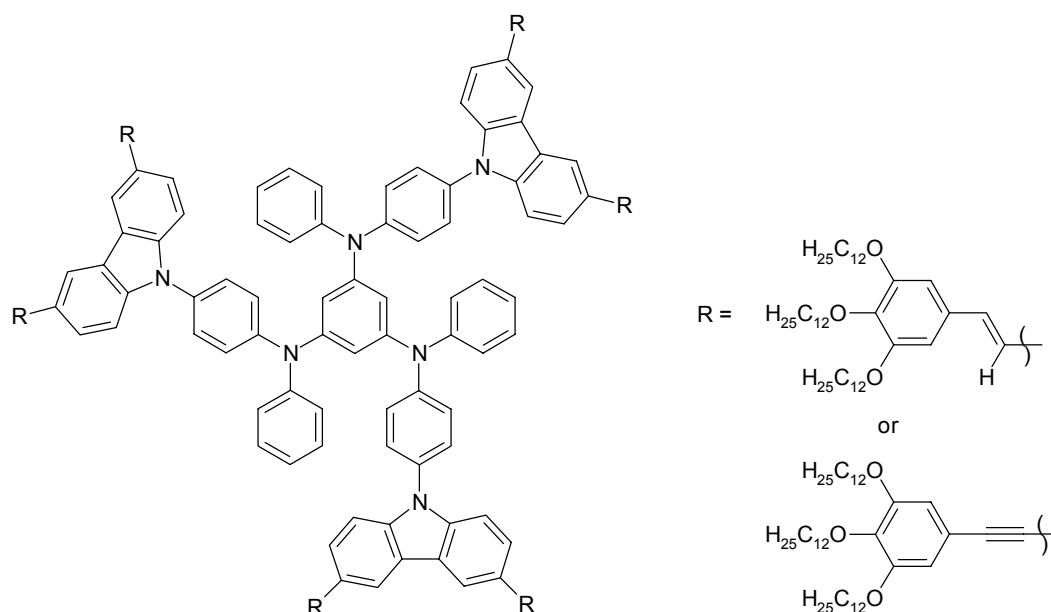
Figure 5.3. *The stars-shaped mixed carbazole oligoaniline proposed as first target molecule (left) substituted with either a phenylevinylene or a phenyleneacetylene as mesogenic groups (right).*

The star-shaped or C_3 symmetrical oligoaniline **11** reported in chapter 4 seems a suitable candidate as basic motif for creating discotic liquid crystalline high-spin molecules. Although it is likely that a rigid central core is required in combination with a flexible periphery in order to get discotic stacking, a very rigid core could negatively influence the stability of the cation radicals. Therefore, as a first attempt introduction of rigidity and flexibility will be done in the periphery of the molecule, by substituting the terminal diphenylamine groups with carbazole moieties. This would still resemble the 1,4-benzenediamine motif, but allows for easy introduction of a variety of different groups on the 3 and 6 position of the carbazole as has been shown by Biemans[10]. Here tridodecylgallic acid derivatives, available in a large variety of different functional groups[11], will be used as mesogenic groups. So as target molecule, a star-shaped carbazole oligoaniline with mesogenic groups is proposed (Figure 5.3).
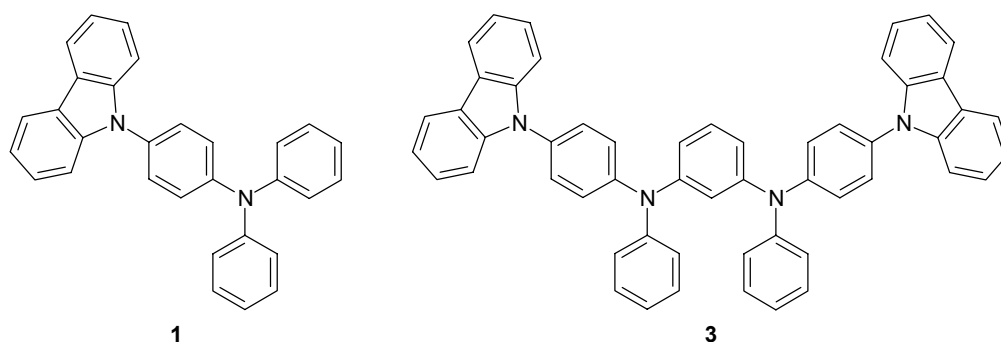

Figure 5.4. *Carbazole oligoanilines **1** and **3** proposed as model compounds for studying their redox, optical, and magnetic properties.*

However, this class of compounds has not been studied before and the stability of the cation radicals when oxidized is unknown. So first dimer **1** and tetramer **3** (Figure 5.4) will be synthesized as model compounds for the investigation of their redox optical and magnetic properties.

5.2 Mixed carbazole aniline oligomers

5.2.1 Synthesis

A similar synthetic strategy as used for the synthesis of the linear *N*-substituted *m-p*-aniline oligomers of chapter 3, is applied for the synthesis of linear carabazole-aniline oligomers, using palladium/ligand catalyst systems developed by Buchwald et al.[12,13]
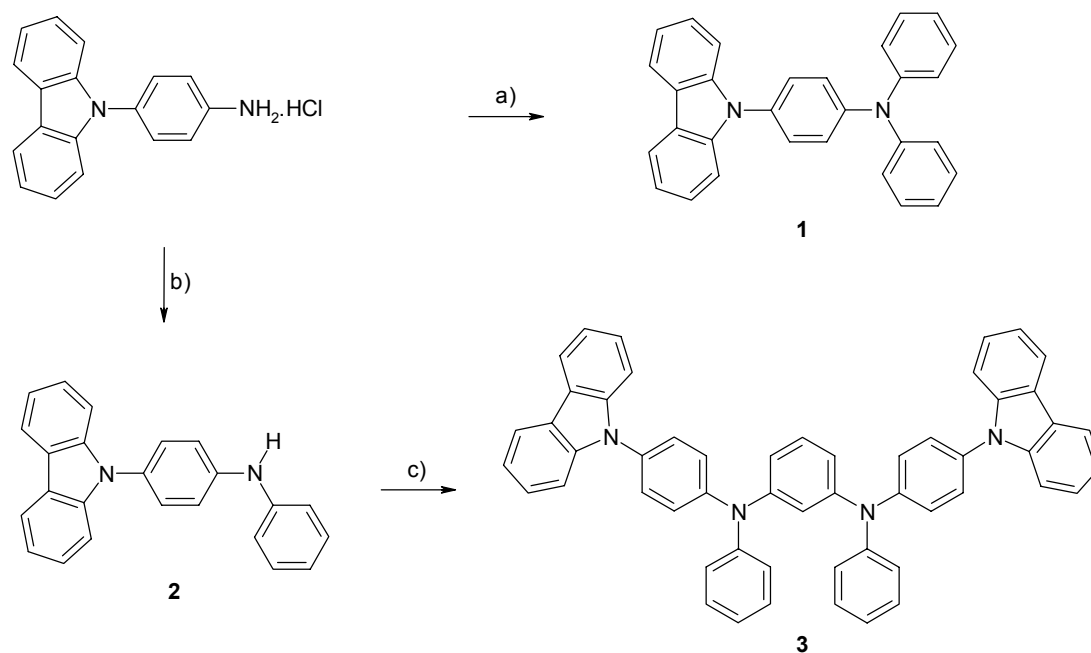
Scheme 5.1. *Synthesis of dimer **1** and tetramer **3**. Reactions and conditions: a) bromobenzene, NatBuO, Pd₂(dba)₃, BPPFA, 90 °C, one week, 45 %, b) bromobenzene, NatBuO, Pd₂(dba)₃, S-BINAP, 90 °C, 18 h, 90 %, c) 1,3-dibromobenzene, NatBuO, Pd₂(dba)₃, PPF-OMe, toluene, 90 °C, 72 h, 64 %.*

Since 4-(*N*-carbazolyl)benzeneamine hydrochloride is commercially available, it is used as starting compound for the preparation of both carbazole oligomers (Scheme 5.1). Two different palladium/ligand catalysts, combined with the use of bromobenzene in large excess, result in two different compounds, **1** and **2**. Here *S*-BINAP as ligand in the catalyst system gives a sufficiently slow reaction rate for the second coupling of

bromobenzene to the aromatic amine. This provides the opportunity to prepare **2** with only small amounts of **1** formed. Subsequent coupling of 1,3-dibromobenzene twice with secondary amine **2** yields tetramer **3**. Column chromatography and crystallization from toluene were used to purify **3**. ^{1}H-NMR spectroscopy of **3** reveals the typical splitting pattern for a 1,3-benzenediamine as well as the carbazole absorptions occurring at higher field as compared to the phenyl group attached to the 1,3-benzenediamine.

5.2.2 Cyclic voltammetry

Electrochemical experiments were carried out according to the general procedure as described in chapter 4. The cyclic voltammogram of **1** revealed one reversible one-electron oxidation occurring at 0.91 V, resulting in the formation of the cation radical of **1** (Figure 1.8, solid line); increasing the voltage gave rise to a second one-electron oxidation towards the dication of **1** at 1.35 V (Figure 1.8, dotted line). Repeated cycling revealed that the second oxidation wave was irreversible due to an increase in current intensity and the gradual appearance of an extra oxidation wave. The anodic and cathodic waves were separated by 64 mV for both E_1^0 and E_2^0, which is in agreement with the theoretical value of 59 mV for a one-electron process. Cyclic voltammetry of *N*-phenyl-carbazole revealed a first irreversible oxidation potential of 1.32 V, which leads to the conclusion that in the first oxidation wave of **1** the triphenylamine unit of the molecule was oxidized followed by the carbazole unit in the second oxidation wave.

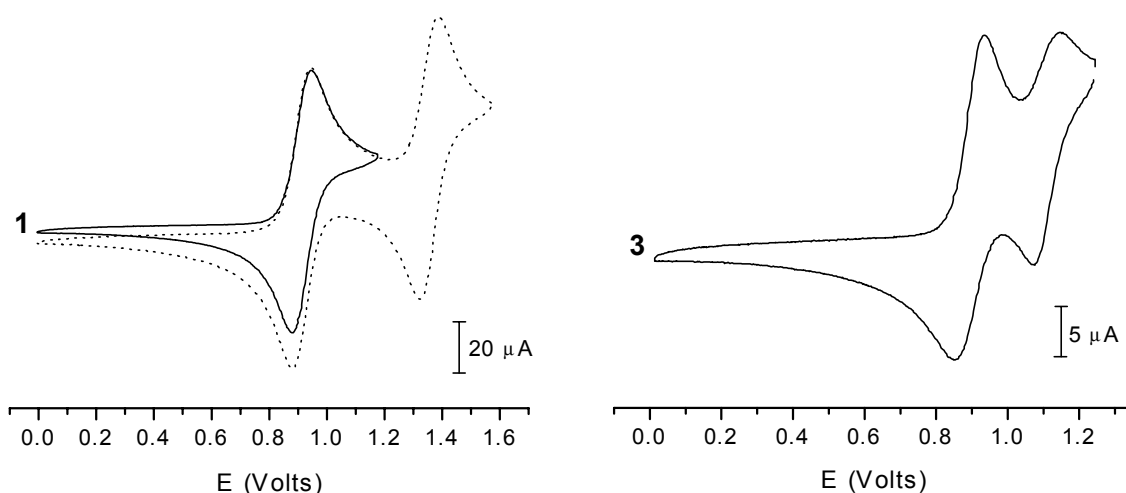**Figure 5.5.** *Cyclic voltammograms of the carbazole oligomers dimer **1** (left) and tetramer **3** (right). Conditions: 0.1 M TBAHF in CH₂Cl₂ at 295 K, scan rate 100 mV/s. Potential vs. SCE reference and calibrated against Fc/Fc+ couple at 0.46 V.*

The redox properties of tetramer **3** showed a similar behavior for the first oxidation at 0.89 V, generating the cation radical of **3** (Figure 1.8). The second chemically reversible oxidation potential at 1.10 V leading to the di(cation radical) of **3**, however, had a much lower intensity as compared to E_1^0. The cathodic and anodic waves of E_1^0 and E_2^0 were splitted by 83 mV and 73 mV, respectively. Increasing the voltage led to completely irreversible oxidation behavior for the generation of trication and tetracation of **3**.

Measuring the cyclic voltammogram of **3** at different scan rates, revealed that the current intensities of the anodic waves of E_1^0 and E_2^0 behave differently. The maximum current intensity I at E_1^0 and E_2^0 can be plotted as a function of the scan rate v in a double logarithmic plot. Curve fitting according to $I = A*v^B$ reveals that the current intensity at E_1^0 follows $I \approx A*v^{0.5}$, expected for a reversible process[14]. This in contrast to the current intensity at E_2^0, which follows $I \approx A*v^{0.36}$. This leads to the conclusion that the formation of $\mathbf{3}^{2(+\bullet)}$ is a diffusion limited quasi reversible electrochemical process.

Table 5.1. *Electrochemical data of the carbazole oligomers* [a]

	E_1^0(V)	E_2^0(V)
Dimer **1**	0.91	1.35
Tetramer **3**	0.89	1.10

[a] *Conditions: 0.1 M TBAHF in CH_2Cl_2 at 295 K. Potential vs. SCE reference and calibrated against Fc/Fc^+ couple at 0.46 V.*

The electrochemistry of the carbazole oligoanilines showed that the electron donating influence of a carbazole group is rather limited when compared to a diphenylamine group (Chapter 4), leading to an increase in the oxidation potentials. The cation radicals of tetramer **3** seem to be localized at both aniline groups, resulting in a lower stability of the di(cation radical) state. These cyclic voltammetry results are comparable with redox characteristics found by Ito et al.[15] for the *m*-oligoanilines, although a more exact comparison is hampered by the absence of Fc/Fc+ value in this publication.

5.2.3 Optical properties of the carbazole oligomers

The oxidation of the carbazole oligoanilines can also be monitored with UV/visible/nearIR spectroscopy. It could give more information about the remarkable oxidation behavior of tetramer **3**. The electronic absorption spectrum of neutral dimer **1**

in CH_2Cl_2 shows three bands at 5.22, 4.21 and 4.00 eV (Figure 4.7), which decreased upon addition of $THI^{+\bullet}ClO_4^-$, to give three cation radical bands at 3.09, 2.39, and 1.04 eV, which are attributed to the formation of $\mathbf{1^{+\bullet}}$. The absorptions bands reached their maximum intensity when **1** was fully oxidized to $\mathbf{1^{+\bullet}}$, and an extra absorption band could be seen at 3.51 eV. Addition of more $THI^{+\bullet}ClO_4^-$ solution led to the appearance of $THI^{+\bullet}ClO_4^-$ absorption bands, indicating that the oxidation strength of $THI^{+\bullet}ClO_4^-$ was insufficient to oxidize the carbazole part of the molecule. Afterwards hydrazine hydrate was added, resulting in a recovery of the neutral spectrum of **1**.
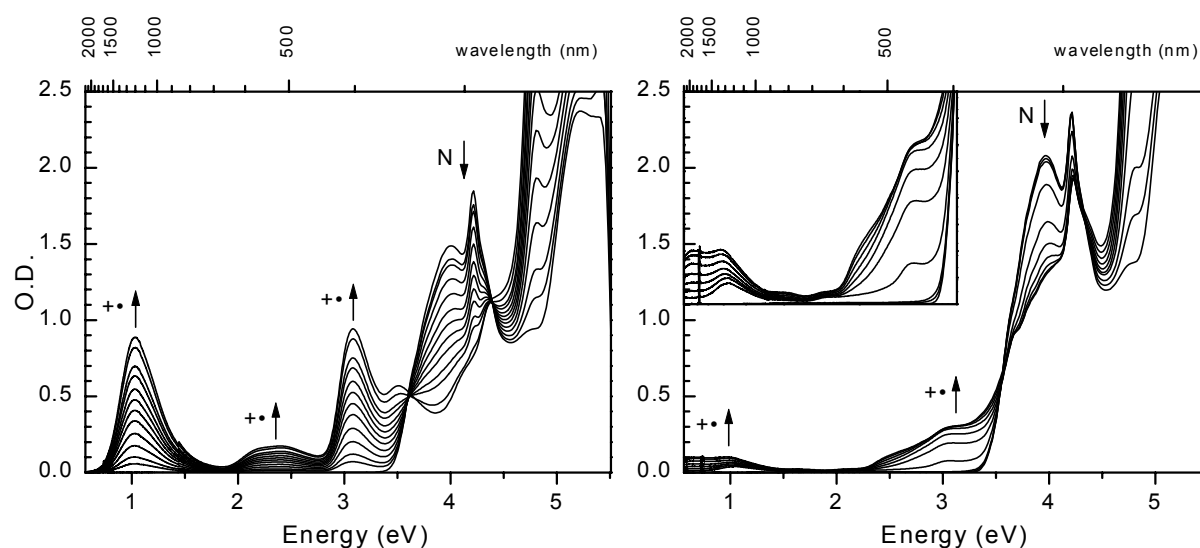

Figure 5.6. *UV/visible/nearIR spectra recorded during the conversion of dimer **1** (left) and tetramer **3** (right) by stepwise oxidation with $THI^{+\bullet}ClO_4^-$ in CH_2Cl_2 at 295 K from the neutral state to their respective cation radical states. Inset right shows magnified low energy area with 'cation radical' absorptions.*

Neutral tetramer **3** in dichloromethane showed three absorption bands at 5.25, 4.21, and 3.97 eV respectively (Figure 4.7), similar to what was found for neutral **1**. Addition of $THI^{+\bullet}ClO_4^-$ solution however, resulted in different optical behavior. Although the upcoming absorption bands at 3.1 and 1 eV initially showed comparable behavior to **1**, soon extra bands came up at the low energy side of the cation radical absorption bands (Figure 4.7, magnified area). Also the intensity of these bands never reached values comparable to the cation radical absorptions of **1**. Clearly the di(cation radical) state of **3** is lacking stability at room temperature and leads to formation of byproducts. A full recovery of the neutral spectrum could therefore not be accomplished by addition of hydrazine hydrate.

Table 5.2. *Optical data of the carbazole oligomers* [a]

	Neutral, eV (nm)			Cation radical, eV (nm)			
Dimer **1**	4.00	4.21	5.22	1.04	2.39	3.09	3.51
	(310)	(295)	(238)	(1192)	(519)	(401)	(353)
Tetramer **3**	3.97	4.21	5.25	±1.0		±3.1	
	(312)	(295)	(236)	(±1240)		(±400)	

[a] *Conditions: CH_2Cl_2, oxidation with $THI^{+\bullet}ClO_4^-$ at 295 K.*

5.2.4 Electron spin resonance spectroscopy

ESR-spectroscopy of $1^{+\bullet}$ recorded at 295 K shows a 5-line hyperfine spectrum in a dilute CH_2Cl_2 solution (Figure 5.7). The 5 lines can be attributed to hyperfine coupling of the unpaired electron with two nitrogen nuclei (I_N = 1). Surprisingly the unpaired electron has spin density on the nitrogen atom of the carbazole unit and shows that this unit contributes to the delocalisation of the unpaired electron. No additional hyperfine couplings could be observed when the spectrum was recorded at low modulation amplitude. The frozen solution spectrum of $1^{+\bullet}$ revealed a narrow signal, typical for a doublet (S = ½) state (Figure 5.7, inset).
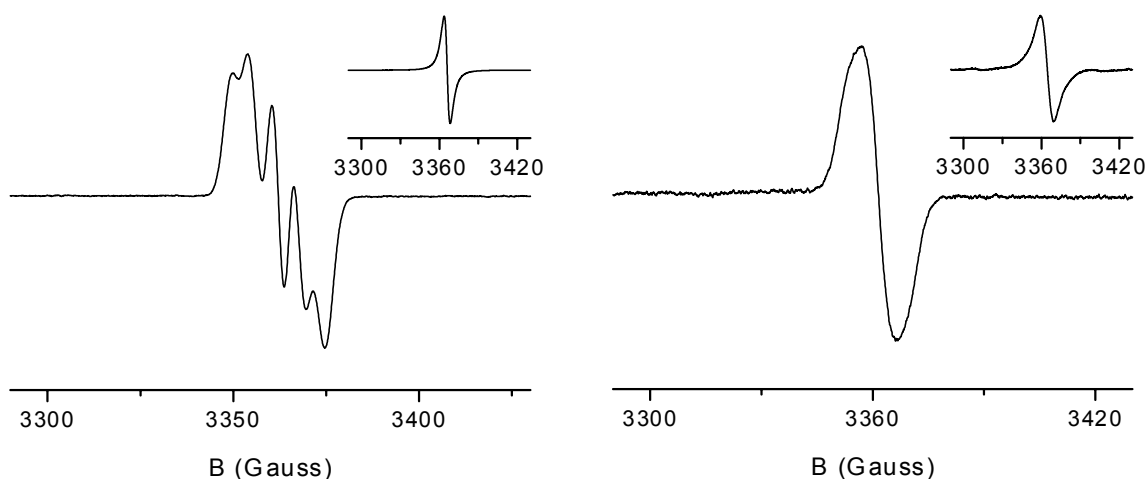
Figure 5.7. *ESR spectra recorded of the cation radical of dimer **1** (left) and the 'di(cation radical)' of tetramer **3** (right) in CH_2Cl_2 obtained by oxidation with $THI^{+\bullet}ClO_4^-$ at 295 K. Insets show the spectra at 125 K.*

Although the electrochemical and UV/visible/nearIR experiments showed the instability of the di(cation radical) of **3** at room temperature, an attempt was made to record an ESR spectrum of $3^{2(+\bullet)}$ in CH_2Cl_2 at 295 K directly after sample preparation (Figure 5.7). The ESR spectrum showed a broad featureless band typical for an

oligo(cation radical), which slowly decreased in intensity as function of the time. The frozen solution spectrum, although much broader as compared to $1^{+\bullet}$ at 125 K, revealed no evidence for a triplet ($S = 1$) state at the $\Delta M_S = \pm 1$ transition, and a $\Delta M_S = \pm 2$ transition could not be observed.

These experiments led to the conclusion that the carbazole aniline oligomers are unsuitable candidates to be used as a core in a star-shaped high-spin molecule with mesogenic groups, for reasons of cation radical instability. Although a similar strategy can be applied as used for the stabilization of cation radicals in m-oligoanilines[16,17], by blocking all relevant positions on the phenyl groups, the mixed carbazole aniline concept was not pursued any further.

5.3 Aniline oligomers with mesogenic groups

Because the carbazole aniline oligomers gave unstable cation radicals at 295 K, the carbazole moiety was again replaced by a N-phenyl-3,4,5-tridodecyloxybenzene-amine group, resulting in a star-shaped oligoaniline **8** (Scheme 5.4).

5.3.1 Synthesis

The synthesis of the mesogenic group, 3,4,5-tridodecyloxybenzeneamine, will be reported elsewhere[11] and is not discussed here. First model compound **5** was synthesized in order to check the feasibility of the synthetic strategy, using mesogenic groups in combination with a palladium/ligand catalyzed C-N coupling (Scheme 5.2). The synthesis starts with reacting 1,4-dibromobenzene twice with 3,4,5-tridodecyloxybenzeneamine, resulting in 1,4-benzenediamine **4**. This was followed by reacting **4** twice with bromobenzene yielding **5**, using bromobenzene as reactant as well as solvent, in order to completely phenylate the secondary amines. All products were purified using column chromatography resulting in wax like solids with increased sensitivity towards oxidation by air. Optical microscopy revealed no indication for liquid crystalline behavior and only melting behavior was observed between 55-60 °C resulting in an isotropic liquid.
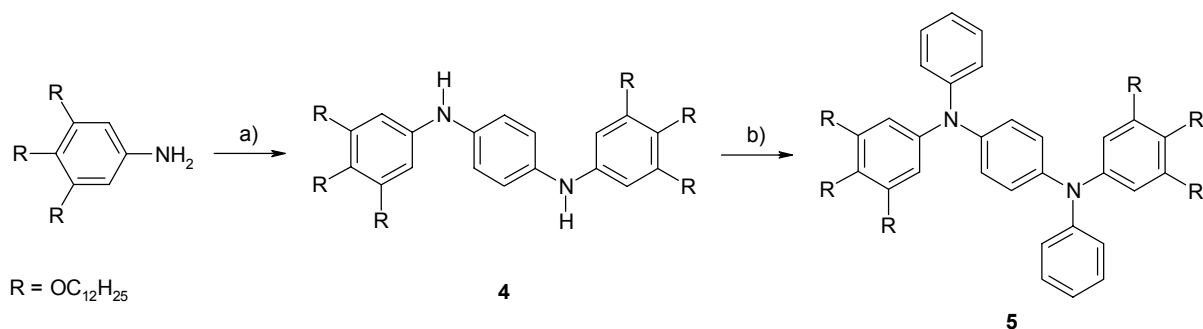
Scheme 5.2. *Synthesis of dimer **5**. Reactions and conditions: a) 1,4-dibromobenzene, NatBuO, Pd₂(dba)₃, S-BINAP, toluene, 90 °C, 19 h, 14%, b) bromobenzene, NatBuO, Pd₂(dba)₃, S-BINAP, 90 °C, 20 h, 52 %.*

The successful synthesis of model compound **5** made it possible to pursue a star-shaped oligoaniline with mesogenic groups. The synthetic strategy involves a reversal of the two steps of the synthetic sequence resulting in **5** (Scheme 5.3). Because reaction of 3,4,5-tridodecyloxybenzeneamine with an excess of 1,4-dibromobenzene not only leads to the formation of the desired secondary amine, but also might result in the formation of oligomeric branched side products. This in contrast to reaction of **6** with an excess of 1,4-dibromobenzene, where fewer side products, most likely dimeric and debrominated products, might be formed. So first secondary amine **6** was prepared by reacting 3,4,5-tridodecyloxybenzeneamine with an excess of bromobenzene. In contrast to the results described previously using the same synthetic methodology, a substantial amount of twice reacted product, *N,N*-diphenyl-3,4,5-tridodecyloxybenzeneamine, was formed during the reaction, but purification by column chromatography yielded pure **6**.

Subsequently, mono reacted product **7** was prepared using an excess of the 1,4-dibromobenzene, which was later recovered by sublimation. Column chromatography afforded intermediate **7** in 93 % yield.
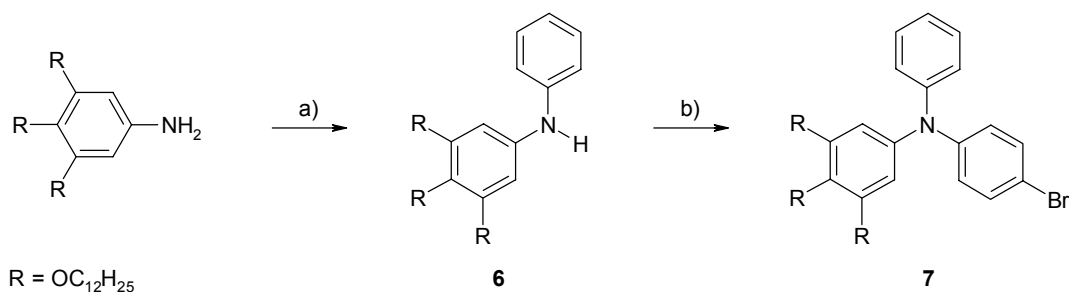
Scheme 5.3. *Synthesis of intermediates **6** and **7**. Reactions and conditions: a) bromobenzene, NatBuO, Pd₂(dba)₃, S-BINAP, 90 °C, 68 h, 87 %, b) 1,4-dibromobenzene, NatBuO, Pd₂(dba)₃, S-BINAP, toluene, 90 °C, 18 h, 93 %.*

Due to purification problems which arose during the synthesis of star-shaped hexamer **14** in chapter 4, the decision was made to use *N,N',N''*-triphenyl-1,3,5-benzenetriamine for a threefold reaction with **7** in the final reaction step, to yield star-shaped hexamer **8** (Scheme 5.4). The once, twice, and three times reacted triamine was separated using preparative size exclusion chromatography (SEC). Since chlorinated solvents generally contain a substantial amount of oxygen, THF without stabilizer was used as eluent in the purification of **8**. Although polyTHF and other by-products are formed during the preparative SEC chromatography of **8**, they could be removed by a simple column filtration.
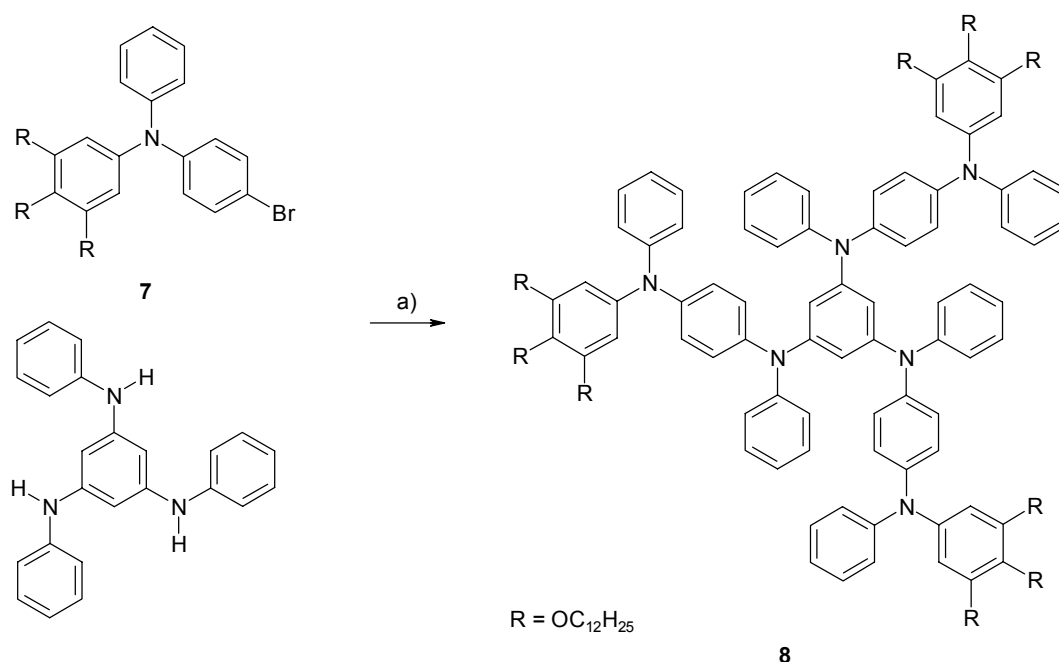
Scheme 5.4. *Synthesis of star-shaped hexamer 8. Reaction conditions: a) NatBuO, Pd₂(dba)₃, BPPFA, toluene, 90 °C, 96 h, 31 %.*

Optical microscopy revealed the absence of a liquid crystalline phase, only a phase transition from a waxy solid to an isotropic liquid was observed around ~ 60 °C. The absence of discotic liquid crystalline behavior might either be due to the absence of a large rigid core in the molecule combined with an insufficient number of alkoxy groups present in the periphery of the molecule.

5.3.2 Cyclic voltammetry

The cyclic voltammogram of **8** is not well resolved, and a large gap between the anodic and cathodic waves can be observed (Figure 5.8). It shows a first oxidation

potential of approximately 0.49 V for **8** with a splitting of 150 mV, at which one-electron is removed. The other multiple electron oxidations at 0.60 and 1.04 V show an even larger anodic/cathodic wave splitting of 180 and 200 mV, respectively. The splitting increases significantly at higher scan rates and is characteristic for a quasi-reversible electrochemical system. In such a system the electron transfer rate becomes comparable with the mass transfer rate at the surface of the electrode. This is probably due to the presence of the long alkoxy groups at the terminal ends of the 1,4-benzenediamine units of star-shaped hexamer **8**. The oxidizable core of the molecule might therefore, be shielded from the electrode surface by the insulating alkoxy groups resulting in a reduced electron transfer rate. Also the current intensity is negatively influenced by the size of the molecule and the molecular weight to the number of 1,4-benzenediamine units ratio, which is larger and higher as compared to star-shaped *N*-methyl-oligoaniline **11** of chapter 4. The cyclic voltammetry is, however, still chemically reversible since scan cycles are identical at constant scan rate. Also the gap between the tri(cation radical) and tri(dication) oxidation potential is still present, allowing for tuning of the oxidation state of the molecule.
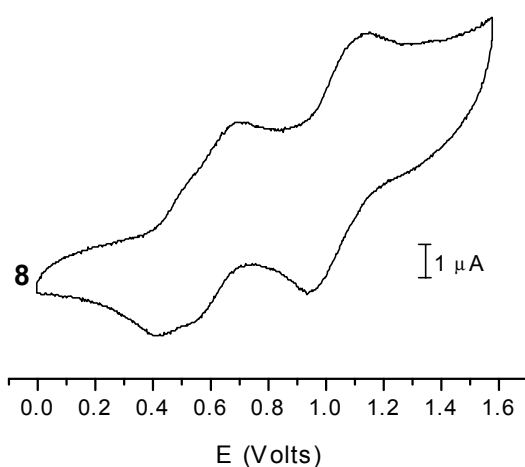
Figure 5.8. *Cyclic voltammogram of star-shaped hexamer 8. Conditions: 0.1 M TBAHF in CH₂Cl₂ at 295 K, scan rate 100 mV/s. Potential vs. SCE reference and calibrated against Fc/Fc⁺ couple at 0.46 V.*

Table 5.3. *Electrochemical data of star-shaped oligomer 8 [a]*

	E_1^0(V)	E_2^0(V)	E_3^0(V)
Hexamer **8**	0.49	0.60[b]	1.04[b]

[a] *Conditions: 0.1 M TBAHF in CH₂Cl₂ at 295 K. Potential vs. SCE reference and calibrated against Fc/Fc⁺ couple at 0.46 V.* [b] *Peaks are unresolved.*

5.3.3 Optical properties

The optical properties of neutral **8** recorded in dichloromethane show one absorption band at 3.93 eV (Figure 5.9). The addition of $THI^{+\bullet}ClO_4^-$ in CH_2Cl_2 initially resulted in two new absorptions at 1.3 and 3.0 eV, which became sharper and red shifted on addition of more oxidant. Also a small shoulder at the blue side of the absorption at 1.14 eV appeared, when **8** was oxidized to the tri(cation radical) state. Oxidation towards the tri(dication) state, resulted in a decrease of the cation radical absorption bands and in between these bands the appearance of unresolved dication band(s). The presence of unreacted thianthrenium perchlorate cannot be excluded completely, since it has an absorption in the same region at ~ 2.25 eV. The neutral spectrum of **8** was recovered after addition of hydrazine hydrate.
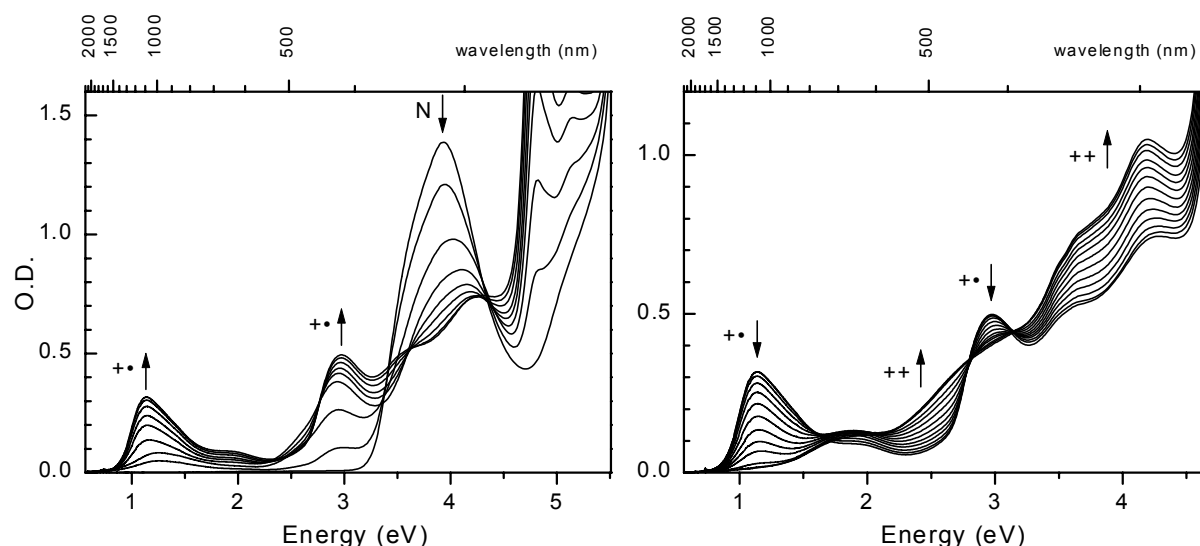
Figure 5.9. *UV/visible/nearIR spectra recorded during the conversion of 8 by stepwise oxidation with THI⁺•ClO₄⁻ in CH₂Cl₂ at 295 K; left: from neutral state to the tri(cation radical); right: from the tri(cation radical) towards the tri(dication).*

In order to check possible aggregation behavior of neutral **8** or its oxidized states in an apolar solvent, dodecane was used as apolar solvent in the solvent mixtures used for the oxidation of **8**. Initially $THI^{+\bullet}ClO_4^-$ in CH_2Cl_2 was used as oxidizing solution, because $THI^{+\bullet}ClO_4^-$ is not soluble in dodecane. However, the resulting neutral thianthrene formed during the stepwise oxidation, precipitated, causing turbid solutions. The use of PIFA in chloroform/TFA (99/1,(v/v) circumvented this problem and reproducible results could be obtained. Star-shaped hexamer **8** recorded in dodecane has a neutral absorption at 3.92 eV, which decreased upon addition of PIFA (Figure 5.10). Two new absorptions came up attributed to the formation of the tri(cation radical) of **8**

at 1.23 and 3.04 eV. A similar observation was made for $\mathbf{8}^{3(+\bullet)}$ in CH_2Cl_2, although the bands are slightly shifted to higher energy. The addition of more oxidant, however, gave much more pronounced spectra for the formation of the tri(dication) of **8** with clear dication absorption bands at 1.81 and 4.07 eV. In this experiment a concentrated oxidant solution was used to minimize the amount of chloroform added to the dodecane solution, in an attempt to keep the solution as apolar as possible. As a result of this, half way the experiment, the solution contained only 1.7 % and at the end 3.5 % of $CHCl_3$/TFA solution.
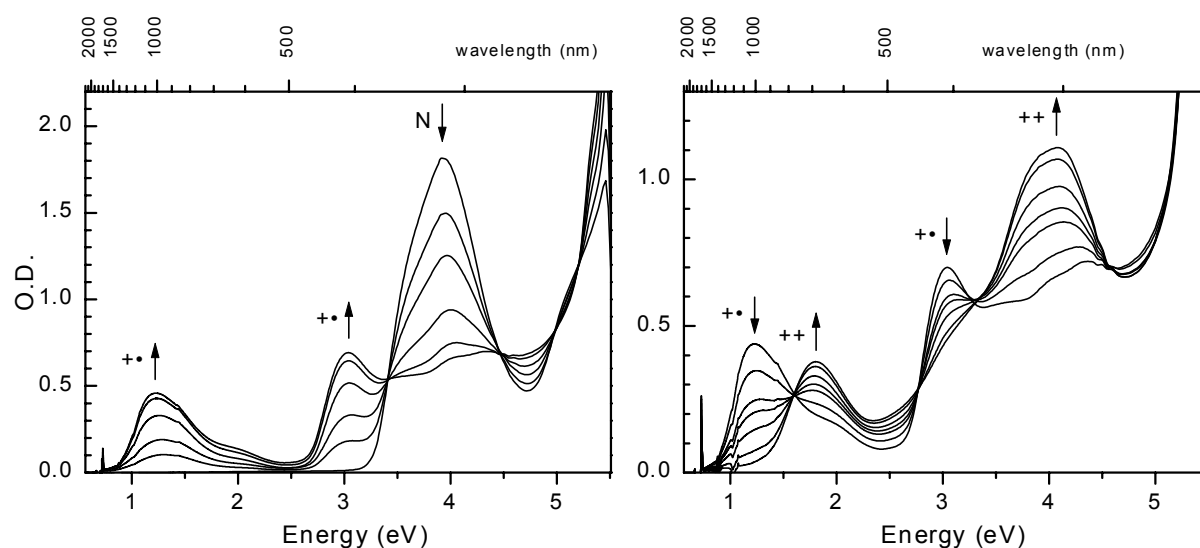
Figure 5.10. *UV/visible/nearIR spectra recorded during the conversion of 8 in dodecane by stepwise oxidation with PIFA in CHCl₃/TFA (99/1 (v/v)) at 295 K; left: from neutral state to the tri(cation radical); right: from the tri(cation radical) to the tri(dication).*

These oxidation experiments show no indication of lyotropic liquid crystalline behavior for **8** in apolar media, since no vibronic absorption bands can be seen. An important result is that a stable tri(cation radical) oxidation state of **8** can be obtained.

Table 5.4. *Optical data of hexamer 8.*

Solvent	Neutral, eV (nm)	Tri(cation radical), eV (nm)		
Dichloromethane [a]	3.93 (316)	1.14 (1088)	2.97 (418)	4.29 (289)
Dodecane [b]	3.92 (316)	1.23 (1008)	3.04 (408)	4.34 (286)

[a] *Conditions: oxidation with THI⁺•ClO₄⁻.* [b] *Conditions: oxidation with PIFA in CHCl₃/TFA (99/1 (v/v)).*

5.3.4 Electron spin resonance spectroscopy

The star-shaped hexamer **8** was oxidized with 3 equivalents of PIFA in dodecane/CHCl$_3$/TFA to the tri(cation radical) state (**8**$^{3(+\bullet)}$). The frozen solution spectrum of **8**$^{3(+\bullet)}$ at 120 K revealed a 5 line zero-field splitting at normal field corresponding to a quartet ($S = 3/2$) state (Figure 4.18). The zero-field parameters $D = 58$ MHz and $E \approx 0$ MHz were obtained from simulation of the anisotropic ESR spectrum at the $\Delta M_S = \pm 1$ transition. This simulation indicated that the intense central line should also be attributed to the presence of doublet impurities. This D value corresponds to an average distance of ~ 11 Å between the unpaired electrons using the dipolar approximation. The electron-donating character of the alkoxy groups located on the outside phenyl rings is probably responsible for the more delocalized nature of the unpaired electrons. The presence of a high-spin state could be confirmed by the observation of a $\Delta M_S = \pm 2$ transition at half field. An unambiguous prove for the quartet state, however, would be the observation of a $\Delta M_S = \pm 3$ transition, but this was not possible due to reasons described in paragraph 4.2.3. In contrast to the ESR experiments on the oligo(cation radicals) of chapter 4, where the best ESR spectra were obtained in butyronitrile, the ESR spectroscopy of **8**$^{3(+\bullet)}$ samples prepared in CH$_2$Cl$_2$ or butyronitrile revealed much more line-broadening and hence less resolved spectra.
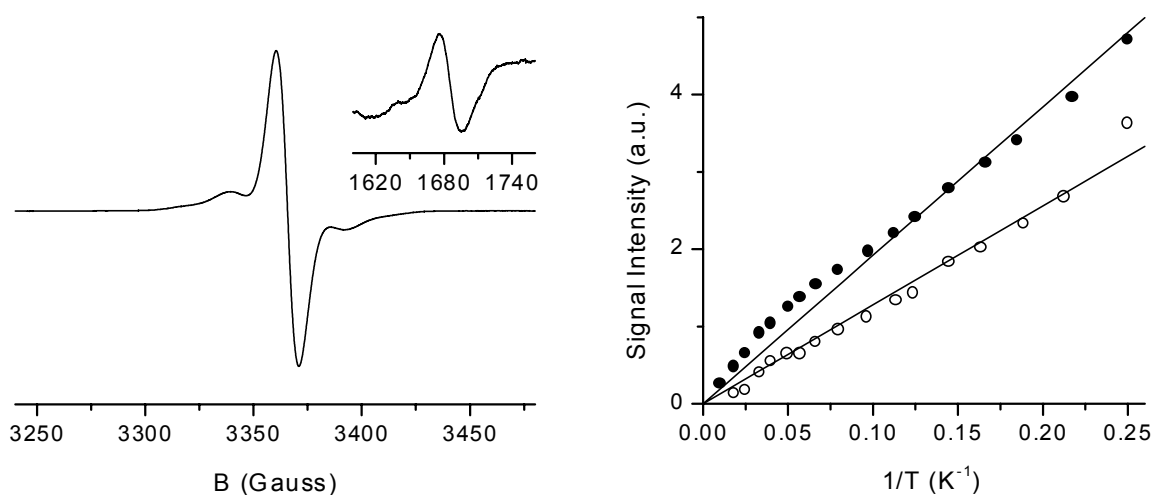
Figure 5.11. *ESR spectra and temperature dependence of the ESR signal intensity of the tri(cation radical) of star shaped hexamer 8 in dodecane/CHCl$_3$/TFA (92/17/1 (v/v/v)) obtained by oxidation with PIFA. Left: recorded at 120 K, inset right shows half-field signal recorded at 4 K. Right: $\Delta M_S = \pm 1$ ($\bullet$) signal and $\Delta M_S = \pm 2$ ($\circ$) signal as a function of the reciprocal temperature, solid lines are linear fits to Curie's law.*

To determine whether the quartet state of $8^{3(+\bullet)}$ is a low energy state, a variable temperature ESR experiment was conducted in the range of $4 - 100$ K. To avoid any contamination by the ESR signal of the doublet impurity, the signal intensities for the $\Delta M_S = \pm 1$ transition were taken from the broad shoulders corresponding to the quartet state. It could be established that the $\Delta M_S = \pm 1$ and $\Delta M_S = \pm 2$ transitions of $8^{3(+\bullet)}$ follow Curie's law ($I = C/T$) (Figure 4.18). This result indicates that the $S = 3/2$ state of $8^{3(+\bullet)}$ is a low energy state of the molecule, which can be degenerate with the corresponding doublet state for reasons described in chapter 4.

5.4 Conclusion

The carbazole oligoaniline dimer **1** and tetramer **3** show reversible oxidation behavior for the preparation of the corresponding cation radical. However, creation of more charges on these oligomers leads to irreversible oxidation behavior at ambient temperatures. Surprisingly, oxidation of the second aniline unit in tetramer **3** already results in an unstable di(cation radical). UV/visible/nearIR spectroscopy confirmed that reversible oxidation of **3** to the di(cation radical) was not possible under the conditions applied here. Therefore, ESR spectroscopy could not reveal any high-spin properties for **3**. The unstable behavior of $3^{2(+\bullet)}$ bears much resemblance with the instability of the di(cation radical) of meta-oligoaniline dimers[15,16] at ambient temperatures. Therefore, the preparation of a star-shaped oligoaniline containing carbazole groups with mesogenic properties was not attempted.

The preparation of the star-shaped oligomer **8** with mesogenic groups proved to be a partially successful first step towards discotic crystalline high-spin molecules. Although liquid crystalline properties could not be observed, the high-spin properties of $8^{3(+\bullet)}$ were established by ESR spectroscopy. The use of dodecane in oxidation experiments could successfully be applied in the UV/visible/nearIR experiments.

These experiments on the carbazole aniline oligomers show the fine balance which exists between rigidity and cation radical stability. Ordering high-spin molecules by making them discotic liquid crystalline, as a first step towards intermolecular ferromagnetic coupling, is presently hampered by the fact that cation radicals based on flexible 1,4-benzenediamine units are more stable but lack liquid crystalline properties, whereas the more rigid carbazole systems seem to lack chemical stability. It would therefore be of interest to use stable neutral radicals in an attempt to make ordered stacks of high-spin molecules. The absence of charged species would eliminate the

electrostatic repulsion, which could help in the formation discotic liquid crystalline stacks.

5.5 Experimental section

General techniques. For general procedures and equipment see experimental sections of chapter 3 and 4. 4-(*N*-carbazolyl)benzeneamine hydrochloride (Lancaster) was used as received. *n*-Dodecane, (FLuka 98%) was dried over an alumina column (ICN Alumina B super I). Chloroform (CHCl$_3$, Acros c.p. stabilized with ethanol) was distilled from P$_2$O$_5$[18]. For preparative size exclusion chromatography Bio-Beads S-X1 (BIORAD, mesh size 200-400, MW limit 14,000) were used. *N,N',N"*-triphenyl-1,3,5-benzenetriamine[19] and 3,4,5-tridodecyloxybenzeneamine[11] were synthesized according to literature procedures.

***N,N*-Diphenyl-4-(*N*-carbazolyl)benzeneamine (1).** An oven-dried Schlenk flask was charged with 4-(*N*-carbazolyl)benzeneamine hydrochloride (0.3 g, 1.0 mmol), sodium *tert*-butoxide (0.41 g, 4.3 mmol), Pd$_2$(dba)$_3$ (4.9 mg, 5.4 µmol), and BPPFA (9.3 mg, 14.7 µmol). After purging with argon, bromobenzene (10 ml, 95 mmol) was added. The reaction mixture was heated for one week at 90 °C and cooled to room temperature. The mixture was taken up in diethyl ether, filtered over Celite 545 and concentrated in vacuo. Column chromatography (SiO$_2$, heptane/CH$_2$Cl$_2$ 2:1) afforded white crystals (0.19 g, 45%). 168-170 mp °C; ^{1}H NMR (CDCl$_3$): δ 8.38 (d, *J* = 7.8 Hz, 2H), 7.46-7.18 (m, 18H), 7.08 (t, *J* = 7.5 Hz, 2H); ^{13}C NMR (CDCl$_3$): δ 147.62, 147.22, 141.02, 131.53, 129.60, 128.00, 125.99, 124.92, 124.51, 123.55, 123.36, 120.43, 119.89, 110.02; IR (ATR, cm^{-1}): 3040, 2924, 1625, 1587, 1509, 1497, 1485, 1451, 1333, 1312, 1273, 1230, 1178, 1147, 1113, 1076, 1027, 913, 897, 837, 757, 742, 719, 695, 628, 565. Anal Calcd for C$_{30}$H$_{22}$N$_2$: C, 87.77; H, 5.40; N, 6.82. Found: C, 87.37; H, 5.44; N, 6.51.

***N*-Phenyl-4-(*N*-carbazolyl)benzeneamine (2).** An oven-dried Schlenk flask was charged with 4-(*N*-carbazolyl)phenylamine hydrochloride (0.29 g, 1.0 mmol), sodium *tert*-butoxide (0.30 g, 3.1 mmol), Pd$_2$(dba)$_3$ (2.9 mg, 3.2 µmol), and *S*-BINAP (4.6 mg, 7.4 µmol). After purging with argon, bromobenzene (10 ml, 95 mmol) was added. The reaction mixture was heated for 18 hours at 90 °C and cooled to room temperature. The mixture was taken up in diethyl ether, filtered over Celite 545 and concentrated in vacuo. Column chromatography (SiO$_2$, heptane/CH$_2$Cl$_2$ 2:1) afforded white crystals (0.30, 90%). ^{1}H NMR (CDCl$_3$): δ 8.14 (dt, *J* = 7.7, 0.9 Hz, 2H), 7.42-7.36 (m, 6H), 7.32 (t, *J* = 7.4 Hz, 2H), 7.27 (t, *J* = 7.1 Hz, 2H), 7.21 (dt, *J* = 8.8, 3.1 Hz, 2H), 7.16 (d, 7.5 Hz, 2H), 7.00 (tt, *J* = 7.4, 1.1 Hz, 1H), 5.83 (bs, 1H); ^{13}C NMR (CDCl$_3$): δ 142.69, 142.32, 141.21, 129.67, 129.42, 128.22, 125.78, 123.01, 121.69, 120.20, 119.57, 118.54, 117.88, 109.73; IR (ATR, cm^{-1}): 3390, 3047, 1625, 1595, 1513, 1493, 1477, 1450, 1402, 1335, 1309, 1229, 1177, 1148, 1117, 1077, 1026, 1014, 998, 911, 877, 823, 744, 722, 692, 623, 565.

***N,N'*-Bis[4-(*N*-carbazolyl)phenyl]-*N,N'*-diphenyl-1,3-benzenediamine (3).** An oven-dried Schlenk flask was charged with **2** (0.3 g, 0.9 mmol), sodium *tert*-butoxide (0.13 g, 1.4 mmol), Pd$_2$(dba)$_3$ (2.6 mg, 2.8 µmol), and PPF-OMe (3.4 mg, 7.8 µmol). After purging with argon, 1,3-dibromobenzene (50 µl, 0.41 mmol) and toluene (5ml) were added. The reaction mixture was heated for 72 hours at 90 °C and cooled to room temperature. The mixture was taken up in diethyl ether, filtered over Celite 545 and concentrated in vacuo. Column chromatography (SiO$_2$, heptane/CH$_2$Cl$_2$ 3:1) and crystallization from toluene resulted in white crystals (0.21, 64 %). 268-270 mp °C; ^{1}H NMR (CDCl$_3$): δ 8.16 (d, *J* = 7.7 Hz, 4H), 7.43-7.39 (m, 12H), 7.37-7.25 (m, 17H), 7.11 (t, *J* = 7.0 Hz, 2H), 7.08 (t, *J* = 2.2 Hz, 1H), 6.89 (dd, *J* = 8.1, 2.2 Hz, 2H); ^{13}C NMR (CDCl$_3$): δ 148.65, 147.35, 146.82, 141.18, 131.79, 130.33, 129.63, 128.01, 126.00, 125.09, 124.44, 123.78, 123.39, 120.44, 120.17, 119.94, 119.00, 110.02; IR (ATR, cm^{-1}): 3034, 1625, 1582, 1509, 1482, 1452, 1333, 1300, 1266, 1230, 1184,

1147, 1120, 1111, 1076, 1015, 914, 857, 838, 772, 750, 723, 693, 629, 566. Anal Calcd for $C_{54}H_{38}N_4$: C, 87.30; H, 5.16; N, 7.54. Found: C, 87.51; H, 5.52; N, 6.91.

N,N'-Bis(3,4,5-tridodecyloxyphenyl)-1,4-benzenediamine (4). An oven-dried Schlenk flask was charged with 3,4,5-tridodecyloxybenzeneamine (1.29 g, 2.0 mmol), 1,4-dibromobenzene (0.24 g, 1.0 mmol), sodium *tert*-butoxide (0.29 g, 3.0 mmol), Pd$_2$(dba)$_3$ (4.9 mg, 5.4 µmol), and *S*-BINAP (12.2 mg, 19.6 µmol). After purging with argon, toluene (10 ml) was added. The reaction mixture was heated for 19 hours at 90 °C and cooled to room temperature. The mixture was taken up in diethyl ether, filtered over Celite 545 and concentrated in vacuo. Column chromatography (SiO$_2$, heptane/CH$_2$Cl$_2$ 1:1) resulted in a waxy solid (0.2 g, 14 %). ^{1}H NMR (CDCl$_3$): δ 6.99 (s, 4H), 6.21 (s, 4H), 5.38 (bs, 2H), 3.91-3.87 (m, 12H), 1.81-1.71 (m, 12H), 1.47-1.41 (m, 12H), 1.38-1.20 (m, 96 H), 0.88 (t, *J* = 6.6 Hz, 18H); ^{13}C NMR (CDCl$_3$): δ 153.94, 140.25, 137.72, 132.74, 120.42, 96.77, 73.82, 69.33, 32.15, 30.56, 29.99, 29.98, 29.93, 29.88, 29.67, 29.63, 29.60, 26.42, 26.34, 22.92, 14.33.

N,N'-Bis(3,4,5-tridodecyloxyphenyl)-N,N'-diphenyl-1,4-benzenediamine (5). An oven-dried Schlenk flask was charged with **4** (0.2 g, 0.14 mmol), sodium *tert*-butoxide (0.14 g, 1.5 mmol), Pd$_2$(dba)$_3$ (2.7 mg, 2.9 µmol), and *S*-BINAP (5.4 mg, 8.7 µmol). After purging with argon, bromobenzene (1 ml, 9.5 mmol) was added. The reaction mixture was heated for 20 hours at 90 °C and cooled to room temperature. The mixture was taken up in diethyl ether, filtered over Celite 545 and concentrated in vacuo. Column chromatography (SiO$_2$, heptane/CH$_2$Cl$_2$ 2:1) resulted in a waxy solid (0.11 g, 52 %). mp 40-41 °C; ^{1}H NMR (CDCl$_3$): δ 7.24-7.19 (m, 4H), 7.05 (dd, *J* = 8.8, 1.1 Hz, 4H), 6.97 (s, 4H), 6.94 (tt, *J* = 7.3, 1.1 Hz, 2H), 6.31 (s, 4H), 3.94 (t, *J* = 6.6 Hz, 4H), 3.82 (t, *J* = 6.6 Hz, 8H), 1.80-1.70 (m, 12H), 1.50-1.38 (m, 12H), 1.35-1.20 (m, 96 H), 0.89 (t, *J* = 6.6 Hz, 18H); ^{13}C NMR (CDCl$_3$): δ 153.69, 148.22, 143.25, 142.79, 134.97, 129.19, 125.06, 122.85, 121.82, 104.57, 73.76, 69.34, 32.16, 30.60, 30.00, 29.98, 29.95, 29.90, 29.88, 29.70, 29.60, 26.40, 26.34, 22.92, 14.34; IR (ATR, cm^{-1}): 2957, 2918, 2851, 1585, 1505, 1493, 1467, 1424, 1378, 1349, 1298, 1280, 1263, 1238, 1221, 1112, 1091, 1032, 997, 980, 823, 781, 747, 738, 721, 696, 682, 657, 629, 602, 583.

N-Phenyl-3,4,5-tridodecyloxybenzeneamine (6). An oven-dried Schlenk flask was charged with 3,4,5-tridodecyloxybenzeneamine (0.65 g, 1.0 mmol), sodium *tert*-butoxide (0.16 g, 1.7 mmol), Pd$_2$(dba)$_3$ (2.7 mg, 2.9 µmol), and *S*-BINAP (5.7 mg, 9.2 µmol). After purging with argon, bromobenzene (6 ml, 57 mmol) was added. The reaction mixture was heated for 68 hours at 90 °C and cooled to room temperature. The mixture was taken up in diethyl ether, filtered over Celite 545 and concentrated in vacuo. Column chromatography (SiO$_2$, heptane/CH$_2$Cl$_2$ 4:5) resulted in slightly yellow viscous oil (0.63 g, 87 %). ^{1}H NMR (CDCl$_3$): δ 7.25 (dd, *J* = 8.4, 7.3 Hz, 2H), 7.02 (dd, *J* = 8.4, 1.1 Hz, 2H), 6.89 (tt, *J* = 7.3, 1.1 Hz, 1H), 6.23 (s, 2H), 5.57 (bs, 1H), 3.94-3.90 (m, 6H), 1.82-1.76 (m, 6H), 1.55-1.42 (m, 6H), 1.39-1.23 (m, 48 H), 0.90 (t, *J* = 6.8 Hz, 9H); ^{13}C NMR (CDCl$_3$): δ 153.74, 144.09, 138.62, 133.39, 129.47, 120.44, 117.21, 98.45, 73.87, 69.38, 32.36, 32.34, 30.75, 30.19, 30.17, 30.13, 30.07, 29.85, 29.82, 29.79, 26.62, 26.53, 23.13, 14.57; IR (ATR, cm^{-1}): 3336, 2956, 2921, 2852, 1593, 1537, 1496, 1467, 1456, 1411, 1387, 1285, 1250, 1232, 1175, 1113, 1034, 1001, 970, 814, 750, 718, 692, 633, 612.

N-4-Bromophenyl-N-phenyl-3,4,5-tridodecyloxybenzeneamine (7). An oven-dried Schlenk flask was charged with **6** (0.3 g, mmol), sodium *tert*-butoxide (0.5 g, 5.2 mmol), Pd$_2$(dba)$_3$ (5.1 mg, 5.5 µmol), *S*-BINAP (10 mg, 16 µmol), and 1,4-dibromobenzene (7.0 g, 30 mmol). After purging with argon, toluene (5 ml) was added. The reaction mixture was heated for 18 hours at 90 °C and cooled to room temperature. The mixture was taken up in diethyl ether, filtered over Celite 545 and concentrated in vacuo. The excess of 1,4-dibromobenzene was largely removed by vacuum sublimation. Column chromatography (SiO$_2$, heptane/CH$_2$Cl$_2$ 3:1) resulted in an amorphous solid (0.34, 93 %). mp 44-45 °C; ^{1}H NMR (CDCl$_3$): δ 7.30 (d, *J* = 8.8 Hz, 2H), 7.23 (dd, *J* = 8.4, 7.3 Hz, 2H), 7.05 (dd, *J* = 8.8, 1.1 Hz, 2H), 6.99 (tt, *J* = 7.3, 1.1 Hz, 1H), 6.92 (d, *J* = 8.8 Hz, 2H), 6.26 (s, 2H), 3.94 (t, *J* = 6.6 Hz, 2H), 3.79 (t, *J* = 6.6 Hz, 4H), 1.80-1.69 (m, 6H), 1.48-1.35 (m, 6H), 1.31-

1.22 (m, 48 H), 0.88 (t, J = 6.6 Hz, 9H); ^{13}C NMR (CDCl$_3$): δ 153.69, 147.44, 147.15, 142.61, 135.24, 132.07, 129.32, 124.60, 123.88, 122.88, 114.30, 104.75, 73.80, 69.38, 32.31, 32.27, 30.75, 30.16, 30.14, 30.09, 30.05, 30.01, 29.82, 29.79, 29.76, 29.70, 29.41, 26.56, 26.45, 23.10, 14.54; IR (ATR, cm^{-1}): 2955, 2917, 2849, 1588, 1486, 1468, 1432, 1382, 1331, 1311, 1292, 1239, 1222, 1113, 1069, 1039, 1008, 952, 886, 819, 783, 752, 721, 712, 693, 669, 658, 585.

N,N',N''-Tris[N-phenyl-N-(3,4,5-tridodecyloxyphenyl)-4-aminophenyl]-N,N',N''-triphenyl-1,3,5-benzenetriamine (8). An oven-dried Schlenk flask was charged with N,N',N''-triphenyl-1,3,5-benzenetriamine (44.7 mg, 0.13 mmol), **7** (0.34 g, 0.39 mmol), sodium *tert*-butoxide (0.1 g, 1.04 mmol), Pd$_2$(dba)$_3$ (2.3 mg, 2.5 μmol), and BPPFA (4.6 mg, 7.5 μmol). After purging with argon, toluene (5 ml) was added. The reaction mixture was heated for 96 hours at 90 °C and cooled to room temperature. The mixture was taken up in diethyl ether, filtered over Celite 545 and concentrated in vacuo. Preparative SEC chromatography (Biobeads column) with THF as eluens and a short column filtration (SiO$_2$, CH$_2$Cl$_2$) resulted in an amorphous white solid (0.11 g, 31 %). mp 55-58 °C; ^{1}H NMR (CDCl$_3$): δ 7.20-7.12 (m, 12H), 7.02 (dd, J = 8.8, 1.1 Hz, 6H), 6.98 (dd, J = 8.4, 1.1 Hz, 6H), 6.95-6.86 (m, 18H), 6.40 (s, 3H), 6.25 (s, 6H), 3.92 (t, J = 6.6 Hz, 6H), 3.77 (t, J = 6.6 Hz, 12H), 1.80-1.65 (m, 18H), 1.50-1.35 (m, 18H), 1.35-1.20 (m, 144H), 0.90-0.85 (m, 27H); ^{13}C NMR (CDCl$_3$): δ 153.54, 149.01, 148.02, 147.41, 143.06, 143.03, 141.95, 134.90, 129.11, 129.02, 125.52, 124.74, 123.40, 122.88, 122.26, 121.79, 113.20, 104.62, 73.80, 69.37, 32.30, 30.76, 30.15, 30.10, 30.05, 30.03, 29.86, 29.78, 29.76, 26.58, 26.50, 23.09, 14.53; IR (ATR, cm^{-1}): 3036, 2921, 2853, 1731, 1586, 1493, 1466, 1436, 1380, 1277, 1236, 1176, 1114, 1036, 803, 748, 722, 694.

5.6 References

1. McConnell, H. M., *J. Chem. Phys.* **1963**, *39*, 1910.
2. Izuoka, A.; Murata, S.; Sugawara, T.; Iwamura, H., *J. Am. Chem. Soc.* **1985**, *107*, 1786.
3. Izuoka, A.; Murata, S.; Sugawara, T.; Iwamura, H., *J. Am. Chem. Soc.* **1987**, *109*, 2631.
4. Zhang, J. P.; Baumgarten, M., *Chem. Phys.* **1997**, *222*, 1.
5. Coomber, A. T.; Beljonne, D.; Friend, R. H.; Bredas, J. L.; Charlton, A.; Robertson, N.; Underhill, A. E.; Kurmoo, M.; Day, P., *Nature* **1996**, *380*, 144.
6. Demus, D.; Goodby, J. W.; Gray, G. W.; Spiess, H.-W.; Vill, V. (Eds.), *Handbook of Liquid Crystals, Vol 1: Fundamentals*, WILEY-VCH, Weinheim **1998**.
7. Palmans, A. R. A.; Vekemans, J.; Havinga, E. E.; Meijer, E. W., *Angew. Chem., Int. Ed.* **1997**, *36*, 2648.
8. Palmans, A. R. A.; Vekemans, J.; Hikmet, R. A.; Fischer, H.; Meijer, E. W., *Adv. Mater.* **1998**, *10*, .
9. Palmans, A. R. A.; Vekemans, J. A. J. M.; Fischer, H.; Hikmet, R. A.; Meijer, E. W., *Chem. Eur. J.* **1997**, *3*, 300.
10. Biemans, H. A. M., *Multi-chromophoric arrays in molecules of high symmetry*, Eindhoven University of Technology, Eindhoven **1997**.
11. Vekemans, J. A. J. M., *to be published*.
12. Wolfe, J. P.; Wagaw, S.; Buchwald, S. L., *J. Am. Chem. Soc.* **1996**, *118*, 7215.
13. Marcoux, J. F.; Wagaw, S.; Buchwald, S. L., *J. Org. Chem.* **1997**, *62*, 1568.
14. Southhampton-Electrochemistry-Group, *Instrumental Methods in Electrochemistry*, Ellis Horwood Limited, Chichester **1985**.

15.   Ito, A.; Saito, T.; Tanaka, K.; Yamabe, T., *Tetrahedron Lett.* **1995**, *36*, 8809.

16.   Yano, M.; Sato, K.; Shiomi, D.; Ichimura, A.; Abe, K.; Takui, T.; Itoh, K., *Tetrahedron Lett.* **1996**, *37*, 9207.

17.   Stickley, K. R.; Blackstock, S. C., *J. Am. Chem. Soc.* **1994**, *116*, 11575.

18.   Armarego, W. L. F.; Perrin, D. D., *Purification of Laboratory Chemicals*, Butterworth-Heinemann, Oxford **1997**.

19.   Buu-Hoï, N. P., *J. Chem. Soc.* **1952**, 4346.

6

Oligo(verdazyl radicals) with mesogenic groups

Abstract: An attempt to create liquid crystalline discotic stacks as an intermediate step towards intermolecular ferromagnetic coupling between high-spin molecules is reported. Two neutral oxo-verdazyl triradicals with mesogenic groups were synthesized, one with a 1,3,5-substituted benzene core and one with a 2,6,10-substituted triphenylene core. These molecules were characterized by means of UV/visible/nearIR spectroscopy and ESR spectroscopy revealing evidence for intramolecular high-spin behavior. Liquid crystalline behavior, however was not be observed. In a second attempt triphenyl verdazyl radicals were used to create a high-spin molecule with mesogenic side groups.

6.1 Introduction

Achieving intermolecular spin coupling will be a major step that may allow us to progress from high-spin molecules towards nanoscopic and mesoscopic magnetic materials under ambient conditions. The assembly of high-spin molecules into functional magnetic materials requires a detailed understanding and precise control at all the levels of hierarchy. In chapter 5 a model was proposed to use liquid crystalline high-spin molecules for creating intermolecular ferromagnetic interactions in extended discotic stacks. The first attempt in that direction by using oligo(cation radicals) of C_3 symmetry was not successful because these molecules lacked the liquid crystalline properties. In this chapter we will pursue the same goal but use stable neutral radicals to enhance the attractive interactions between the conjugated systems.
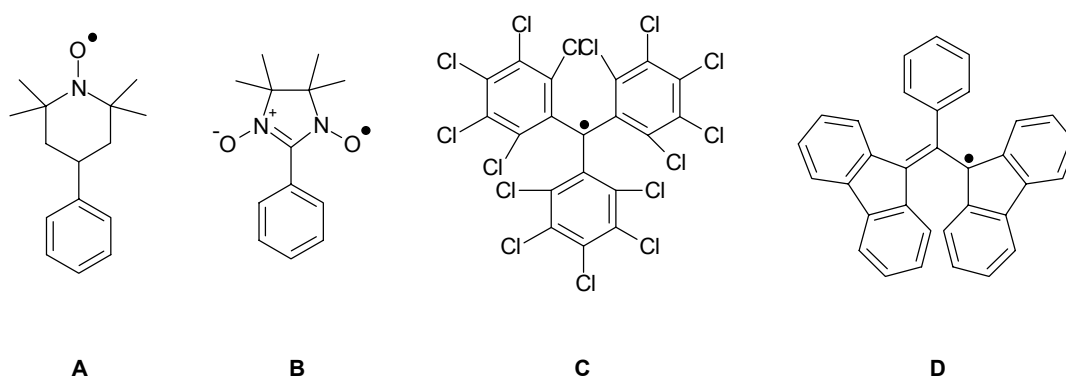

Figure 6.1. *Stable neutral radicals. From left to right: TEMPO radical (**A**), nitronyl nitroxide (**B**), perchlorotriphenylmethyl radical (**C**), Koelsch free radical (**D**).*

Various stable neutral radicals are known which might be used in a ferromagnetic material[1-3]. Aminoxyl type radicals like the TEMPO radical (Figure 6.1, **A**) are suitable candidates with respect to their stability under aerobic conditions. However, due to absence of π-conjugation, the possibilities for through-bond and hence ferromagnetic coupling are limited. Nitronyl nitroxides (**B**) are also very stable radicals but do not exhibit a high-spin ground state in a 1,3,5-tri(radical)benzene type configuration[4]. Here the intramolecular spin-spin coupling is limited because of a low extent of spin delocalisation into the phenyl ring. In contrast the perchlorotriphenylmethyl radical[5] (**C**) has been used to prepare very stable neutral radicals with high-spin properties[6]. A drawback is that they do not allow for easy synthetic modification[7], and seem not suitable for use in discotic liquid crystals, because of out-of-plane twisting resulting in a non-planar molecule. Koelsch free radical[8] (**D**) is an another example of a stable carbon centered radical with high-spin properties in a 1,3-benzenediradical configuration[9]. This type of radical in principle allows for synthetic modification, but only a few derivatives

are known so far[10,11]. For nitrogen centered verdazyl radicals, on the other hand, a large variety of mono radicals has been reported[12,13](Figure 6.2). These verdazyl radicals also exhibit high-spin properties[14-17] in 1,3-di(radical)benzene and 1,3,5-tri(radical)benzene systems and are therefore of interest to prepare high-spin discotic liquid crystals.
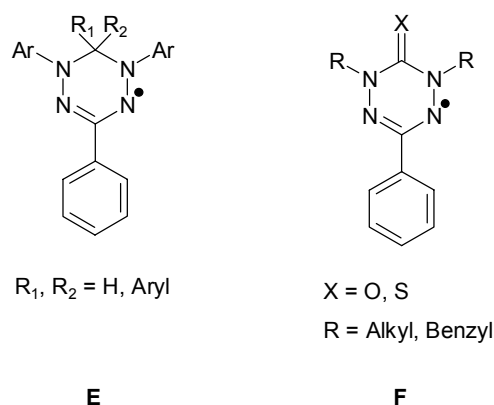

Figure 6.2. *Two classes of verdazyl radicals: triphenyl verdazyl radical (E) and oxo- or thio-verdazyl radical (F).*

Verdazyl radicals can roughly be differentiated in two classes; the triarylverdazyls (Figure 6.2, **E**) and the oxo- or thio-verdazyls[18] (**F**). Synthetically the latter are better accessible since the core and the periphery of the molecule can be constructed in parallel and thus allow for easy modification of the R-groups. The oxo and thio-verdazyl are, however, some what less stable than the triphenylverdazyls. Another important aspect is that the desired radicals can be generated in a controllable way from their precursors by stepwise oxidation. Triaryl verdazyl radicals and their precursors are usually constructed in a sequence of reactions on one starting molecule, sometimes even in a one-pot procedure, ending with a ring closure and oxidation by air, producing the very stable free radical in low yields.
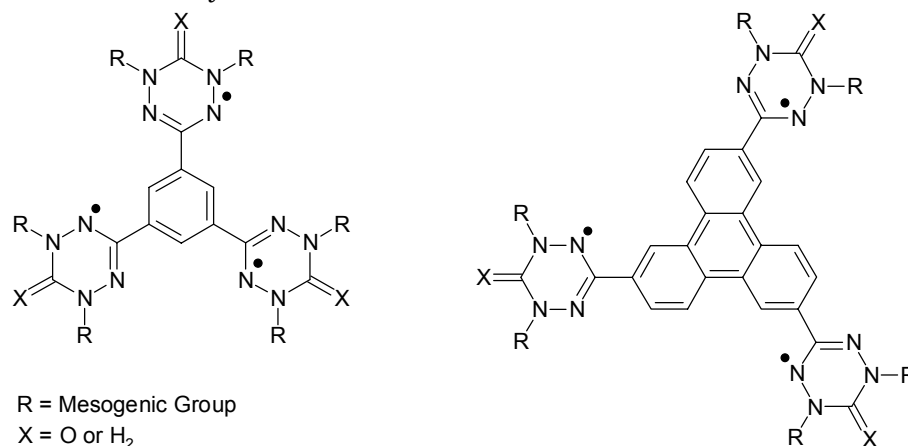

Figure 6.3. *Target molecules.*

Recently oxo-verdazyl biradicals with high-spin properties[19] as well as phosphorus containing verdazyl radicals[20] were reported, adding to the diversity of the verdazyl radicals. Because oxo-verdazyl radicals are synthetically better accessible and easier modified they are used here. In this chapter the synthesis and characterization of a 1,3,5-tri(oxo-verdazyl radical)benzene with dodecyl substituents as mesogenic groups is reported, in an attempt to check the high-spin properties of these oxo-verdazyl radicals. In a next step the benzene is replaced by a triphenylene core to create an organic high-spin discotic liquid crystal via the extension of the core. Although triphenylene has not been used so far as an intramolecular ferromagnetic coupling unit the basic rules for alternation of spin polarization predict that two substitution patterns may produce the required in phase periodicity of spin polarization: 1,5,9 or 2,6,10. The 1,4,5,8,9,12 positions are synthetically difficult to modify in contrast to the 2,3,6,7,10,11 positions, for which a range of hexa-substituted triphenylene molecules have been reported[21,22]. These type of molecules received considerable attention for their discotic liquid crystalline behavior[23] combined with interesting redox and photoconducting properties[24,25]. Only a few triphenylenes with a 2,6,10 substitution pattern are known. One example is 2,6,10-trialkoxy triphenylene reported by Ringsdorf et al. This system exhibits no discotic liquid crystalline behavior, except for the trialkoxytribromotriphenylene which has a small discotic liquid crystalline regime[26,27](Figure 6.4, **G**). The synthesis of 2,6,10-trimethyltriphenylene (Figure 6.4, **H**) has been reported[28] from 4-methylcyclohexanone, using a zirconium halide catalyst, in a cyclodehydration reaction, followed by dehydrogenation. In theory the methyl substituents give access to a wide range of functional groups, of which the aldehyde functionality is of special interest here since it allows for conversion into verdazyl radicals. Finally the design of a 1,3,5-tris(triphenylverdazyl radical)benzene precursor with mesogenic groups will be described.
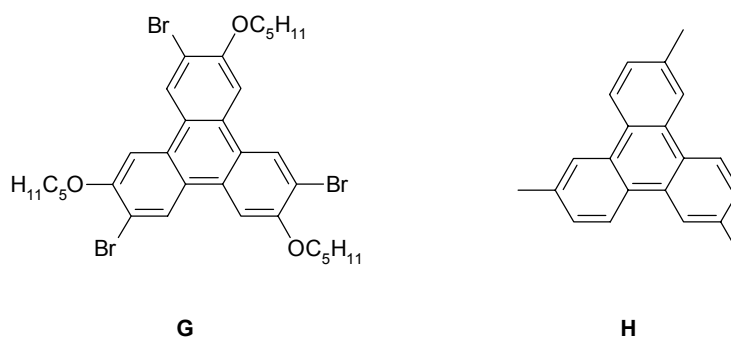

G   **H**

Figure 6.4. *2,6,10-Substituted triphenylenes of Ringsdorf et al. (**G**) and Shirai et al.(**H**).*

## 6.2 Oxo-verdazyl radicals with dodecyl-groups

6.2.1 Synthesis

1,4,5,6-Tetrahydro-1,2,4,5-tetrazin-3(2H)-ones are precursors to the oxo-verdazyl radicals, which are prepared by a condensation of the appropriate carbonohydrazide with an aldehyde when substituted with methyl or benzyl groups at the 2 and 4 position. Starting with a simple alkyl chain as a mesogenic group, dodecylhydrazine **1** was prepared by reaction of 1-bromododecane with hydrazine hydrate in large excess[29] followed by vacuum distillation. To prepare the carbonohydrazide **2**, a twofold excess of dodecylhydrazine was used in the reaction with phosgene, using a solution of phosgene. The hydrochloric acid produced during the reaction, is neutralized by the excess of dodecylhydrazine and the corresponding hydrochloric acid salt was removed by filtration during work-up. After column chromatography carbonohydrazide **2** could be isolated in a yield of 60 %.
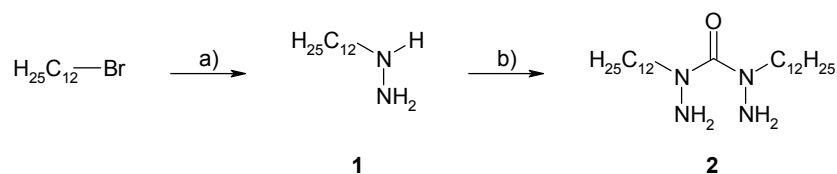
Scheme 6.1. *Synthesis of 2,4-didodecyl-carbonohydrazide **2**. Reactions and conditions: a) H$_2$NNH$_2$.H$_2$O, ethanol, reflux, 18 h, 69 %, b) phosgene, CHCl$_3$, toluene, 0 °C, 2 h, 60 %.*

This synthetic route enables the preparation of various different tetrazinones using **2** in a condensation reaction with various different arylaldehydes. Starting with benzaldehyde, model compound **3** could be prepared at ambient temperature. Reaction of **2** with 1,3,5-triformylbenzene yielded star-shaped compound **4**. Both **3** and **4** showed isotropic melting behavior with polarized optical microscopy.

2,6,10-Trimethyltriphenylene was prepared according to the procedure reported by Shirai et al.[28] using 4-methylcyclohexane and zirconium tetrachloride in stoichiometric amount instead of a catalytic amount, followed by dehydrogenation with Pd/C. There are several options for converting a benzylic methyl group into an aldehyde functionality, either by direct oxidation or by an indirect route using a radical bromination followed by oxidation. An attempt to directly oxidize the methyl groups to the aldehyde using tetrapyridinesilver(II) peroxydisulfate, failed because of partial oxidation of the aromatic core[30].
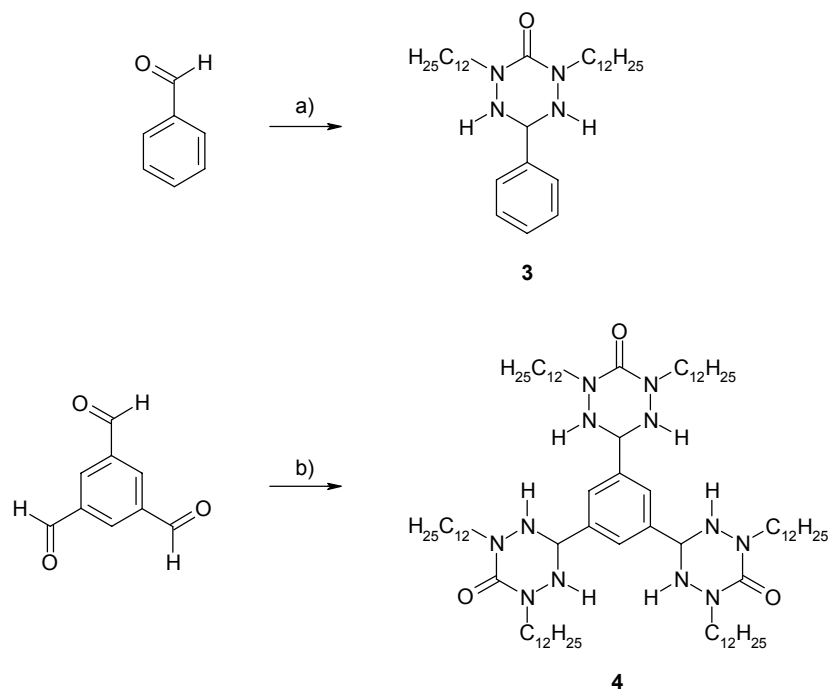
Scheme 6.2. *Synthesis of model compound **3** and star-shaped compound **4**. Reactions and conditions: a) **2**, methanol, 295 K, 2 h, 31 %, b) **2**, THF, reflux, 48 h, 36 %.*

After an elaborate search for the right reaction conditions it was possible to achieve bromination of the methyl groups in absence of aromatic bromination. However, it was not possible to exclusively mono-brominate all methyl positions. In practice some double bromination was unavoidable. In the optimized procedure 4 equivalents of NBS and benzoylperoxide were used for fast and complete radical bromination, resulting in a trimethyltriphenylene with an average of four bromines, **5** (Scheme 6.3). The benzylbromide groups as well as the benzyldibromide can be converted to an trialdehyde under the same reaction conditions[31], resulting in the 2,6,10-trifomaldehyde **6**.
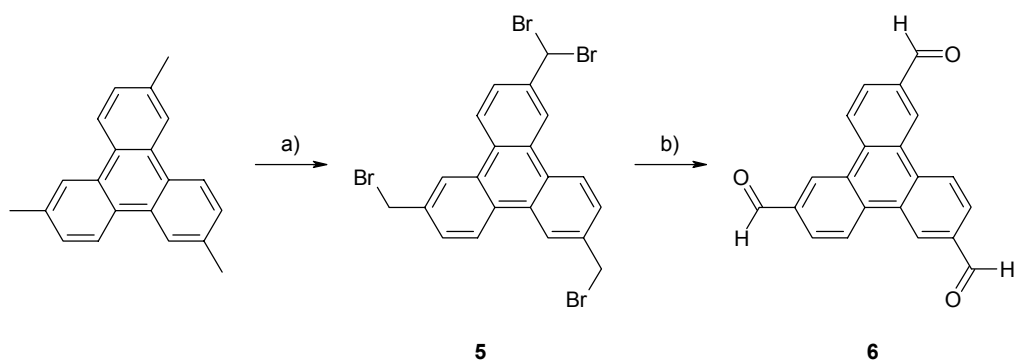
Scheme 6.3. *Synthesis of 2,6,10-triformyltriphenylene **6**. Reactions and conditions: a) N-bromosuccinimide (NBS), CCl₄, benzoylperoxide, UV-irradiation, reflux, 30 min, 76 %, b) **5**, NaHCO₃, DMSO, 115 °C, 6 h, 45 %.*

Analogous to the synthesis of **4**, reaction of **6** with 2,4-didodecyl-carbonohydrazide **2** yielded triphenylene **7**, which was separated from once and twice reacted 2,6,10-triformyltriphenylene using column chromatography (Scheme 6.4). Decomposition upon a phase transition to an isotropic liquid was observed for **7** with polarized optical microscopy.
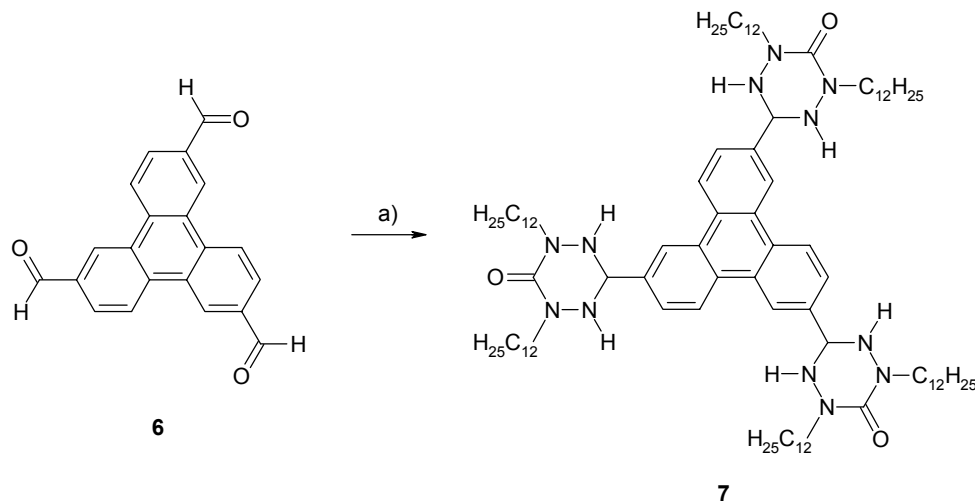
Scheme 6.4. *Synthesis of **7**. Reaction conditions: a) **2**, DMF, 90 °C, 48 h, 35 %.*

6.2.2 Cyclic voltammetry

The cyclic voltammogram of **3** shows a large oxidation wave (Figure 1.8) which decreased during the first couple of cycles and reached steady state situation at which the oxidation reaction rate equals the diffusion rate of **3** to the electrode. The corresponding reduction wave was absent, indicating that an irreversible oxidation reaction takes place consistent with the conversion of **3** into the corresponding oxo-verdazyl radical. After the first cycle a new redox wave can be seen at 0.81 V, appearing as a shoulder on the redox wave at 1.05 V. This new oxidation wave is assigned to the formation of the oxo-verdazyl cation, **3$^+$** (Scheme 6.5), similar to cyclic voltammetry reported by Fico et al.[19] on oxo-verdazyl biradicals.
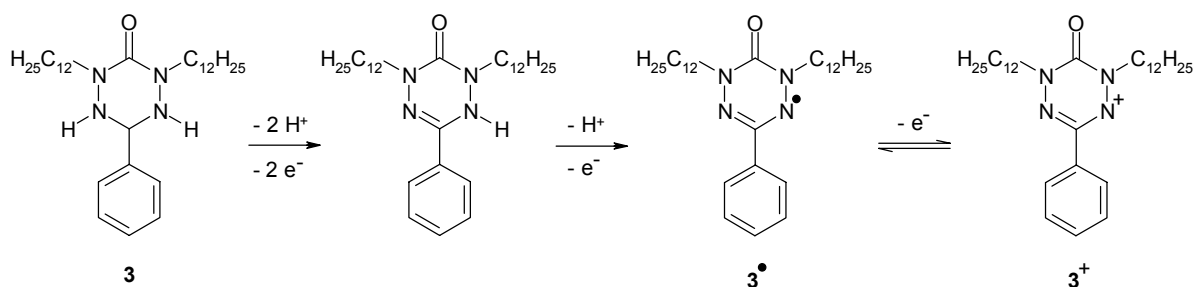
Scheme 6.5. *The irreversible oxidation of **3** to **3$^\bullet$** and the reversible oxidation to **3$^+$**.*

The anodic wave at 0.81 V and the cathodic wave at 0.70 V of the verdazyl radical showed reversible behavior indicated by the constant current intensity through out the experiment. Measuring at different scan rates (v) revealed a quasi-reversible behavior for the reduction wave at 0.70 V; the increase in current intensity follows $v^{0.5}$. The fact that the splitting between the anodic and cathodic wave increases at higher scan rates is an additional indication for quasi-reversible behavior.
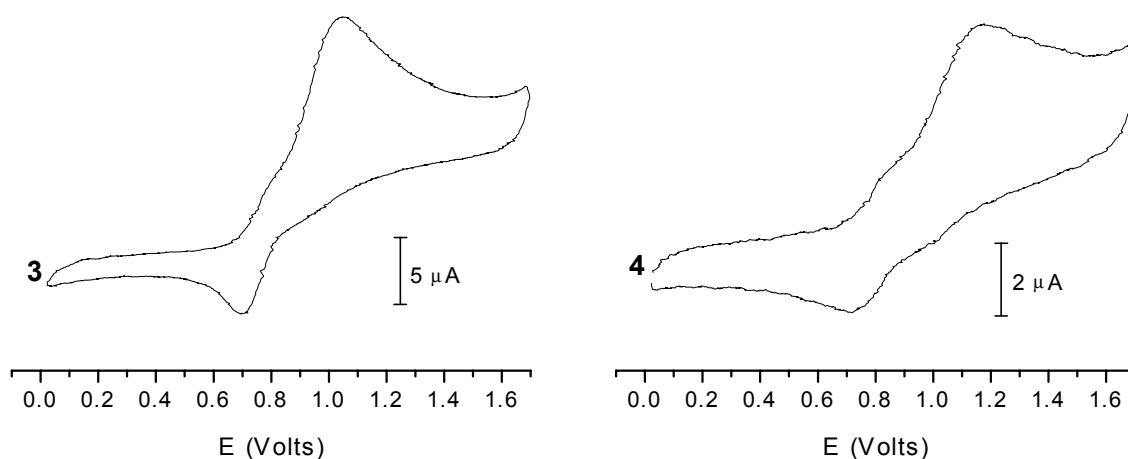

Figure 6.5. *Cyclic voltammograms of the oxo-verdazyl precursors; left: monoverdazyl* **3**; *right: triverdazyl* **4**. *Conditions: 0.1 M TBAHF in CH$_2$Cl$_2$ at 295 K, scan rate 100 mV/s. Potential vs. SCE reference and calibrated against Fc/Fc$^+$ couple at 0.46 V.*

A similar result was obtained for **4**. The cyclic voltammogram shows an intense oxidation wave at 1.16 V without a corresponding reduction wave and a small shoulder at 0.88 V after the first cycle. The reduction wave at 0.7 V, when measured at different scan rates, increases in intensity with $v^{0.5}$, indicating quasi reversible behavior. The observed splitting between the anodic and cathodic wave at 0.79 V is larger as compared to mono-verdazyl **3**. This phenomenon can be explained in two ways; either the increase of the splitting is due to formation tri(cation radical) of **4** by three consecutive one-electron oxidations which overlap or, as found for star-shaped compound **8** of chapter 5, the increased splitting is a result of the long alkyl chains limiting the electron transfer rate to the same order of magnitude as the diffusion rate. A combination of these processes is also possible so no unambiguous conclusion can be made. In conclusion, the redox behavior of **3** and **4** is consistent with the irreversible nature of the oxidation process for preparation of oxo-verdazyl radicals. The oxo-verdazyl radicals formed exhibit a quasi reversible oxidation which appears as a new oxidation curve at a potential less than that of the precursor.

6.2.3 Optical properties

1,2,4,5-Tetrazinones are commonly oxidized to oxo-verdazyl radicals using PbO_2, $K_3Fe(CN)_6/Na_2CO_3$, or $KMnO_4$ as oxidants. This oxidation reaction is irreversible since not only electrons but also protons are removed from the tetrazinones and consumed during the process, resulting in the formation of the oxo-verdazyl radical. Therefore, oxidizing agents like $NOBF_4$ or thianthrenium perchlorate are not suitable to use here. Since PbO_2 is insoluble in organic solvents and the mixture of $K_3Fe(CN)_6/Na_2CO_3$ is commonly dissolved in water, $KMnO_4$ in acetonitrile (ACN) was used as oxidant solution. A disadvantage of using $KMnO_4$ is the formation of MnO_2 particles in the redox reaction, which scatter the light. Therefore, after each addition of oxidant solution MnO_2 was allowed to settle on the bottom of the cell before the spectrum was recorded. Nevertheless, some light scattering effects can be observed in the spectra indicated by an decrease in absorption at the high energy side of the spectrum upon addition of more oxidizing agent as the particles become sufficiently large to precipitate from the solution.

Figure 6.6. *UV/visible/nearIR spectra recorded during the conversion of **3** by stepwise oxidation with $KMnO_4$ in acetonitrile at 295 K; left: from reduced state to the mono verdazyl radical; inset left: magnified part of the final spectrum of the monoverdazyl radical; right: magnified low energy area. Dotted line is the absorption spectrum of **3**.*

The electronic absorption spectrum of **3** in acetonitrile shows an intense absorption at ±5.9 eV and a weaker band at 4.2 eV (Figure 6.6). Stepwise addition of the $KMnO_4$ solution to the acetonitrile solution of **3** resulted in several new absorptions of which the absorption at 5.0 eV (248 nm) is the most intense. The absorptions around 3 eV and 2.5

eV show vibronic fine structure (Table 4.5) comparable to the spectrum of 1,5-dimethyl-3-phenyl-6-oxoverdazyl in dioxane, recorded by Neugebauer et al.[18]. The appearance of $KMnO_4$ absorptions around 2.5 eV (not shown) at the end of the stepwise oxidation, is an indication that the correct oxidation state had been reached and the complete conversion of **3** to the oxo-verdazyl radical had been accomplished.

Triverdazyl precursor of **4** dissolved in butyronitrile shows absorptions at 5.57 and 4.12 eV, similar to **3** (Figure 4.7). Upon addition of $KMnO_4$ in acetonitrile, the characteristic absorptions attributed to the formation of oxo-verdazyl radicals appear, although light scattering by MnO_2 particles obscures some of the details of the spectrum, especially in the area around 3 eV. Upon reaching the triradical state, the spectrum shows an intense absorption at 4.86 (255 nm) and weaker absorptions at 3 and 2.5 eV (Table 4.5) with some vibronic splitting similar to **3$^•$**. Addition of more oxidant solution results in the appearance of $KMnO_4$ absorptions around 2.5 eV. The ε values for the final oxo-verdazyl radical spectra of **3** and **4** differ by a factor ±2.5, in fair agreement with the number of verdazyl radical groups in the molecules.
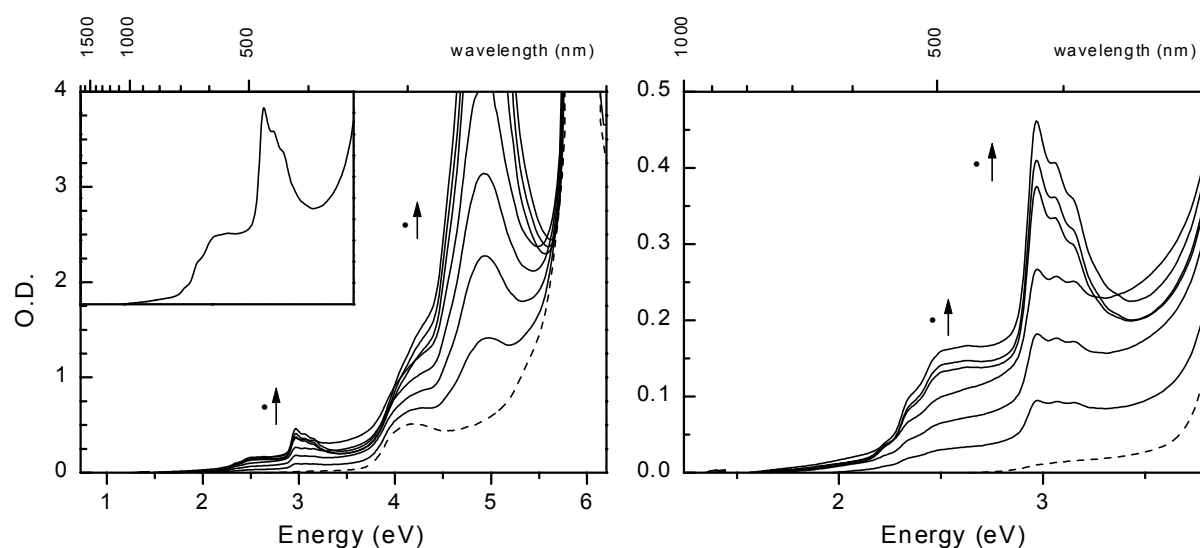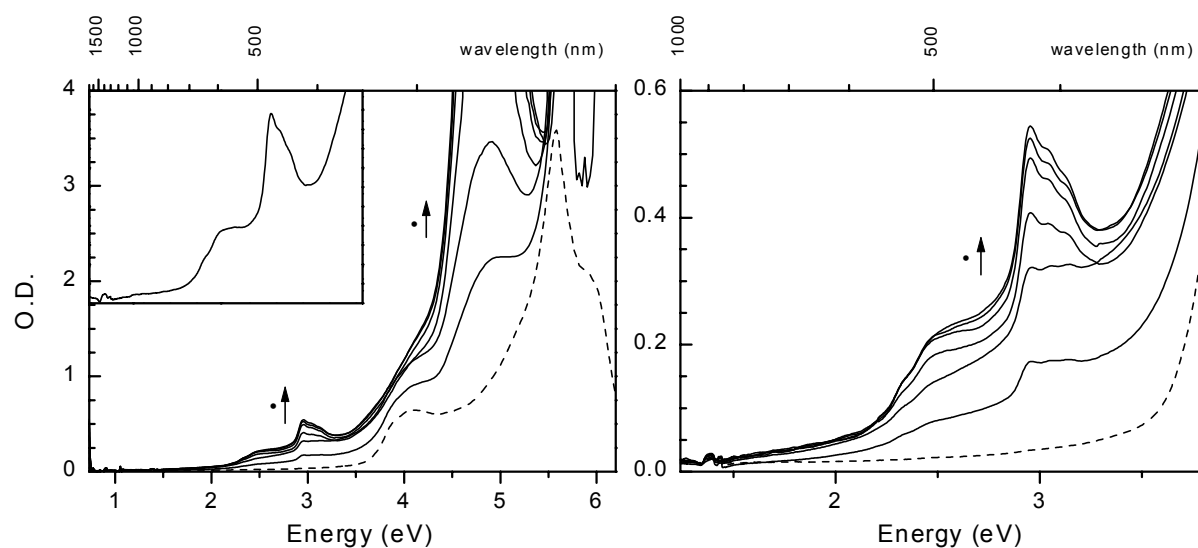

Figure 6.7. *UV/visible/nearIR spectra recorded during the conversion of 4 in butyronitrile by stepwise oxidation with KMnO₄ in acetonitrile at 295 K; left: from reduced state to the triverdazyl radical; inset left: magnified part of the final spectrum of the triverdazyl radical; right: magnified low energy area. Dotted line is the absorption spectrum of 4.*

These experiments show that the tetrazinones **3** and **4** can be converted in a controlled fashion to the corresponding oxo-verdazyl radical molecule, exhibiting distinct and characteristic spectra.

Table 6.1. *Optical data of the oxo-verdazyl radicals* [a]

	eV (nm); log ε							
3$^\bullet$	2.25	2.38	2.52	2.64	3.00	3.08	3.18	5.00
	(550);	(520);	(492);	(470);	(413);	(403);	(390);	(248);
	1.94	2.47	2.64	2.62	3.08	3.02	2.88	3.65
4$^{3\bullet}$	2.24	2.37	2.51	2.62	2.95	3.03	3.13	4.86
	(554);	(524);	(494);	(473);	(420);	(409);	(396);	(255);
	2.51	2.88	3.04	3.06	3.47	3.43	3.37	-

[a] *Conditions: Acetonitrile or butyronitrile, oxidation with KMnO₄, 295 K.*

6.2.4 Electron spin resonance spectroscopy

The ESR spectrum of **3$^\bullet$** in acetonitrile recorded at 295 K shows a highly resolved hyperfine coupling pattern (Figure 4.12) with approximately 37 lines. Comparing this spectrum with the ESR-spectrum obtained for 1,5-dimethyl-3-phenyl-6-oxoverdazyl recorded in benzene by Neugebauer et al.[32] shows that the very small hyperfine interactions with the protons of the phenyl group remain unresolved here. The spectrum of **3$^\bullet$** could be simulated[33] with the following hyperfine coupling constants: A_N = 18.4 MHz (2N); A_N = 14.6 MHz (2N); A_H = 8.7 MHz (4H). These hyperfine couplings can be assigned to the interaction of the unpaired electron with two sets of two equivalent nitrogen nuclei, $N_{1,5}$ and $N_{2,4}$, and four equivalent hydrogen nuclei of the first CH_2-group of the dodecyl chains. The anisotropic ESR spectrum of **3$^\bullet$** recorded at 110 K shows a broad spectrum with a peak-to-peak linewidth of 45 MHz, due to randomly oriented dipolar hyperfine interactions of this doublet state monoverdazyl.
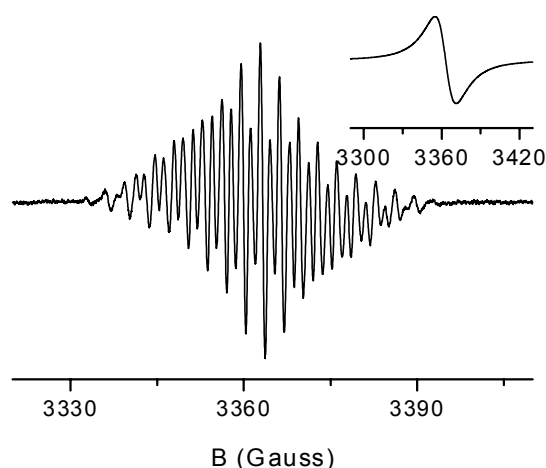

Figure 6.8. *ESR spectrum of **3$^\bullet$** in acetonitrile obtained by oxidation with KMnO₄ recorded at 295 K, inset shows spectrum recorded at 110 K.*

After oxidation of a concentrated solution of **4** in hexane (0.3 M) with $K_3Fe(CN)_6/Na_2CO_3$ an ESR spectrum was recorded at 295 K, which exhibits a single line possibly indicating the presence of multiple verdazyl radicals per molecule. Cooling to 120 K resulted in a broad ESR transition with a peak to peak line width of 28 MHz without characteristic features attributable to a quartet state (Figure 4.13). However, a weak $\Delta M_S=\pm2$ transition could be detected indicating the presence of high-spin species. A change of solvent from hexane to butyronitrile using a less concentrated solution of **4** (0.25 mM) oxidized with three equivalents of $KMnO_4$ with subsequent filtering, resulted in a similar anisotropic ESR spectrum at 110 K with a peak to peak line width of 37 MHz. In this case no $\Delta M_S=\pm2$ transition could be detected. Additional attempts using UV/visible/nearIR spectroscopy for converting **4** into the triverdazyl radical, did not give rise to an ESR-spectrum exhibiting evidence for a high-spin state.
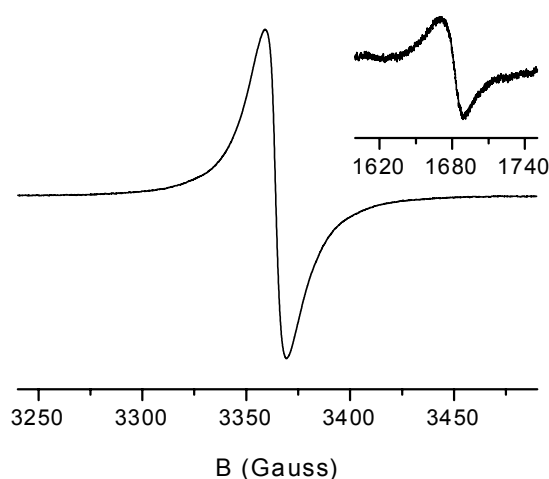
Figure 6.9. *ESR spectrum of $\mathbf{4^{3\bullet}}$ in hexane obtained by oxidation with $K_3Fe(CN)_6/Na_2CO_3$ recorded at 120 K, inset shows half-field signal recorded at 120 K.*

Similar to the oxidation of **4**, a hexane solution of the triverdazyl radical of triphenylene compound **7** was prepared by oxidation of **7** with $K_3Fe(CN)_6/Na_2CO_3$ and work up. The ESR spectrum recorded at 295 K (Figure 6.10) reveals some partially resolved hyperfine couplings similar to the ESR spectrum of $\mathbf{3^{\bullet}}$ which indicates either incomplete oxidation to the triradical or weak dipole-dipole interactions between the radical centers. At 120 K a broad featureless ESR-spectrum is obtained with a splitting of 45 MHz as well as a very weak $\Delta M_S=\pm2$ transition at half field indicating the presence of high-spin species.
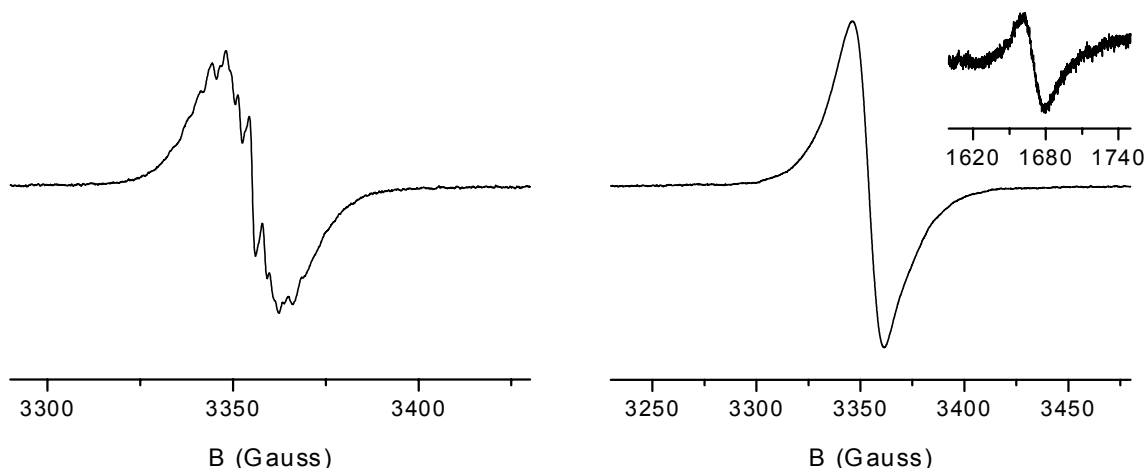
Figure 6.10. *ESR spectrum of $7^{3\bullet}$ in hexane obtained by oxidation with $K_3Fe(CN)_6/Na_2CO_3$. Left: recorded at 295 K. Right: recorded at 120 K, inset shows half-field signal recorded at 120 K.*

The ESR spectra of the oxo-verdazyl compounds $4^{3\bullet}$ and $7^{3\bullet}$ show no features attributable to a quartet ($S = 3/2$) state. However, the observation of a $\Delta M_S=\pm2$ transition gives some evidence for cooperative behavior of the spins. Therefore, the exchange integral of the oxo-verdazyl radicals seems to be rather small due to negligible delocalization of the spins into the central aromatic core. An explanation might be that this is due to a small increase in the angle between the verdazyl moiety and the aromatic ring compared to the methyl substituted verdazyls of Fico et al.[19]

6.3 Attempted synthesis of a tris(diphenyl verdazyl radical)benzene with mesogenic groups

Since triphenylverdazyl radicals have been shown to yield high-spin molecules when placed in a 1,3-benzene or 1,3,5-benzene substituted configuration[14], attention was shifted to the possibility of synthesizing a star-shaped tris(diphenylverdazyl radical) molecule with mesogenic groups. First, the reported molecules were synthesized to establish their high-spin states once again. ESR spectroscopy showed that both the 1,3-bis(diphenylverdazyl) and the 1,3,5-tris(diphenylverdazyl)benzene exhibited high-spin states (Figure 6.11)
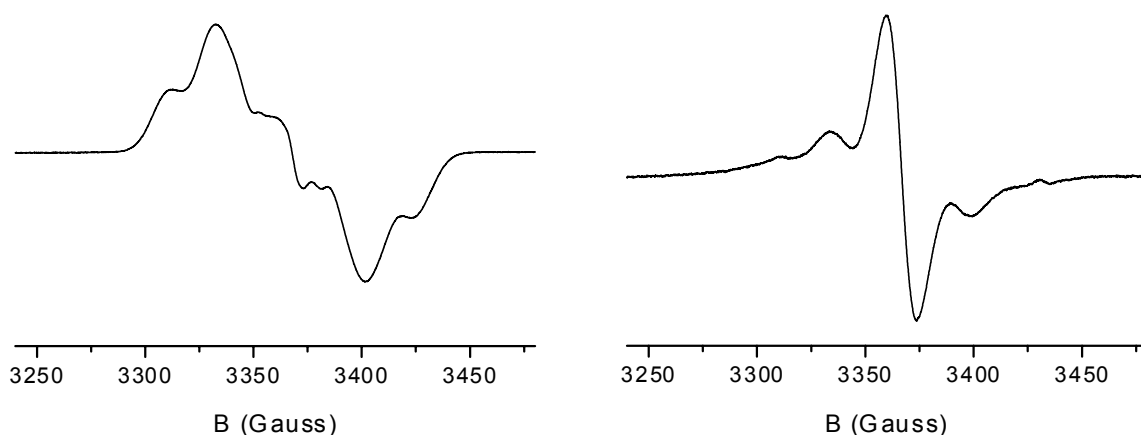
Figure 6.11. *ESR spectra of the oligo(diphenylverdazyls) of Kuhn et al. in dichloromethane at 120 K obtained by oxidation with BaO/Ba(OH)₂. Left: triplet spectrum of 1,3-bis(diphenylverdazyl)benzene. Right: quartet spectrum of 1,3,5-tris(diphenylverdazyl)benzene.*

One of the drawbacks of triphenylverdazyl radicals is that it is difficult to quantitatively prepare the oligo(verdazyl radical) from its precursor. The high-spin molecules reported were previously purified by crystallization, with poor yields for the desired radical compounds. This method of purification is not possible for molecules with long flexible side chains.

Two possible routes have been considered to prepare a tris(diphenylverdazyl radical) molecule with mesogenic groups (Scheme 6.6);

1) the mesogenic or alkyl group is directly attached to the phenyl groups and is present from the start of the synthesis.

2) the mesogenic groups are coupled to the star-shaped molecule at the end of the synthesis, just before or just after the preparation of the verdazyl radicals.

Route 1 required the preparation of an alkoxy or alkyl substituted phenylhydrazine as well as benzeneamine. Because tridodecylbenzeneamine (**9**) is available, an attempt was made to convert the primary amine into the hydrazine (**8**). Due to the very electron rich nature and amorphous character of the hydrazine, it could not be identified as well as isolated, using *o*-mesitylenesulfonylhydroxylamine (MSH) as aminating reagent[34-36].
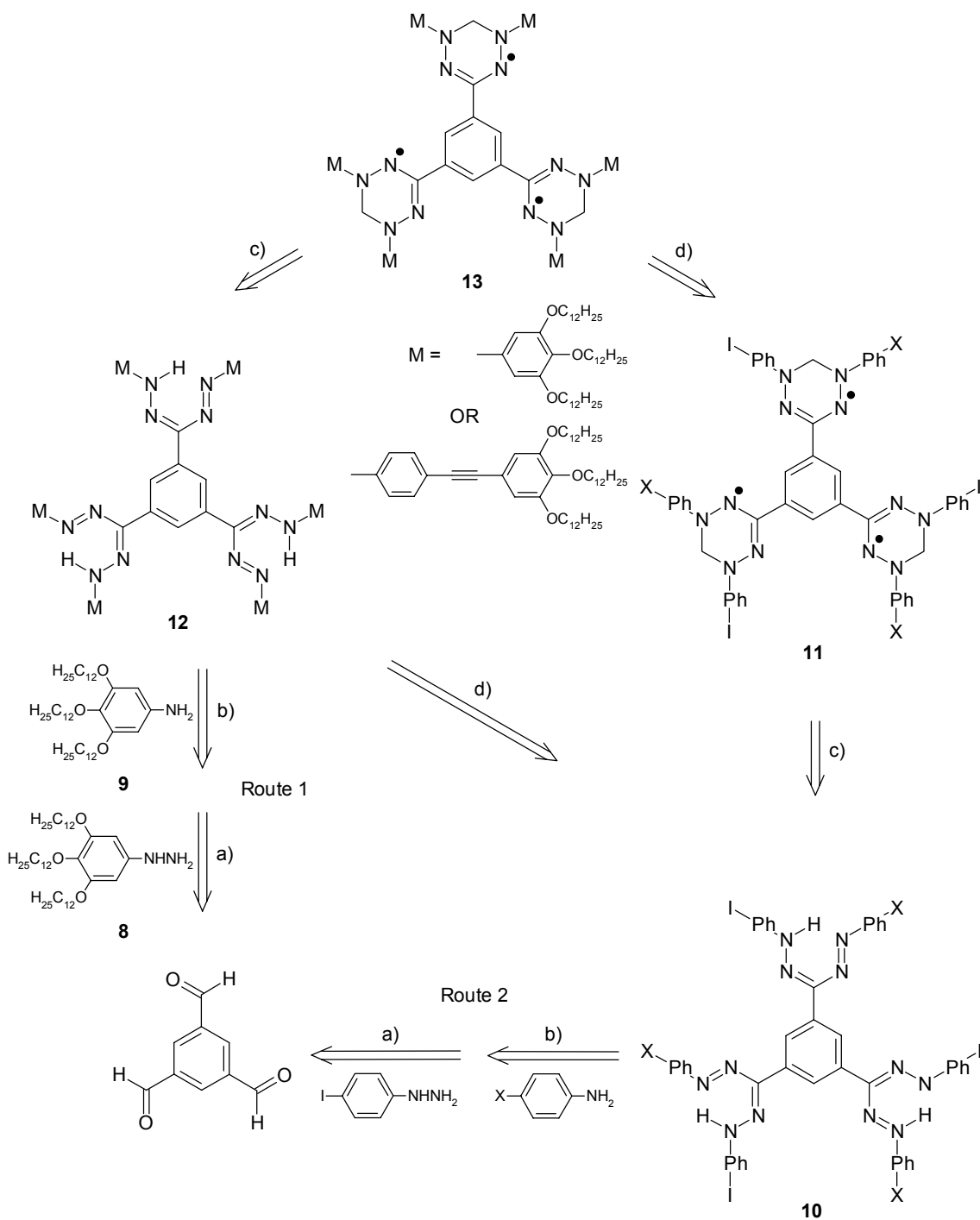
Scheme 6.6. *Retrosynthesis of a tris(triphenylverdazyl radical) molecule with mesogenic groups. Reactions and conditions: a) H⁺, ethanol, b) HCl, NaNO₂, 0 °C ,c) iodomethane or formaldehyde, NaOH, DMF, d) 3,4,5-tridodecyloxyphenylacetylene, Pd(PPh₃)₂Cl₂, CuI, triethylamine/THF.*

Route 2 required a functional group at the phenyl group for the attachment of a mesogenic group in the first step. Also here a tridodecylgallic acid derivative, tridodecylphenylacetylene, was chosen as a mesogenic group. This phenylacetylene can be coupled to a aryl halide using a Hagihara reaction[37], but disappointingly in a test

reaction a triphenylverdazyl monoradical did not quantitatively survive under the reaction conditions of the Hagihara coupling. This suggested that synthesis of **13** via preparation of **11** would not give a quantitative survival of the verdazyl radicals.

As a consequence, the synthesis of **13** via verdazyl precursor **12** was attempted. At first only three iodine groups were incorporated in the star-shaped molecule by a condensation of 4-iodo-phenylhydrazine with 1,3,5-triformylbenzene. However, reaction of this condensation product with phenyldiazonium hydrochloride, resulted in a very low yield of the desired product which was hard to purify (**10**, X = H). Nevertheless, attachment of the mesogenic groups was accomplished before the preparation of the verdazyl radicals (**12**) and purified by preparative SEC. As suspected, it was not possible to separate the triradical molecule (**13**) from products resulting from non-quantitative formation of the verdazyl radicals, being mono- and diradical molecules, because the difference in size and/or polarity between these molecules was to small.

6.4 Conclusion

Two oxo-verdazyl triradicals have been synthesized with dodecyl groups as mesogenic groups in an attempt to prepare a high-spin molecule with discotic liquid crystalline properties that would give rise to π-stacks exhibiting intermolecular ferromagnetic coupling. Synthetically the introduction of dodecyl groups on the oxo-verdazyl radicals proved not to be very difficult, although the amorphous character of these compounds resulted in a more elaborate purification. The control over the substitution pattern of triphenylene, shown by the synthesis of a 2,6,10-substituted triphenylene with aldehyde groups, enables the use of a triphenylene core as ferromagnetic coupling unit.

UV/visible/nearIR spectroscopy showed the possibility to convert compounds **3** and **4** in a controllable way into their respective oxo-verdazyl radicals as evidenced by the change in the optical properties of the compounds. Some evidence for the high-spin character of the triradical compounds has been found using ESR spectroscopy, as indicated by the observation of $\Delta M_S = \pm 2$ transitions. However, the ESR spectra recorded at normal field for **4**$^{3\bullet}$ and **7**$^{3\bullet}$ do not give any indication for the presence quartet species. An explanation for this behavior is that **4**$^{3\bullet}$ and **7**$^{3\bullet}$ possess a thermally accessible quartet state with a doublet ground state. However, this explanation is not supported by a recent report by Fico et al.[19], establishing the high-spin ground state of bis(oxo-verdazyl) biradicals in a 1,3-benzene and 1,4-benzene type configuration. The ability of triphenylene to act as a ferromagnetic coupling unit (FCU) makes it interesting to

investigate the use of a triphenylene core as FCU in combination with other types of radicals extending the work of Blackstock et al.[38] who used naphtalene as a FCU.

The combination of high spin triphenyl verdazyl radicals with mesogenic groups was not successful. The synthetic methodology used to prepare this kind of verdazyl radicals does not allow for quantitative conversion, preventing its use in an glassy material like a liquid crystalline disc.

The results for the oxo-verdazyl radicals show that they are promising candidates for use in a discotic liquid crystalline stack, combining synthetic accessibility, tune-ability, and radical stability. The synthetic route for the triradical molecules makes it possible to easily modify the substituents of the oxo-verdazyl radical group, allowing for preparation of a range of triradicals with different mesogenic groups, thus increasing the possibility to find a discotic liquid crystalline material with high-spin properties. Even asymmetric substitution of the oxo-verdazyl radical, although synthetically more tedious, is possible as shown by Neugebauer et al.[39], opening up the possibility to combine mesogenic groups with intramolecular ferromagnetic coupling units like metal complexing or hydrogen bonding groups.

6.5 Experimental section

General techniques. For general procedures and equipment see experimental sections of chapter 3 and 4. Dodecylbromide (Merck), phosgene in toluene (Fluka, 20%), benzaldehyde (Fluka), were used as received. 1,3,5-triformylbenzene[40,41] was prepared according to literature procedures. 2,6,10-Trimethyltriphenylene[28] was prepared in a modified literature procedure using $ZrCl_4$ in stoichiometric instead of catalytic amount.

Dodecylhydrazine[29] (1). A mixture of 1-bromododecane (15 ml, 62.5 mmol), hydrazine monohydrate (25 ml, 0.52 mol), and ethanol (35 ml) was stirred at reflux for 18 h and cooled to room temperature. After addition of aqueous sodium hydroxide (50 ml, 2.5 M), it was extracted with diethyl ether (3 * 50 ml). The combined extracts were dried over Na_2SO_4, filtered and concentrated in vacuo. Vacuum distillation afforded dodecylhydrazine that became an amorphous solid after standing (8.58 g, 69 %). b.p. 184 °C at 0.16 mbar (lit[42]: b.p. 176-177 °C at 0.15 mbar): ^{1}H NMR (CDCl$_3$): δ 3.10 (bs, 3H), 2.76 (t, J = 7.1 Hz, 2H), 1.48 (q, J = 7.1 Hz, 2H), 1.35-1.25 (m, 18 H), 0.88 (t, J = 6.6 Hz, 3H); ^{13}C NMR (CDCl$_3$): δ 56.62, 31.84, 29.59, 29.56, 29.53, 29.50, 29.28, 27.67, 27.12, 22.62, 14.05; IR (ATR, cm^{-1}): 3081, 2923, 2851, 1583, 1557, 1465, 1438, 1418, 1389, 1297, 1254, 1229, 1108, 1089, 1027, 987, 888, 857, 839, 827, 742, 723, 667, 612, 570.

2,4-Didodecyl-carbonohydrazide[43] (2). To a stirred solution of **1** (4.6 g, 23 mmol) in chloroform (15 ml) at 0 °C was added dropwise phosgene in toluene solution (20 %, 2.9 ml, 5.5 mmol). After stirring for 2 h, the solution was filtered and the residue was washed with chloroform, after which the filtrate was concentrated in vacuo. Column chromatography (SiO$_2$, ethyl acetate/CH$_2$Cl$_2$ 1:3.5) afforded **2** as a white solid (1.4 g, 60 %). mp 178-180 °C; ^{1}H NMR (CDCl$_3$): δ 4.02 (bs, 4H), 3.27 (t, J = 7.5 Hz, 4H), 1.75-1.6 (m, 4H), 1.35-1.25 (m, 36 H), 0.88 (t, J = 6.7 Hz, 6H); ^{13}C NMR (CDCl$_3$): δ 166.36, 53.91, 31.86, 29.57, 29.44, 29.30, 27.08, 26.75, 22.63, 14.05; IR (ATR, cm^{-1}): 3254, 3165, 2953, 2915, 2848, 2785, 1662, 1636, 1536, 1466, 1374, 1314, 1300, 1278, 1257, 1246, 1223, 1191, 1151, 1090, 1061, 1045, 1036, 1020, 990, 972, 959, 924, 881, 721.

2,4-Didodecyl-6-phenyl-1,4,5,6-tetrahydro-1,2,4,5-tetrazin-3(2*H***)-one (3).** A solution of **2** (0.85 g, 2.0 mmol) in methanol (2 ml) was added to a stirred solution of benzaldehyde (0.21 g, 2 mmol) in methanol (2 ml). Stirring for 2 h resulted in a 2-phase system, which was concentrated in vacuo. Column chromatography (SiO$_2$, ethyl acetate/CH$_2$Cl$_2$ 1:19) afforded **3** as a white solid (0.32 g, 31 %). ^{1}H NMR (CDCl$_3$): δ 7.53 (d, *J* = 8.2 Hz, 2H), 7.45-7.35 (m, 3H), 4.92 (t, *J* = 11.3 Hz, 1H), 4.15 (d, *J* = 11.3 Hz, 2H), 3.58 (dt, *J* = 13.6, 7.2 Hz, 2H), 3.45 (dt, *J* = 13.6, 7.0 Hz, 2H), 1.68-1.58 (m, 4H), 1.37-1.22 (m, 36 H), 0.88 (t, *J* = 6.7 Hz, 6H); ^{13}C NMR (CDCl$_3$): δ 154.37, 135.29, 128.81, 128.67, 126.24, 70.05, 49.98, 31.91, 31.88, 29.64, 29.50, 29.36, 29.03, 27.35, 26.89, 22.69, 14.11; IR (ATR, cm^{-1}): 3225, 2922, 2853, 1703, 1595, 1458, 1377, 1316, 1172, 1105, 1073, 1007, 773, 722, 693.

1,3,5-Tris(1,5-didodecyl-6-oxo-hexahydro-1,2,4,5-tetrazin-3-yl)benzene (4). A solution of **2** (0.40 g, 0.94 mmol) and 1,3,5-triformylbenzene (50 mg, 30 μmol) in THF (2ml) was stirred at reflux for 2 days, after which it was concentrated in vacuo. Column chromatography (SiO$_2$, ethyl acetate/CH$_2$Cl$_2$ 1:3) afforded **4** as a white solid (0.15 g, 36 %). m.p. 170-172 °C; ^{1}H NMR (CDCl$_3$): δ 7.72 (s, 3H), 4.97 (t, *J* = 9.6 Hz, 3H), 4.27 (d, *J* = 9.6 Hz, 6H), 3.63 (dt, *J* = 13.7, 7.3 Hz, 6H), 3.38 (dt, *J* = 13.7, 7.1 Hz, 6H), 1.68-1.55 (m, 12H), 1.35-1.20 (m, 108 H), 0.88 (t, *J* = 6.6 Hz, 18H); ^{13}C NMR (CDCl$_3$): δ 154.33, 136.60, 125.29, 69.68, 49.97, 31.91, 29.71, 29.67, 29.57, 29.37, 27.56, 26.96, 22.68, 14.11; IR (ATR, cm^{-1}): 3224, 2956, 2919, 2851, 1678, 1598, 1455, 1374, 1301, 1182, 965, 864, 722, 631, 575.

2-(Dibromomethyl)-6,10-di(bromomethyl)triphenylene[44] (5). A mixture of 2,6,10-trimethyltriphenylene (0.21 g, 0.78 mmol), *N*-bromosuccinimide (0.55 g, 3.1 mmol), benzoyl peroxide (0.38 g, 1.6 mmol) in carbon tetrachloride (35 ml) was stirred and heated by UV radiation for 30 min at reflux, using a suntanning lamp (120 W). After evaporation of the solvent, ethyl acetate was added and the solution was heated, cooled, and filtered. The ethyl acetate fraction was washed with 0.1 M Na$_2$CO$_3$ (3*75 ml), water (75 ml), dried over MgSO$_4$, and concentrated in vacuo. The resulting solid was heated in heptane/CH$_2$Cl$_2$ (3/1) yielding **5** as a yellow powder after filtration (0.32 g, 70 %). mp 210 °C (d.c.); ^{1}H NMR (CDCl$_3$): δ 8.62 (dd, *J* = 12.9, 1.8 Hz, 1H), 8.58-8.48 (m, 5H), 7.95-7.90 (m, 1H), 7.72-7.67 (m, 2H), 6.93 (d, *J* = 1.3 Hz, 1H), 4.76 (s, 4H); IR (ATR, cm^{-1}): 1901, 1691, 1503, 1436, 1413, 1306, 1246, 1209, 1143, 952, 906, 885, 832, 771, 734, 707, 700, 667, 654, 610, 595, 568. Anal Calcd for C$_{21}$H$_{14}$Br$_4$: C, 43.05; H, 2.41. Found: C, 43.51; H, 2.51. DIP-MS 585.

2,6,10-Triformyltriphenylene[31] (6). A mixture of **5** (0.25 g, 0.43 mmol) and sodium bicarbonate (1,58 g, mmol) in DMSO (10 ml) was heated under argon for 6 h at 115 °C. The salts were removed by filtration, after which the residue was precipitated in ethyl acetate, filtered and concentrated in vacuo. The (DMSO) solution was precipitated in acetonitrile yielding **6** as a white powder after filtration (60 mg, 45%). mp >280 °C; ^{1}H NMR (CDCl$_3$): δ 10.29 (s, 3H), 9.40 (d, *J* = 1.2 Hz, 3H), 9.04 (d, *J* = 8.5 Hz, 3H), 8.21 (dd, *J* = 8.5, 1.4 Hz, 3H); IR (ATR, cm^{-1}): 2827, 1689, 1615, 1578, 1504, 1426, 1380, 1347, 1313, 1242, 1190, 1120, 1008, 896, 832, 754, 638, 587.

2,6,10-Tris(1,5-didodecyl-6-oxo-hexahydro-1,2,4,5-tetrazin-3-yl)triphenylene (7). A solution of **6** (25 mg, 80 μmol) and **2** (0.12 g, 0.27 mmol) in DMF (2ml) was stirred at 90 °C for 48 h, after which it was concentrated in vacuo. Column chromatography (SiO$_2$, ethyl acetate/CH$_2$Cl$_2$ 2:3) afforded **7** as a white solid (0.04 g, 35 %). ^{1}H NMR (CDCl$_3$): δ 8.93 (d, *J* = 8.6 Hz, 3H), 8.15 (d, *J* = 8.5, 3H), 7.46 (s, 3H), 4.90 (t, *J* = 9.3 Hz, 3H), 4.32 (d, *J* = 9.3 Hz, 6H), 3.75-3.60 (m, 6H), 3.50-3.35 (m, 6H), 1.70-1.50 (m, 12H), 1.40-1.10 (m, 108 H), 0.89 (t, *J* = 6.5 Hz, 18H).

Preparation of the ESR-sample of the mono-oxo-verdazyl radical of 3. A solution of **3** (0.707 mg, 1.37 μmol) and KMnO$_4$ (0.218 mg, 1.38 μmol) in acetonitrile (1.50 ml) was stirred for 1 hour in a glovebox. Filtration

of this solution, using a syringe equipped with a 0.2 μm filter, yielded a red solution, which was subsequently transferred into a quartz ESR tube.

Preparation of the ESR-sample of the tri-oxo-verdazyl radical of 4. A solution of **4** (0.08 g, 0.06 mmol) in THF (2 ml) was mixed with a solution of $K_3Fe(CN)_6$ (0.17 g, 0.52 mmol) in 0.5 N Na_2CO_3 (2 ml) and stirred for 3 h. Extraction of the mixture with CH_2Cl_2, drying of the extract with $MgSO_4$, filtration and evaporation of the solvent resulted in a red amorphous solid which was dissolved in hexane (0.2 ml).

Preparation of the ESR-sample of the tri-oxo-verdazyl radical of 7. A solution of **7** (0.04 g, 0.03 mmol) in THF (2 ml) was mixed with a solution of $K_3Fe(CN)_6$ (0.08 g, 0.24 mmol) in 0.5 N Na_2CO_3 (2 ml) and stirred for 3 h. After the work up procedure described above the red amorphous solid was dissolved in hexane (0.2 ml).

6.6 References

1.   Braun, D., *Pure App. Chem.* **1972**, *30*, 41.
2.   Griller, D.; Ingold, K., *Acc. Chem. Res.* **1976**, *9*, 13.
3.   Forrester, A. R.; Hay, J. M.; Thomson, R. H., *Organic Chemistry of Stable Free Radicals*, Academic Press, London **1968**.
4.   Izuoka, A.; Fukada, M.; Sugawara, T.; Sakai, M.; Bandow, S., *Chem. Lett.* **1992**, 1627.
5.   Ballester, M., *Acc. Chem. Res.* **1985**, *18*, 380.
6.   Veciana, J.; Rovira, C.; Crespo, M. I.; Armet, O.; Domingo, V. M.; Palacio, F., *J. Am. Chem. Soc.* **1991**, *113*, 2552.
7.   Ruizmolina, D.; Veciana, J.; Palacio, F.; Rovira, C., *J. Org. Chem.* **1997**, *62*, 9009.
8.   Koelsch, C. F., *J. Am. Chem. Soc.* **1957**, *79*, 4439.
9.   Tukada, H.; Mutai, K., *Tetrahedron Lett.* **1992**, *33*, 6665.
10.   Kuhn, R.; Neugebauer, F. A., *Monatsh. Chem.* **1964**, *95*, 3.
11.   Plater, M. J.; Kemp, S.; Lattmann, E., *J. Chem. Soc., Perkin Trans. 2* **2000**, *1*, 971.
12.   Kuhn, R.; Trischmann, H., *Monatsh. Chem.* **1964**, *95*, 457.
13.   Dormann, E.; Winter, H.; Dyakonow, W.; Gotschy, B.; Lang, A.; Naarmann, H.; Walker, N., *Ber. Bunsen-Ges.* **1992**, *96*, 922.
14.   Kuhn, R.; Neugebauer, F. A.; Trischmann, H., *Monatsh. Chem.* **1966**, *97*, 525.
15.   Mukai, K.; Azuma, N.; Shikata, H.; Ishizu, K., *Bull. Chem. Soc. Jpn.* **1970**, *43*, 3958.
16.   Kothe, G.; Neugebauer, F. A.; Zimmermann, H., *Angew. Chem.* **1972**, *84*, 890.
17.   Azuma, N.; Kazuhiko, I.; Mukai, K., *J. Chem. Phys.* **1974**, *61*, 2294.
18.   Neugebauer, F. A.; Fischer, H.; Siegel, R., *Chem. Ber.* **1988**, *121*, 815.
19.   Fico, R. M.; Hay, M. F.; Reese, S.; Hammond, S.; Lambert, E.; Fox, M. A., *J. Org. Chem.* **1999**, *64*, 9386.
20.   Hicks, R. G.; Hooper, R., *Inorg. Chem.* **1999**, *38*, 284.
21.   Chapuzet, J.-M.; Simonet, J., *Tetrahedron* **1991**, *47*, 791.
22.   Matheson, I. M.; Musgrave, O. C.; Webster, C. J., *Chem. Commun.* **1965**, 278.
23.   Boden, N.; Borner, R. C.; Bushby, R. J.; Cammidge, A. N.; Jesudason, M. V., *Liq. Cryst.* **1993**, *15*, 851.

24. Arikainen, E. O.; Boden, N.; Bushby, R. J.; Clements, J.; Movaghar, B.; Wood, A., *J. Mater. Chem.* **1995**, *5*, 2161.

25. Adam, D.; Schuhmacher, P.; Simmerer, J.; Haussling, L.; Siemensmeyer, K.; Etzbach, K. H.; Ringsdorf, H.; Haarer, D., *Nature* **1994**, *371*, 141.

26. Henderson, P.; Kumar, S.; Rego, J. A.; Ringsdorf, H.; Schuhmacher, P., *J. Chem. Soc., Chem. Commun.* **1995**, 1059.

27. Rego, J. A.; Kumar, S.; Dmochowski, I. J.; Ringsdorf, H., *Chem. Commun.* **1996**, 1031.

28. Shirai, H.; Amano, N.; Hashimoto, Y.; Fukui, E.; Ishii, Y.; Ogawa, M., *J. Org. Chem.* **1991**, *56*, 2253.

29. Brown, D. M.; Jones, G. H.; Looker, B. E.; McLean, C. D.; Middleton, S., *J. Chem. Soc., Perkin Trans. 1* **1977**, 2052.

30. Firouzabadi, H.; Salehi, P.; Sardarian, A. R.; Seddighi, M., *Synth. Commun.* **1991**, *21*, 1121.

31. Helms, A.; Heiler, D.; McLendon, G., *J. Am. Chem. Soc.* **1992**, *114*, 6227.

32. Neugebauer, F. A.; Fischer, H., *Angew. Chem.* **1980**, *92*, 766.

33. Solution and powder ESR spectra were simulated using WINEPR Simfonia, Shareware Version 1.25, Brüker Analytische Messtechnik GmbH, Copyright © 1994-1996.

34. Krause, J. G., *Synthesis* **1972**, 140.

35. Tamura, Y.; Minamikawa, J.; Sumoto, K.; Fujii, S.; Ikeda, M., *J. Org. Chem.* **1973**, *38*, 1239.

36. Carpino, L. A., *J. Am. Chem. Soc.* **1960**, *82*, 3133.

37. Sonogashira, K.; Tohda, Y.; Hagihara, N., *Tetrahedron Lett.* **1975**, 4467.

38. Selby, T. D.; Blackstock, S. C., *J. Am. Chem. Soc.* **1999**, *121*, 7152.

39. Neugebauer, F. A.; Fischer, H.; Krieger, C., *J. Chem. Soc., Perkin Trans. 2* **1993**, *2*, 535.

40. Storck, W.; Manecke, G., *Makromol. Chem.* **1975**, *176*, 97.

41. Fourmigue, M.; Johannsen, I.; Boubekeur, K.; Nelson, C.; Batail, P., *J. Am. Chem. Soc.* **1993**, *115*, 3752.

42. Westphal, O., *Chem. Ber.* **1941**, *74*, 759.

43. Neugebauer, F. A.; Fischer, H.; Siegel, R.; Krieger, C., *Chem. Ber.* **1983**, *116*, 3461.

44. Xu, L.; Keehn, P. M.; Gnaim, J. M.; Green, B. S., *J. Org. Chem.* **1992**, *57*, 3208.

7

Investigations on intramolecular spin coupling of cation radicals through σ-bonds

Abstract: Oligo(triarylamines) have been designed and characterized with the aim to use hexahydrotriazine or spirofluorene moieties as intramolecular ferromagnetic coupling units. After oxidation of the triarylamines to the corresponding oligo(cation radicals), ESR spectroscopy revealed in both cases no indication of exchange coupling through the σ-bonds.

7.1 Introduction

The search for new exchange pathways for intra- and intermolecular ferromagnetic spin-spin coupling is of continuing interest, and as a result various interesting materials and ideas have been proposed. One of the areas of new ideas concerns the development and experimental verification of new ferromagnetic coupling units (FCU). Heterocyclic rings, like e.g. triazine, are interesting as FCU in the search for an intramolecular ferromagnetic coupling by hydrogen bonding, resulting in supramolecular aggregates[1]. Therefore, triazine rings have been the subject of extensive theoretical investigations[1-5], which predicted that a 1,3-triazinebiradical is an effective FCU. Baumgarten et al.[1] predict triazine to be an effective FCU in a high-spin ground state for a triplet 1,3-triazinebiradical as well as in a quartet 1,3,5-triazinetriradical. In contrast, Tanaka et al.[6]. calculated that the ground state of a 1,3,5-triradicaltriazine is a doublet low-spin state. Recently this was experimentally verified by Blackstock et al.[7] who synthesized and oxidized two 1,3,5-triazines (Figure 6.1, **A**). Only the tri(cation radical) of the *p*-anisyl substituted derivative was found to be stable enough for ESR spectroscopy. It was found that the doublet state is the ground state, while the quartet state is a low-lying excited state.
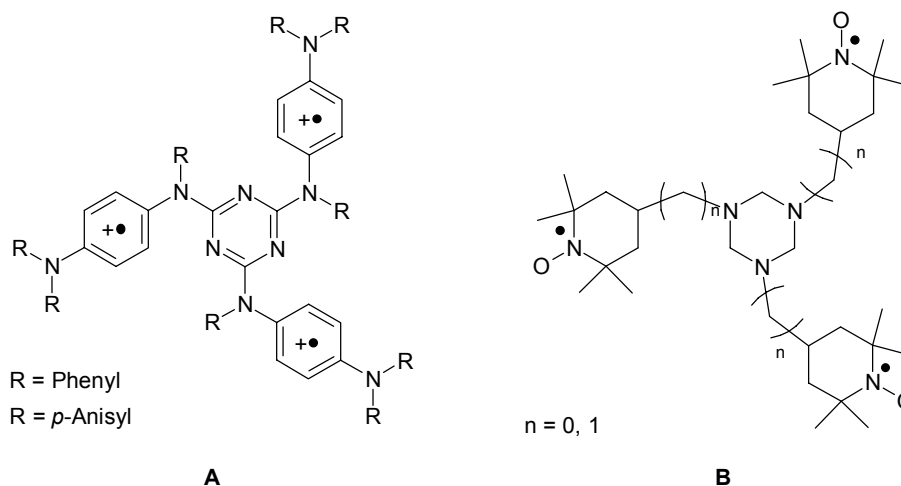

Figure 7.1. *Triradicals with heterocyclic FCU. Left: star-shaped triazines of Blackstock et al.[7](A), hexahydrotriazines of Golubev et al.[8] (B).*

In the report of Tanaka et al.[6] also the ferromagnetic coupling capability of the non-aromatic form, hexahydrotriazine was investigated. According to these calculations a 1,3,5-hexahydrotriazinetriradical has a degenerate doublet-quartet ground state. This interesting proposal suggests that intramolecular ferromagnetic spin-spin coupling can possibly be achieved with the σ-bonds present in hexahydrotriazine functioning as an

exchange pathway for spin alignment resulting in high-spin molecules. The use of σ-bonds as exchange pathway has already proved to be a successful approach for the design of high-spin molecules, see *N,N'*dioxyl-1,3,5,7-tetramethyl-2,6-diaza-adamantane[9,10]. However, only one report on hexahydrotriazine triradicals exists, in which very stable TEMPO radicals have been used by Golubev et al.[8] for the purpose of synthesizing spin labels and spin probes (Figure 6.1, **B**). In contrast, piperazines, belonging to the same class of compounds as hexahydrotriazines, have been used by Nakatsuji et al.[11] (Figure 7.2, **C**) and by Rey et al.[12] (Figure 7.2, **D**) in pursue of ferromagnetic charge transfer complexes containing stable neutral radicals. The bis(TEMPO radical) of Nakatsuji et al.[11] exhibited a thermally accessible triplet state with a singlet ground state, in contrast to the bis(nitronyl nitroxide radical) of Rey et al.[12] were no intramolecular spin-spin interaction could be observed.
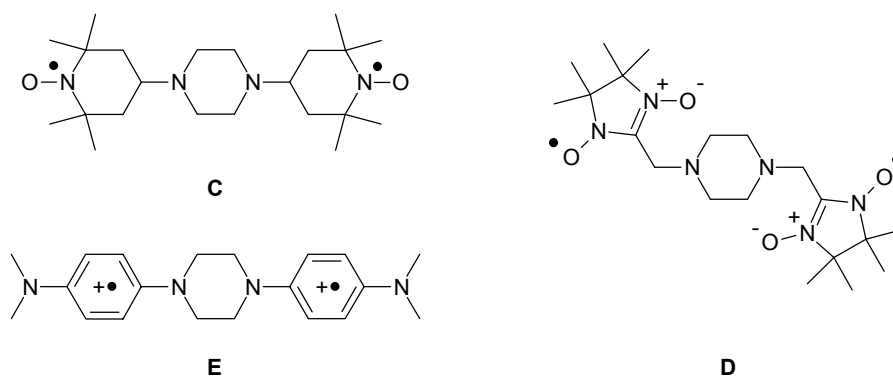

Figure 7.2. *Piperazine biradicals. Top, left: bis(TEMPO radical) of Nakatsuij et al.[11] (C), right: bis(nitronyl nitroxide radical) of Rey et al.[12] (D), bottom, left : piperazine di(cation radical) of Nelsen et al.[13] (E).*

The previous chapters have shown that 1,4-benzenediamine motifs can be oxidized to bear stable cation radicals. The work of Nelsen et al.[13] (Figure 7.2, **E**) and Brouwer et al.[14] is of interest in this respect because molecules were reported consisting of piperazine rings with 1,4-benzenediamine motifs. These molecules could be reversibly oxidized to the corresponding cation radical. As a straight forward extension a molecule can be designed which combines the 1,4-benzenediamine motif with a hexahydrotriazine ring (Figure 7.3). A similar hexahydrotriazine with methyl groups has already been reported by Giumanini et al.[15] (Figure 7.3, **F**), who were interested in a practical synthetic method for the preparation of hexahydrotriazines, but the redox or high-spin properties were not investigated. In this chapter two molecules of this class of compounds have been synthesized and characterized by means of cyclic voltammetry,

UV/visible/nearIR spectroscopy and ESR spectroscopy in an attempt to design a high-spin molecule with intramolecular ferromagnetic spin-spin coupling through σ-bonds.
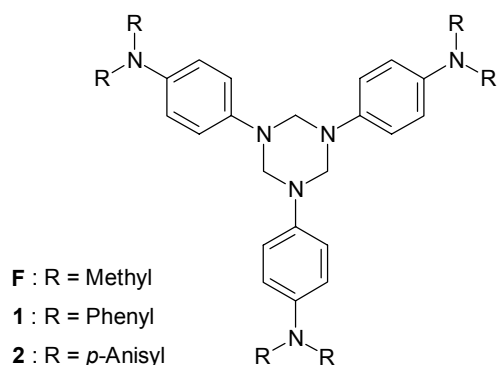

F : R = Methyl
1 : R = Phenyl
2 : R = *p*-Anisyl

Figure 7.3. *Hexahydrotriazine by Giumanini et al.[15] (**F**) and target hexahydrotriazine molecules 1 and 2.*

An other type of interesting σ-bond FCU are the new and interesting class of the spiro compounds which are used in LED's[16-20] and organic solar cells[21]. They combine π-conjugation with glass like behavior and solubility. The spiro-TAD and spiro-MeOTAD of Salbeck et al. are interesting molecules not only as a hole transport material but also for possible high-spin characteristics, since the benzidine motifs are spiroconjugated by the sp[3] carbon atom. A through-bond or though-space spin-spin coupling mechanism could give a ferromagnetic alignment of the spins if both sides of the molecule are oxidized to the cation radical. A recent report by Frank et al.[22] showed that this is indeed possible for nitronyl nitroxide radicals, where a thermally accessible triplet state could be observed for a spiroconjugated biradical (Figure 7.4, **G**). Therefore, in this chapter also the spiro-TAD molecules of the group of Salbeck are investigated for possible high-spin behavior when oxidized to the corresponding di(cation radical).
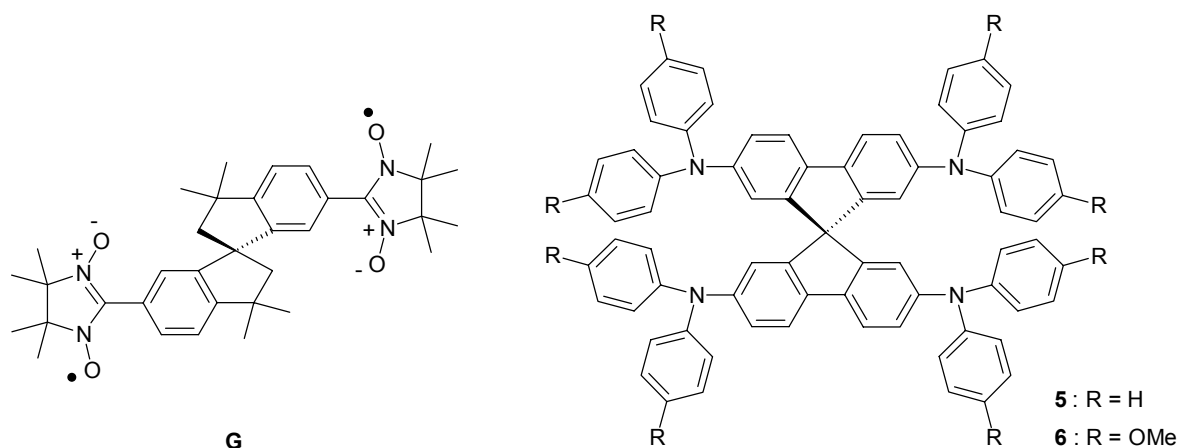

G

5 : R = H
6 : R = OMe

Figure 7.4. *Spiro biradicals. Left: spiroconjugated nitronyl nitroxide biradical of Frank et al.[22] Right: spiro-TAD molecules 5 and 6 by Salbeck et al.[17]*

## 7.2 Spin-spin coupling in 1,3,5-hexahydrotriazines

7.2.1 Synthesis

The synthetic methodology of Giumanini et al.[15] requires a *para*-substituted aniline to form the hexahydrotriazine ring by a condensation with formaldehyde. Therefore, *N,N*-diphenyl-1,4-benzenediamine, the precursor to hexahydrotriazine **1**, was synthesized using Haeussermann's[23] modification of the method developed by Herz[24] involving the nitration of triphenylamine with subsequent reduction of the nitro group by zinc/acetic acid to the primary amine[25]. Since 4,4'-dimethoxy-diphenylamine is commercially available, the precursor of **2** was made using a more recently developed synthetic method involving palladium catalyzed C-N bond formation, which allows for coupling of very electron poor substrates, like 4-bromo-nitrobenzene, to a secondary amine, using Cs_2CO_3 as a weak base[26] (Scheme 5.1). Reduction of the resulting triphenylamine **3** with zinc/acetic acid yields the *N,N*-bis(4-methoxyphenyl)-1,4-benzenediamine **4** after crystallization.
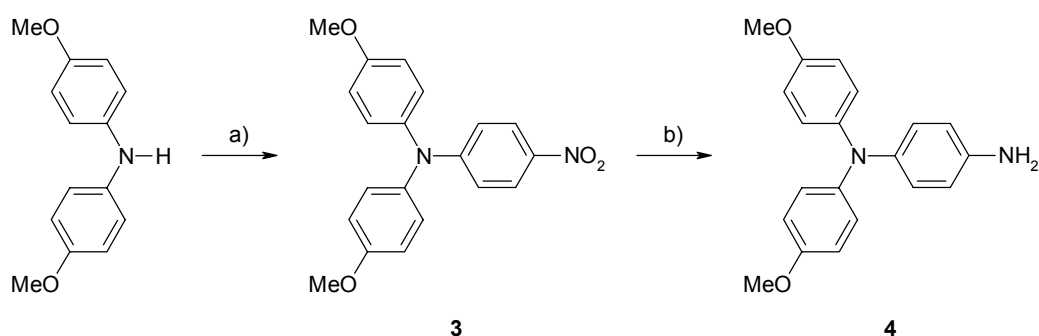
Scheme 7.1. *Synthesis of 1,4-benzenediamine* **4**. *Reactions and conditions: a) 4-bromo-nitro-benzene, Cs_2CO_3, $Pd_2(dba)_3$, S-BINAP, 90 °C, one week, 89 %, b) Zn, acetic acid, ethanol, 295 K, 1 h, 82 %.*

Hexahydrotriazine rings, resulting from the reaction of aniline with formaldehyde, have been accidentally discovered in the search for a stable *N*-methyleneaniline as an useful reactive synthon and have eluded positive identification for a long time[27,28]. These hexahydrotriazines can easily be prepared by using the method of Giumanini et al.[15] Reaction of aniline derivatives with paraformaldehyde also results in the formation of higher cyclic analogues, mostly tetramer, as well. So reaction of *N,N*-diphenyl-1,4-benzenediamine or primary amine **4** with parafomaldehyde in refluxing toluene yields **1** and **2**, respectively (Scheme 7.2). Removal of the side-products was accomplished by twofold precipitation from CH_2Cl_2/methanol in case of **1** and crystallization from petroleum ether/toluene in case of **2**.
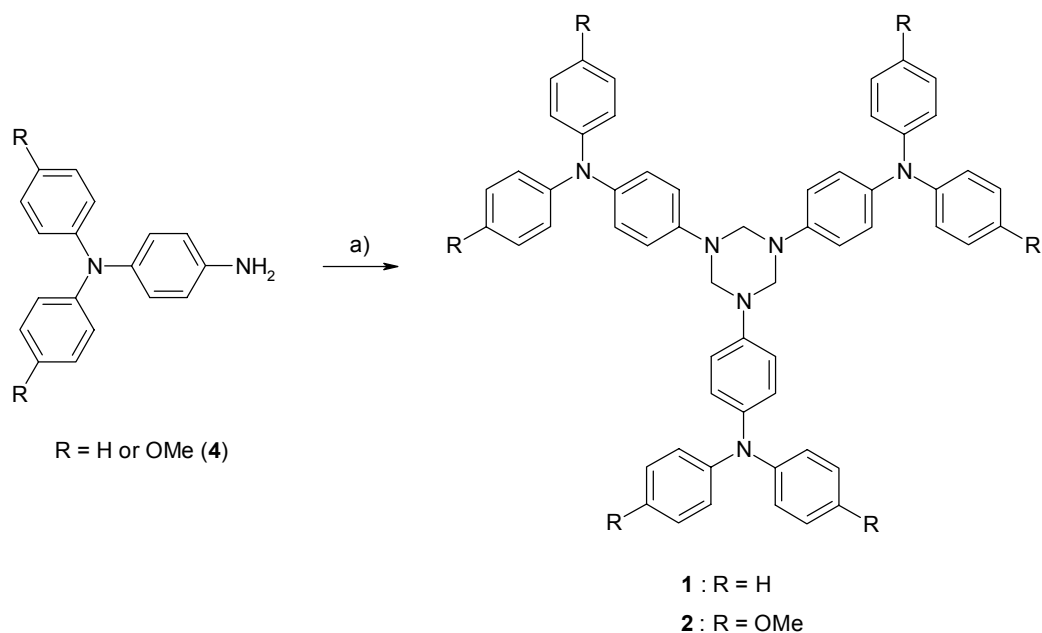
Scheme 7.2. *Synthesis of hexahydrotriazines* **1** *and* **2**. *Reaction conditions: a) parafomaldehyde, toluene, reflux, 30 min,* **(1)** *63 %,* **(2)** *40 %.*

7.2.2 Cation radicals by cyclic voltammetry

The redox characteristics of hexahydrotriazines **1** and **2** are depicted in Figure 1.8 and all electrochemical data is summarized in Table 7.1.
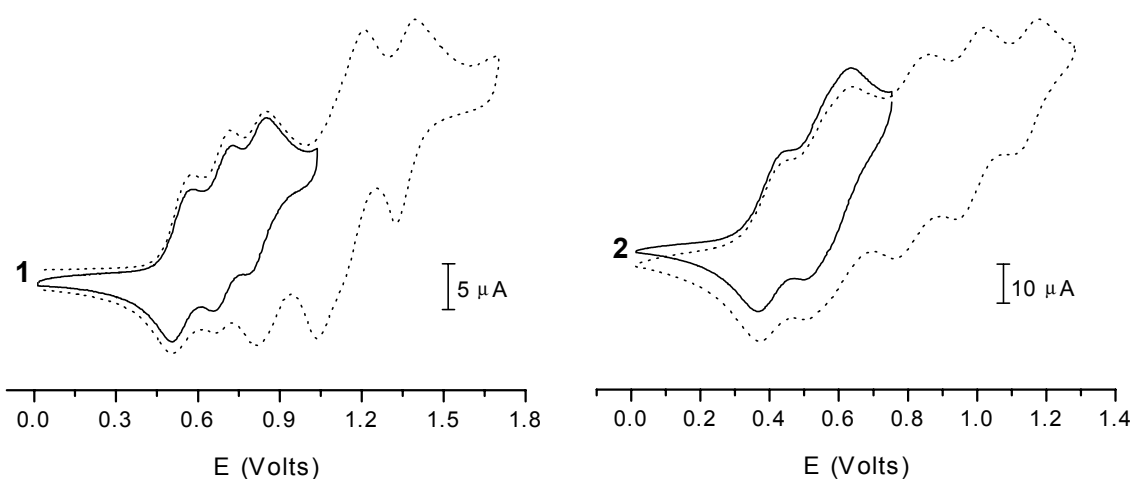

Figure 7.5. *Cyclic voltammograms of hexahydrotriazines* **1** *(left) and* **2** *(right). Conditions: 0.1 M TBAHF in CH₂Cl₂, scan rate 100 mV/s, at 295 K. Potential vs. SCE reference and calibrated against Fc/Fc⁺ couple at 0.46 V.*

Cyclic voltammetry of **1** shows three reversible oxidation waves at 0.54, 0.69, and 0.81 V, resulting in the tri(cation radical), $\mathbf{1}^{3(+\bullet)}$. The anodic/cathodic peak splittings were on average 74 mV, indicating an one-electron oxidation process. Measurement of the voltammogram at higher scan rates resulted in an increase of the anodic/cathodic peak splitting characteristic for quasi-reversible oxidation behavior. An increase of the potential to 1.7 V resulted in irreversible oxidation behavior. The first cycle shows a strong increase of the current for the reduction waves. Continuous cycling showed, next to a further increase of the current intensity, also the appearance of additional oxidation waves.

The cyclic voltammogram of **2** shows two reversible oxidation waves corresponding to the oxidation to the tri(cation radical), $\mathbf{2}^{3(+\bullet)}$. The first and second wave had a peak-peak splitting of 95 mV and 137 mV, respectively. Careful examination of the cyclic voltammogram of **2** reveals a small shoulder at the second oxidation wave, indicating that two one-electron oxidations are overlapping. The current slowly increases with the number of repeating cycles when the potential is increased to 1.3 V. From this irreversible oxidation behavior three separate one-electron waves can be distinguished yielding the hexacation of **2**. The partial reversibility shows that the methoxy groups at the *para*-positions are insufficient for stabilizing oxidation states higher than the tri(cation radical) of **2**.

Table 7.1. *Electrochemical data of the hexahydrotriazines[a]*

	E_1^0(V)	E_2^0(V)	E_3^0(V)	E_4^0(V)[c]	E_5^0(V)[c]	E_6^0(V)[c]
1	0.54	0.69	0.81	1.12[b]	1.12[b]	1.36
2	0.41	0.57[b]	0.57[b]	0.81	0.98	1.14

[a] Conditions: 0.1 M TBAHF in CH₂Cl₂, 295 K. Potential vs. SCE reference and calibrated against Fc/Fc⁺ couple at 0.46 V. [b] Peaks are unresolved. [c] Irreversible redox potentials.

7.2.3 Optical properties of the cation radicals

The oxidation of the hexahydrotriazines can also be accomplished with chemical oxidizing agents. The stepwise oxidation of **1** and **2** with thianthrenium perchlorate in hexafluoroisopropanol was monitored with UV/visible/nearIR spectroscopy. In this case hexafluoroisopropanol is used as solvent since it is known to strongly stabilize cation radicals.
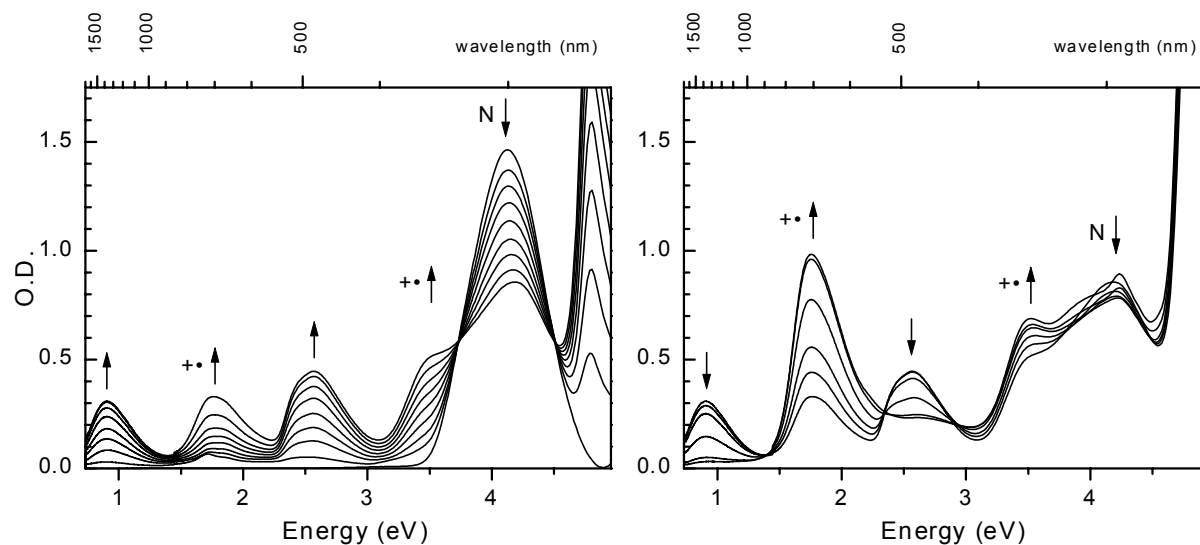
Figure 7.6. *UV/visible/nearIR spectra recorded during the conversion of **1** by stepwise oxidation with THI*$^{+\bullet}$*ClO$_4^-$ in hexafluoroisopropanol at 295 K. Left: from neutral to di(cation radical) state. Right: from di(cation radical) to tri(cation radical) state.*

Oxidation of **1** shows a decrease of the neutral absorption at 4.13 eV and the appearance of four absorption bands at 0.90, 1.76, 2.57, and, 3.53 eV, respectively. When **1** is approximately oxidized to the di(cation radical) state, the bands at 0.90 and 2.57 eV start to the decrease. Simultaneously the band at 1.76 eV shows a strong increase in absorption. Both the bands at 1.76 and 3.53 eV are attributed to the presence of cation radicals. The bands at 0.90 eV and 2.57 eV might be due to the reversible formation of benzidine species by coupling of the *para*-positions of the phenyl-groups. Further oxidation results in bands attributed to unreacted thianthrenium perchlorate. Reduction with hydrazine hydrate failed to completely restore the neutral spectrum. This might be due to instability of **1**$^{3(+\bullet)}$ or a possible reactivity of hexahydrotriazine rings towards reducing agents.

To validate the assumption that benzidines are formed during the oxidation of **1** to **1**$^{3(+\bullet)}$, *N,N'*-bis(3-methylphenyl)-*N,N'*-diphenylbenzidine (TPD) was oxidized with THI$^{+\bullet}$ClO$_4^-$ in dichloromethane (Figure 7.7). Oxidation of TPD results in a decrease of the neutral absorptions at 3.52 and 4.00 eV and the appearance of two new absorptions at 0.89 and 2.56 eV, attributed to the formation of TPD$^{+\bullet}$. Further oxidation of TPD$^{+\bullet}$ to TPD^{2+} results in an intense absorption band at 1.68 eV and a decrease of the cation radical bands. These results are strong indication that during the oxidation of **1** benzidines are formed.
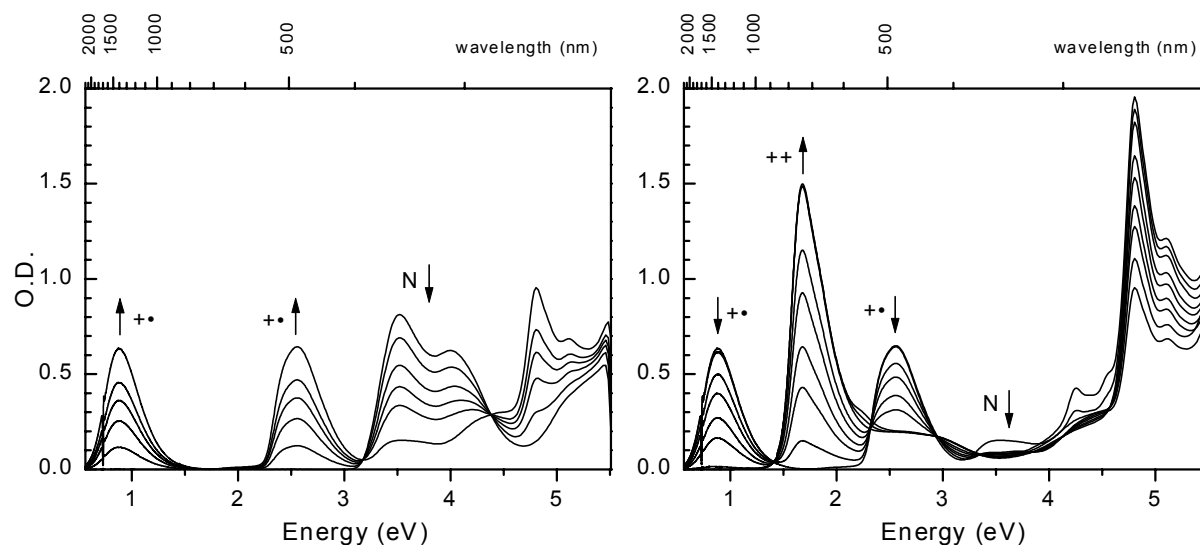
Figure 7.7. *UV/visible/nearIR spectra recorded during the conversion of N,N'-bis(3-methylphenyl)-N,N'-diphenylbenzidine by stepwise oxidation with THI$^{+\bullet}$ClO$_4^-$ in CH$_2$Cl$_2$ at 295 K. Left: from neutral to cation radical state. Right: from cation radical to dication state.*

The spectrum of neutral **2** in hexafluoroisopropanol shows two absorption bands at 4.28 and 3.29 eV (Figure 7.8). Addition of oxidator results in a decrease of the band at 4.28 eV. In contrast, the band at 3.29 eV increases together with a new absorption band at 1.59 eV upon addition of more THI$^{+\bullet}$ClO$_4^-$. The absence of absorptions bands around 1 and 2.5 eV shows that in this case no benzidines are formed, since the *para*-positions are blocked with methoxy-groups. Upon reaching the tri(cation radical) state a small shoulder at 2.0 eV becomes visible next to an intense band at 1.59 eV. Also here reduction of the oxidized solution with hydrazine hydrate does not completely restore the neutral spectrum. The acidity of hexafluoroisopropanol might be causing the irreversible nature of these oxidation experiments, since protonation of the hexahydrotriazine ring could result in a ring opening reaction and disintegration into separate molecules. Therefore, dichloromethane was tried as solvent for the oxidation of **2**. The spectrum of neutral **2** shows an absorption at 4.05 eV. Upon oxidation three absorption bands appear at 1.59, 1.98, and 3.31 eV, almost at identical positions compared to the oxidation experiment in hexafluoroisopropanol. Addition of hydrazine hydrate to the dichloromethane solution at the end of the oxidation experiment did not to completely restore the spectrum of neutral **2**.
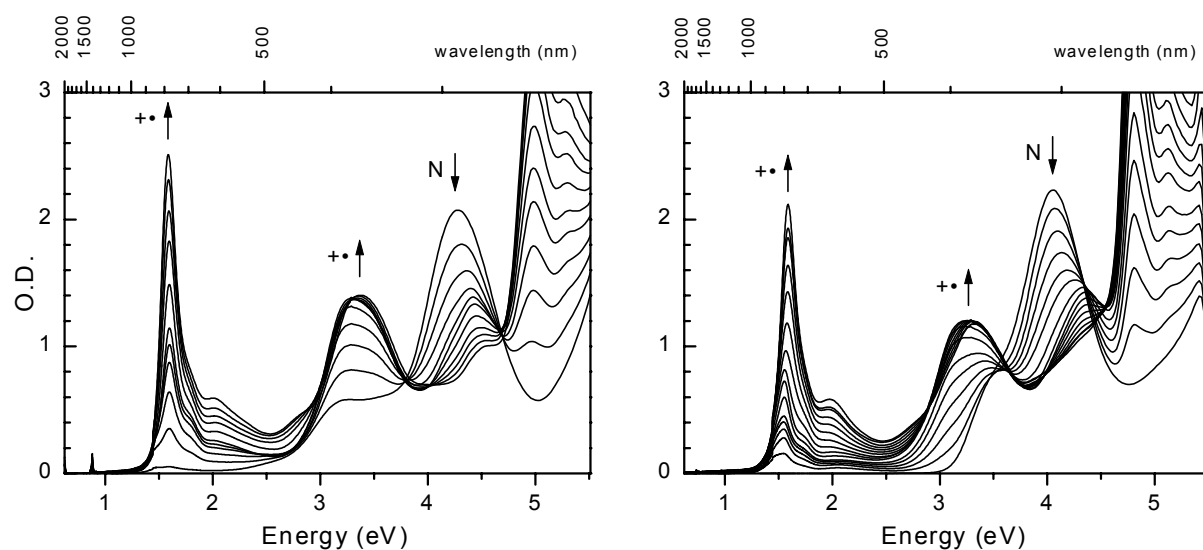
Figure 7.8. *UV/visible/nearIR spectra recorded in different solvents during the conversion of **2** to $2^{3(+\bullet)}$ by stepwise oxidation with THI$^{+\bullet}$ClO$_4^-$ at 295 K. Solvents: hexafluoroisopropanol (left), dichloromethane (right).*

As a control experiment, primary amine **4** was oxidized with THI$^{+\bullet}$ClO$_4^-$ in dichloromethane (Figure 7.9) resulting in the same absorption characteristics as for $2^{3(+\bullet)}$ in dichloromethane. Here absorptions come up at 1.56, 2.00, and 3.33 eV for the cation radical of **4**. The spectrum of neutral **4** was completely restored after reduction with hydrazine hydrate. These UV/visible/nearIR spectroscopy measurements show that it is very likely that the hexahydrotriazine rings in compounds **1** and **2** are not stable under these oxidative and/ or solvent conditions.
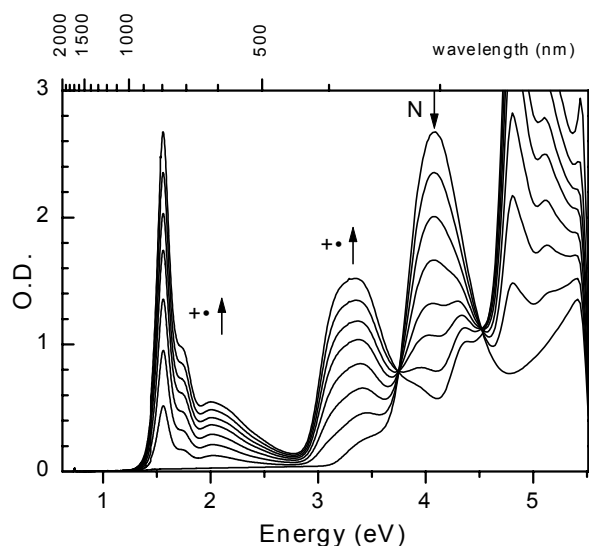

Figure 7.9. *UV/visible/nearIR spectra recorded in dichloromethane during the conversion of **4** to $4^{+\bullet}$ by stepwise oxidation with THI$^{+\bullet}$ClO$_4^-$ at 295 K.*

Table 7.2. *Optical data of the hexahydrotriazines*

	Neutral, eV (nm)		Oligo(cation radical), eV (nm)		
1[a]		4.13 (300)	1.76 (704)	2.57 (482)	3.53 (352)
2[a]	3.29 (375)	4.28 (289)	1.59 (780)	2.00 (619)	3.38 (367)
2[b]		4.05 (305)	1.59 (780)	1.98 (627)	3.31 (373)
4[b]		4.07 (304)	1.56 (797)	2.00 (619)	3.33 (372)
TPD[b]	3.52 (352)	4.00 (310)	0.89 (1398)	2.56 (485)	

[a] *Conditions: hexafluoroisopropanol, oxidation with* $THI^{+\bullet}ClO_4^-$*, 295 K.* [b] *Conditions: dichloromethane, oxidation with* $THI^{+\bullet}ClO_4^-$*, 295 K.*

7.2.4 Electron spin resonance spectroscopy

Although the UV/visible/nearIR spectroscopy measurements indicated that the oligo(cation radicals) of hexahydrotriazines **1** and **2** are unstable under chemical oxidizing conditions, it is of interest to check whether an intramolecular ferromagnetic spin coupling can be observed. The ESR spectrum of $1^{+\bullet}$ in hexafluoroisopropanol at ambient temperatures (Figure 7.10) shows at least seven shoulders as a result of hyperfine coupling with the nitrogen nuclei and the ring protons. Further oxidation of $1^{+\bullet}$ to $1^{3(+\bullet)}$ and subsequent cooling down to 120 K reveals an ESR spectrum with a broad transition for the frozen solution of $1^{3(+\bullet)}$. No indication for a high-spin state could be found. Measurement at half field failed to show a $\Delta M_S=\pm 2$ transition. These results indicate that there is no strong interaction between the unpaired electrons in $1^{3(+\bullet)}$.
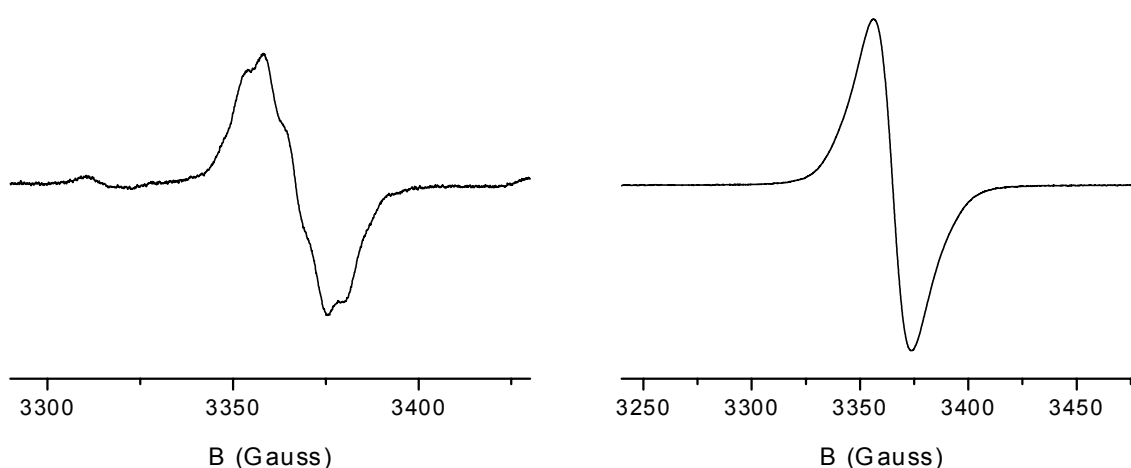

Figure 7.10. *ESR spectra of $1^{+\bullet}$ (left) at 295 K and $1^{3(+\bullet)}$ (right) at 120 K in hexafluoroisopropanol obtained by oxidation with $THI^{+\bullet}ClO_4^-$.*

Because of failure to observe significant interactions between the spins the concept of spin coupling of nitrogen centered cation radicals via σ-bonds in hexahydrotriazines was not pursued any further.

7.3 Spin-spin coupling in diarylamine substituted spirofluorenes

The spiro compounds (Figure 7.4), 2,2',7,7'-tetrakis-(*N*,*N*-diphenylamino)-9,9'-spirofluorene (spiro-TAD) **5** and 2,2',7,7'-tetrakis-(*N*,*N*-di-4-methoxyphenylamino)-9,9'-spirofluorene (spiro-MeOTAD) **6**, were generously provided by the group of prof. J. Salbeck. To allow for comparison with other aniline oligomers, the redox and optical properties of spiro compounds **5** and **6** have been investigated[29].

7.3.1 Cation radicals by cyclic voltammetry

The cyclic voltammogram of **5** shows three reversible oxidation waves at 0.67, 0.81, and 1.01 V (Figure 7.11). E_1^0 and E_2^0 are one-electron oxidations with a peak-peak splitting of 69 and 59 mV, respectively. At E_3^0 two electrons are removed from $5^{2(+•)}$, leading to the formation of 5^{4+} with a peak-peak splitting of 62 mV. Measuring at different scan rates revealed the quasi-reversible nature of these oxidation processes, indicated by an increased peak-peak splitting at higher scan rates.
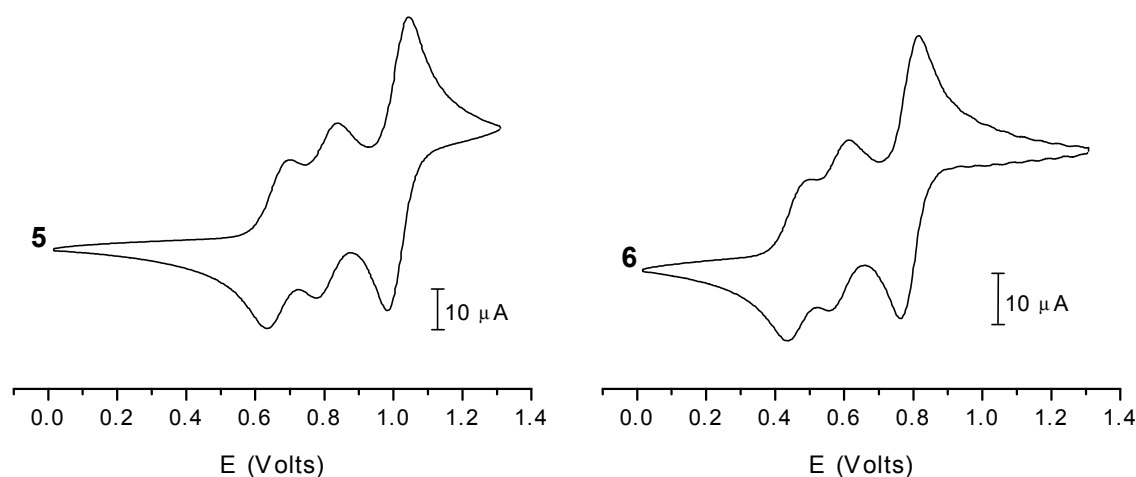

Figure 7.11. *Cyclic voltammograms of spiro compounds **5** (left) and **6** (right). Conditions: 0.1 M TBAHF in CH₂Cl₂, scan rate 100 mV/s, at 295 K. Potential vs. SCE reference and calibrated against Fc/Fc⁺ couple at 0.46 V.*

The redox properties of **6** showed a similar behavior and three reversible oxidation waves at 0.47, 0.59, and 0.79 V could be observed. The anodic and cathodic waves were splitted by 69 mV, 57 mV, and 49 mV, respectively. The significantly decreased peak-peak splitting of E_3^0 is an indication for a coupled two-electron oxidation process. Interestingly, the oxidation potentials show an average decrease of 0.2 V compared to **5** due to the presence of methoxy substituents in **6**. The electrochemistry of the spirofluorenes **5** and **6** showed that stable di(cation radicals) can be obtained at ambient temperature.

Table 7.3. *Electrochemical data of the spiro-TADs* [a]

	E_1^0(V)	E_2^0(V)	E_3^0(V)
5	0.67	0.81	1.01[b]
6	0.47	0.59	0.79[b]

[a] *Conditions: 0.1 M TBAHF in CH_2Cl_2, 295 K. Potential vs. SCE reference and calibrated against Fc/Fc^+ couple at 0.46 V.* [b] *Two-electron oxidation.*

7.3.2 Optical properties of the cation radicals

The optical properties of **5** and **6** were measured using UV/visible/nearIR spectroscopy. The electronic absorption spectrum of neutral **5** in dichloromethane shows two absorption bands at 4.01 and 3.28 eV (Figure 7.12). Oxidation of **5** with $THI^{+\bullet}ClO_4^-$ results in a decrease of the neutral bands and two new absorption bands come up at 2.43 and 0.94 eV. Complete oxidation to $\mathbf{5}^{2(+\bullet)}$ reveals the presence of an extra band at 3.58 eV previously obscured by the absorption of neutral **5**. The optical spectrum of neutral **6** exhibits two absorptions at 4.03 and 3.24 eV. Addition of $THI^{+\bullet}ClO_4^-$ results in two new absorption bands at 2.38 and 0.82 eV. Upon reaching the di(cation radical) state of **6**, four absorption bands are visible at 3.33, 2.38, 1.83, and 0.82 eV. The neutral absorption spectra of molecules **5** and **6** reappeared after addition of hydrazine hydrate, indicative for a chemically reversible process.

Table 7.4. *Optical data of the spiro-TADs* [a]

	Neutral, eV (nm)		Di(cation radical), eV (nm)			
5	3.28 (378)	4.01 (309)	0.94 (1321)	2.43 (508)	3.58 (347)	
6	3.24 (384)	4.03 (306)	0.82 (1514)	1.83 (678)	2.38 (521)	3.33 (371)

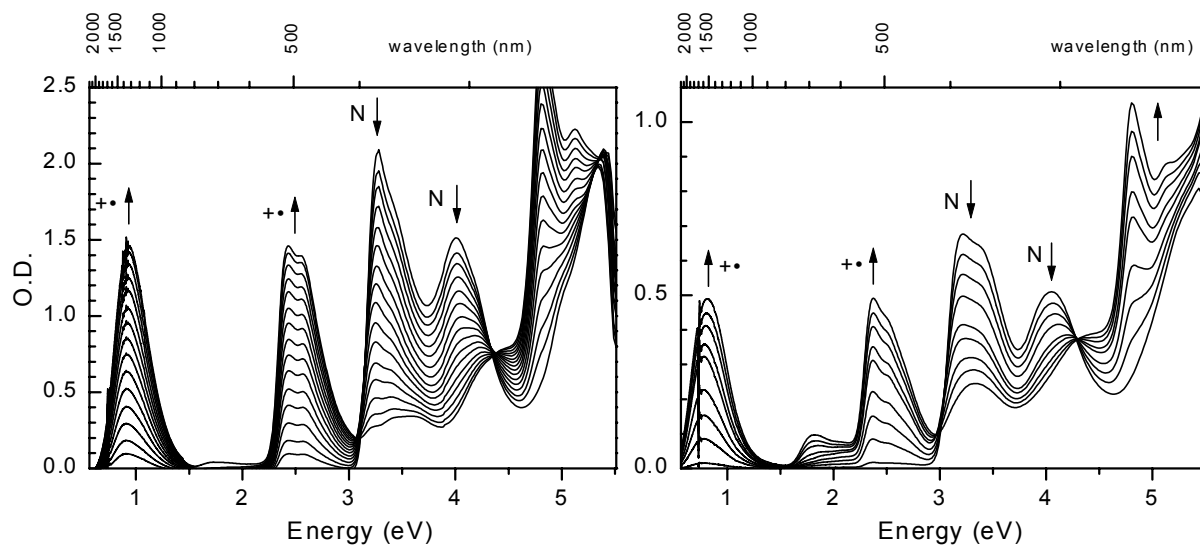[a] *Conditions: dichloromethane, oxidation with $THI^{+\bullet}ClO_4^-$, 295 K.*

Figure 7.12. *UV/visible/nearIR spectra recorded during the conversion of **5** (left) and **6** (right) by stepwise oxidation with $THI^{+\bullet}ClO_4^-$ at 295 K in CH_2Cl_2 from the neutral state to the di(cation radical).*

7.3.3 Electron spin resonance spectroscopy

The ESR spectra of $\mathbf{5^{(+\bullet)}}$ (not shown) and $\mathbf{5^{2(+\bullet)}}$ (Figure 7.13) in dichloromethane at ambient temperature only differed in signal intensity and show a spectrum with a peak-to-peak linewidth of 24 MHz. A narrow transition with a peak-to-peak linewidth of 15.5 MHz could be observed for the frozen solution of $\mathbf{5^{2(+\bullet)}}$ at 125 K with the addition of TFA. The absence of a $\Delta M_S=\pm 2$ transition at half field shows that there are no ferromagnetic or antiferromagnetic interactions between the two spins in $\mathbf{5^{2(+\bullet)}}$.
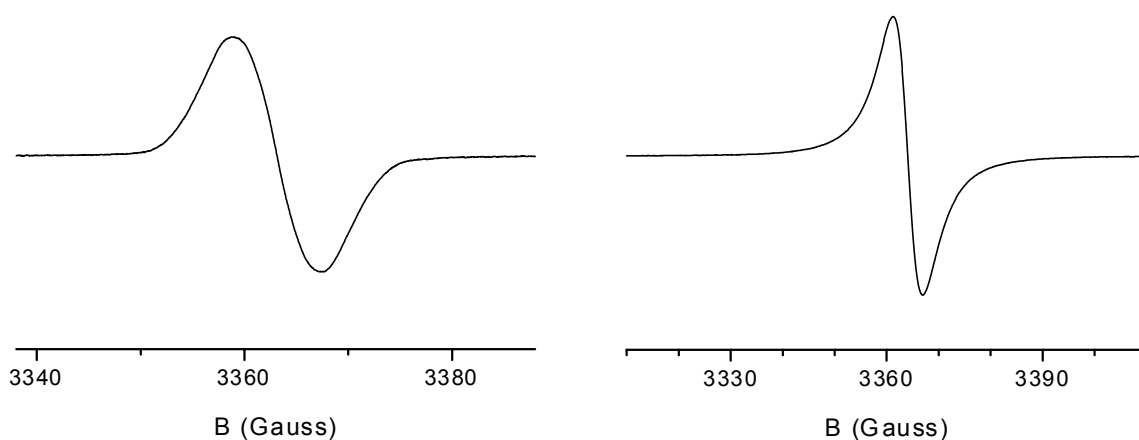

Figure 7.13. *ESR spectra of $\mathbf{5^{2(+\bullet)}}$ at 295 K (left) in dichloromethane and at 125 K (right) in dichloromethane/TFA (99/1) obtained by oxidation with $THI^{+\bullet}ClO_4^-$.*

Spiro-MeOTAD **6** was oxidized with two equivalents of $THI^{+\bullet}ClO_4^-$ in dichloromethane to the di(cation radical) $\mathbf{6^{2(+\bullet)}}$. At ambient temperature an ESR spectrum was obtained with a small hyperfine coupling of approximately 5.5 MHz attributed to the interaction of the cation radicals with the hydrogen and nitrogen nuclei (Figure 7.14). Since the linewidth of the spectrum is small, the cation radical seems to interact with only two nitrogen nuclei and is therefore localized at one of the benzidine parts in the molecule. The anisotropic ESR spectrum of $\mathbf{6^{2(+\bullet)}}$ at 125 K shows a narrow transition with a peak-to-peak linewidth of 18.6 MHz. A $\Delta M_S = \pm 2$ transition at half field could not be observed.
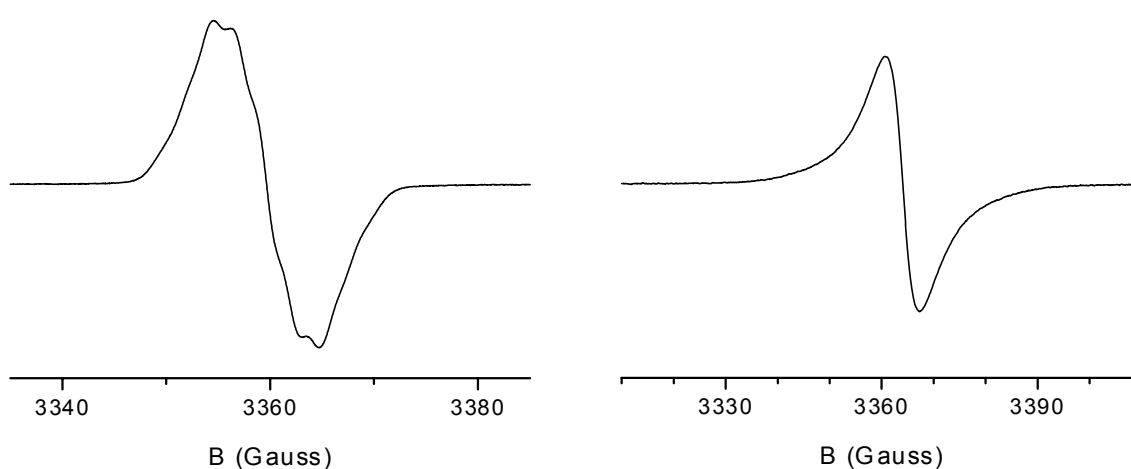
Figure 7.14. *ESR spectra of $\mathbf{6^{2(+\bullet)}}$ at 295 K (left) in dichloromethane and at 125 K (right) in dichloromethane/TFA (99/1) obtained by oxidation with $THI^{+\bullet}ClO_4^-$.*

The ESR spectra of di(cation radicals) of **5** and **6** clearly show that the exchange coupling between the cation radicals in these spiro compounds is close to zero. In case of an antiferromagnetic exchange coupling either no transition or a transition with a very low intensity due to cancellation of spins would be found.

7.4 Conclusion

The results with the hexahydrotriazines **1** and **2** show that the hexahydrotriazine ring is not suitable for intramolecular ferromagnetic interaction between cation radicals generated by oxidative doping. Either because the hexahydrotriazine is cleaved due to the acidic and/or oxidative conditions used or because the spin polarization mechanism through the σ-bonds is not strong enough to result in an exchange overlap/interaction.

This does leave open the use of other types of radicals in combination with hexahydrotriazine rings, either generated under reductive conditions or already present as stable neutral radicals before ring closure, to investigate the possibility of hexahydrotriazines acting as ferromagnetic coupling units.

In the spiro compounds **5** and **6**, both halves of the molecule are held strictly perpendicular by the central sp³ carbon, hampering any overlap between the molecular orbitals. Therefore, the spirofluorene part might be a bit to rigid too facilitate a spin polarization mechanism through the σ-bonds which must serve as exchange pathway for an intramolecular ferromagnetic coupling. Only one prerequisite for an intramolecular ferromagnetic coupling is met here; the cation radicals are occupying orthogonal molecular orbitals. The other prerequisite, an substantial exchange coupling between the unpaired electrons, is not fulfilled, resulting in the cation radicals behaving like they are on different molecules.

These results show that spin coupling of ionic radicals through σ-bonds is not as predictable as it is for π-bonds. The stability of σ-bonds and rigidity of the construction probably play a major role in the design of high-spin molecules with through-σ-bond intramolecular interactions of ionic radicals.

7.5 Experimental section

General techniques. For general procedures and equipment see experimental sections of chapter 3 and 4. *N,N*-bis(4-methoxyphenyl)amine (Lancaster), 1-bromo-4-nitrobenzene, and *N,N'*-bis(3-methylphenyl)-*N,N'*-diphenylbenzidine (Aldrich) were used as received. *N,N*-Diphenyl-1,4-benzenediamine was prepared according to literature procedures[23,24]

_N,N_-Bis(4-methoxyphenyl)-4-nitro-benzenamine (3). An oven-dried Schlenk flask was charged with *N,N*-bis(4-methoxyphenyl)amine (1.26 g, 5.50 mmol), 1-bromo-4-nitrobenzene (1.31 g, 6.48 mmol), cesium carbonate (2.68 g, 8.23 mmol), Pd$_2$(dba)$_3$ (12.6 mg, 13.8 µmol), and *S*-BINAP (24.0 mg, 38.5 µmol). After alternate applying of vacuum and argon three times, toluene (20ml) was added. The reaction mixture was heated for one week at 90 °C and cooled to room temperature. The mixture was taken up in diethyl ether, filtered over Celite 545 and concentrated in vacuo. Column chromatography (SiO$_2$, heptane/CH$_2$Cl$_2$ 2:3) resulted in an orange solid (1.72 g, 89 %). mp 123-125 °C; ^{1}H NMR (CDCl$_3$): δ 7.99 (d, *J* = 9.3 Hz, 2H), 7.13 (d, *J* = 8.8 Hz, 4H), 6.91 (d, *J* = 8.8 Hz, 4H), 6.75 (d, *J* = 9.3 Hz, 2H), 3.82 (s, 6H); ^{13}C NMR (CDCl$_3$): δ 157.92, 154.38, 139.23, 138.51, 128.35, 125.80, 115.98, 115.44, 55.74; IR (ATR, cm^{-1}): 3042, 3009, 2966, 2933, 2906, 2840, 1608, 1583, 1493, 1461, 1446, 1314, 1285, 1238, 1180, 1164, 1105, 1035, 1023, 831, 815, 781, 748, 729, 716, 691, 644, 628, 605, 576.

_N,N_-Bis(4-methoxyphenyl)-1,4-benzenediamine (4)^{25}. To a solution of **3** (1.68 g, 4.77 mmol) and zinc (2.88 g, 44.1 mmol) in ethanol (100 ml) was added drop wise acetic acid (4 ml, mmol) and stirred for 1 h at room temperature. After filtration and evaporation of the solvent, it was dissolved in CH$_2$Cl$_2$ and subsequently washed with 1 N sodium hydroxide and water, dried over MgSO$_4$, filtered and concentrated in vacuo. crystallization from petroleum ether(60-80)/toluene (5:1, v/v) resulted in a white solid (1.26 g, 82 %). mp 128-

130 °C; ^{1}H NMR (CDCl$_3$): δ 6.95 (d, J = 9.0 Hz, 4H), 6.88 (d, J = 8.8 Hz, 2H), 6.77 (d, J = 9.0 Hz, 4H), 6.60 (d, J = 8.8 Hz, 2H), 3.77 (s, 6H), 3.52 (bs, 2H); ^{13}C NMR (CDCl$_3$): δ 154.83, 142.50, 141.96, 140.49, 125.96, 124.54, 116.33, 114.66, 55.75; IR (ATR, cm^{-1}): 3456, 3372, 3232, 3033, 3003, 2968, 2928, 2836, 1635, 1499, 1468, 1460, 1440, 1275, 1264, 1232, 1181, 1165, 1107, 1028, 913, 833, 818, 779, 724, 715, 708.

1,3,5-Tris(*N,N*-diphenyl-4-aminophenyl)hexahydro-1,3,5-triazine (1). A solution of *N,N*-diphenyl-1,4-benzenediamine (0.15 g, 0.58 mmol) and paraformaldehyde (0.06 g, 2 mmol) in toluene (10 ml) was stirred at reflux for 30 min, after which half of the toluene was distilled off, and it was concentrated in vacuo. Twofold precipitation from CH$_2$Cl$_2$/methanol afforded **1** as a white solid (0.1 g, 63 %). mp 108-110 °C; ^{1}H NMR (CDCl$_3$): δ 7.2-7.15 (m, 12H), 7.03 (d, J = 7.6 Hz, 12H), 7.0-6.9 (m, 15H), 4.79 (s, 6H), 3.76 (s, 18H); ^{13}C NMR (CDCl$_3$): δ 147.96, 144.58, 141.35, 129.05, 125.80, 123.33, 122.01, 119.18, 69.66; IR (ATR, cm^{-1}): 3036, 1587, 1506, 1489, 1387, 1326, 1275, 1221, 1174, 1155, 1076, 1029, 985, 932, 824, 751, 694, 620.

1,3,5-Tris(*N,N*-bis(4-methoxyphenyl)-4-aminophenyl)hexahydro-1,3,5-triazine (2). A solution of **4** (0.17 g, 0.53 mmol) and paraformaldehyde (0.02 g, 0.67 mmol) in toluene (10 ml) was stirred at reflux for 30 min, after which half of the toluene was distilled off, and it was concentrated in vacuo. Crystallisation from petroleum ether(60-80)/toluene (7:3, v/v) afforded **2** as a white powder (0.07 g, 40 %). mp 120-122 °C; ^{1}H NMR (CDCl$_3$): δ 6.97 (d, J = 9.0 Hz, 12H), 6.90 (d, J = 9.0 Hz, 6H), 6.84 (d, J = 9.0 Hz, 6H), 6.76 (d, J = 9.0 Hz, 12H), 4.79 (s, 6H), 3.76 (s, 18H); ^{13}C NMR (CDCl$_3$): δ 155.25, 143.56, 142.74, 141.95, 125.44, 123.56, 119.50, 114.74, 70.32, 55.72; IR (ATR, cm^{-1}): 2995, 2935, 2836, 1499, 1466, 1443, 1388, 1322, 1262, 1235, 1218, 1178, 1147, 1107, 1033, 993, 982, 929, 911, 821, 780, 717, 602, 569.

7.6 References

1. Zhang, J. P.; Baumgarten, M., *Chem. Phys.* **1997**, *214*, 291.
2. Zhang, J. P.; Wang, R. S.; Wang, L. X.; Baumgarten, M., *Chem. Phys.* **1999**, *246*, 209.
3. Zhang, J. P.; Lahti, P. M.; Wang, R. S., *J. Phys. Org. Chem.* **1999**, *12*, 53.
4. Ito, A.; Miyajima, H.; Yoshizawa, K.; Tanaka, K.; Yamabe, T., *J. Org. Chem.* **1997**, *62*, 38.
5. Ito, A.; Miyajima, H.; Yoshizawa, K.; Tanaka, K.; Yamabe, T., *Synth. Met.* **1997**, *85*, 1777.
6. Saito, T.; Ito, A.; Tanaka, K., *J. Phys. Chem. A* **1998**, *102*, 8021.
7. Selby, T. D.; Stickley, K. R.; Blackstock, S. C., *Org. Lett.* **2000**, *2*, 171.
8. Golubev, V. A.; Rashba, Y. É., *Bull. Acad. Sci. USSR, Div. Chem. Sci.* **1982**, *31*, 2445.
9. Chiarelli, R.; Rassat, A.; Rey, P., *J. Chem. Soc., Chem. Commun.* **1992**, 1081.
10. Chiarelli, R.; Novak, M. A.; Rassat, A.; Tholence, J. L., *Nature* **1993**, *363*, 147.
11. Nakatsuji, S.; Mizumoto, M.; Takai, A.; Anzai, H.; Teki, Y.; Tajima, K., *Mol. Cryst. Liq. Cryst. Sci. Technol., Sect. A* **1999**, *334*, 205.
12. Vostrikova, K. E.; Belorizky, E.; Pecaut, J.; Rey, P., *Eur. J. Inorg. Chem.* **1999**, 1181.
13. Nelsen, S. F.; Yunta, M. J. R., *J. Phys. Org. Chem.* **1994**, *7*, 55.
14. Brouwer, A. M.; Wiering, P. G.; Zwier, J. M.; Langkilde, F. W.; Wilbrandt, R., *Acta Chem. Scand.* **1997**, *51*, 217.
15. Giumanini, A. G.; Verardo, G.; Zangrando, E.; Lassiani, L., *J. Prakt. Chem.* **1987**, *329*, 1087.

16. Steuber, F.; Staudigel, J.; Stossel, M.; Simmerer, J.; Winnacker, A.; Spreitzer, H.; Weissortel, F.; Salbeck, J., *Adv. Mater.* **2000**, *12*, 130.
17. Salbeck, J.; Yu, N.; Bauer, J.; Weissortel, F.; Bestgen, H., *Synth. Met.* **1997**, *91*, 209.
18. Salbeck, J., *Ber. Bunsen-Ges.* **1996**, *100*, 1667.
19. Yu, W. L.; Pei, J.; Huang, W.; Heeger, A. J., *Adv. Mater.* **2000**, *12,* 828.
20. Salbeck, J.; Weissörtel, F.; Bauer, J., *Macromol. Symp.* **1997**, *125*, 121.
21. Bach, U.; Lupo, D.; Comte, P.; Moser, J. E.; Weissortel, F.; Salbeck, J.; Spreitzer, H.; Gratzel, M., *Nature* **1998**, *395*, 583.
22. Frank, N. L.; Clerac, R.; Sutter, J. P.; Daro, N.; Kahn, O.; Coulon, C.; Green, M. T.; Golhen, S.; Ouahab, L., *J. Am. Chem. Soc.* **2000**, *122*, 2053.
23. Haeussermann, C., *Chem. Ber.* **1906**, *39*, 2762.
24. Herz, E., *Chem. Ber.* **1890**, *23*, 2536.
25. Gambarjan, S., *Chem. Ber.* **1908**, *41*, 3507.
26. Wolfe, J. P.; Buchwald, S. L., *Tetrahedron Lett.* **1997**, *38*, 6359.
27. Layer, R. W., *Chem. Rev.* **1963**, *63*, 489.
28. Sprung, M. M., *Chem. Rev.* **1940**, *26*, 297.
29. Similar studies have been conducted by prof. J. Salbeck and co-workers using spectroelectrochemistry.

Summary

Whereas molecular materials with functional optical and electrical properties find their way into commercial applications, molecular magnetic materials remain a challenge for physical organic chemistry. The preparation of organic molecules with ferromagnetically aligned electron spins is limited by the reactive nature of free radicals and weak magnetic interactions. Several design strategies exist to engage in this challenge, of which high-spin molecules form a promising option to obtain room temperature stable magnetic materials . The research presented in this thesis has been focused on the design, synthesis, assembly, and characterization of organic molecules in which multiple free electrons ferromagnetically couple to a high-spin state. Furthermore, as a first step towards intermolecular ferromagnetic interactions, high-spin molecules with possible liquid crystalline properties have been designed to create ferromagnetically ordered stacks.

Doped aniline oligomers with 1,4-benzenediamine motifs have a fair chemical stability under ambient conditions and are known to possess high-spin properties when connected via ferromagnetic coupling units. The recent progress in C-N bond formation synthetic methodologies made it possible to improve and extend the synthesis of this type of high-spin molecules. A series of *N*-methyl-*m*-*p*-aniline oligomers has been synthesized with different topologies. The well known 1,3-benzene or 1,3,5-benzene ferromagnetic coupling unit has been used for their construction. The free radicals were generated by oxidative doping of the 1,4-benzenediamine moieties and the properties of these cation radicals were studied with UV/visible/nearIR spectroscopy and ESR spectroscopy. The observed properties were consistent with low energy high-spin states. For the first time it has been possible to obtain high-spin oligo(cation radicals) of this length and shows that the concept of a polaronic ferromagnet is viable for extension to longer systems. It has also been possible to obtain a ferromagnetic coupling in two-dimensional branched oligomers. This research provides the basis for the development of linear and branched high-spin polymers.

An intermolecular ferromagnetic coupling between the individual high-spin molecules is a prerequisite for obtaining a material with magnetic properties. The specific structural orientation of the molecules in such a material is of high importance in this respect. It has been established theoretically that a helical packing of discotic high-spin molecules could lead to an one-dimensional ferromagnetic stack. As a first step towards such a stack, an attempt to design a discotic liquid crystalline high-spin molecules has been undertaken. Since carbazoles allow for facile substitution at the 3- and 6-position with e.g. mesogenic groups, mixed carbazole aniline oligomers have been

prepared and characterized. The introduction of the carbazole, however, caused a decreased stability of the oligo(cation radicals) at ambient temperatures. Next, a star-shaped aniline oligomer with mesogenic groups at the periphery was synthesized and oxidized to the tri(cation radical). Although a low lying high-spin state could be confirmed, lyotropic or thermotropic liquid crystalline properties were not observed.

Stable neutral verdazyl radicals were investigated instead of nitrogen-centered cation radicals to overcome coulombic repulsion which occurs between equally charged molecules. Here oxo-verdazyl radicals with dodecyl groups were used for the construction of a discotic liquid crystalline high-spin molecule. In addition to a 1,3,5-substituted benzene also a 2,6,10-substitued triphenylene core has been used to increase the rigidity of the central core. Although, both triradicals exhibited a transition at half field with ESR-spectroscopy characteristic of ferromagnetic coupling of unpaired electrons, no unambiguous evidence could be found for a high-spin state or for liquid crystalline behavior.

In most high-spin molecules ferromagnetic intramolecular spin-spin coupling occurs via π-bonds acting as exchange pathways. It is of interest to investigate new exchange pathways as well. Two types of molecules in which a ferromagnetic intramolecular coupling might occur via σ-bonds have been studied. Stable oxidation to the corresponding oligo(cation radical) could be accomplished electrochemically and chemically both for hexahydrotriazine as well as spirofluorene derivatives. However, these molecules showed no evidence for a ferromagnetic intramolecular interaction via σ-bonds and only low-spin states were observed with ESR-spectroscopy.

Samenvatting

Waar moleculaire materialen met functionele elektrische en optische eigenschappen momenteel intensief bestudeerd worden en de gang naar commerciële toepassing maken, vormen organische en polymere materialen met magnetische eigenschappen een tot op heden niet gerealiseerde wetenschappelijke uitdaging. Het creëren van ferromagnetische gekoppelde elektronspins in organische moleculen en moleculaire polymeren stelt hoge eisen aan het ontwerp omdat chemische stabiliteit van intrinsiek reactieve radicalen gecombineerd moet worden met een coöperatief gedrag van veelal zwakke magnetische interacties. Het promotieonderzoek was gericht op het ontwerpen, synthetiseren, assembleren en karakteriseren van organische hoge-spin moleculen, waarin meerdere vrije elektronen ferromagnetisch koppelen tot een hoge-spin toestand. In dergelijke systemen ontstaat een netto magnetisch moment door combinatie van de individuele magnetische momenten van de vrije elektronen.

Het is bekend dat (poly)anilines door middel van oxidatieve doping omgezet kunnen worden in stabiele geladen radicalen. Deze materialen worden onder meer toegepast als electrisch geleidend materiaal en als electromagnetische afscherming. De hoge-spin moleculen die in dit onderzoek ontwikkeld werden, zijn opgebouwd uit anilinefragmenten die via een zogenaamde meta-para of een meta-meta topologie met elkaar verbonden zijn. Na oxidatieve doping kan deze specifieke topologie via spinpolarisatie leiden tot een relatief sterke intramoleculaire ferromagnetische wisselwerking van elektronspins. Door gebruik te maken van recent ontwikkelde homogene palladium gekatalyseerde reacties zijn omvangrijke, goed-gedefinieerde, lineaire en stervormige moleculen gesynthetiseerd. De elektrochemische, optische en magnetische eigenschappen van deze oligo-anilines en de corresponderende oligoradicaalkationen zijn intensief bestudeerd met cyclische voltammetrie, UV/vis/nearIR en elektronspin resonantie (ESR) spectroscopie. In de grondtoestand blijken alle elektronspins binnen het molecuul (*intra*moleculair) ferromagnetisch gekoppeld te zijn. Niet eerder konden zulke lange high-spin oligoradicaalkationen gerealiseerd worden. Voorts bleek het mogelijk om ferromagnetische koppeling te bewerkstelligen in een tweedimensionaal systeem. Hiermee is de synthetische basis gelegd voor de ontwikkeling van lineaire en vertakte high-spin polymeren.

Omdat magnetisme een materiaaleigenschap is, moet er ook een *inter*moleculaire ferromagnetische koppeling tussen de hoge-spin moleculen zijn in een organische ferromagneet. Met het realiseren van deze, unieke, stap zouden moleculaire magnetische materialen echt binnen bereik komen. Aandachtspunt in het ontwerp is dat de magnetische interactie sterk afhankelijk is van de specifieke onderlinge oriëntatie

van de moleculen. Theoretisch is af te leiden dat een helische stapeling van vlakke geconjugeerde high-spin moleculen zou kunnen leiden tot een ferromagnetisch aggregaat van nanoscopische afmetingen. Als eerste stap in die richting zijn moleculen ontworpen die een high-spin grondtoestand combineren met discotisch vloeibaar kristallijn gedrag. De drijvende kracht achter vloeibaar kristallijn gedrag komt vaak voort uit de combinatie van twee totaal verschillende eigenschappen, in dit geval star en flexibel, binnen één molecuul, dat dan zorgt voor een soort van fasescheiding binnen het materiaal waarin de flexibele delen en starre delen aparte geordende domeinen vormen. Om dit mesogene karakter van de moleculen te verkrijgen zijn uitgebreide starre aromatische kernen gebruikt en zijn flexibele alifatische groepen in de periferie van het molecuul aangebracht. Zowel geladen oligo-aniline radicaalkationen als neutrale oligoverdazylradicalen zijn toegepast als dragers van de elektronspins. Ofschoon diverse nieuwe high-spin moleculen gemaakt konden worden, bleek de combinatie met vloeibaar kristallijn gedrag vooralsnog niet te realiseren.

Moleculaire magneten blijven daarmee een uitdaging voor synthetisch en fysisch organische chemie.

Curriculum Vitae

Martin Struijk werd geboren op 15 augustus 1971 te Doesburg. Na het doorlopen van het VWO aan het Newman College in Breda begon hij in 1989 aan de studie Scheikundige Technologie aan de Technische Universiteit Eindhoven. Het propaedeutisch examen werd in 1990 behaald en het afstudeerproject binnen de vakgroep Organische Chemie (prof.dr. E.W. Meijer) werd in 1996 afgerond. Vanaf april 1996 tot april 2000 was hij als onderzoeker in opleiding in dienst van de Nederlandse Organisatie voor Wetenschappelijk Onderzoek. Onder leiding van prof.dr.ir. René Janssen en prof.dr. E.W. Meijer in de capaciteitsgroep Macromoleculaire en Organische Chemie werkte hij aan zijn promotieonderzoek waarvan de resultaten in dit proefschrift beschreven staan.

Martin Struijk was born in Doesburg (The Netherlands) on the 15th of August 1971. In 1989, after he obtained his high school degree at the 'Newman College' in Breda, he started his study in Chemical Engineering at the Eindhoven University of Technology. In 1996 he graduated with a major in Organic Chemistry (prof.dr. E.W. Meijer). From April 1996 to April 2000 he was employed by the Netherlands Organization for Scientific Research. In the group of 'Macromolecular and Organic Chemistry' he worked under the guidance of prof.dr. R.A.J. Janssen and prof.dr. E.W. Meijer on his PhD-research of which the results are described in this thesis.

Dankwoord

Ook al ben ik nu echt aan het einde van mijn promotieperiode gekomen, nog steeds is het moeilijk voor te stellen dat het boekje er werkelijk ligt. Dat het allemaal zover is gekomen is dan ook mede te danken aan de hulp, afleiding en steun van diverse mensen in mijn omgeving.

Allereerst wil ik mijn promotoren René Janssen en Bert Meijer bedanken. Jullie geduld, inzet en enthousiaste begeleiding zijn van grote invloed geweest op mijn ontwikkeling als onderzoeker. De vrijheid om mijn eigen onderzoek te sturen en de onderwerpen te bestuderen waarin ik geloofde, heb ik zeer op prijs gesteld. Ik voel me dan ook erg bevoorrecht dat ik in deze uitgebalanceerde vakgroep heb mogen meedraaien.

I would like to thank dr. Martin Baumgarten for taking a position in my manuscript committee and for your valuable suggestions to my thesis. Verder wil ik prof.dr. H. H. Brongersma bedanken voor het lezen van het manuscript en het plaatsnemen in mijn promotie commissie. I'm grateful to prof. J. Salbeck for his generous providing of the spirofluorenes, although unfortunately they did not behave like we expected. Henk Claessens en Hervé Cottet, ook al staan de resultaten van de samenwerking niet in dit proefschrift, ik wil jullie toch bedanken voor het interessante uitstapje op het gebied van de analytische chemie.

Rob Peerlings en Bert Groenendaal wil ik bedanken voor hun enthousiaste dagelijkse begeleiding gedurende mijn jaren als student binnen de groep. Het is ook mede dankzij jullie dat ik verder ben gegaan in de organische chemie. Ook Martijn Wienk en John van Haare ben ik erkentelijk voor het wegwijs maken in de diverse fysisch organische meettechnieken gedurende de eerste jaren van mijn promotie.

Jef Vekemans bedank ik voor de synthetische adviezen en discussies, Jolanda Spiering voor de diverse producten die ik heb mogen afnemen, maar zeker ook voor de jaarlijkse volleybal traditie.

Joost van Dongen, allereerst ben ik je dankbaar voor de hulp bij de diverse scheidingsproblemen die ik gedurende mijn promotieperiode ben tegengekomen, maar ook voor de muzikale uitstapjes en gezellige auditorium lunches. Ook wil ik hierbij Tonny Bosman, Luc Brunsveld, Henk Janssen en Emiel Peeters bedanken voor hun aandeel in die momenten van ontspanning naast het werk en de fijne discussies over het dagelijks nieuws.

Het is altijd makkelijk als je iemand hebt die net een klein beetje voorloopt en het dus allemaal al eens heeft moeten regelen, daarom ben ik Jan-Willem Weener als schrijfkamergenoot dankbaar voor de diverse tips op bureaucratisch, schrijf en sollicitatiegebied maar ook voor de oeverloze verhalen waar uiteindelijk waarheid over ging in fictie. Mijn dank gaat ook uit naar Albert Schenning voor zijn medewerking aan het polyactyleen project dat uiteindelijk niet helemaal werkte maar toch een interessante zijsprong was.

Uiteraard ben ik Ingrid Dirkx, Henk Eding, Hanny van der Lee en Hanneke Veldhoen dank verschuldigd voor het feit dat ze ervoor hebben gezorgd dat de vakgroep en mijn promotie soepel draaiden gedurende de afgelopen jaren. Hans Damen, bedankt voor alle 'informatie' uitwisselingen en conversaties gedurende de koffiepauzes 's ochtends en 's middags, jouw kritische kijk heb ik zeer gewaardeerd.

Mijn kamergenoot Robert van Mullekom wil ik niet alleen bedanken voor de prettige samenwerking tijdens - naar wat nu blijkt - een trendsettend vakgroepsuitje, maar ook voor je humor en taalgrappen. Koen Pieterse, nu jij nog, als laatste van een memorabele generatie. Bedankt ook voor Brugge maar zeker ook voor de gezellige uitstapjes onder andere in het teken van science fiction samen met Marcel van Genderen, die ik hier ook tevens voor bedank.

Ik bedank ook alle (ex)bewoners van Lab zuidoost en kernlab één voor de fijne werksfeer. Rest mij nog alle mensen die door de jaren heen een grote of kleine bijdrage hebben geleverd aan mijn promotieonderzoek te bedanken voor hun medewerking.

Lieve familie, ook al denk ik dat jullie de afgelopen jaren inhoudelijk weinig van mijn promotie hebben begrepen, zonder jullie warmte en steun om op terug te vallen zou promoveren voor mij een hele moeilijke opgave zijn geworden. Het feit dat ik er straks echt sta komt ook mede door jullie. Niet te min wil ik toch nog een aantal van jullie in het bijzonder bedanken.

Joke, door jou en jouw gezin kreeg mijn sportieve kant een positieve impuls. Ook was het bijzonder fijn om zomaar aan te kunnen schuiven en af en toe de auto te mogen lenen.

Oma Noordzij, voor al die dinsdagavonden waarin de wandelingen door het park mij niet alleen hielpen om op de hoogte blijven van alle familie perikelen, maar tevens momenten van ontspanning waren.

Thea, Petra en Harry, voor de culinaire uitspattingen, wijsheid en hulp gedurende de afgelopen jaren.

En natuurlijk Ard en Anne-Hélène, voor de momenten van gezelligheid en onvoorwaardelijke steun aan die 'kleine' broer.

Pa en Ma, ik weet dat jullie ontzettend meegeleefd hebben en altijd voor mij klaar stonden de afgelopen jaren. Ma, jouw creativiteit en enthousiasme werken aanstekelijk. Pa, jouw adviezen en visie op onderzoek heb ik altijd als zeer waardevol beschouwd.

Judith, je weet nog niet half hoeveel energie ik uit onze relatie heb geput om deze schrijfperiode door te komen. Alle momenten samen waren bijzonder en zullen in de toekomst vast nog mooier worden.